CRUSTACEAN REPRODUCTIVE PHYSIOLOGY AND ITS APPLICATIONS

EDITED BY: Haihui Ye, Chaoshu Zeng, Naoaki Tsutsui and Heinrich Dircksen

PUBLISHED IN: Frontiers in Marine Science and Frontiers in Physiology

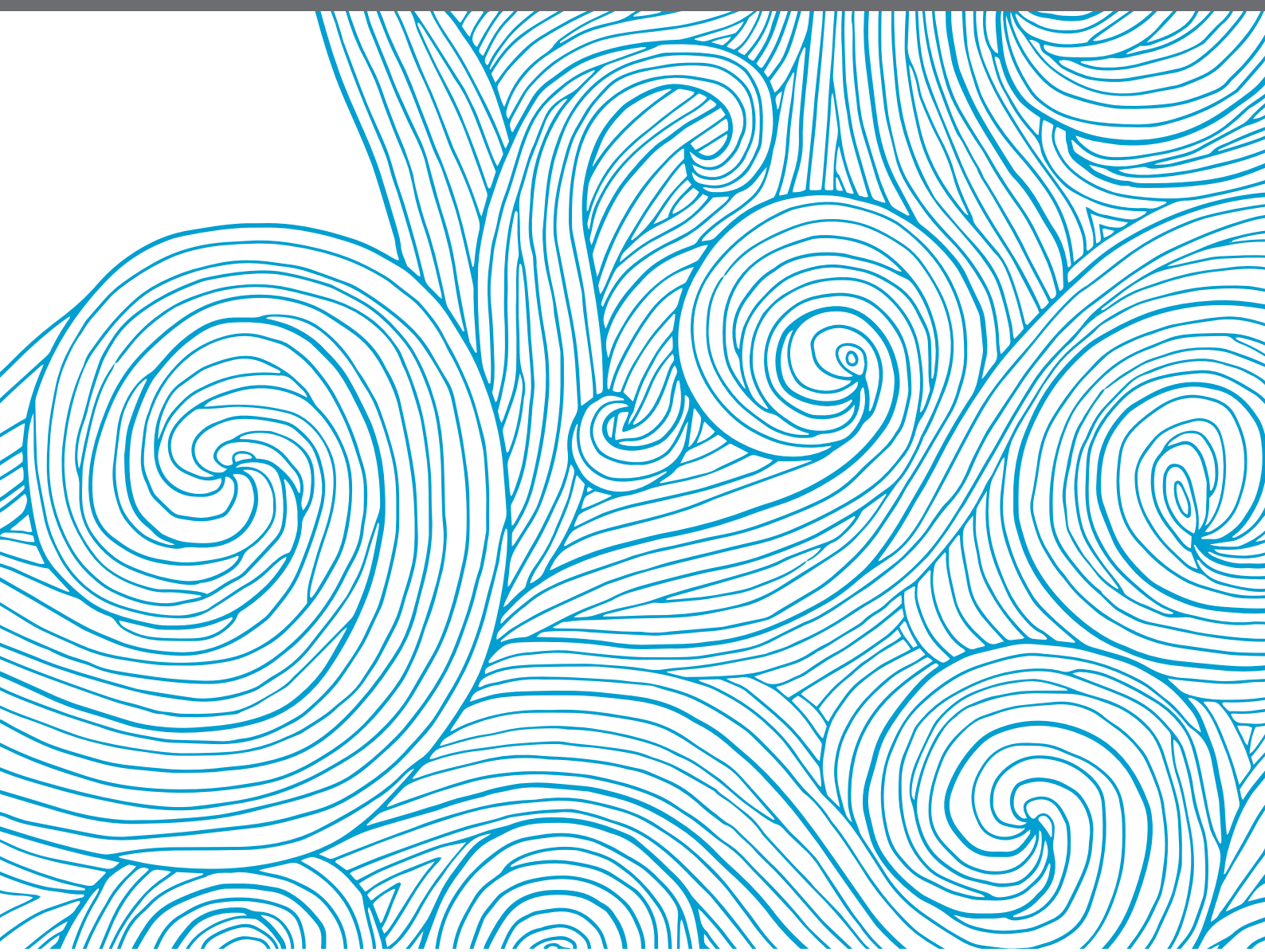

frontiers Research Topics

frontiers

ISSN 1664-8714
ISBN 978-2-83250-206-8
DOI 10.3389/978-2-83250-206-8

About Frontiers

Frontiers is more than just an open-access publisher of scholarly articles: it is a pioneering approach to the world of academia, radically improving the way scholarly research is managed. The grand vision of Frontiers is a world where all people have an equal opportunity to seek, share and generate knowledge. Frontiers provides immediate and permanent online open access to all its publications, but this alone is not enough to realize our grand goals.

Frontiers Journal Series

The Frontiers Journal Series is a multi-tier and interdisciplinary set of open-access, online journals, promising a paradigm shift from the current review, selection and dissemination processes in academic publishing. All Frontiers journals are driven by researchers for researchers; therefore, they constitute a service to the scholarly community. At the same time, the Frontiers Journal Series operates on a revolutionary invention, the tiered publishing system, initially addressing specific communities of scholars, and gradually climbing up to broader public understanding, thus serving the interests of the lay society, too.

Dedication to Quality

Each Frontiers article is a landmark of the highest quality, thanks to genuinely collaborative interactions between authors and review editors, who include some of the world's best academicians. Research must be certified by peers before entering a stream of knowledge that may eventually reach the public - and shape society; therefore, Frontiers only applies the most rigorous and unbiased reviews.
Frontiers revolutionizes research publishing by freely delivering the most outstanding research, evaluated with no bias from both the academic and social point of view. By applying the most advanced information technologies, Frontiers is catapulting scholarly publishing into a new generation.

What are Frontiers Research Topics?

Frontiers Research Topics are very popular trademarks of the Frontiers Journals Series: they are collections of at least ten articles, all centered on a particular subject. With their unique mix of varied contributions from Original Research to Review Articles, Frontiers Research Topics unify the most influential researchers, the latest key findings and historical advances in a hot research area! Find out more on how to host your own Frontiers Research Topic or contribute to one as an author by contacting the Frontiers Editorial Office: frontiersin.org/about/contact

CRUSTACEAN REPRODUCTIVE PHYSIOLOGY AND ITS APPLICATIONS

Topic Editors:
Haihui Ye, Jimei University, China
Chaoshu Zeng, James Cook University, Australia
Naoaki Tsutsui, Mie University Tsu, Japan
Heinrich Dircksen, Stockholm University, Sweden

Citation: Ye, H., Zeng, C., Tsutsui, N., Dircksen, H., eds. (2022). Crustacean Reproductive Physiology and its Applications. Lausanne: Frontiers Media SA. doi: 10.3389/978-2-83250-206-8

Table of Contents

frontiers | Frontiers in Physiology

TYPE Editorial
PUBLISHED 15 September 2022
DOI 10.3389/fphys.2022.1018481

OPEN ACCESS

EDITED AND REVIEWED BY
Pung Pung Hwang,
Academia Sinica, Taiwan

*CORRESPONDENCE
Haihui Ye,
hhye@jmu.edu.cn

SPECIALTY SECTION
This article was submitted to Cardiac Electrophysiology, a section of the journal Frontiers in Physiology

RECEIVED 13 August 2022
ACCEPTED 18 August 2022
PUBLISHED 15 September 2022

CITATION
Ye H, Zeng C, Tsutsui N and Dircksen H (2022), Editorial: Crustacean reproductive physiology and its applications.
Front. Physiol. 13:1018481.
doi: 10.3389/fphys.2022.1018481

Editorial: Crustacean reproductive physiology and its applications

Haihui Ye[1]*, Chaoshu Zeng[2], Naoaki Tsutsui[3] and Heinrich Dircksen[4]

[1]College of Fisheries, Jimei University, Xiamen, China, [2]College of Science and Engineering, James Cook University, Townsville, QLD, Australia, [3]Department of Marine Bioresources, Faculty of Bioresources, Mie University, Tsu, Japan, [4]Department of Zoology, Stockholm University, Stockholm, Sweden

KEYWORDS

reproduction, metabolic regulation, growth, genetics, neuropeptides, crustacea

Editorial on the Research Topic
Crustacean reproductive physiology and its applications

Crustacea constitute an important taxonomic group in aquatic ecosystems and form an important sector of aquaculture industry. Novelties in studies on crustacean reproductive physiology help shedding new lights on deeper understanding of the mechanisms of sex determination and differentiation of crustaceans. The application of established and innovative techniques based on such knowledge will contribute significantly to progress in the crustacean aquaculture industry. The objective of this Special Issue was to provide a forum for researchers to report upon their cutting-edge research in Crustacean Reproductive Physiology and its Applications. This Research Topic comprises ten original research articles.

In particular, in this Special Issue, the roles of several neuropeptides in regulating crustacean reproduction have been reported for several decapod crustacean species of importance for aquaculture. In the giant freshwater prawn *Macrobrachium rosenbergii*, Ao et al. revealed that recombinant neuroparsins NP1 and NP2 stimulate expression of the vitellogenin (Vg) gene, and silencing of NP1 and NP2 genes suppresses Vg, Vg receptor, and CyclinB gene expressions. In the mud crab *Scylla olivacea*, double strand RNA technology (dsRNA) was used to inhibit transcription of vitellogenesis-inhibiting hormone (VIH), i.e. dsRNA-VIH accelerates ovarian maturation by increasing hemolymph vitellogenin concentration and the gonadosomatic index (Duangprom et al.). In the swimming crab *Portunus trituberculatus*, Tu et al. confirmed via *in vitro* experiments that the expressions of Vg, VgR, cyclinB, and Cdc2 in ovary explants is induced by synthetic corazonin, but reduced by corazonin receptor dsRNA. Tu et al. also suggested that the corazonin/corazonin receptor signaling system stimulates the biosynthesis of ecdysteroids. It is known that crustacean female sex hormone (CFSH) plays a pivotal role in the development of secondary sex characteristics in dioecious species. The roles of CFSH were reported for the first time in female reproductive

physiology in the hermaphrodite cleaner shrimp *Lysmata vittata* in this Special Issue. CFSH1a was found to be indispensable for the development of female gonopores, but was probably not involved in the control of vitellogenesis in this species. In terms of male reproductive physiology, CFSH1a appeared to suppress the mRNA expression of the insulin-like androgenic gland hormone 2 (IAG2) in short-term silencing and recombinant protein injection experiments. However, CFSH1a did not affect male sexual differentiation in long-term silencing experiments (Liu et al.).

Up to the present date, autocrine and paracrine mechanisms are poorly understood in crustaceans. Thus, as an important novelty in this Special Issue, Yang et al. revealed that in the ovary of the mud crab *Scylla paramamosain*, bone morphogenetic protein 2 (BMP2) is exclusively detected in oocytes, whereas BMP2-receptors are expressed in both follicle cells and oocytes. RNAi tests further suggested that BMP2 promotes oocyte maturation through an autocrine/paracrine pathway. It is reasonable but novel that autocrine/paracrine regulation of gonadal function by the transforming growth factor β (TGFβ) superfamily, which is well known in vertebrates, also exists in crustaceans.

RNA -Seq is a powerful tool for uncovering molecular events in gonadal development. Wang et al. applied full-length transcriptome sequencing and comparative transcriptomic analysis to provide insights into the ovarian maturation of the ridge tail white shrimp *Exopalaemon carinicauda*. Li et al. identified a novel Vg specifically expressed in the hepatopancreas of the Pacific white shrimp *Litopenaeus vannamei*, and revealed an exogenous nutrient transfer and accumulation mechanism from the hepatopancreas to ovary in Penaeid shrimps.

Male reproductive physiology in crustaceans often appears to attract too little attention. In this Special Issue, RNAi analyses in the oriental river prawn *Macrobrachium nipponense* revealed that ferritin positively affects mRNA expression of IAG and the secretion of testosterone, thus positively affecting testis development in this species (Jin et al.).

In addition, the genetic mechanism of sex determination in the Chinese shrimp *Fenneropenaeus chinensis* was explored by Wang et al. The authors applied resequencing of data to detect sex-linked variants and female-specific sequences, and found these clearly suggestive of a female heterogametic (ZW) sex determination system.

Copepods are small planktonic crustaceans often serving as excellent prey for larval rearing in hatcheries. Wang et al. investigated the embryonic development and effects of temperature, salinity and light intensity on egg hatching of the calanoid copepod *Bestiolina amoyensis*, and suggested that *B. amoyensis* is a good candidate as live feed for larval rearing.

We hope the readers will benefit from these articles in their research and enjoy reading these subjects as much as we did while editing them. We sincerely thank all authors and reviewers for their participation and commitment that made publication of this Research Topic possible.

Author contributions

HY wrote the draft. CZ, HD, and NT revised the text. All authors contributed to the article and approved the submitted version.

Conflict of interest

The authors declare that the research was conducted in the absence of any commercial or financial relationships that could be construed as a potential conflict of interest.

Publisher's note

frontiers in Marine Science

ORIGINAL RESEARCH
published: 31 August 2021
doi: 10.3389/fmars.2021.743727

Evidences of Z- and W-Linked Regions on the Genome of *Fenneropenaeus chinensis*

Qiong Wang[1,2†], Jianjian Lv[1,2†], Xianyun Ren[1,2], Jiajia Wang[1,2], Shaoting Jia[1,2], Yuying He[1,2] and Jian Li[1,2*]*

[1] *Key Laboratory for Sustainable Utilization of Marine Fisheries Resources, Ministry of Agriculture and Rural Affairs, Yellow Sea Fisheries Research Institute, Chinese Academy of Fishery Sciences, Qingdao, China,* [2] *Function Laboratory for Marine Fisheries Science and Food Production Processes, Qingdao National Laboratory for Marine Science and Technology, Qingdao, China*

Fenneropenaeus chinensis is a commercially cultured shrimp in China. *F. chinensis* adults show significant sexual dimorphism, with larger females than males. However, sex determination (SD) of *F. chinensis* has not yet been elucidated. Clarification of the sex-determining system of *F. chinensis* could enrich our knowledge of the sex differentiation mechanism in crustaceans and facilitate the study of sex-controlling technologies. Here, we studied the sex-determining system of *F. chinensis* using the fixation index (F_{ST}) between the sexes to detect the genetic differentiation in resequencing data of multiple males and females. We located the candidate sex chromosome in the genome of *F. chinensis* and concluded the female heterogametic (ZW) SD system. We also assembled female-specific sequences, which could be used as molecular markers to identify the sex of *F. chinensis*. However, the differentiation of the *F. chinensis* Z and W chromosome is limited. RNA-seq data detected many genes with male-biased expression in the Z-specific region, which possibly could further intensify the divergency between the Z and W chromosomes.

Keywords: Crustacea, sex differentiation, shrimp, genome, Z chromosome

OPEN ACCESS

Edited by:
Haihui Ye,
Jimei University, China

Reviewed by:
Deborah Charlesworth,
University of Edinburgh, United Kingdom
Hongyu Ma,
Shantou University, China

****Correspondence:***
Yuying He
heyy@ysfri.ac.cn
Jian Li
lijian@ysfri.ac.cn

† These authors have contributed equally to this work

Specialty section:
This article was submitted to Aquatic Physiology, a section of the journal Frontiers in Marine Science

Received: *19 July 2021*
Accepted: *12 August 2021*
Published: *31 August 2021*

Citation:
Wang Q, Lv J, Ren X, Wang J, Jia S, He Y and Li J (2021) Evidences of Z- and W-Linked Regions on the Genome of Fenneropenaeus chinensis. Front. Mar. Sci. 8:743727. doi: 10.3389/fmars.2021.743727

INTRODUCTION

The evolution of chromosomes carrying the sex determination (SD) factor is an interesting form of genomic evolution (Charlesworth and Charlesworth, 2000; Bachtrog et al., 2011). In some cases, selection for close linkage may promote suppressed recombination in the SD region, because the region includes a sexually antagonistic polymorphism (Bull, 1985; Bergero and Charlesworth, 2009; Wright et al., 2016). Once recombination becomes suppressed, sex-specific evolutionary pressures act on the evolving sex chromosomes (Lahn and Page, 1997; Moghadam et al., 2012), leading to adaptive and non-adaptive processes that produce distinct differences between the X and Y (or Z and W) chromosomes (Muller, 1918; Bergero and Charlesworth, 2009; Bachtrog, 2013; Li et al., 2021). However, in many species, loss of recombination near the SD locus does not spread across the sex chromosomes, which may remain heteromorphic, and display only limited differentiation (Telgmann-Rauber et al., 2007; Spigler et al., 2008; Tennessen et al., 2016; Pucholt et al., 2017) (**Figure 1A**).

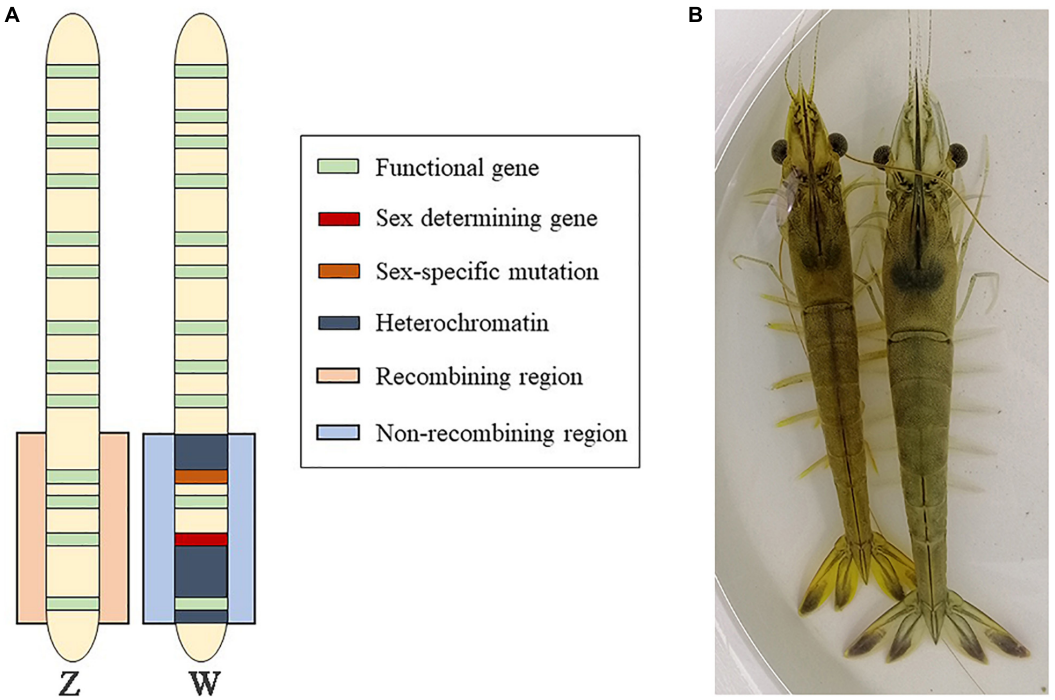

FIGURE 1 | Background for the sex chromosome analysis of *F. chinensis*. **(A)** Model of the early-stage sex chromosome. **(B)** *F. chinensis* (male on the left and female on the right).

Fenneropenaeus chinensis is a commercially cultured shrimp in China, whose adults are sexually dimorphic. Female shrimps tend to be blue, whereas the males are yellow; the adult females are larger and heavier than the adult males (Wang et al., 2019) (**Figure 1B**). Studies on the sex of *F. chinensis* are valuable. In Crustacea, both XX/XY and ZZ/ZW system existed (Shi et al., 2018; Fang et al., 2020). The sex-determining region of a predominant aquaculture shrimp species, the Pacific white shrimp (*Litopenaeus vannamei*), was mapped by the integrating linkage and association analyses (Yu et al., 2017). The results supported female heterogamety. The sex-determining regions of two other *Penaeus* shrimps, *Penaeus monodon* and *Penaeus japonicus*, have been mapped using high-density linkage analysis (Li et al., 2003; Robinson et al., 2014), but not fine-mapped. However, even some closely related species have different SD loci (Phillip et al., 2001; Miura, 2007; Mank and Avise, 2009; Pucholt et al., 2017). For *F. chinensis*, several sex-related markers have been identified by QTL mapping, but no direct evidence of their connection with SD was found (Meng et al., 2021). We therefore studied the SD mechanism of *F. chinensis* to improve our knowledge of the sex differentiation mechanism in crustaceans and facilitate the study of sex-controlling technologies, and provide sex-linked markers to identify the sexes at early developmental stages. The genome of *F. chinensis* released this year (Wang et al., 2021) makes it realizable to study the sex chromosome. In this study, we used resequencing data to detect sex-linked variants, including female-specific sequences, and preliminarily conclude that the species had a female heterogametic (ZW) SD system.

MATERIALS AND METHODS

Sample Collection and Sequencing

We randomly selected 10 female and 11 male *F. chinensis* "Huanghai No. 1" shrimps (age, 4 months) from the conservation base of Haifeng Aquaculture Co., Ltd. (Weifang, Shandong Province, China). The DNA samples of these 21 shrimps were obtained from the muscle and sequenced individually using the BGISEQ platform (BGI, Shenzhen, China), with paired ends of 150 bp. We obtained 219.9 Gb of clean DNA data (female: 104.5 Gb, male: 115.4 Gb). In addition, one female and one male were deeply sequenced, yielding 51.2 and 50.9 Gb clean data, respectively, approximately 35x cover depth.

The genome sequencing data were mapped to the improved reference genome of *F. chinensis* (Wang et al., 2021) using BWA (v0.7.15) (Li and Durbin, 2010) with default parameters. The bam files of 10 females and 11 males were merged into two pools by sex, and further convert to pileup file by using SAMtools (v1.9) (Li et al., 2009).

Analysis of Genetic Differentiation Between the Sexes

To evaluate the genetic differentiation between the sexes across the genome, we used PoPoolation2 software (Kofler et al., 2011) to convert the pileup file into sync file with a minimum base quality of 20. F_{ST} between the sexes and nucleotide diversity values, π, were estimated for all site types, using PoPoolation2 with the following set parameters: window size

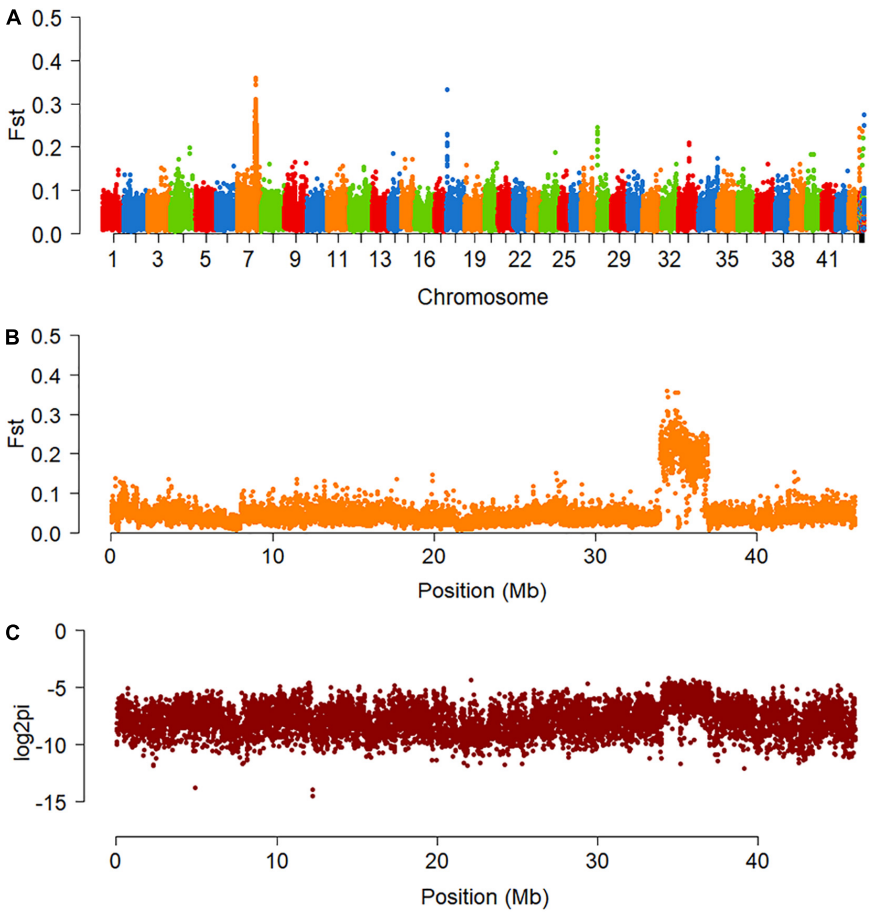

FIGURE 2 | Genomic differentiation of the two sexes of *F. chinensis*. **(A)** Genome-wide scan of the fixation index (F_{ST}) between the two sexes of *F. chinensis*. **(B)** F_{ST} on pseudochromosome Chr7. **(C)** Nucleotide diversity (π) on pseudochromosome Chr7 of the female. Value of π is represented in logarithm.

of 10 kb, step size of 5 kb, minimum allele count of 4, minimum coverage of 10, and maximum coverage of 200. F_{ST} was calculated using the merged data of all females and males, whereas π values were estimated using the two deep-sequenced individuals.

Information on mapping depth along the genome was extracted with bedtools (v2.25.0) (Quinlan and Hall, 2010) in 1 kb windows. The depth was normalized by the total read count. The ratio of the depth of male to female was $\log_2$-transformed.

Female-Specific Sequence Assembly

Besides the 21 "Huanghai No. 1" *F. chinensis* shrimps, we also sequenced 15 female and six male *F. chinensis* shrimps captured from the wild, again using the BGISEQ platform, with paired ends of 150 bp. In total, we obtained 436.3 Gb of clean resequencing data (female: 251.9 Gb, male: 184.4).

We expected a female heterogametic, or ZX system. Candidate W-linked sequences can be detected because they are female-specific. Therefore, we attempted to assemble female-specific sequences according to the method used for the snakehead (*Channa argus*) (Ou et al., 2017), with some adjustments. Briefly, the pooled sequencing data from the females were mapped to the reference genome, which was constructed from a male. The unmapped reads were assembled using SOAPdenovo (Luo et al., 2012), with Kmer = 31, and then aligned back to the assembled sequence to assess the accuracy of the assembly. Homozygous SNPs could reflect assembly error. The assembled contigs were mapped back to the reference genome using NCBI BLAST (v2.2.29 +) (Johnson et al., 2008) with evalue 1e-1. We deleted contigs for which more than 60% of the fragments that could be mapped to the reference genome. The resequencing data from both the males and the females were mapped to the assembled female-specific contigs. We retained only contigs with male mapping depth = 0 and female mapping depth > 30, representing W-linked candidates.

Validation With PCR Amplification

The candidate W-linked fragments based on the "Huanghai No. 1" strain and captured wild shrimps used for the female-specific sequence assembly were validated by PCR amplification in samples from four populations, containing two other population, "Huanghai No. 3" and wild shrimp bred for a generation. Primers were designed for the female-specific sequences with

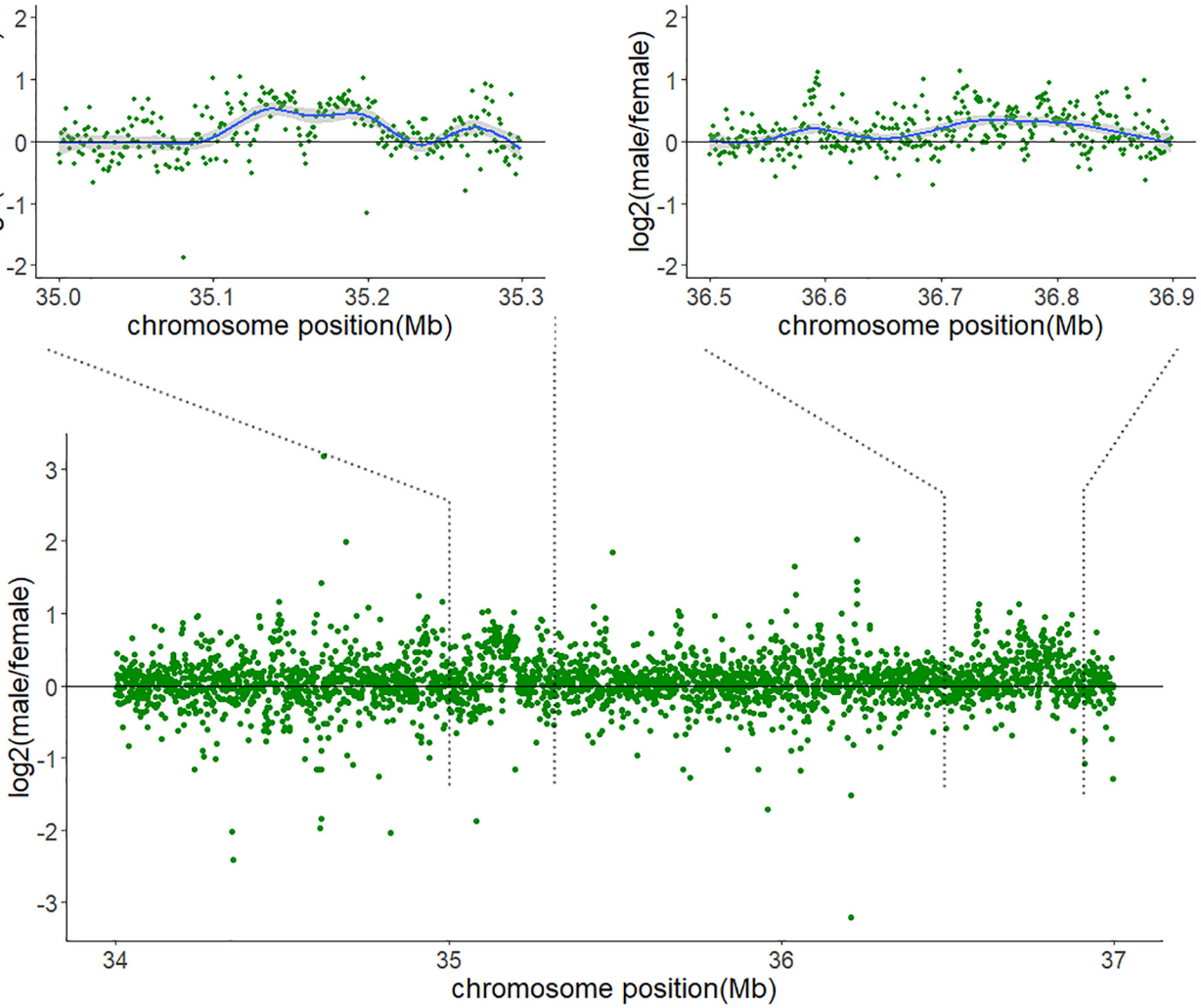

FIGURE 3 | Sequencing depth ratios of male to female in the 34–37 Mb interval of Chr7. The values of the read depth ratios are represented in logarithm.

the web tool Primer3[1] and synthesized by Sangon Biotech (China). We designed a pair of reference primers that could amplify the sequence in both sexes, but with a different sequence length in the females.

Female and male DNA pools of the four populations were used as PCR templates for the preliminary primer screening. Primers that generated PCR product only in female pools were selected for further validation in the individual samples of the four populations (10 females and 10 males of "Huanghai No. 1," 10 females and 10 males of "Huanghai No. 3," 12 females and 12 males of wild shrimp bred for a generation, and 10 females and six males of captured wild shrimp).

RNA-Seq Data Processing

The RNA-seq data have been described in a previous study (NCBI BioProject accession number: PRJNA591354) (Wang et al., 2019). Briefly, the gonad and muscle of female and male *F. chinensis* shrimps at 5 months of age were collected, and total RNA was extracted. We used three biological replicates for each tissue and sex. The 12 libraries were sequenced using the Illumina NovaSeq S4 platform, with paired ends of 150 bp. Clean reads from each RNA-seq library were aligned to the reference genome using HISAT (Kim et al., 2015). The gene expression of each sample was analyzed with HTSEQ (Anders et al., 2015).

[1]https://primer3.ut.ee/

RESULTS

Resequencing Data Identified a Candidate Sex-Linked Region

The fixation index (F_{ST}), which measures population differentiation (Weir and Cockerham, 1984; Holsinger and Weir, 2009), was calculated across the genome. Increased F_{ST} was observed on chromosome 7 (Chr7), spanning a region of approximately 3 Mb, from 34 to 37 Mb (**Figures 2A,B**). In the female, nucleotide diversity (π) increased in the same

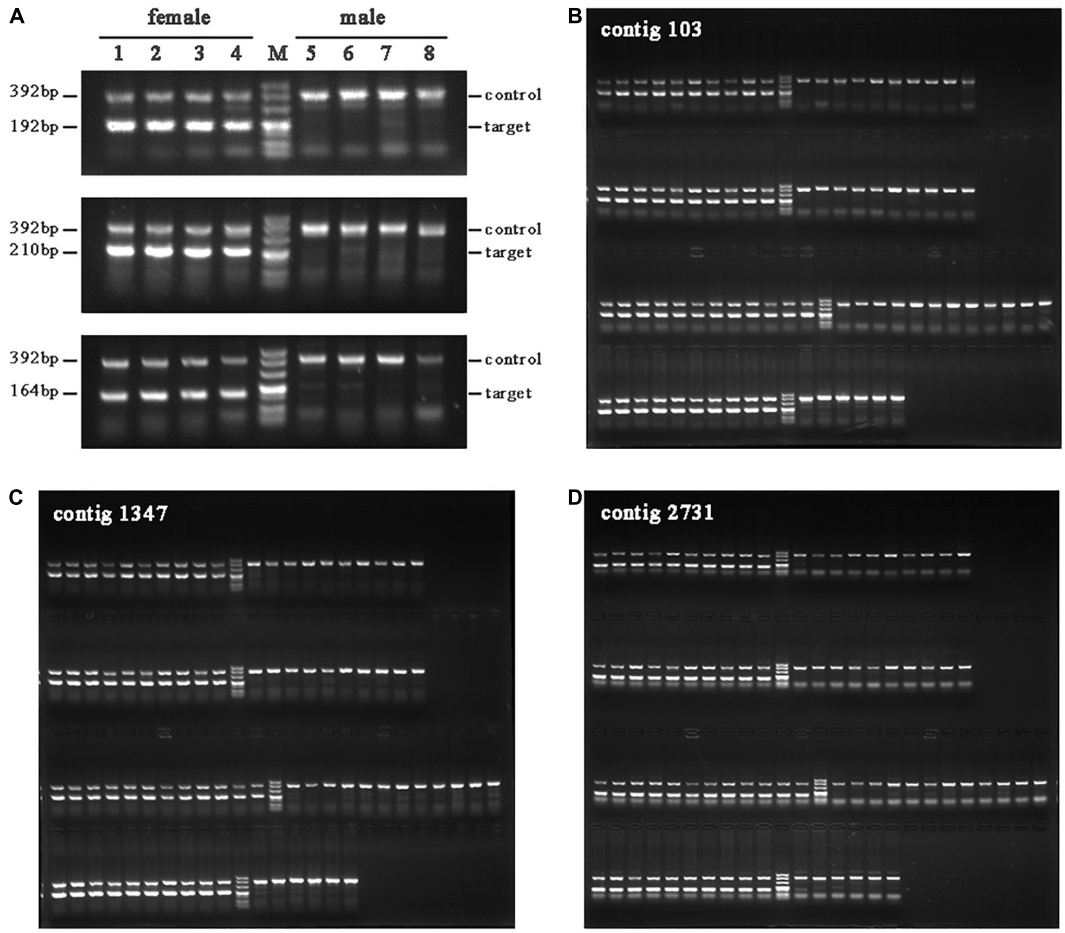

FIGURE 4 | PCR amplification of the female-specific sequences in female and male shrimps. **(A)** Female-specific sequence amplification with mixed DNA templates. Lanes 1–4 refer to females of "Huanghai No. 1," "Huanghai No. 3," wild shrimp bred for a generation, and captured wild shrimp, respectively; lanes 5–8 refer to male shrimps in the same order. The three lines from top to bottom correspond to three contigs (contig 103, contig 1347, and contig 2731). **(B–D)** The three contigs were amplified with individual DNA templates.

interval, as expected in a system of female heterogamety (**Figure 2C**), whereas in males, it was similar to the values in the rest of the genome. There are 60 genes located on this 3 Mb interval according to the genomic annotation file of *F. chinensis*.

The mapping depth was estimated across Chr7. More reads aligned to the 34–37 Mb interval in the males than in the females (**Supplementary Figure 1**), and the ratio of male to female coverage in some zones was close to 2:1 (**Figure 3**).

Assembly and Validation of Female-Specific Sequences

Among the 1.68 billion clean reads in the female pool, 92.01% mapped to the reference genome (**Supplementary Table 1**), and 134.12 million unmapped reads were also extracted and used in the assembly. In total, we obtained 103.25 Mb of fragments, consisting 435,866 contigs, with 70 contigs longer than 2,000 bp (**Supplementary Table 2**). Alignment of the unmapped reads showed a high coverage and low error rate (**Supplementary Table 3**). After further screening, we obtained 363 candidate female-specific contigs.

We selected 16 of the longest candidate female-specific contigs for validation. Sequences from three contigs amplified only with female DNA pools (**Figure 4A**). Further validation was performed using individual DNA templates (**Figures 4B–D**).

RNA-Seq Data Detected Male-Biased Expression Genes in the Interval on Chr7

To obtain information on the expression of genes on Chr7, we re-analyzed the RNA-seq data reported in a previous study (Wang et al., 2019) (**Supplementary Figure 2**). In muscle and gonad tissue of 5-month-old animals, we detected abundant differentially expressed genes (DEGs). In the muscle, 743 genes had male-biased expression and 2,291 genes had female-biased expression (**Supplementary Figure 3**). In the gonad, there were 1,713 male-biased and 1,352 female-biased genes (**Supplementary Figure 4**). DEGs in the gonad showed a higher

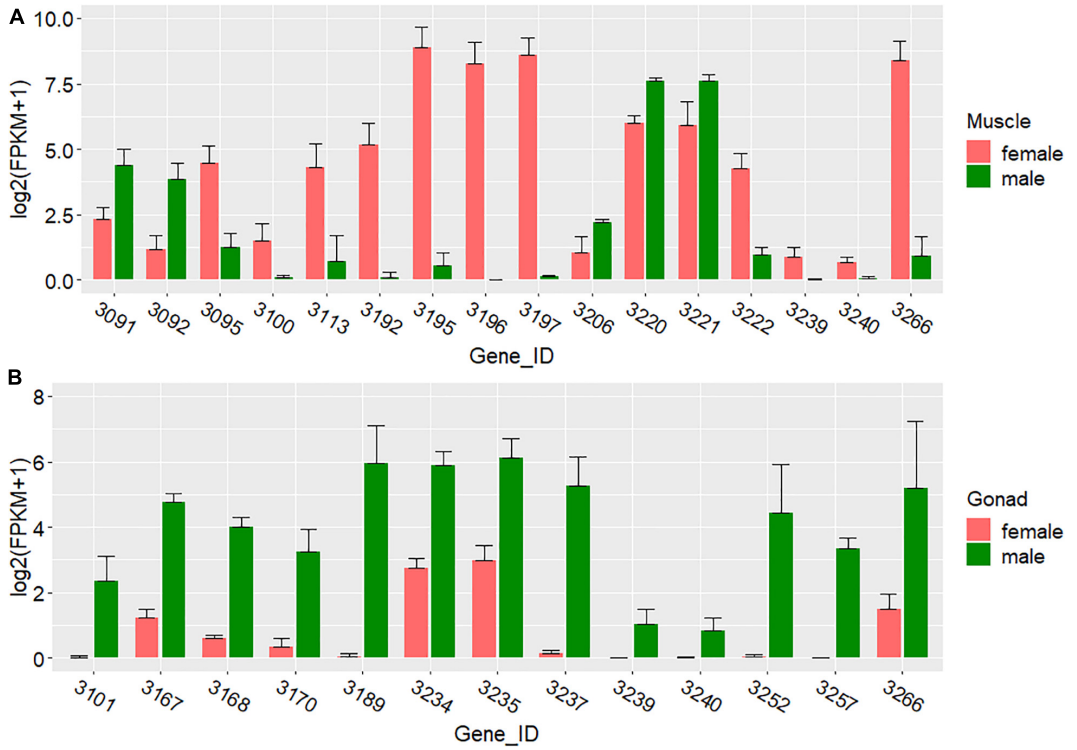

FIGURE 5 | Expression of DEGs in the 34–37 Mb interval of Chr7. **(A)** Expression in the muscle. **(B)** Expression in the gonad.

proportion (71.21%) of male-biased expression on Chr7 than other chromosomes (**Supplementary Table 4**).

In the 34–37 Mb interval of Chr7, we found five genes with male-biased and 11 with female-biased expression in the muscle (**Figure 5A** and **Supplementary Table 5**). In the gonad, the expression of all 13 DEGs in this region was male-biased; even expression of the adjacent genes was male-biased (**Figure 5B** and **Supplementary Table 6**).

DISCUSSION

The F_{ST} analysis located the sex-differentiation region on Chr7, which was regarded as the candidate sex chromosome in this study. In the differentiation region, the higher read mapping depth in males than females suggests that the sex-linked region is hemizygous in females, and the increased π in the females indicating that the SD system of *F. chinensis* is female heterogametic (female: ZW, male: ZZ). However, this species does not have differentiated Z and W chromosomes. Most fragments of the candidate "Z chromosome" were indistinguishable from autosomal sequences, according to the F_{ST} values and gene expression analyses. The sex chromosome formation of this species may only stay a primary stage.

During sex chromosome divergence, the suppression of recombination leads to the accumulation of mutations, which can result in highly heteromorphic sex chromosomes (Wright et al., 2016). At the primary stage of the divergence, the loss of recombination near the SD locus does not spread across the sex chromosomes. The sex chromosomes display only limited levels of differentiation. There are 60 genes annotated in the interval of 34–37 Mb of Chr7; compared to the 790 genes on Chr7 (46 Mb), and 25,026 genes on the whole genome (1.45 Gb), the gene density is slightly higher, which might be caused by the intergenic region loss in the initial process of recombination suppression.

However, if recombination becomes suppressed in a large genome region carrying a sex-determining locus, transcriptional degeneration of the W (or Y) allele can occur quickly (Bachtrog et al., 2008; Papadopulos et al., 2015). The enrichment of sex-biased expression genes in such an SD region may occur before loss of genes from the sex-limited chromosome (Bergero and Charlesworth, 2011; Chibalina and Filatov, 2011; Muyle et al., 2012; Pucholt et al., 2017). All the DEGs in and near the candidate Z-linked region exhibited male-biased expression, suggesting that many mutations causing male-biased expression have accumulated. These DEGs may be related to sex development and responsible for sexual dimorphism or reproduction. However, further studies need to be performed to analyze the functions of the DEGs.

The female-specific sequences detected in our analysis may have been derived from a W chromosome-like region. However, the Z and W regions appear to carry highly similar sequences, and some of our primers were designed for both of them (**Supplementary Figure 5**).

DATA AVAILABILITY STATEMENT

The datasets presented in this study can be found in online repositories. The names of the repository/repositories and accession number(s) can be found below: NCBI (accession: PRJNA591354).

AUTHOR CONTRIBUTIONS

QW collected the samples and carried out genetic differentiation analysis. XR extracted DNA and RNA for sequencing. JJL carried out female-specific fragment assembly. XR processed the RNA-seq data. JW and SJ performed verification experiment. JL conceived this project. YH supervised the work. QW and JJL wrote the manuscript. All authors contributed to the final manuscript.

FUNDING

This work was supported by the National Key R&D Program of China (No. 2019YFD0900403), China Agriculture Research System of MOF and MARA (No. CARS-48), National Natural Science Foundation of China (No. 31902367), and Central Public-interest Scientific Institution Basal Research Fund of CAFS (No. 2020TD46).

ACKNOWLEDGMENTS

We would like to appreciate our colleagues of the Key Laboratory for Sustainable Utilization of Marine Fisheries Resources of Yellow Sea Fisheries Research Institute, for their assistance on sample collection and helpful comments on the manuscript.

SUPPLEMENTARY MATERIAL

The Supplementary Material for this article can be found online at: https://www.frontiersin.org/articles/10.3389/fmars.2021.743727/full#supplementary-material

REFERENCES

Bachtrog, D., Kirkpatrick, M., Mank, J. E., McDaniel, S. F., Pires, J. C., Rice, W., et al. (2011). Are all sex chromosomes created equal? *Trends Genet* 27, 350–357. doi: 10.1016/j.tig.2011.05.005

Charlesworth, B., and Charlesworth, D. (2000). The degeneration of Y chromosomes. *Philos Trans R Soc Lond B Biol Sci* 355, 1563–1572. doi: 10.1098/rstb.2000.0717

Bergero, R., and Charlesworth, D. (2009). The evolution of restricted recombination in sex chromosomes. *Trends Ecol Evol* 24, 94–102. doi: 10.1016/j.tree.2008.09.010

Bull, J. J. (1985). Sex determining mechanisms: an evolutionary perspective. *Experientia* 41, 1285–1296. doi: 10.1007/bf01952071

Wright, A. E., Dean, R., Zimmer, F., and Mank, J. E. (2016). How to make a sex chromosome. *Nat Commun* 7, 12087. doi: 10.1038/ncomms12087

Lahn, B. T., and Page, D. C. (1997). Functional coherence of the human Y chromosome. *Science* 278, 675–680. doi: 10.1126/science.278.5338.675

Moghadam, H. K., Pointer, M. A., Wright, A. E., Berlin, S., and Mank, J. E. (2012). W chromosome expression responds to female-specific selection. *Proc Natl Acad Sci U S A* 109, 8207–8211. doi: 10.1073/pnas.1202721109

Muller, H. J. (1918). Genetic Variability, Twin Hybrids and Constant Hybrids, in a Case of Balanced Lethal Factors. *Genetics* 3, 422–499. doi: 10.1093/genetics/3.5.422

Li, M., Zhang, R., Fan, G., Xu, W., Zhou, Q., Wang, L., et al. (2021). Reconstruction of the origin of a neo-Y sex chromosome and its evolution in the spotted knifejaw, Oplegnathus punctatus. *Mol Biol Evol* 38, 2615–2626. doi: 10.1093/molbev/msab056

Bachtrog, D. (2013). Y-chromosome evolution: emerging insights into processes of Y-chromosome degeneration. *Nat Rev Genet* 14, 113–124. doi: 10.1038/nrg3366

Pucholt, P., Wright, A. E., Conze, L. L., Mank, J. E., and Berlin, S. (2017). Recent Sex Chromosome Divergence despite Ancient Dioecy in the Willow Salix viminalis. *Mol Biol Evol* 34, 1991–2001. doi: 10.1093/molbev/msx144

Telgmann-Rauber, A., Jamsari, A., Kinney, M. S., Pires, J. C., and Jung, C. (2007). Genetic and physical maps around the sex-determining M-locus of the dioecious plant asparagus. *Mol Genet Genomics* 278, 221–234. doi: 10.1007/s00438-007-0235-z

Tennessen, J. A., Govindarajulu, R., Liston, A., and Ashman, T. L. (2016). Homomorphic ZW chromosomes in a wild strawberry show distinctive recombination heterogeneity but a small sex-determining region. *New Phytol* 211, 1412–1423. doi: 10.1111/nph.13983

Spigler, R. B., Lewers, K. S., Main, D. S., and Ashman, T. L. (2008). Genetic mapping of sex determination in a wild strawberry, Fragaria virginiana, reveals earliest form of sex chromosome. *Heredity (Edinb)* 101, 507–517. doi: 10.1038/hdy.2008.100

Wang, Q., He, Y., and Li, J. (2019). Conjoint Analysis of SMRT- and Illumina-Based RNA-Sequencing Data of Fenneropenaeus chinensis Provides Insight Into Sex-Biased Expression Genes Involved in Sexual Dimorphism. *Front Genet* 10:1175. doi: 10.3389/fgene.2019.01175

Shi, X., Waiho, K., Li, X., Ikhwanuddin, M., Miao, G., Lin, F., et al. (2018). Female-specific SNP markers provide insights into a WZ/ZZ sex determination system for mud crabs Scylla paramamosain, S. tranquebarica and S. serrata with a rapid method for genetic sex identification. *BMC Genomics* 19:981. doi: 10.1186/s12864-018-5380-8

Fang, S., Zhang, Y., Shi, X., Zheng, H., Li, S., Zhang, Y., et al. (2020). Identification of male-specific SNP markers and development of PCR-based genetic sex identification technique in crucifix crab (Charybdis feriatus) with implication of an XX/XY sex determination system. *Genomics* 112, 404–411. doi: 10.1016/j.ygeno.2019.03.003

Yu, Y., Zhang, X., Yuan, J., Wang, Q., Li, S., Huang, H., et al. (2017). Identification of Sex-determining Loci in Pacific White Shrimp Litopeneaus vannamei Using Linkage and Association Analysis. *Mar Biotechnol (NY)* 19, 277–286. doi: 10.1007/s10126-017-9749-5

Robinson, N. A., Gopikrishna, G., Baranski, M., Katneni, V. K., Shekhar, M. S., Shanmugakarthik, J., et al. (2014). QTL for white spot syndrome virus resistance and the sex-determining locus in the Indian black tiger shrimp (Penaeus monodon). *BMC Genomics* 15:731. doi: 10.1186/1471-2164-15-731

Li, Y. T., Byrne, K., Miggiano, E., Whan, V., Moore, S., Keys, S., et al. (2003). Genetic mapping of the kuruma prawn Penaeus japonicus using AFLP markers. *Aquaculture* 219, 143–156. doi: 10.1016/S0044-8486(02)00355-1

Phillip, R. B., Konkol, N. R., Reed, K. M., and Stein, J. D. (2001). Chromosome painting supports lack of homology among sex chromosomes in Oncorhynchus, Salmo, and Salvelinus (Salmonidae). *Genetica* 111, 119–123. doi: 10.1023/a:1013743431738

Miura, I. (2007). An evolutionary witness: the frog rana rugosa underwent change of heterogametic sex from XY male to ZW female. *Sex Dev* 1, 323–331. doi: 10.1159/000111764

Mank, J. E., and Avise, J. C. (2009). Evolutionary diversity and turn-over of sex determination in teleost fishes. *Sex Dev* 3, 60–67. doi: 10.1159/000223071

Meng, X., Fu, Q., Luan, S., Luo, K., Sui, J., and Kong, J. (2021). Genome survey and high-resolution genetic map provide valuable genetic resources for Fenneropenaeus chinensis. *Sci Rep* 11, 7533. doi: 10.1038/s41598-021-87237-4

Wang, Q., Ren, X., Liu, P., Li, J., Lv, J., Wang, J., et al. (2021). Improved genome assembly of Chinese shrimp (Fenneropenaeus chinensis) suggests adaptation to the environment during evolution and domestication. *Mol Ecol Resour* doi: 10.1111/1755-0998.13463

Li, H., and Durbin, R. (2010). Fast and accurate long-read alignment with Burrows-Wheeler transform. *Bioinformatics* 26, 589–595. doi: 10.1093/bioinformatics/btp698

Li, H., Handsaker, B., Wysoker, A., Fennell, T., Ruan, J., Homer, N., et al. (2009). The Sequence Alignment/Map format and SAMtools. *Bioinformatics* 25, 2078–2079. doi: 10.1093/bioinformatics/btp352

Kofler, R., Pandey, R. V., and Schlotterer, C. (2011). PoPoolation2: identifying differentiation between populations using sequencing of pooled DNA samples (Pool-Seq). *Bioinformatics* 27, 3435–3436. doi: 10.1093/bioinformatics/btr589

Quinlan, A. R., and Hall, I. M. (2010). BEDTools: a flexible suite of utilities for comparing genomic features. *Bioinformatics* 26, 841–842. doi: 10.1093/bioinformatics/btq033

Ou, M., Yang, C., Luo, Q., Huang, R., Zhang, A. D., Liao, L. J., et al. (2017). An NGS-based approach for the identification of sex-specific markers in snakehead (Channa argus). *Oncotarget* 8, 98733–98744. doi: 10.18632/oncotarget.21924

Luo, R., Liu, B., Xie, Y., Li, Z., Huang, W., Yuan, J., et al. (2012). SOAPdenovo2: an empirically improved memory-efficient short-read de novo assembler. *Gigascience* 1, 18. doi: 10.1186/2047-217X-1-18

Johnson, M., Zaretskaya, I., Raytselis, Y., Merezhuk, Y., McGinnis, S., and Madden, T. L. (2008). NCBI BLAST: a better web interface. *Nucleic Acids Res* 36, W5–W9. doi: 10.1093/nar/gkn201

Kim, D., Langmead, B., and Salzberg, S. L. (2015). HISAT: a fast spliced aligner with low memory requirements. *Nat Methods* 12, 357–360. doi: 10.1038/nmeth.3317

Anders, S., Pyl, P. T., and Huber, W. (2015). HTSeq–a Python framework to work with high-throughput sequencing data. *Bioinformatics* 31, 166–169. doi: 10.1093/bioinformatics/btu638

Weir, B. S., and Cockerham, C. C. (1984). Estimating F-Statistics for the Analysis of Population Structure. *Evolution* 38, 1358–1370. doi: 10.1111/j.1558-5646.1984.tb05657.x

Holsinger, K. E., and Weir, B. S. (2009). Genetics in geographically structured populations: defining, estimating and interpreting F(ST). *Nat Rev Genet* 10, 639–650. doi: 10.1038/nrg2611

Bachtrog, D., Hom, E., Wong, K. M., Maside, X., and de Jong, P. (2008). Genomic degradation of a young Y chromosome in Drosophila miranda. *Genome Biol* 9, R30. doi: 10.1186/gb-2008-9-2-r30

Papadopulos, A. S., Chester, M., Ridout, K., and Filatov, D. A. (2015). Rapid Y degeneration and dosage compensation in plant sex chromosomes. *Proc Natl Acad Sci U S A* 112, 13021–13026. doi: 10.1073/pnas.1508454112

Muyle, A., Zemp, N., Deschamps, C., Mousset, S., Widmer, A., and Marais, G. A. (2012). Rapid de novo evolution of X chromosome dosage compensation in Silene latifolia, a plant with young sex chromosomes. *PLoS Biol* 10:e1001308. doi: 10.1371/journal.pbio.1001308

Bergero, R., and Charlesworth, D. (2011). Preservation of the Y transcriptome in a 10-million-year-old plant sex chromosome system. *Curr Biol* 21, 1470–1474. doi: 10.1016/j.cub.2011.07.032

Chibalina, M. V., and Filatov, D. A. (2011). Plant Y chromosome degeneration is retarded by haploid purifying selection. *Curr Biol* 21, 1475–1479. doi: 10.1016/j.cub.2011.07.045

Conflict of Interest: The authors declare that the research was conducted in the absence of any commercial or financial relationships that could be construed as a potential conflict of interest.

Publisher's Note: All claims expressed in this article are solely those of the authors and do not necessarily represent those of their affiliated organizations, or those of the publisher, the editors and the reviewers. Any product that may be evaluated in this article, or claim that may be made by its manufacturer, is not guaranteed or endorsed by the publisher.

frontiers in Marine Science

ORIGINAL RESEARCH
published: 08 October 2021
doi: 10.3389/fmars.2021.748928

Bone Morphogenetic Protein 2 Is Involved in Oocyte Maturation Through an Autocrine/Paracrine Pathway in *Scylla paramamosain*

*Yanan Yang, Peng Zhang, Zhaoxia Cui and Chenchang Bao**

School of Marine Science, Ningbo University, Ningbo, China

Ovary-secreted autocrine/paracrine factors play important roles in regulating oocyte maturation via the autocrine/paracrine pathway. This study aimed to evaluate the functions of bone morphogenetic protein 2 (BMP2) in oocyte maturation and communication between follicle cells and oocytes. In our study, we first identified BMP2 from the mud crab *Scylla paramamosain*. Quantitative real-time PCR showed that BMP2 was detected in diverse tissues, notably in the ovary, stomach and gill. The expression levels of BMP2 transcripts increased during vitellogenesis. Spatial expression of BMP2 and receptors in the ovary revealed that BMP2 was exclusively detected in oocytes, whereas the receptors were expressed in both follicle cells and oocytes. RNAi tests revealed that the expression of cyclin B first decreased at 2 h and then increased at 4 h after BMP2 knockdown. These combined findings suggest that BMP2 may promote oocyte maturation through an autocrine/paracrine pathway in *S. paramamosain*.

Keywords: bone morphogenetic protein 2, oocyte maturation, autocrine/paracrine pathway, oocytes and follicle cells, mud crab

OPEN ACCESS

Edited by:
Naoaki Tsutsui,
Mie University, Japan

Reviewed by:
Radha Chaube,
Banaras Hindu University, India
Yilei Wang,
Jimei University, China

****Correspondence:***
Chenchang Bao
baochenchang@nbu.edu.cn

Specialty section:
This article was submitted to Aquatic Physiology, a section of the journal Frontiers in Marine Science

Received: *28 July 2021*
Accepted: *21 September 2021*
Published: *08 October 2021*

Citation:
Yang Y, Zhang P, Cui Z and Bao C (2021) Bone Morphogenetic Protein 2 Is Involved in Oocyte Maturation Through an Autocrine/Paracrine Pathway in Scylla paramamosain. Front. Mar. Sci. 8:748928. doi: 10.3389/fmars.2021.748928

INTRODUCTION

In vertebrates, oocyte maturation is a complicated mutual interaction between extraovarian and intraovarian signals (Ge, 2005; Emori and Sugiura, 2014). In vertebrates, oocyte maturation is generally activated by luteinizing hormone (LH), which is produced and secreted from the pituitary (Nagahama and Yamashita, 2008). In addition to this classical endocrine pathway, growing evidence suggests that many intraovarian autocrine/paracrine factors, such as transforming growth factor β (TGFβ) and epidermal growth factor (EGF), play critical roles in oocyte maturation via the autocrine/paracrine pathway (Ge, 2005; Clelland and Peng, 2009). Bone morphogenetic protein (BMP), a member of the TGFβ superfamily, has been demonstrated to play intraovarian autocrine/paracrine roles in development and follicular formation (Glister et al., 2004; Knight and Glister, 2006). For example, rat BMP9 plays an autocrine role in regulating steroidogenesis in ovarian granulosa cells (Hosoya et al., 2015). BMP2 is located in granulosa cells, and its receptors are expressed in both granulosa cells and oocytes. BMP2 stimulates steroidogenesis in granulosa cells through an autocrine pathway (Inagaki et al., 2009).

The mud crab *Scylla paramamosain* (Crustacea: Decapoda: Brachyura) is an economically important and nutritious crab species in China and South Asia. Ovarian development in *S. paramamosain* has been divided into undeveloped (stage I), pre-vitellogenic (stage II), early vitellogenic (stage III), late vitellogenic (stage IV), and mature (stage V) stages (Bao et al., 2018). In the late vitellogenic stage, the size of the oocyte nucleus reaches a maximum of almost 40 μm, the oocyte germinal vesicle (GV) becomes obvious, and the oocytes are usually arrested at the prophase of the first meiosis (Yang et al., 2019). Meiotic arrest resumes by a stimulus, and the first clear sign of meiosis initiation is germinal vesicle breakdown (GVBD) (Eppig, 1982). It has been reported that oocytes in the GV stage could be induced to mature by 5-HT (Yang et al., 2019). Recent studies found that short neuropeptide F (sNPF), BMP7 and BMP9/10 can play roles as intraovarian autocrine/paracrine factors by regulating oocyte maturation in mud crabs (Bao et al., 2018; Yang et al., 2018, 2021). As a paracrine factor, BMP7 plays a potentially inhibitory role in oocyte maturation, which is induced by 17α,20β-dihydroxyprogesterone (DHP) (Shu et al., 2016; Yang et al., 2018). However, the effects of other autocrine/paracrine factors on oocyte maturation are still unknown.

In this study, we focused on the effects of BMP2 on oocyte maturation. We analyzed the expression patterns of ligand and receptors of BMP2 in follicle cells and oocytes, then characterized BMP2 expression at the GV and GVBD stages. We reveal the function of BMP2 in oocyte maturation via an autocrine/paracrine pathway in *S. paramamosain*.

MATERIALS AND METHODS

Experimental Animals

According to the morphological and histological features, the mud crab vitellogenesis was classified into the pre-vitellogenic stage, the early vitellogenic stage and the late vitellogenic stage (Huang et al., 2014). Crabs were purchased from the eight market in Xiamen, Fujian Province, China. All crabs were under normal physiological conditions without any induction or treatment in this study. Prior to dissections, crabs were anaesthetized on ice for 30 min. Our study did not involve endangered or protected species.

Sequence Analysis of Bone Morphogenetic Protein 2

The sequence of BMP2 cDNA was obtained from transcriptome data (NCBI SRA database: SRR3086589, SRR3086590, and SRR3086592) and was verified by DNA sequencing. The obtained BMP2 cDNA sequence was compared with the NCBI nucleotide database using the NCBI BLAST tool[1]. The deduced amino acid sequence was translated using DNAStar BioEdit software. Then, multiple sequence alignments were performed using the LaTEX TexShade package to present the conserved sequence motifs and show the LOGO.

[1]http://blast.ncbi.nlm.nih.gov/Blast.cgi

RNA Extraction and cDNA Synthesis

Total RNA was extracted using TRIzol RNA isolation reagent (Invitrogen) according to the manufacturer's instructions. The concentration and quality of RNA were determined using a NanoOne spectrophotometer. First-strand cDNA was synthesized from 2 μg of total RNA using the PrimeScript^{TM} RT reagent kit with gDNA Eraser (TaKaRa).

Tissue Distribution and Expression Profile of Bone Morphogenetic Protein 2

Total RNA was isolated from various tissues, including the eyestalk ganglion, cerebral ganglion, thoracic ganglion, ovary, stomach, hepatopancreas and gill. Fluorescence quantitative real-time PCR (qRT–PCR) was carried out to detect the mRNA distribution in different tissues and the temporal expression profile in the ovary. Gene-specific primers for BMP2 (**Table 1**) were used to amplify the corresponding products. The housekeeping gene β-actin (GenBank ID: GU992421) was used to compare the relative expression levels of BMP2 in the samples. qRT–PCR measurements were performed using the Applied Biosystems 7500 Real-time PCR System (Carlsbad, CA United States) version 2.4 software. qRT–PCR was carried out in a total volume of 20 μl, containing 10 μl of SYBR Premix Ex Taq^{TM} (Takara), 0.4 μl of ROX^{TM} Reference Dye (Takara), 0.5 μl of each primer (10 mM), 2 μl of the diluted cDNA and 6.6 μl of ddH_2O. The thermal profile for qRT–PCR was 30 s at 95°C for 1 cycle, 5 s at 95°C, 30 s at 56°C, and 30 s at 72°C for 42 cycles. All experiments were repeated independently at least three times.

In addition, the temporal expression pattern of BMP2 was estimated using qRT–PCR as described above.

Separation of Oocytes and Follicle Cells

Follicle cells were separated from the corresponding oocytes as previously described (Yang et al., 2018). Ovaries at the late

TABLE 1 | Details of primers for this study.

Gene name	Primer sequence (5′–3′)	Purpose
Cyclin B	GACGCTCTTCCTCACTGTTGG	qRT-PCR
	GTCTGGGCAAACCATCTCCTC	qRT-PCR
BMP2	GTGAGAGCACGGACCAAAGA	Semi quantitative PCR and qRT-PCR
	ACGCTGCACTACACCTTTGT	Semi quantitative PCR and qRT-PCR
BMP2	TGCCACTCGCTCCTCTGA	RNAi
	CTCGGCTTTCCCAGCTACCTAT	RNAi
BMPRIB	TCTTCCTCCCTTGCTGACC	Semi quantitative PCR
	GGTCAGGTGGCACAAGGTCA	Semi quantitative PCR
BMPRII	GGTGGTGCGAAACAAAGCC	Semi quantitative PCR
	TTGCCTCAGCATCGTAGTCCC	SEMI quantitative PCR
GFP	TGGGCGTGGATAGCGGTTTG	qRT-PCR
	GGTCGGGGTAGCGGCTGAAG	qRT-PCR
β-actin	GAGCGAGAAATCGTTCGTGAC	Semi quantitative PCR and qRT-PCR
	GGAAGGAAGGCTGGAAGAGAG	Semi quantitative PCR and qRT-PCR

vitellogenic stage were dissected from the crabs and then placed in a plastic culture dish with modified crab saline (11.3 mM KCl, 440 mM NaCl, 26 mM $MgCl_2$, 13.3 mM $CaCl_2$, 23 mM Na_2SO_4, 10 mM HEPES, pH 7.4). Follicle layers were gently removed with fine forceps. The denuded oocytes and separated follicle layers were collected for RNA extraction, with three biological replicates.

Expression Pattern of Bone Morphogenetic Protein 2 and Receptors in the Ovary by Semiquantitative PCR

Semiquantitative PCR was used to determine the expression profiles of BMP2 and BMPRs in the ovary, follicle cells and denuded oocytes. The specific primers of BMPRs for PCR were designed according to the cDNA sequences (GenBank: KU985444 and KU985443). Negative (β-actin) and blank controls (no template) were carried with the target gene together. Semiquantitative PCR was carried out in a volume of 25 μl containing 12.5 μl of 2 × Premix Ex Taq II (Takara), 2 μl of cDNA template, 1 μM each primer and 8.5 μl of H_2O. The thermal profile for the PCR was 3 min at 95°C for 1 cycle, 30 s at 94°C, 30 s at 56°C, and 30 s at 72°C for 38 cycles, followed by an extension at 72°C for 10 min. The PCR products were analyzed by 1.5% agarose gel electrophoresis. PCR was conducted in quadruplicate for each individual sample. All the primers were listed in **Table 1**.

Expression of Bone Morphogenetic Protein 2 in the Germinal Vesicle and Germinal Vesicle Breakdown Stages

Ovaries at the late vitellogenic and mature stages were selected to obtain oocytes in the GV and GVBD stages. Briefly, oocytes in the GV and GVBD stages were determined using a clearing solution (formaldehyde, ethanol, acetic acid, 30:42:1) followed by microscopic examination. Four biological replicates were used for BMP2 detection. qRT–PCR was carried out as described above.

Effect of Bone Morphogenetic Protein 2 on Cyclin B Expression *in vitro*

We first designed specific primers to amplify the sequences of BMP2 and the green fluorescent protein (GFP) gene (as an exogenous control gene) (**Table 1**). Then, the pure DNA templates were used to synthesize the dsRNA with T7 and SP6 polymerases. The remaining DNA template in dsRNA solution was digested with RNase-free DNase I (TaKaRa). Finally, the quality, concentration and integrity of dsRNA were detected using a NanoOne spectrophotometer and agarose gel electrophoresis.

The dissection and treatment of ovarian explants were carried out as described in a previous study (Liu et al., 2019). Female crabs at the late vitellogenic stage were anaesthetized for 15 min on ice and sterilized in 75% ethanol for 10 min. Then, ovarian tissues at the GV stage were dissected and washed 6 times with modified crab saline. Subsequently, the ovary samples were cut into 50-mg fragments and then placed in a well of a 24-well tissue culture plate with 1.5 ml 2 × L15 medium containing streptomycin (300 IU ml^{-1}) and penicillin G (300 IU ml^{-1}). The experiment included three treatments, namely, dsRNA for BMP2 and GFP (negative control), as well as a blank control (no dsRNA), with each treatment performed in four replicates ($n = 4$). The ovarian explants were cultured with dsRNA at 25°C and then collected at 1, 2, 4, 6, and 8 h for gene expression analysis to determine the effect of dsRNA. After the target gene was silenced, the expression of cyclin B was analyzed by qRT–PCR, as described above, using the primers listed in **Table 1**.

Data Analysis

BMP2 expression relative to the control was determined by the $2^{-\Delta\Delta Ct}$ method. All data are presented as the mean ± SD. Statistical analyses were performed using SPSS 20 software. Data were normally distributed, as assessed with normality tests (Shapiro–Wilk test). Independent samples *t*-tests were used to analyze BMP2 expression between follicle cells and oocytes and the GV and GVBD stages. Data for different vitellogenic stages and RNAi experiments were first subjected to Levene's test for testing the homogeneity of variances and then subjected to one-way analysis of variance (ANOVA) with Scheffé's method *post hoc* analysis. *P*-values less than 0.05 were considered statistically significant.

RESULTS

Sequence of Bone Morphogenetic Protein 2 cDNA

In the transcriptome data of *S. paramamosain*, a 2,594-bp transcript was found to encode BMP2. The nucleotide sequence showed high conservation to orthologs of other known BMP2 transcripts from different decapods, especially from the Chinese mitten crab *Eriocheir sinensis*. The BMP2 transcript was composed of a 1,224-bp open reading frame (ORF), a 580-bp 5′-untranslated region and a 790-bp 3′-untranslated region. This ORF encoded a 407-aa protein, and the calculated molecular mass was 46.4 kDa. A BLAST search of the *S. paramamosain* BMP2 protein sequence showed high scoring identities to BMP2 proteins from other species; the highest score was an 88% identity to the amino acid sequence from the swimming crab *Portunus trituberculatus*. The alignment of the deduced amino acid sequences in different species is shown in **Figure 1**.

Tissue Distribution and Expression Profile of Bone Morphogenetic Protein 2

qRT–PCR was used to detect the expression levels of BMP2 in seven tissues (eyestalk, cerebral ganglia, thoracic ganglia, ovary, stomach, hepatopancreas and gill) of *S. paramamosain* (**Figure 2**). The results indicated that BMP2 was detected in various tissues. A predominant transcript expression level of BMP2 was detected in the ovary, stomach and gill (**Figure 2**).

To determine whether BMP2 acts on ovarian development, qRT–PCR was employed to detect its expression in different vitellogenic stages. As demonstrated in **Figure 3**, BMP2 was increased from pre-vitellogenic stage to the early and late vitellogenic stages.

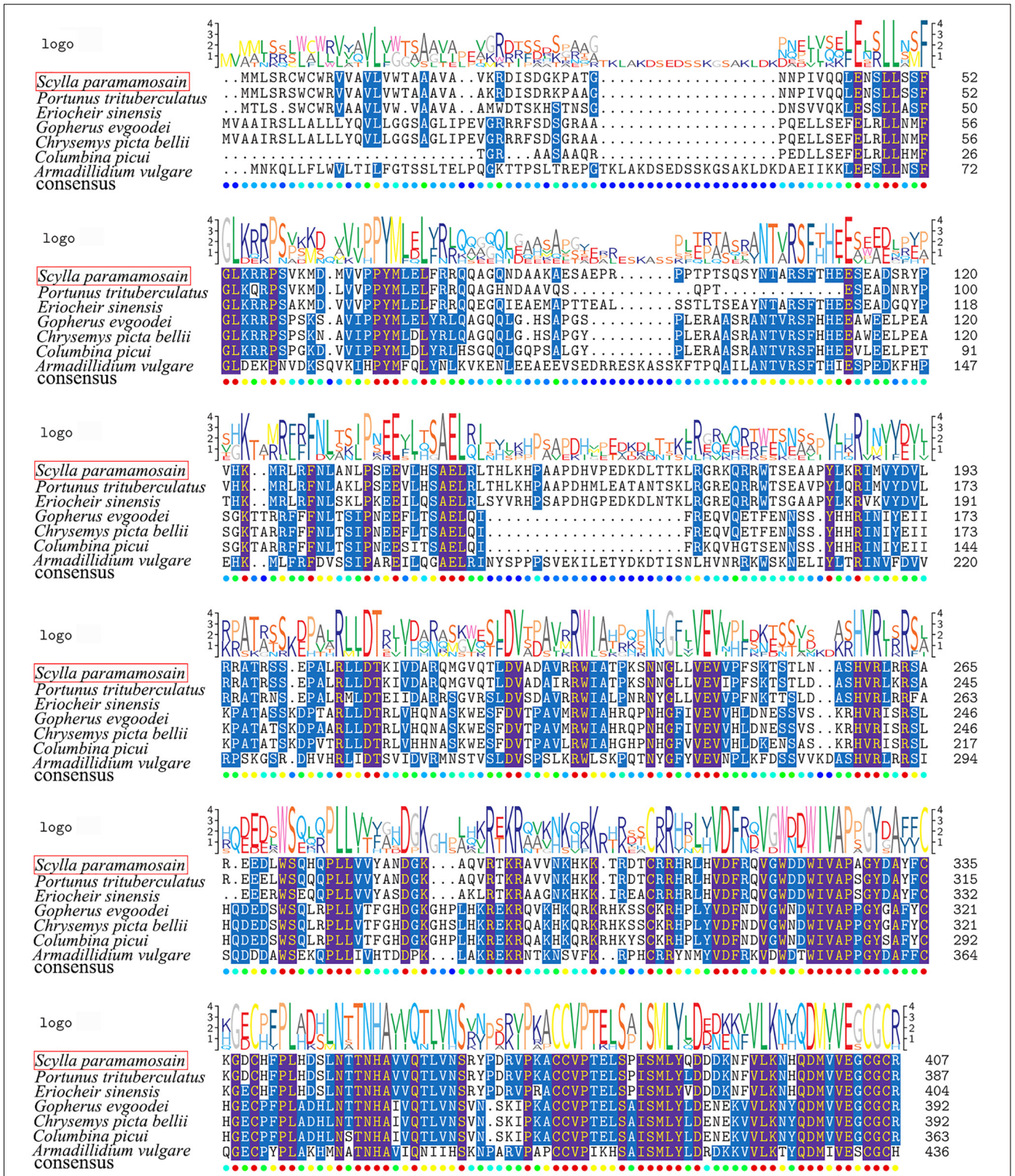

FIGURE 1 | Comparative amino acid sequence alignment of BMP2 from *S. paramamosain* with BMP2 proteins from other species. Sequences used in the alignment included *Portunus trituberculatus* (GenBank accession number: MPC22470.1); *Eriocheir sinensis* (GenBank accession number: QKI80004.1); *Gopherus evgoodei* (GenBank accession number: XP_030413884.1); *Chrysemys picta bellii* (GenBank accession number: XP_005287486.1); *Columbina picui* (GenBank accession number: NWQ78677.1); and *Armadillidium vulgare* (GenBank accession number: RXG59312.1). The sequence logo is shown above the alignments.

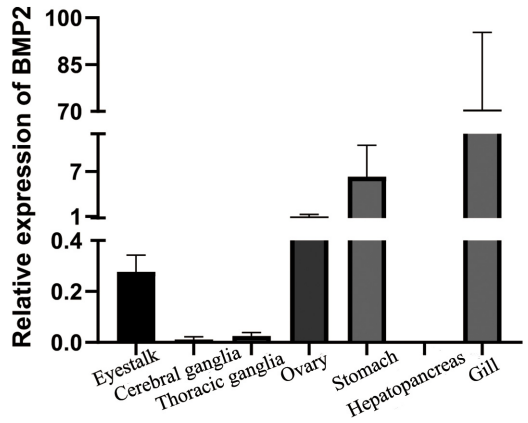

FIGURE 2 | Tissue distribution of BMP2 in *S. paramamosain*. Expression of β-actin was used as internal control. The relative expression of BMP2 was analyzed by qRT–PCR.

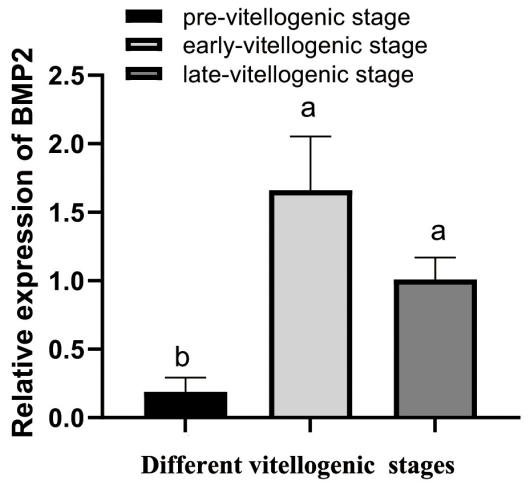

FIGURE 3 | Temporal expression profile of *S. paramamosain* BMP2 in ovarian development. The expression level of BMP2 was investigated by qRT–PCR and normalized to β-actin. The relative expression abundances are presented as the means ± SD ($n = 4$). Different letters above the bars demonstrate significant differences between different vitellogenic stages ($P < 0.05$).

Spatial Expression of Bone Morphogenetic Protein 2 and BMPRs in the Ovary

We used semiquantitative PCR to determine the mRNA expression level of BMP2 and its receptors in follicle cells and oocytes derived from the ovaries at the late vitellogenic stage (stage IV). The results revealed that BMP2 and its receptors show a distinctive distribution pattern in follicle cells and oocytes. BMP2 was exclusively detected in oocytes (**Figure 4**). Unlike the ligand, the receptors bone morphogenetic protein receptor IB (BMPRIB) and bone morphogenetic protein receptor II (BMPRII) were located in both follicle cells and oocytes (**Figure 4**). β-actin (used as the housekeeping gene) was concurrently tested in all cDNA templates, while no signal was detected in the blank control (distilled water was used to serve as the template during PCR).

Role of Bone Morphogenetic Protein 2 in Oocyte Maturation

To research the function of BMP2 in oocyte maturation, the expression level of BMP2 was detected in the GV and GVBD stages. BMP2 showed a higher expression level in the GV stage (**Figure 5**). Afterward, we used dsRNAs to silence BMP2 in ovaries in the GV stage and analyzed the expression patterns using qRT–PCR. The results revealed that BMP2 was significantly silenced at 1 and 2 h (**Figure 6A**). Then, we analyzed the expression of cyclin B, which was decreased first at 2 h and then increased at 4 h (**Figure 6B**).

DISCUSSION

In our study, we cloned BMP2 from *S. paramamosain*, which was similar to the sequence of BMP2 in *E. sinensis* (Yang et al., 2020). Similar to BMP7 in the mud crab, a TGF-b propeptide is located in the BMP2 N-terminus region (Shu et al., 2016). The C-terminus of BMP2 has a TGF-β-DPP domain that is found in *Drosophila melanogaster* protein decapentaplegic (Dpp) and is responsible for development (Allendorph et al., 2007). Thus, data from the sequence of BMP2 indicated that this sequence is a member of the BMP family (Xiao et al., 2007).

Higher expression levels of BMP2 were observed in the gill and stomach of *S. paramamosain*. BMP2 is also expressed at a high level in the gill of *E. sinensis* (Yang et al., 2020). In crustaceans, a thin chitin layer covers the external surface of the gill (Flemister, 1959), and the gastric mill is a masticating apparatus that is a part of the stomach and also contains a chitin layer (Yonge, 1926). The higher expression levels of BMP2 in the gill and stomach implied that BMP2 may be related to chitin formation. In mammals, BMP2 is a vital protein for bone formation and development (Rosen, 2009). However, crustaceans have a chitin carapace instead of the bones found in mammals (Rodriguez-Chanfrau et al., 2019). In crustaceans, BMP2 may be related to chitin formation. Moreover, BMP2 was also highly expressed in the ovary. Higher expression levels of some BMPs in the ovary have been identified in both mammals and crustaceans (Lima et al., 2012; Shu et al., 2016) and are responsible for ovary development and oocyte maturation (Peng et al., 2009; Yang et al., 2018).

To determine the relationship between BMP2 and reproduction, the expression pattern of BMP2 was subsequently analyzed during ovarian development. A significantly low expression was observed at the pre-vitellogenic stage, while relatively abundant expression of BMP2 was observed in the early vitellogenic and late vitellogenic stages, indicating that BMP2 might be involved in vitellogenesis and late ovarian development. This finding was obviously incompatible with the expression profile of BMP2b in zebrafish, which showed a peak at the pre-vitellogenic stage and declined steadily toward the end of folliculogenesis (Li and Ge, 2011). The tendencies of BMP2

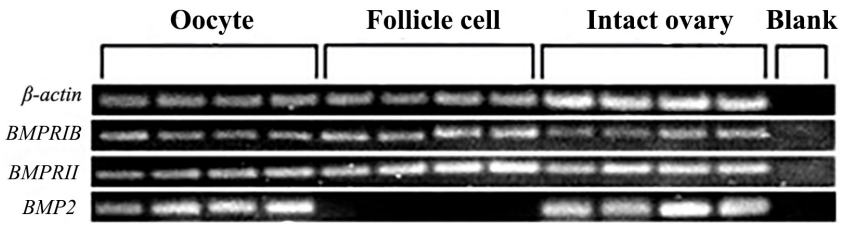

FIGURE 4 | Localization of BMP2 and two BMPRs in the ovary. BMP2 transcript was exclusively expressed in the oocytes. In contrast, two BMP receptors (BMPRIB and BMPRII) were located on both follicle cells and denuded oocytes. The housekeeping gene (β-actin) was detected in each sample, while no signal was detected in the blank control.

expression at different vitellogenic stages of the mud crab were also different from other BMP members, such as BMP7 in the mud crab and growth differentiation factor 9 (GDF9) in ricefield eel (He et al., 2012; Shu et al., 2016). It is possible that this discrepancy was due to species diversity. The expression profile of BMP2, combined with the expression levels of BMP receptors, was significantly higher in the early and late vitellogenic stages (Shu et al., 2016), suggesting a potential role for BMP2 in ovarian maturation. BMP2 and other BMPs have also been reported to be involved in ovarian maturation in other species, such as BMP2 in buffalo and BMP15 in zebrafish (Peng et al., 2009; Rajesh et al., 2018).

BMPs, as members of the TGFβ superfamily, act on oocyte maturation in an autocrine/paracrine manner (Ge, 2005; Clelland and Peng, 2009). Similar to the TGFβ superfamily, BMPs have been shown to act via two types of BMPRI (BMPRIA and BMPRIB) and BMPRII (Wang and Roy, 2009). In this study, we detected the spatial expression of BMP2 and BMPRs in the ovary. BMP2 was exclusively expressed in oocytes, and receptors were detected in both follicle cells and oocytes. The localization of BMP2 and BMPRs revealed that there was a potential autocrine/paracrine pathway in the mud crab ovary, as in the study of *S. paramamosain* BMP7 (Yang et al., 2018). These findings were consistent with reports from mammals (Brankin et al., 2005; Inagaki et al., 2009). For example, BMP2 was found in granulosa

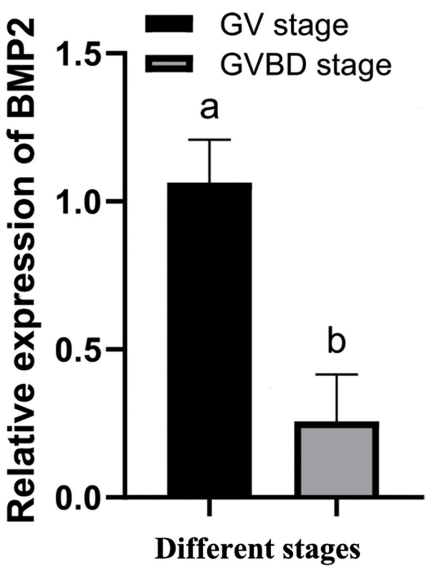

FIGURE 5 | Temporal expression profiles of BMP2 at the GV and GVBD stages. The relative expression levels are shown as the means ± SD (n = 4). Different letters above the bars demonstrate significant differences between the oocytes at the GV and GVBD stages ($P < 0.05$, independent t-test).

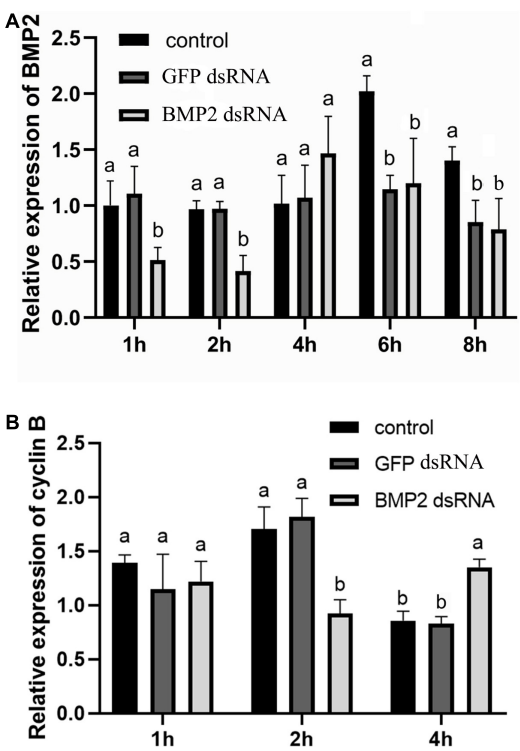

FIGURE 6 | Effect of BMP2 dsRNA on cyclin B expression in *S. paramamosain*. **(A)** Levels of BMP2 expression were detected at 1, 2, 4, 6, and 8 h postaddition of BMP2 dsRNAs (5 μg/ml). **(B)** The expression levels of cyclin B were detected at 1, 2, and 4 h postaddition of BMP2 dsRNAs. GFP dsRNAs and distilled water in equal amounts were concurrently employed as negative and blank controls, respectively. The relative expression levels of target genes are presented as the means ± SD (n = 4). Significant differences between different treatments are represented by different letters above the bars ($P < 0.05$).

cells, receptors were found in oocytes and granulosa cells of rats, and BMP2 can regulate estradiol production in granulosa cells in the autocrine pathway (Inagaki et al., 2009). Porcine BMP2 and BMPRs were observed in granulosa cells and oocytes, and BMP2 in oocytes acted in a paracrine manner to suppress progesterone production in granulosa cells (Brankin et al., 2005). Our results suggested that BMP2 may be involved in similar autocrine/paracrine signaling in *S. paramamosain*.

To investigate the role of BMP2 in oocyte maturation, an RNAi experiment was carried out to knock down the expression of BMP2. The expression level of cyclin B was decreased first at 2 h, which indicated that cyclin B might be regulated by BMP2. However, the expression level of cyclin B was increased at 4 h after the addition of BMP2 dsRNA. There is much cross-reactivity among different BMP ligands and type-I receptors (Shimasaki et al., 2004). It could be speculated that the BMP2 deficiency was offset by other BMP subtypes, which was similar to the study of BMP7 in *S. paramamosain* (Yang et al., 2018). During oocyte maturation, BMP2 regulated the expression of cyclin B, with higher expression levels evident at the GV stage than at the GVBD stage. These results were similar to the study of BMP9/10 in mud crabs, which also showed higher expression levels in the GV stage and regulated cyclin A and cyclin B (Yang et al., 2021). In our previous study, we found that BMP7 was secreted from follicle cells and suppressed DHP-induced oocyte maturation in mud crabs (Yang et al., 2018), whereas BMP2 secreted from oocytes may promote oocyte maturation. BMPs play vital roles in regulating follicle maturation in vertebrates (Wang et al., 2015). As demonstrated in previous studies, BMP6 can promote the maturation of mouse preantral follicle maturation, and GDF9 and BMP15 can regulate canine cumulus maturation (Wang et al., 2015; Ramirez et al., 2020). In porcine oocytes, the expression levels of BMP15 and GDF9 were significantly increased at GVBD compared with GV stages and participated in oocyte maturation (Lin et al., 2014). Consequently, we hypothesize that BMP2 plays a critical role in oocyte maturation of *S. paramamosain*, possibly through an autocrine/paracrine pathway.

CONCLUSION

In our study, we first identified BMP2 from the mud crab *Scylla paramamosain*. The spatial expression of BMP2 and receptors in ovary revealed that, the BMP2 might be an autocrine/paracrine factor. The expression of BMP2 mRNA increased along the ovarian development implied that BMP2 was probably involved in vitellogenesis and late ovarian development. Furthermore, the expression of cyclin B was decreased after the BMP2 knockdown. These combined findings suggest that BMP2 may promote oocyte maturation through an autocrine/paracrine pathway in *S. paramamosain*.

DATA AVAILABILITY STATEMENT

The datasets presented in this study can be found in online repositories. The names of the repository/repositories and accession number(s) can be found below: https://www.ncbi.nlm.nih.gov/genbank/, KU985443; https://www.ncbi.nlm.nih.gov/genbank/, KU985444; https://www.ncbi.nlm.nih.gov/, SRR3086589; https://www.ncbi.nlm.nih.gov/, SRR3086590; https://www.ncbi.nlm.nih.gov/, SRR3086592.

AUTHOR CONTRIBUTIONS

YY: conceptualization, sample collection, experiment, and writing–original draft. PZ: experiment. ZC: supervision. CB: sample collection, editing, and supervision. All authors contributed to the article and approved the submitted version.

FUNDING

This study was supported by the National Natural Science Foundation of China (grant no: 31902350) and the K. C. Wong Magna Fund in Ningbo University.

REFERENCES

Allendorph, G. P., Isaacs, M. J., Kawakami, Y., Izpisua Belmonte, J. C., and Choe, S. (2007). BMP-3 and BMP-6 structures illuminate the nature of binding specificity with receptors. *Biochemistry* 46, 12238–12247. doi: 10.1021/bi700907k

Bao, C. C., Yang, Y. N., Huang, H. H., and Ye, H. H. (2018). Inhibitory role of the mud crab short neuropeptide F in vitellogenesis and oocyte maturation via autocrine/paracrine signaling. *Front. Endocrinol.* 9:390. doi: 10.3389/fendo.2018.00390

Brankin, V., Quinn, R. L., Webb, R., and Hunter, M. G. (2005). Evidence for a functional bone morphogenetic protein (BMP) system in the porcine ovary. *Domest. Anim. Endocrinol.* 28, 367–379. doi: 10.1016/j.domaniend.2005.01.001

Clelland, E., and Peng, C. (2009). Endocrine/paracrine control of zebrafish ovarian development. *Mol. Cell. Endocrinol.* 312, 42–52. doi: 10.1016/j.mce.2009.04.009

Emori, C., and Sugiura, K. (2014). Role of oocyte-derived paracrine factors in follicular development. *Anim. Sci. J.* 85, 627–633. doi: 10.1111/asj.12200

Eppig, J. J. (1982). The relationship between cumulus cell-oocyte coupling, oocyte meiotic maturation, and cumulus expansion. *Dev. Biol.* 89, 268–272. doi: 10.1016/0012-1606(82)90314-1

Flemister, S. C. (1959). Histophysiology of gill and kidney of crab *Ocypode albicans*. *Biol. Bull.* 116, 37–48. doi: 10.2307/1539154

Ge, W. (2005). Intrafollicular paracrine communication in the zebrafish ovary: the state of the art of an emerging model for the study of vertebrate folliculogenesis. *Mol. Cell. Endocrinol.* 237, 1–10. doi: 10.1016/j.mce.2005.03.012

Glister, C., Kemp, C. F., and Knight, P. G. (2004). Bone morphogenetic protein (BMP) ligands and receptors in bovine ovarian follicle cells: actions of BMP-4, -6 and -7 on granulosa cells and differential modulation of Smad-1 phosphorylation by follistatin. *Reproduction* 127, 239–254. doi: 10.1530/rep.1.00090

He, Z., Wu, Y., Xie, J., Wang, T., Zhang, L., and Zhang, W. (2012). Growth differentiation factor 9 (GDF9) was localized in the female as well as male germ cells in a protogynous hermaphroditic teleost fish, ricefield eel *Monopterus albus*. *Gen. Comp. Endocrinol.* 178, 355–362. doi: 10.1016/j.ygcen.2012.06.016

Hosoya, T., Otsuka, F., Nakamura, E., Terasaka, T., Inagaki, K., Tsukamoto-Yamauchi, N., et al. (2015). Regulatory role of BMP-9 in steroidogenesis by rat ovarian granulosa cells. *J. Steroid Biochem. Mol. Biol.* 147, 85–91. doi: 10.1016/j.jsbmb.2014.12.007

Huang, X. S., Ye, H. H., Huang, H. Y., Yang, Y. N., and Gong, J. (2014). An insulin-like androgenic gland hormone gene in the mud crab, *Scylla paramamosain*,

extensively expressed and involved in the processes of growth and female reproduction. *Gen. Comp. Endocrinol.* 204, 229–238. doi: 10.1016/j.ygcen.2014.06.002

Inagaki, K., Otsuka, F., Miyoshi, T., Yamashita, M., Takahashi, M., Goto, J., et al. (2009). p38-Mitogen-activated protein kinase stimulated steroidogenesis in granulosa cell-oocyte cocultures: role of bone morphogenetic proteins 2 and 4. *Endocrinology* 150, 1921–1930. doi: 10.1210/en.2008-0851

Knight, P. G., and Glister, C. (2006). TGF-β superfamily members and ovarian follicle development. *Reproduction* 132, 191–206. doi: 10.1530/rep.1.01074

Li, C. W., and Ge, W. (2011). Spatiotemporal expression of bone morphogenetic protein family ligands and receptors in the zebrafish ovary: a potential paracrine-signaling mechanism for oocyte-follicle cell communication. *Biol. Reprod.* 85, 977–986. doi: 10.1095/biolreprod.111.092239

Lima, I. M. T., Brito, I. R., Rossetto, R., Duarte, A. B. G., Rodrigues, G. Q., Saraiva, M. V. A., et al. (2012). BMPRIB and BMPRII mRNA expression levels in goat ovarian follicles and the *in vitro* effects of BMP-15 on preantral follicle development. *Cell Tissue Res.* 348, 225–238. doi: 10.1007/s00441-012-1361-4

Lin, Z. L., Li, Y. H., Xu, Y. N., Wang, Q. L., Namgoong, S., Cui, X. S., et al. (2014). Effects of growth differentiation factor 9 and bone morphogenetic protein 15 on the *in vitro* maturation of porcine oocytes. *Reprod. Domest. Anim.* 49, 219–227. doi: 10.1111/rda.12254

Liu, A., Liu, F., Shi, W. Y., Huang, H. Y., Wang, G. Z., and Ye, H. H. (2019). C-type allatostatin and its putative receptor from the mud crab serve an inhibitory role in ovarian development. *J. Exp. Bio.* 222:21. doi: 10.1242/jeb.207985

Nagahama, Y., and Yamashita, M. (2008). Regulation of oocyte maturation in fish. *Dev. Growth Differ.* 50, s159–s219. doi: 10.1111/j.1440-169X.2008.01019.x

Peng, C., Clelland, E., and Tan, Q. (2009). Potential role of bone morphogenetic protein-15 in zebrafish follicle development and oocyte maturation. *Comp. Biochem. Physiol. A Mol. Integr. Physiol.* 153, 83–87. doi: 10.1016/j.cbpa.2008.09.034

Rajesh, G., Mishra, S. R., Paul, A., Punetha, M., Vidyalakshmi, G. M., Narayanan, K., et al. (2018). Transcriptional and translational abundance of bone morphogenetic protein (BMP) 2, 4, 6, 7 and their receptors BMPR1A, 1B and BMPR2 in buffalo ovarian follicle and the role of BMP4 and BMP7 on estrogen production and survival of cultured granulosa cells. *Res. Vet. Sci.* 118, 371–388. doi: 10.1016/j.rvsc.2018.04.002

Ramirez, G., Palomino, J., Aspee, K., and De los Reyes, M. (2020). GDF-9 and BMP-15 mRNA levels in canine cumulus cells related to cumulus expansion and the maturation process. *Animals* 10:462. doi: 10.3390/ani10030462

Rodriguez-Chanfrau, J. E., Rodriguez-Riera, Z., and Gamiotea-Turro, D. (2019). Trimethylchitosan hydrochloride obtained from lobster carapace chitin on a bench scale. *Biointerface Res. Appl. Chem.* 9, 4279–4283. doi: 10.33263/BRIAC95.279283

Rosen, V. (2009). BMP2 signaling in bone development and repair. *Cytokine Growth Factor Rev.* 20, 475–480. doi: 10.1016/j.cytogfr.2009.10.018

Shimasaki, S., Moore, R. K., Otsuka, F., and Erickson, G. F. (2004). The bone morphogenetic protein system in mammalian reproduction. *Endocr. Rev.* 25, 72–101. doi: 10.1210/er.2003-0007

Shu, L., Yang, Y. N., Huang, H. Y., and Ye, H. H. (2016). A bone morphogenetic protein ligand and receptors in mud crab: a potential role in the ovarian development. *Mol. Cell. Endocrinol.* 434, 99–107. doi: 10.1016/j.mce.2016.06.023

Wang, C., and Roy, S. K. (2009). Expression of bone morphogenetic protein receptor (BMPR) during perinatal ovary development and primordial follicle formation in the hamster: possible regulation by FSH. *Endocrinology* 150, 1886–1896. doi: 10.1210/en.2008-0900

Wang, X., Su, L., Pan, X., Yao, J., Li, Z., Wang, X., et al. (2015). Effect of BMP-6 on development and maturation of mouse preantral follicles *in vitro*. *Biotechnol. Biotechnol. Equip.* 29, 336–344. doi: 10.1080/13102818.2014.996605

Xiao, Y. T., Xiang, L., and Shao, J. Z. (2007). Bone morphogenetic protein. *Biochem. Biophys. Res. Commun.* 362, 550–553. doi: 10.1016/j.bbrc.2007.08.045

Yang, T., Wei, B. H., Hao, S. L., Wei, Y. L., and Yang, W. X. (2020). Bone morphogenetic protein 2 (BMP2) mediates spermatogenesis in Chinese mitten crab *Eriocheir sinensis* by regulating kinesin motor KIFC1 expression. *Gene* 754:144848. doi: 10.1016/j.gene.2020.144848

Yang, Y. N., Lin, D. D., Bao, C. C., Huang, H. Y., and Ye, H. H. (2019). Serotonergic mechanisms of oocyte germinal vesicle breakdown in the mud crab, *Scylla paramamosain*. *Front. Physiol.* 10:797. doi: 10.3389/fphys.2019.00797

Yang, Y. N., Shu, L., Jiang, Q. L., Huang, H. Y., and Ye, H. H. (2018). Does the bone morphogenetic protein 7 inhibit oocyte maturation by autocrine/paracrine in mud crab? *Gen. Comp. Endocrinol.* 26, 119–125. doi: 10.1016/j.ygcen.2018.05.004

Yang, Y. N., Zhang, Y., Zhuang, Y., Zhang, C. Y., Bao, C. C., and Cui, Z. X. (2021). Identification of differentially abundant mRNA transcripts and autocrine/paracrine factors in oocytes and follicle cells of mud crabs. *Anim. Reprod. Sci.* 230:106784. doi: 10.1016/j.anireprosci.2021.106784

Yonge, C. M. (1926). Structure and physiology of the organs of feeding and digestion in *Ostrea edulis*. *J. Mar. Biol. Assoc. U.K.* 14, 295–386. doi: 10.1017/S002531540000789x

Conflict of Interest: The authors declare that the research was conducted in the absence of any commercial or financial relationships that could be construed as a potential conflict of interest.

Publisher's Note: All claims expressed in this article are solely those of the authors and do not necessarily represent those of their affiliated organizations, or those of the publisher, the editors and the reviewers. Any product that may be evaluated in this article, or claim that may be made by its manufacturer, is not guaranteed or endorsed by the publisher.

frontiers in Marine Science

ORIGINAL RESEARCH
published: 15 December 2021
doi: 10.3389/fmars.2021.791965

Roles of Crustacean Female Sex Hormone 1a in a Protandric Simultaneous Hermaphrodite Shrimp

*Fang Liu[1], Wenyuan Shi[2], Lin Huang[2], Guizhong Wang[2], Zhihuang Zhu[3] and Haihui Ye[1]**

[1] College of Fisheries, Jimei University, Xiamen, China, [2] College of Ocean and Earth Sciences, Xiamen University, Xiamen, China, [3] Fisheries Research Institute of Fujian, Xiamen, China

Crustacean female sex hormone (CFSH) plays a pivotal role in the development of secondary sex characteristics in dioecious crustaceans. However, until now the knowledge concerning its functions in hermaphroditic species is scanty. Herein, we explored the function of CFSH (*Lvit-CFSH1a*) in the peppermint shrimp *Lysmata vittata*, a species characterized by a rare reproductive system of protandric simultaneous hermaphroditism (PSH). *Lvit-CFSH1a* cDNA was 1,220-bp in length with a 720-bp ORF encoded a polypeptide of 239-aa. RT-PCR showed that *Lvit-CFSH1a* was exclusively expressed in the eyestalk ganglion. For female physiology, it was found that *Lvit*-CFSH1a was indispensable for the development of female gonopores, but it might not involve vitellogenesis of the species. For male physiology, *Lvit*-CFSH1a suppressed *Lvit-IAG2* expression in short-term silencing experiment and recombinant protein injection experiment, but did not affect male sexual differentiation in long-term silencing experiment. In addition, silencing the *Lvit-CFSH1a* gene impeded individual growth in *L. vittata.*

Keywords: sexual differentiation, CFSH, PSH, reproductive endocrine, crustaceans

OPEN ACCESS

Edited by:
Valerio Matozzo, University of Padua, Italy

Reviewed by:
Dong Zhang, Chinese Academy of Fishery Sciences, China
Tania Rodríguez Ramos, University of Waterloo, Canada
Fernando Diaz, Center for Scientific Research and Higher Education in Ensenada (CICESE), Mexico
Hui Qiao, Chinese Academy of Fishery Sciences, China

****Correspondence:***
Haihui Ye
hhye@jmu.edu.cn

Specialty section:
This article was submitted to Aquatic Physiology, a section of the journal Frontiers in Marine Science

Received: *09 October 2021*
Accepted: *23 November 2021*
Published: *15 December 2021*

Citation:
Liu F, Shi W, Huang L, Wang G, Zhu Z and Ye H (2021) Roles of Crustacean Female Sex Hormone 1a in a Protandric Simultaneous Hermaphrodite Shrimp. Front. Mar. Sci. 8:791965. doi: 10.3389/fmars.2021.791965

INTRODUCTION

Gonochorism is the most common reproductive strategy in decapod crustacean species (Juchault, 1999). In dioecious decapod crustaceans, androgenic gland hormone (AGH) and insulin-like androgenic gland hormone (IAG) secreted mainly by androgenic gland (AG), play critical roles in sexual differentiation (Manor et al., 2007). Implantation of AG into females induced masculinization in the red swamp crayfish *Procambarus clarkii* (Taketomi and Nishikawa, 1996), the giant freshwater prawn *Macrobrachium rosenbergii* (Nagamine et al., 1980; Malecha et al., 1992) and the red claw crayfish *Cherax quadricarinatus* (Khalaila et al., 2001; Barki et al., 2003), and vice versa (Barki et al., 2006). Likewise, silencing of IAG genes in males blocked male sexual differentiation while stimulating feminization. For instance, knockdown of *IAG* led to the arrest of testicular spermatogenesis and incomplete development of secondary sexual characteristics (appendices masculinae) in young *M. rosenbergii* males (Ventura et al., 2009). Moreover, silencing IAG gene could also feminize male-related phenotypes in the intersex *C. quadricarinatus* (Rosen et al., 2010) and the male Chinese mitten crab *Eriocheir sinensis* (Fu et al., 2020), and even induce fully sex reversal in young *M. rosenbergii* males (Ventura et al., 2009). Therefore, by virtue of its universal role as a master regulator of crustacean male development, IAG was also termed the

sexual "IAG-switch" (Levy and Sagi, 2020). It was presumed that females arose as the absence of AG or IAG (Ventura et al., 2009).

In 2014, Zmora and Chung (2014) identified a neurohormone from the eyestalk ganglion in the Atlantic blue crab *Callinectes sapidus*. The neurohormone was named crustacean female sex hormone (CFSH) as its pivotal roles in the development of the female's mating and egg brooding systems, including the gonopores and ovigerous setae (Zmora and Chung, 2014). In recent years, more and more full-length transcripts for CFSH orthologs have also been found in decapod crustacean species (Ventura et al., 2014; Veenstra, 2015, 2016; Nguyen et al., 2016; Kotaka and Ohira, 2018; Liu et al., 2018; Tsutsui et al., 2018; Thongbuakaew et al., 2019). Interestingly, CFSH genes were not exclusively expressed in the eyestalk ganglion in certain numbers of crustacean species (Veenstra, 2015; Nguyen et al., 2016; Tsutsui et al., 2018; Thongbuakaew et al., 2019). For instance, *MroCFSH1a* was specifically identified in the central nervous system (CNS), ovary, and testis; while *MroCFSH2b* was expressed in various tissues excluding heart, and muscle (Thongbuakaew et al., 2019). It was also noteworthy that more than one CFSH transcripts were identified in some species (Veenstra, 2015, 2016; Kotaka and Ohira, 2018; Tsutsui et al., 2018; Thongbuakaew et al., 2019). Such examples were shown in *P. clarkii* (*Prc-CFSH*, *Prc-CFSH-like 1,* and *Prc-CFSH-like 2*) (Veenstra, 2015), *E. sinensis* (*Esi-CFSH1*, *Esi-CFSH2a,* and *Esi-CFSH2b*) (Veenstra, 2016) and *M. rosenbergii* (*MroCFSH1a*, *MroCFSH1b*, *MroCFSH2a,* and *MroCFSH2b*) (Thongbuakaew et al., 2019). Interestingly, the expression levels of CFSH showed no significant difference between males and females in the eastern rock lobster *Sagmariasus verreauxi* (Ventura et al., 2014), and similar phenomenon was observed in prepubertal individuals of the mud crab *Scylla paramamosain* (Liu et al., 2018). Even so, function studies of CFSHs were demonstrated only in a few dioecious crustacean species (Liu et al., 2018; Tsutsui et al., 2018; Thongbuakaew et al., 2019; Jiang et al., 2020). In the mud crab *S. paramamosai*n, CFSH not only regulated sexual differentiation of early juveniles (Jiang et al., 2020), but also acted as an inhibitor of IAG in prepubertal males (Liu et al., 2018). In the kuruma prawn *Marsupenaeus japonicus*, *Maj-CFSH-ov*, which was dominantly expressed in the ovary, might be involved in some reproductive process other than vitellogenesis (Tsutsui et al., 2018). However, *Mro*CFSHs were suggested to be involved in vitellogenesis induced by 5-hydroxytryptamine (5-HT) addition in ovary explants of *M. rosenbergii* (Thongbuakaew et al., 2019).

Interestingly, a review of the literature shows that Caridean shrimps exhibit several other protandry sexual systems apart from gonochorism (Bauer, 2000). To date, however, there are rare reports elaborating sexual differentiation mechanism in protandric crustaceans. In the strictly sequential protandric hermaphroditism (SPH) shrimp *Pandalus platyceros*, *Pnp-IAG* knockdown elevated the expression of *vitellogenin* in the hepatopancreas and promoted transformation of the gonad from ovotestis to ovary (Levy et al., 2020). In the protandric simultaneous hermaphroditism (PSH) shrimp *Lysmata wurdemanni*, it was suggested that IAG was possibly responsible for the maintenance of the male reproductive activity in euhermaphrodite phase (Zhang et al., 2017). More detailed studies were performed in another PSH shrimp *L. vittata*. It was demonstrated that *Lvit-IAG1* and *Lvit-IAG2* jointly regulated male sexual differentiation (Liu et al., 2021a,b). Meanwhile, *Lvit*-IAG1 was also suggested to regulate the ovarian development by inhibiting *Lvit-GIHs* expression (Liu et al., 2021b). Recently, two CFSH transcripts (*Lvit-CFSH1a* and *Lvit-CFSH1b*) have been identified from *L. vittata* by transcriptomic analysis (Bao et al., 2020), however, no further in-depth studies are conducted.

In this study, we explored the function of *Lvit*-CFSH1a in *L. vittata*, a species that displays the unique PSH sexual system, whereby individuals first mature as males; and then, with increasing age and size, acquire reproductive functions of both males and females (Bauer, 2000; Alves et al., 2019). Considering that CFSH acts as an inhibitor of IAG (Liu et al., 2018), we hypothesized that *Lvit*-CFSH1a not only regulated female sexual differentiation, but also involved male sexual differentiation via inhibiting *Lvit-IAGs* expression of the PSH species. To validate this hypothesis, we performed both short-term and long-term gene knockdown via RNA interference (RNAi). In addition, we expressed recombinant *Lvit*-CFSH1a mature peptide (r*Lvit*-CFSH1a) using a prokaryotic expression system, and carried out *in vivo* experiment to examine the effect of *Lvit*-CFSH1a on the expression of *Lvit-IAG1*, *Lvit-IAG2*, *Lvit-Vg,* and *Lvit-VgR*.

MATERIALS AND METHODS

Animals

The experimental animals (*L. vittata*) were artificial-bred at the Fisheries Research Institute of Fujian Province, in Xiamen, China. After transport to the laboratory, shrimps were acclimated in seawater aquaria at temperature of 26 ± 1°C and salinity of 32 ± 1 PSU for 2 days. During that period, they were fed with a commercially formulated shrimp diet daily. Two developmental phases covering four gonadal development stages were defined and described for *L. vittata* according to the previous research (Chen et al., 2019).

cDNA Cloning of *Lvit-CFSH1a*

Total RNA was extracted from the eyestalk ganglion of shrimps at gonadal development stage III using TRIzol® reagent (Invitrogen) according to the manufacturer's instructions. The first-strand cDNA for fragment and 3′-untranslated region (3′ UTR) cloning was generated with 1 μg total RNA using RevertAid First Strand cDNA Synthesis Kit (Fermentas). Fragment of *Lvit-CFSH1a* was obtained from a *de novo* transcriptomic library of *L. vittata* and polymerase chain reaction (PCR) by primer pair (CFSH1aF/CFSH1aR) was performed to verify its accuracy. Seminested PCR was performed for 3′ UTR cloning. The 5′ UTR of *Lvit-CFSH1a* was obtained by a method of rapid amplification of cDNA ends (RACE) with SMART™ RACE cDNA Amplification Kit (Clontech) according to the manufacturer's protocol. Primers used in cDNA cloning were list in **Table 1**.

Genomic DNA Amplification of *Lvit-CFSH1a*

EasyPure® Marine Animal Genomic DNA Kit (TransGen) was used to extract the genomic DNA from the eyestalk ganglion of *L. vittata* at gonadal development stage III. Specific primers were designed for amplification of *Lvit-CFSHs* genomic DNA (gDNA) (**Table 1**). The PCR reaction was performed with LA-Taq polymerase (TaKaRa) under the following conditions: 95°C for 5 min; 35 cycles of 95°C for 30 s, 60°C for 30 s, and 72°C for 2 min, followed by 72°C for 10 min final extension.

The Quantitative Real-Time PCR Assays

Primers used for quantitative real-time PCR (qRT-PCR) were from previous studies (Liu et al., 2021a,b). Amplification efficiency of each primer pair was determined before used for qRT-PCR assays. The cDNA was diluted fourfolds using RNase-free water before it was utilized in qRT-PCR detection. Components including, 10 μl TB Green Premix Ex Taq II (2X) (TaKaRa), 2 μl diluted cDNA, 0.5 μl forward/reverse primer (10 μM), as well as and 7 μl RNase-free water, were used for a 20 μl qRT-PCR reaction system. The reaction was performed using in 7500 Real-Time PCR (Applied Biosystems): 95°C for 30 s, followed by 40 cycles of 95°C for 15 s, 58.5°C for 15 s and 72°C for 30 s. The result was calculated using $2^{-\Delta\ \Delta\ Ct}$ method, whereby *Lvit-β-actin* (GenBank accession number: MT114194) was utilized as the reference gene.

TABLE 1 | Summary of primers used in this study.

Primer	Sequence (5′–3′)	Application
CFSH1aF	CCTTAGCTCAGCAGCAGGGTGT	Fragment validation
CFSH1aR	GGCGGCAGTTCCTTCGTCA	
UPM	CTAATACGACTCACTATAGG GCAAGCAGTGGTATCAACGCAGAGT	5′RACE
5CFSH1aout	GCCTCGGCTCTCCATTTGATGTGCT	
5CFSH1ain	GGGTATGGAGCCGGAAGGTCCAGGTCA	
3adaptor	AAGCAGTGGTATCAACGCAGAGTAC TTTTTTTTTTTTTTTTTTTTTTTTTTTTTTVN	3′RACE
3GSP	AAGCAGTGGTATCAACGCAGAG	
3CFSH1ain	GGATGAACCTCCACAGGAACCACG	
3CFSH1aout	CATACCCGAAGCCCTTCTTCCTGC	
gCFSH1aF	ATATAGCGACACAAGAAACTCCACC	cDNA/gDNA validation
gCFSH1aR	TGATGAGTCATTTTTATTGGATAATTGA	
CFSH1adsF	TGGCTCCACATCGACCACCGA	dsRNA synthesis
CFSH1adsR	ATCATCGCCGTCCTTGTTCCTCTTC	
GFPdsF	TGGGCGTGGATAGCGGTTTG	
GFPdsR	GGTCGGGGTAGCGGCTGAAG	
T7primer	TAATACGACTCACTATAGGG	
SP6primer	ATTTAGGTGACACTATAG	
SP6primer	ATTTAGGTGACACTATAG	
CFSH1ayhF	CCGGAATTCCCGAACAAGG ACGGCGATGATGAGCTCG	Prokaryotic expression
CFSH1ayhR	CTAGCTAGCCTAGTTTTGTA CAGCGGCAGCGAAGACG	

Tissue Expression of *Lvit-CFSH1a* in *L. vittata*

The total RNA was extracted from various tissues (eyestalk ganglion, brain, thoracic ganglion, abdominal ganglion, ovary, testis, androgenic gland, hepatopancreas, stomach, intestine, heart, gill, and muscle) as described in section "cDNA Cloning of *Lvit-CFSH1a.*" The first-strand cDNA was produced from 1 μg total RNA using PrimeScript™ RT reagent Kit with gDNA Eraser (Perfect Real Time) (TaKaRa). Tissue expression profile was determined by RT-PCR under the following conditions: 95°C for 5 min; 35 cycles of 95°C for 30 s, 58.5°C for 30 s, and 72°C for 30 s, followed by 72°C for 5 min final extension. Meanwhile, *Lvit-β-actin* (GenBank accession number: MT114194) was amplified as a positive control. RT-PCR products were examined using 1.5% agarose gel imaged by UV detector (Geldoc, Thermo Fisher Scientific).

Expression Profile of *Lvit-CFSH1a* During Gonadal Development

In order to examine expression profile of *Lvit-CFSH1a* during gonadal development, total RNA was extracted from eyestalk ganglion of *L. vittata* at different gonadal development stages (n = 5). It was followed by the synthesis of cDNA as described in section "Tissue Expression of *Lvit-CFSH1a* in *L. vittata*" and qRT-PCR detection as described in section "The Quantitative Real-Time PCR Assays," respectively.

dsRNA Preparation

Fragment of *Lvit-CFSH1a* and green fluorescent protein gene (*GFP*) (exogenous gene control) were cloned into pGEM-T Easy Vector (Promega). dsRNA synthesis was performed using T7 RNA Polymerase (Takara) and SP6 RNA Polymerase (TaKaRa) according to standard protocols. Finally, dsRNA was diluted with 10 mM phosphate-buffered saline (PBS, pH 7.4).

Short-Term Silencing Experiment *in vivo*

To evaluate the efficacy of gene knockdown via RNA interference (RNAi), a short-term silencing experiment was carried out with *L. vittata* at gonadal development stage I. A total of 15 shrimps (carapace length 2.99 ± 0.10 mm, body weight 42.79 ± 4.28 mg) were randomly and equally assigned to following 3 treatment groups (n = 5): dsRNA *Lvit-CFSH1a*-injected, dsRNA *GFP*-injected and PBS-injected. dsRNA (2 μg/g) (Liu et al., 2021a,b) was delivered via intramuscular injection in the abdominal segment of shrimp. Meanwhile, the PBS-injected group received an equivalent volume of PBS. Sampling was performed 24 h after injection (Shi et al., 2020). Following anesthesia on ice for 5 min, eyestalk ganglion (EG) and androgenic gland (AG) were collected to test the effect of dsRNA-mediated silencing on the specific genes by qRT-PCR. While RNA extraction and qRT-PCR were performed as described above in sections " cDNA Cloning of *Lvit-CFSH1a*" and "The Quantitative Real-Time PCR Assays," the first-strand cDNA was generated with 200 ng total RNA by TransScript® II One—Step gDNA Removal and cDNA short SuperMix Kit (TransGen).

Long-Term Silencing Experiment *in vivo*

A long-term silencing experiment was conducted to determine the potential roles played by *Lvit-CFSH1a* in sexual differentiation and gonadal development. Shrimps (carapace length 3.12 ± 0.17 mm, body weight 47.80 ± 6.42 mg) at gonadal development stage I were randomly divided into three groups (n = 13) as described in section "Short-Term Silencing Experiment *in vivo*." Similar dose of dsRNA (2 μg/g) or equal volume of PBS was injected into the abdominal segment of shrimp once every 4 days for a total of 8 injections in 29-days duration during which shrimps were kept in seawater aquaria under the following conditions: temperature, 26 ± 1°C; salinity, 32 ± 1 PSU; 12L:12D photoperiod. On day 30 (24 h after the 8th injection), all of the shrimp were sampled after anesthetization on ice (Shi et al., 2020). Measurements of carapace length and body weight were recorded. Changes in external sexual features and gonadal development were assessed and recorded as described in our laboratory (Liu et al., 2021a,b). Samples of eyestalk ganglion, androgenic gland, ovarian region of the gonad and hepatopancreas were collected to test the effect of long-term silencing on *Lvit-CFSH1b* (GenBank accession number: MT114198), *Lvit-IAG1* (GenBank accession number: MT114196), *Lvit-IAG2* (GenBank accession number: MT114197), *Lvit-Vg* (GenBank accession number: MT113122) and *Lvit-VgR* (GenBank accession number: MT114195) by qRT-PCR. RNA extraction, the first-strand cDNA synthesis, qRT-PCR were also performed as described in section "Short-Term Silencing Experiment *in vivo*." The remaining gonad tissue was fixed in modified Bouin's fixative (25 ml 37–40% formaldehyde, 75 ml saturation picric acid and 5 ml glacial acetic acid) at 4°C for 24 h, followed by gradient alcohol dehydration, paraffin embedding, preparation of 6 μm sections and staining with hematoxylin and eosin (H & E) for histological observation.

In vivo Effect of *rLvit-CFSH1a* on Gene Expression

r*Lvit*-CFSH1a was expressed using a prokaryotic expression system and purified by immobilized metal-affinity chromatography (IMAC) (Bornhorst and Falke, 2000). The fragment encoding the mature peptide of *Lvit*-CFSH1a was cloned into pET-His vector with restriction enzyme sites (*Eco*RI and *Nhe*I). The generated constructs (pET-His-CFSH1a) was transformed into *E. coli TransB* (DE3) and induced at 16°C after adding isopropyl-beta-D-thiogalactopyranoside (IPTG, 0.2 mM final concentration). After 20 h, bacterial cells were harvested by centrifugation. Because r*Lvit*-CFSH1a expressed as inclusion bodies (**Supplementary Figure 1A**), purification was performed under denaturing conditions (8M urea) with Ni Sepharose™ 6 Fast Flow (GE Healthcare) according to the manufacturer's instructions (**Supplementary Figure 1B**). Purified r*Lvit*-CFSH1a was renatured by graded urea dialysis and confirmed by Western blot analysis. Samples were separated by 12% SDS-PAGE gel electrophoresis. The electrophoresed proteins were transferred to a PVDF membrane and blocked with 5% bull serum albumin (BSA)-PBS for 1 h at room temperature. Following blocking, the membrane was washed three times with PBS. After that, it was incubated in ProteinFind® Anti-His Mouse Monoclonal Antibody (1:2,000, TransGen) for 1 h at 37°C. Horseradish peroxidase activity was detected with Western Blotting Mouse IgG DAB Chromogenic Reagent Kit (incubated with Goat Anti-Mouse IgG/HRP, 1:4,000, 1 h, 37°C; Solarbio) according to the manufacturer's instructions.

A total of 10 shrimps (carapace length 5.17 ± 0.22 mm, body weight 179.02 ± 29.41 mg) at gonadal development stage II were randomly and equally assigned to following 2 treatment groups (n = 5): r*Lvit*-CFSH1a-injected and PBS-injected. r*Lvit*-CFSH1a (2 μg/g) was delivered via intramuscular injection in the abdominal segment of shrimp. Meanwhile, the PBS-injected group received an equivalent volume of PBS. Sampling was performed 24 h after injection. After shrimps were anesthetized on ice for 5 min, AG, ovarian region and hepatopancreas were obtained to test the effect of r*Lvit*-CFSH1a-injection on the specific genes by qRT-PCR. RNA extraction, the first-strand cDNA synthesis, qRT-PCR were also performed as described in section "Short-Term Silencing Experiment *in vivo*."

Bioinformatics Analyses

The primers used for cDNA cloning, gDNA cloning, dsRNA preparation and prokaryotic expression were designed with Primer 5.0. The open reading frame (ORF) was predicted by ORF Finder software[1]. We adopted the SignalP-5.0 Server[2] to predict the signal peptides, whereas cysteine residues and putative disulfide bonds were predicted via DiANNA 1.1 web server[3]. Further, sequence alignment of deduced amino acid sequences with reported sequences was performed using the Clustal Omega website[4]. N-glycosylation motif was predicted by NetNGlyc 1.0 Server[5].

The Maximum Likelihood method with 1000 bootstrap replicates based on the JTT matrix-based model in MEGA7 was applied to generate a phylogenetic tree entailing the deduced amino acid sequence of decapoda CFSH mature peptides. Most of CFSH sequences were borrowed from previous works (Thongbuakaew et al., 2019); other sequences were shown in **Table 2**.

[1]https://www.ncbi.nlm.nih.gov/orffinder/
[2]http://www.cbs.dtu.dk/services/SignalP/
[3]http://clavius.bc.edu/~clotelab/DiANNA/
[4]https://www.ebi.ac.uk/Tools/msa/clustalo/
[5]http://www.cbs.dtu.dk/services/NetNGlyc/

TABLE 2 | Summary of sequences used in multiple sequence alignment and phylogenetic analysis.

Sequence	Species	GenBank accession number
Csa-CFSH1	*Callinectes sapidus*	GU016328
Lvit-CFSH1a	*Lysmata vittata*	MT114199
Pj-CFSH2	*Penaeus japonicus*	LC224021
Sp-CFSH	*Scylla paramamosain*	MF489232

A

>*Lvit-CFSH1a*

```
ACATGGGGATATAGCGACACAAGAAACTCCACCATGGCTCCACATCGACCACCGAGCTCCACCT   64
                                M  A  P  H  R  P  P  S  S  T
CCAGATTCTGCAGTAGCCTCACCCTAGTTGGCGCCGTCGTCCTCGCCTTAGCTCAGCAGCAGGG  128
S  R  F  C  S  S  L  T  L  V  G  A  V  V  L  A  L  A  Q  Q  Q  G
TGTCAAGAGTGACCTGGACCTTCCGGCTCCATACCCGAAGCCCTTCTTCCTGCGAGAGTGGGAG  192
 V  K  S  D  L  D  L  P  A  P  Y  P  K  P  F  F  L  R  E  W  E
GAGGACGATCTCAGGGACTTCAAGTGGTCGGACGCACTTCGAAACTCCCTGAAGAGGAACAAGG  256
 E  D  D  L  R  D  F  K  W  S  D  A  L  R  N  L  S  K  R  N  K
ACGGCGATGATGAGCTCGGAAACGACCCCTTACAGTACTTCTCCGAGGAGCAAGTCAACGCCGC  320
D  G  D  D  E  L  G  N  D  P  L  Q  Y  F  S  E  E  Q  V  N  A  A
CATGAAGGCCGAGTACAAGGTCGTCCCCCATCCGGTCGTCTACACATCTCAGATCCTTCGCGAG  384
  M  K  A  E  Y  K  V  V  P  H  P  V  V  Y  T  S  Q  I  L  R  E
GGCGTCAACTGCTCCTCCATTAGGATGAACCTCCACAGGAACCACGTCAAGCCAGAGTTGCAAC  448
 G  V  N  C  S  S  I  R  M  N  L  H  R  N  H  V  K  P  E  L  Q
TCAGACCCGACTGGATCCACAAGTCGGACTTCATAGGCGACTGCCCCGCCCACTACGTGACGAA  512
L  R  P  D  W  I  H  K  S  D  F  I  G  D  C  P  A  H  Y  V  T  K
GGAACTGCCGCCCATGTATTCACCCGCGGTCATCCTGGAGGCTGTCTGCACCTGCGGGGGATCG  576
  E  L  P  P  M  Y  S  P  A  V  I  L  E  A  V  C  T  C  G  G  S
CAGTGCTCAAGGAGCGGACACCAGTGTGTCCCTGTCTCTCGCCATGTCCCCGTATGGGTGCGAC  640
 Q  C  S  R  S  G  H  Q  C  V  P  V  S  R  H  V  P  V  W  E  R
GGGGTCCTAACTTTCACGTACTGGACGTCGAAGAAGTCACCGTTGCTTGCGCATGCGTCAGGAG  704
R  G  P  N  F  H  V  L  D  V  E  E  V  T  V  A  C  A  C  V  R  R
ACCCAGCGGCGAGGGGAATTTCGTTTTCGCTGCCGCTGTACAAAATTAACACAGTCCCTTTTCC  768
  P  S  G  E  G  N  F  V  F  A  A  A  V  Q  N  *
TTTTCATCCTCCTTTATCCAACGCTCCCAAAACAATAGTTATTAACTTTCAAAATTTCATTTTT  832
CAAGCCATTGTAAAATTAGGTGAAAAAAAAGCTTAAAATCAGTTTAAGAATTGTATGAATCCAG  896
TAGAATTTACTCCATAAATAGTCGTTAAACACCACTTCCACGCCGTTAGGTAGCTTTTAAAAAC  960
CAGTTAGACCTAGGGAGAAGAAAGGTTTAACTGGCAACACTGCTTTAAAGAAAGCAGCAGGTTT 1024
TGTGCGGTTGGTTACAACAAGGACATCCCCTTGGGAGGGATATTATATCCGAATTCTGTTAATT 1088
GATTTCAATTTTATGAATTCTTTGGATTGTGTGCTTTTTTTTTTCTTTTTTTTTTTTGGTTTCG 1152
GGTTTGATTATTCAATTATCCAATAAAAATGACTCATCACAAAAAAAAAAAAAAAAAAAAAAAA 1216
AAAA                                                               1220
```

B

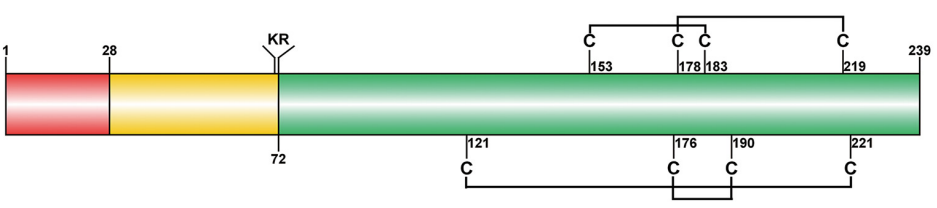

FIGURE 1 | Molecular characterization of *Lvit-CFSH1a*. **(A)** The nucleotide and deduced amino acid sequence of *Lvit-CFSH1a*. The signal peptide was shown in black box, the CFSH precursor-related peptide was in bold italics, the dibasic cleavage site (KR) was boxed in gray, the N-glycosylation motif was shown in blue background and the putative polyadenylation signal (AATAAA) is underlined. **(B)** Schematic diagram of preproprotein of *Lvit*-CFSH1a. Signal peptide (red box), CFSH precursor-related peptide (yellow box), a dibasic cleavage site KR, and the mature hormone (green box) were shown. The eight cysteine residues were predicted, and four putative disulfide bridges were connected with lines.

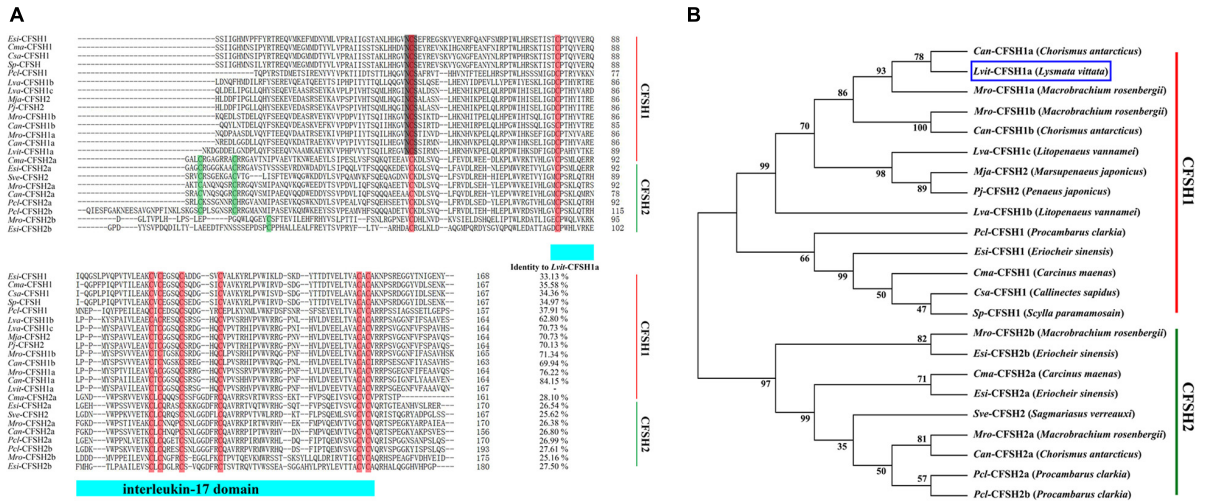

FIGURE 2 | Multiple sequence alignment and phylogenetic tree of CFSH mature peptides in decapoda. **(A)** Multiple sequence alignment of putative mature peptides. Most of CFSH sequences were borrowed from previous works by Thongbuakaew et al. (2019); other sequences were shown in **Table 2**. The eight conserved cysteine residues were boxed in red and other cysteine residues were shown in green. The light blue bar showed conserved IL-17domain. The N-glycosylation motif was shown in gray background. **(B)** Phylogenetic tree of CFSHs in decapod crustaceans. Sequences used in the alignment were the same as those used in multiple sequence alignment. Phylogenetic analysis was conducted by Maximum Likelihood method based on the JTT matrix-based model in MEGA7. The percentage of replicate trees in which the associated taxa clustered together in the bootstrap test (1,000 replicates) was shown next to the branches. *Lvit-CFSH1a* was indicated with blue box.

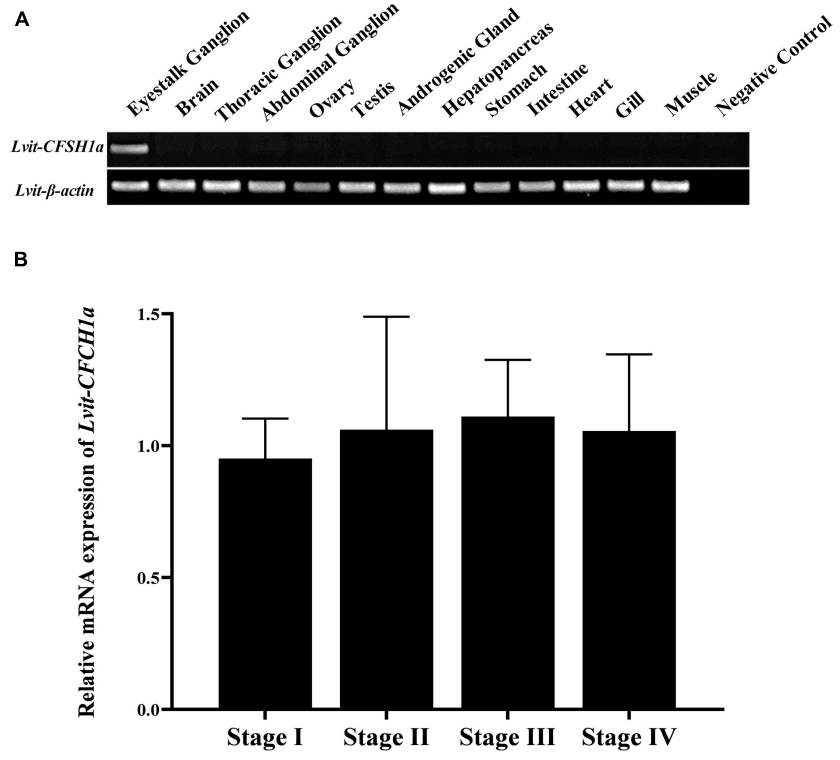

FIGURE 3 | Spatial and temporal expression profiles of *Lvit-CFSH1a*. **(A)** Tissue distribution profiles of *Lvit-CFSH1a*. The analysis was generated by PCR assays with cDNAs from various tissues of individuals at the gonadal development stage III. **(B)** Expression profiles of *Lvit-CFSH1a* in the eyestalk ganglion during gonadal development by qRT-PCR. The *Lvit-CFSH1a* expression levels standardized by *Lvit*-β-*actin* expression levels were represented as mean ± SD (one-way ANOVA followed by Tukey's multiple range tests; $n = 5$).

Statistical Analyses

Normality of data was established by the Kolmogorov-Smirnov test. All the data were presented in a normal distribution and tested for variances homogeneity by the Levene's test. All statistical analyses were performed using the SPSS 18.0 software. Statistical significance ($p < 0.05$) of data regarding *Lvit*-CFSH1a expression profile and silencing experiments was determined using one-way ANOVA followed by Tukey's multiple range tests. The *t*-test was used to analyze the data of r*Lvit*-CFSH1a injection experiment. All data were presented as mean ± SD.

RESULTS

Full Length of *Lvit-CFSH1a*

Lvit-CFSH1a (GenBank accession number: MT114199) cDNA was 1,220-bp in length with a 34-bp 5′-UTR, a 720-bp ORF, and a 467-bp 3′-UTR with a polyA tail in order (**Figure 1A**). The ORF encoded a polypeptide of 239-aa, including a 34-aa signal peptide, a 44-aa CFSH-precursor-related peptide, a dibasic processing signal (Lys-Arg), and a 161-aa mature peptide (**Figure 1**). A single polyadenylation signal ATTAAA is present in the 3′UTR of *Lvit-CFSH1a* (**Figure 1A**). Eight cysteine residues forming four disulfide bridges were found in *Lvit-CFSH1a* (**Figure 1B**). Genomic DNA of *Lvit-CFSH1a* was also cloned but no intron was found.

Homology and Phylogenetic Analysis

Multiple sequence alignment of deduced mature peptide of CFSHs was shown in **Figure 2A**. Eight conserved cysteine residues and an interleukin 17 (IL-17) domain were found in *Lvit*-CFSH1a, and that was faultlessly aligned with other CFSHs (**Figure 2A**). According to the former studies (Kotaka and Ohira, 2018; Tsutsui et al., 2018), the CFSHs were grouped into two subtypes: type I and type II. The type I CFSHs possessed a single conserved N-glycosylation motif while the type II CFSHs contained additional one or two cysteine residues (**Figure 2A**). *Lvit*-CFSH1a mature peptide shared the highest identity with *Can*-CFSH1a (84.15%).

Phylogenetic analysis demonstrated that the CFSHs in the decapod crustaceans formed two major clades: type I and type II CFSH. *Lvit*-CFSH1a was classified into type I CFSH (**Figure 2B**).

Expression Profiles of *Lvit-CFSH1a*

RT-PCR was performed on *L. vittata* at the gonadal development stage III to determine the spatial distribution profile of *Lvit-CFSH1a*. The findings were that *Lvit-CFSH1a* was exclusively expressed in the eyestalk ganglion (**Figure 3A**). The relative expression of *Lvit-CFSH1a* in the eyestalk ganglion during gonadal development was also assessed by qRT-PCR. No significant difference was observed in *Lvit-CFSH1a* expression levels during gonadal development ($F_{3,\ 16} = 0.265$, $p = 0.850$) (**Figure 3B**).

Short-Term Silencing Experiment *in vivo*

The findings revealed that in comparison to the PBS-injected treatment, transcripts of *Lvit-CFSH1a* were 83.7% inhibited [$F_{(2,\ 12)} = 37.675$, $p < 0.05$]; while no significant changes in *Lvit-CFSH1b* expression levels were observed ($F_{(2,\ 12)} = 0.254$, $p = 0.780$]. Meanwhile, knockdown of *Lvit-CFSH1a* resulted in extremely significant upregulation of *Lvit-IAG2* levels [$F_{(2,\ 12)} = 115.993$, $p < 0.05$] but almost did not affect the expression levels of *Lvit-IAG1* [$F_{(2,\ 12)} = 0.008$, $p = 0.992$] (**Figure 4**).

Long-Term Silencing Experiment *in vivo*

Effects of *Lvit-CFSH1a* Silencing on Gene Expression

Compared to the PBS treatment, transcript of *Lvit-CFSH1a* was 81.7% inhibited [$F_{(2,\ 15)} = 20.686$, $p < 0.05$] (**Figure 5**). The

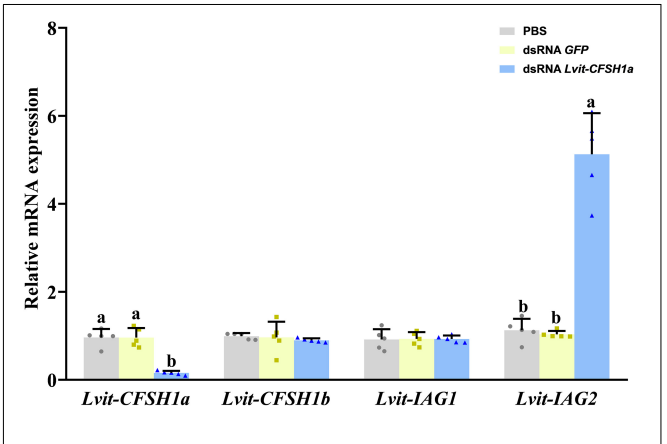

FIGURE 4 | Effects of short-term *Lvit-CFSH1a* silencing on gene expression of *L. vittata*. The efficacy of gene knockdown in the short-term *Lvit-CFSH1a* silencing experiment was evaluated by qRT-PCR. The expression levels of *Lvit-CFSH1a*, *Lvit-CFSH1b*, *Lvit-IAG1,* and *Lvit-IAG2* were detected following *in vivo* injection with PBS, dsRNA *GFP* or dsRNA *Lvit-CFSH1a*. The gene expression levels were standardized by *Lvit-β-actin* expression levels and represented as mean ± SD ("a and b," $p < 0.05$; one-way ANOVA followed by Tukey's multiple range tests; $n = 5$).

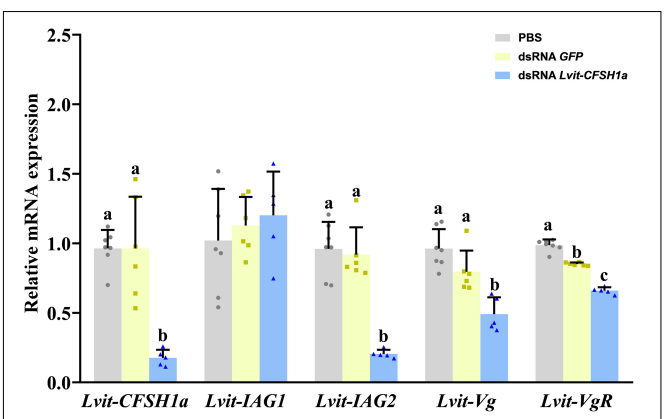

FIGURE 5 | Effects of long-term *Lvit-CFSH1a* silencing on gene expression of *L. vittata*. The efficacy of gene knockdown in the long-term *Lvit-CFSH1a* silencing experiment was evaluated by qRT-PCR. The expression levels of *Lvit-CFSH1a*, *Lvit-IAG1*, *Lvit-IAG2*, *Lvit-Vg,* and *Lvit-VgR* were detected following *in vivo* injection with PBS, dsRNA *GFP* or dsRNA *Lvit-CFSH1a*. The gene expression levels were standardized by *Lvit-β-actin* expression levels and represented as mean ± SD ("a, b and c," $p < 0.05$; one-way ANOVA followed by Tukey's multiple range tests; $n = 5$–7).

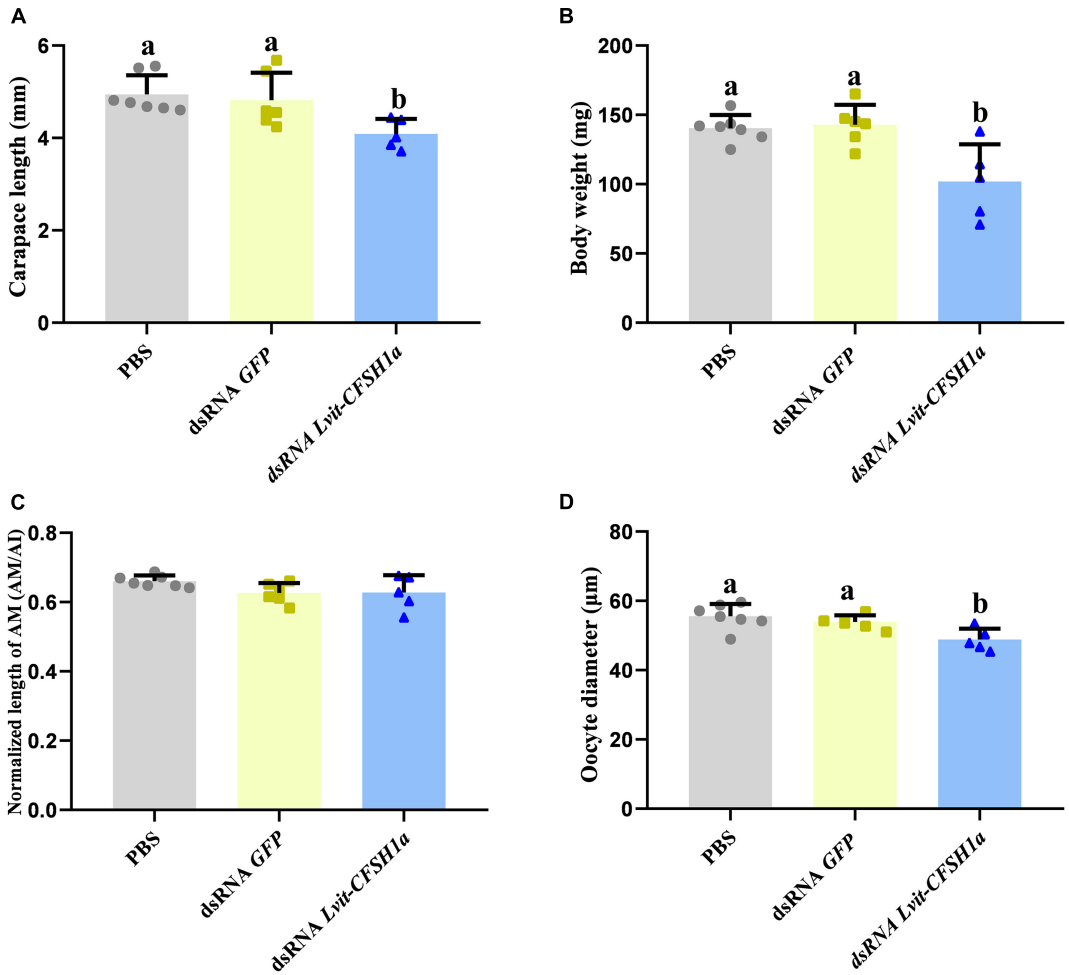

FIGURE 6 | Effects of *Lvit-CFSH1a* silencing on carapace length, body weight, AM length and oocyte diameter of *L. vittata*. **(A)** Carapace length; **(B)** body weight; **(C)** the normalized length of AM (AM/AI); **(D)** the oocyte diameter. Data were represented as mean ± SD ("a and b," $p < 0.05$; one-way ANOVA followed by Tukey's multiple range tests; $n = 5–7$).

relative expression of genes associated with gonadal development and sexual differentiation were also assessed by qRT-PCR. Results showed that the expression of *Lvit-IAG2* in the androgenic gland was significantly reduced [$F_{(2,\ 15)} = 34.597$, $p < 0.05$], but no significant difference was detected for *Lvit-IAG1* expression [$F_{(2,\ 15)} = 0.524$, $p = 0.603$]. Meanwhile, *Lvit-Vg* mRNA expression level in the hepatopancreas [$F_{(2,\ 15)} = 16.651$, $p < 0.05$] and *Lvit-VgR* mRNA expression level in the ovary [$F_{(2,\ 15)} = 175.194$, $p < 0.05$] were found significantly down-regulated (**Figure 5**).

Effects of *Lvit-CFSH1a* Silencing on Growth and Development of Sexual Characteristics

At the end of the 30-day long-term trial, we recorded the average carapace length and bodyweight of the shrimps. Compared with individuals from the PBS (4.94 ± 0.06 mm, 140.36 ± 1.37 mg) or dsRNA *GFP* (4.82 ± 0.09 mm, 142.90 ± 2.05 mg) treatments, shrimps in dsRNA *Lvit-CFSH1a* (4.09 ± 0.05 mm, 101.90 ± 3.84 mg) treatment were significantly smaller [carapace length: $F_{(2,\ 15)} = 5.441$, $p < 0.05$; body weight: $F_{(2,\ 15)} = 9.124$, $p < 0.05$] (**Figures 6A,B**). Moreover, changes in female and male sexual characteristics were also documented through photography (**Figure 7**). On the one hand, *Lvit-CFSH1a* gene knockdown led to retardation of female sexual characteristics. In the PBS and dsRNA *GFP* treatment, gonophores bulged out like a frustum surrounded by lush feathery setae (**Figures 7A,B**). Female gonophores in dsRNA *Lvit-CFSH1a* treatment were hypogenesis (**Figure 7C**). Contrary to the controls, gonophores were less visually evident or completely disappeared. The feathery setae surrounding the female gonopores located at the base of the third pair of pereiopods were substantially sparse (**Figure 7C**). On the other hand, no significant difference in male characteristics (cincinnuli, AM and male gonopore) was observed (**Figures 6C, 7D–L**).

Effects of *Lvit-CFSH1a* Silencing on Gonadal Development

Morphological and histological characteristics of gonads following *Lvit-CFSH1a* knockdown were recorded. Knockdown

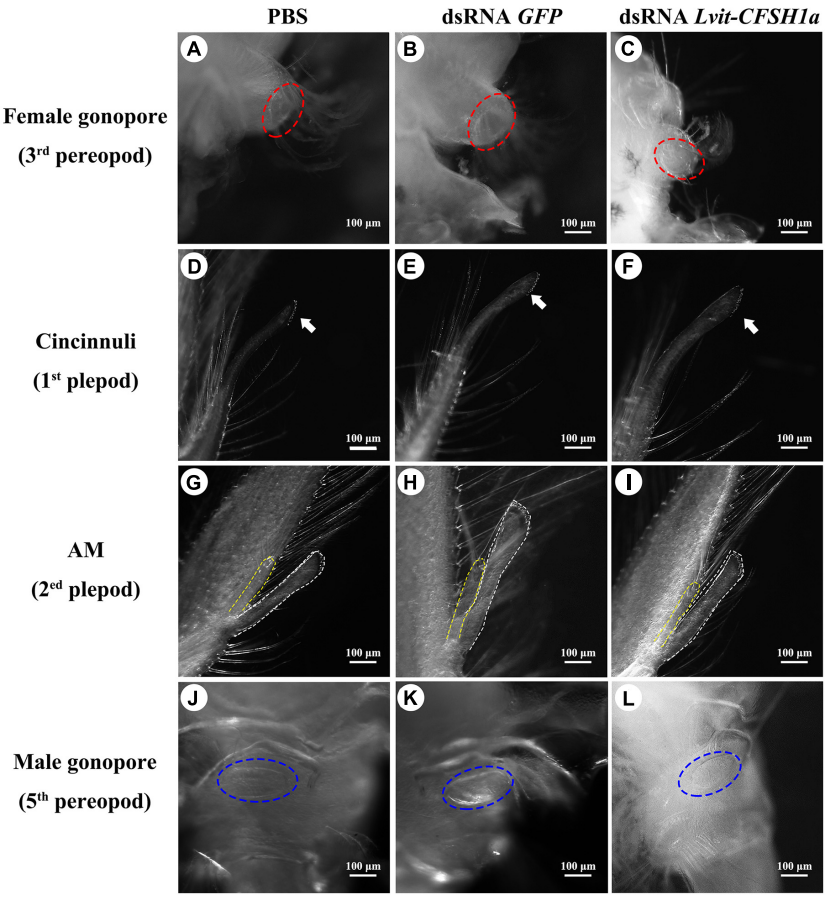

FIGURE 7 | (A–L) Effects of *Lvit-CFSH1a* silencing on development of female and male sexual characteristics. Both female characteristics (female gonopore) and male characteristics (cincinnuli, AM, male gonopore) were photographed at the end of the long-term silencing experiment. Female gonopores were noted by red dotted circle **(A–C)**. Cincinnuli was marked with solid white arrows **(D–F)**. The AI was marked by white dashed lines, while the AM was marked by yellow dashed lines **(G–I)**. Male gonopores were noted by blue dotted circle **(J–L)**. AM, appendices masculinae; AI, appendix interna.

of *Lvit-CFSH1a* led to retardation of ovarian region. In dsRNA *Lvit-CFSH1a* treatment, the ovarian region was thinner (**Figure 8C**). Additionally, the oocyte size significantly decreased following injection of dsRNA *Lvit-CFSH1a* (**Figures 6D**, **8D–F**). For the PBS and dsRNA *GFP* treatment, the average oocyte diameter was 55.57 ± 0.51 μm (n = 7) and 53.87 ± 0.28 μm (n = 6), respectively. Following knockdown of *Lvit-CFSH1a*, the oocyte diameter decreased to 48.81 ± 0.46 μm (n = 5). However, *Lvit-CFSH1a* knockdown had no significant effect on testicular development. Testicular regions of the three treatments were cloudy white (**Figures 8A–C**). Gonadal histology further showed that similar compositions of germ cell types were observed among the three treatments. Abundant of spermatocytes I (Sc I), spermatid (Sd), and spermatozoa (Sz) were found in the testicular region of the three treatments (**Figures 8G–I**).

In vivo Effect of *rLvit-CFSH1a* on Gene Expression

To determine the effect of *Lvit*-CFSH1a on *Lvit-IAG1*, *Lvit-IAG1*, *Lvit-Vg,* and *Lvit-VgR*, two experimental groups were injected with either r*Lvit*-CFSH1a or carrier only (PBS). The findings revealed that injection of r*Lvit*-CFSH1a resulted in extremely significant downregulation of *Lvit-IAG2* levels (p = 0.0028) but almost did not affect the expression levels of *Lvit-IAG1*, *Lvit-Vg,* and *Lvit-VgR* (**Figure 9**).

DISCUSSION

CFSH is a crucial hormone involved in development of female-related phenotypes in dioecious crustaceans (Zmora and Chung, 2014; Jiang et al., 2020). However, the biological functions of CFSH in PSH crustaceans have been rarely investigated.

In our current study, we established a transcript of CFSH (*Lvit-CFSH1a*) in the PSH shrimp, *L. vittata*. By cloning of *Lvit-CFSH1a* gDNA sequence, we confirmed that transcripts of *Lvit-CFSH1a* and *Lvit-CFSH1b* were derived from different genes. Though abundant of nuclear sequence of CFSHs were reported in decapod crustaceans, to date, only two type I CFSHs, *Csa*-CFSH1 (*Callinectes sapidus*), and *Sp*-CFSH (*Scylla paramamosain*), have been proved to stimulate female sexual

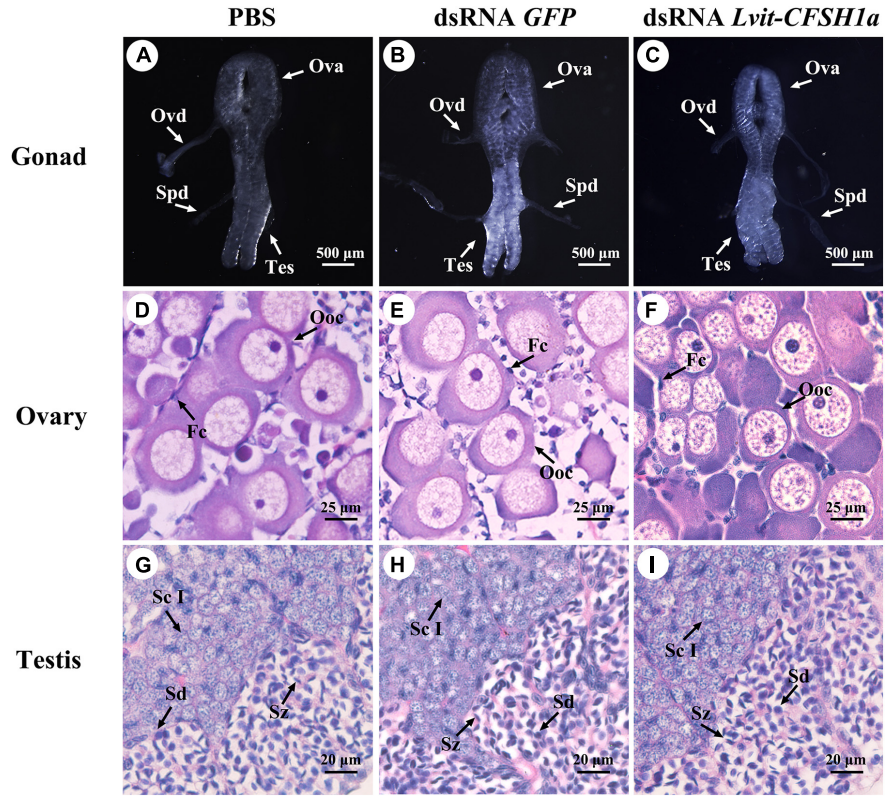

FIGURE 8 | Effects of *Lvit-CFSH1a* silencing on gonadal development of *L. vittata*. Gonad morphology and characteristics were photographed following *in vivo* injection of PBS **(A)**, dsRNA *GFP* **(B)** or dsRNA *Lvit-CFSH1a* **(C)**. Hematoxylin and eosin (H&E)-stained sections was used for follow-up structure description of ovarian region **(D–F)** and testicular region **(G–I)**. Ova, ovary; Tes, testis; Ovd, oviduct; Spd, sperm duct; Ooc, oocytes; Fc, follicular cell; Sc I, primary spermatocyte; Sd, spermatid; Sz, spermatozoa.

differentiation (Ventura et al., 2014; Zmora and Chung, 2014; Veenstra, 2015, 2016; Nguyen et al., 2016; Kotaka and Ohira, 2018; Liu et al., 2018; Tsutsui et al., 2018; Thongbuakaew et al., 2019; Jiang et al., 2020). While expression of CFSH transcripts were detected in a variety of tissues (Veenstra, 2015; Nguyen et al., 2016; Tsutsui et al., 2018; Thongbuakaew et al., 2019), *Csa*-CFSH1 and *Sp*-CFSH were exclusively expressed in the eyestalk ganglion (Zmora and Chung, 2014; Jiang et al., 2020). In this study, *Lvit*-CFSH1a shared similar characteristics with other type I CFSHs (Kotaka and Ohira, 2018; Tsutsui et al., 2018). Phylogenetic tree analysis further demonstrated that *Lvit*-CFSH1a was classified into type I CFSH. Besides, *Lvit*-CFSH1a was also exclusively expressed in the eyestalk ganglion, which was consistent with studies in *C. sapidus* and *S. paramamosain* (Zmora and Chung, 2014; Jiang et al., 2020). Thus, *Lvit*-CFSH1a was possibly involved in development of female-related phenotypes of the PSH species. Alternatively, the constant and stable expression of *Lvit-CFSH1a* during the life cycle of the PSH species suggested that *Lvit*-CFSH1a might not participate in gonad development.

Our findings revealed that RNAi induced a specific knockdown of the *Lvit-CFSH1a* transcripts level by 83.7% in a short-term experiment, and by 81.7% in a long-term experiment. Furthermore, we assessed the influence of *Lvit*-CFSH1a on the development of female features by comparing

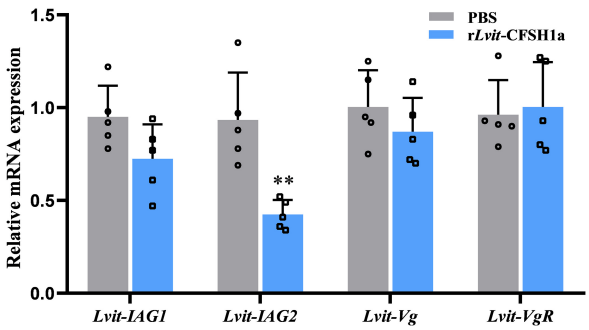

FIGURE 9 | Effects of r*Lvit-CFSH1a* on gene expression of *L. vittata in vivo*. The expression levels of *Lvit-IAG1*, *Lvit-IAG2*, *Lvit-Vg,* and *Lvit-VgR* were detected following *in vivo* injection with PBS or r*Lvit*-CFSH1a. The gene expression levels were standardized by *Lvit*-β-*actin* expression levels and represented as mean ± SD (*t*-test, with $^{**}p < 0.01$; $n = 5$).

female external features and ovarian development status. In the present study, we found that *Lvit-CFSH1a* gene knockdown led to retardation of female sexual characteristics. Numbers of feathery setae surrounding the female gonopores were substantially sparse. This result is similar to those described in *C. sapidus* and *S. paramamosain* (Zmora and Chung, 2014;

Jiang et al., 2020). However, results varied when it came to the influences on ovarian development. In fact, to date the effect of CFSH on ovarian development remains obscure. In *C. sapidus*, knockdown of *Cs-CFSH* showed no significant effect on the ovarian development (Zmora and Chung, 2014). Study in *M. japonicus* suggested that CFSH might participate in some reproductive process other than vitellogenesis (Tsutsui et al., 2018). Research in *M. rosenbergii* also demonstrated that both type I and type II CFSHs had unknown effect on ovarian development (Thongbuakaew et al., 2019). In the present study, a repression phenomenon was observed in the ovarian region of *L. vittata* in long-term silencing experiment. Contrary to the controls, ovarian region in the *Lvit-CFSH1a* silencing treatment was less developed with significantly smaller oocytes. Moreover, qRT-PCR data lent support to histomorphological results. It is known that both the *Vg* gene expression levels in hepatopancreas and *VgR* gene expression levels in ovary are approved indexes of ovarian development (Warrier and Subramoniam, 2002; Subramoniam, 2011; Jia et al., 2013; Urtgam et al., 2015). Following *Lvit-CFSH1a* knockdown, *Lvit-Vg* expression in the hepatopancreas and *Lvit-VgR* expression in the ovary were found significantly down-regulated. It seemed plausible that *Lvit*-CFSH1a stimulated ovarian development via promoting vitellogenesis. We also purified *Lvit*-CFSH1a mature peptide and conducted a further *in vivo* injection experiment in the study. However, results of r*Lvit*-CFSH1a administration demonstrated that r*Lvit*-CFSH1a affect neither vitellogenin synthesis in the hepatopancreas nor vitellogenesis in the gonad. Moreover, no significant difference was observed in *Lvit-CFSH1a* expression levels during gonadal development (**Figure 3**). These results jointly suggested that *Lvit*-CFSH1a might regulate ovarian development via some unknown process other than vitellogenesis. It is worth noting that, as shown in **Figures 6A,B**, *Lvit-CFSH1a* silencing induced significantly slower growth in the treated shrimps. It is known that growth and reproduction are closely related, gonadal development and fecundity usually increase with body size (Heino and Kaitala, 2001; Michalakis et al., 2013). The same phenomenon has also been observed in *L. vittata* (Chen et al., 2019). Thus, another possibility is that long-term *Lvit-CFSH1a* silencing caused significantly slower growth in the treated shrimps and this indirectly hindered the ovarian development, along with smaller oocytes and down-regulation of *Lvit-Vg* and *Lvit-VgR* expression.

Simultaneously, we evaluated the effects of *Lvit*-CFSH1a on male development in the study. In *S. paramamosain*, it was reported that CFSH acts as an inhibitor of IAG (Liu et al., 2018). In dioecious decapod crustaceans, there is usually one IAG gene in a species (Li et al., 2012; Chung, 2014; Huang et al., 2017). Transcripts generated by alternative splicing of the same IAG gene have different functions in different organs (Li et al., 2012; Chung, 2014; Huang et al., 2017). Nevertheless, two IAG genes were identified in the PSH shrimp *L. vittata*, and they cooperatively modulated male sexual differentiation of the species (Liu et al., 2021a,b). Specifically, *Lvit*-IAG1 was suggested to be closely related to the development of both AM and male gonopores, and participated in primary-to-secondary spermatocyte transition (Liu et al., 2021b); whereas *Lvit*-IAG2 was somewhat related to the development of AM, and participated in secondary spermatocyte-to-spermatid transition (Liu et al., 2021a). In the present study, results of short-term silencing experiment and r*Lvit*-CFSH1a injection experiment demonstrated that *Lvit*-CFSH1a acted as an inhibitor of *Lvit*-IAG2 rather than *Lvit*-IAG1. Thus, we speculated that knockdown of *Lvit-CFSH1a* might slightly stimulate male sexual differentiation in long-term silencing experiment, such as relatively longer AM and more spermatid/spermatozoa in the testicular regions. However, at the end of the 30-day long-term trial, no significant promotion in male sexual differentiation was observed. Long-term *Lvit-CFSH1a* knockdown affected neither testicular maturation nor development of male-related phenotypes. Notably, *Lvit-IAG2* expression was significantly suppressed, which was contradictory to the above hypothesis. The following may explain these apparently contradictory results. Previous studies suggested that *Lvit*-IAG2 is more than a sexual differentiation regulator, and it also stimulates the growth of the PSH species (Liu et al., 2021a). In the present study, silencing the *Lvit-CFSH1a* gene impeded individual growth of the species. Moreover, no significant difference was observed in *Lvit-CFSH1a* expression levels during the life cycle of the PSH species (**Figure 3**). Based on the above results, we proposed that *Lvit*-CFSH1a might involve some unknown biological processes and ultimately influence individual growth. In the short-term trial (**Figures 4**, **9**), *Lvit-IAG2* expression was significantly suppressed by *Lvit*-CFSH1a, but in the long-term experiment the adverse effects of *Lvit*-CFSH1a silencing on growth became more obvious (**Figure 6**), and it in turn affected expression of growth-related gene (e.g., *Lvit-IAG2*). With the decrease of *Lvit-IAG2*, the rate of male differentiation in dsRNA *Lvit-CFSH1a* treatment was slower than the PBS or dsRNA *GFP* treatment, which eventually led to similar development of male-related phenotypes among the three treatments.

In summary, we characterized a CFSH gene, *Lvit-CFSH1a*, from the eyestalk ganglion of the PSH species *L. vittata*. This study showed that *Lvit*-CFSH1a regulated female-related phenotypes, but didn't evidently affect the male sexual differentiation. In addition, *Lvit*-CFSH1a might participate in the regulation of individual growth.

DATA AVAILABILITY STATEMENT

The datasets presented in this study can be found in online repositories. The names of the repository/repositories and accession number(s) can be found in the article/**Supplementary Material**.

AUTHOR CONTRIBUTIONS

FL contributed to conceptualization, methodology, software, validation, formal analysis, investigation, data curation, visualization, and writing—original draft preparation of the study. HY contributed to conceptualization, methodology, validation, data curation, writing—review and editing,

supervision, project administration, and funding acquisition. WS and LH contributed to investigation. GW contributed to funding acquisition. ZZ contributed to funding acquisition and provided resources. All authors contributed to manuscript revision, read, and approved the submitted version.

FUNDING

This work was supported by the Special Fund of Marine and Fishery Structure Adjustment in Fujian (2020HYJG01 and 2020HYJG08).

ACKNOWLEDGMENTS

We thank all laboratory members for their constructive suggestions and discussions. We are also grateful to the reviewers for their valuable suggestions.

SUPPLEMENTARY MATERIAL

The Supplementary Material for this article can be found online at: https://www.frontiersin.org/articles/10.3389/fmars.2021.791965/full#supplementary-material

REFERENCES

Alves, D. F. R., Greco, L. S. L., Barros-Alves, S. D., and Hirose, G. L. (2019). Sexual system, reproductive cycle and embryonic development of the red-striped shrimp *Lysmata vittata*, an invader in the western Atlantic Ocean. *PLoS One* 14:e0210723. doi: 10.1371/journal.pone.0210723

Bao, C. C., Liu, F., Yang, Y. A., Lin, Q., and Ye, H. H. (2020). Identification of peptides and their GPCRs in the peppermint shrimp *Lysmata vittata*, a protandric simultaneous hermaphrodite species. *Front. Endocrinol.* 11:226. doi: 10.3389/fendo.2020.00226

Barki, A., Karplus, I., Khalaila, I., Manor, R., and Sagi, A. (2003). Male-like behavioral patterns and physiological alterations induced by androgenic gland implantation in female crayfish. *J. Exp. Biol.* 206(Pt 11), 1791–1797. doi: 10.1242/jeb.00335

Barki, A., Karplus, I., Manor, R., and Sagi, A. (2006). Intersexuality and behavior in crayfish: the de-masculinization effects of androgenic gland ablation. *Horm. Behav.* 50, 322–331. doi: 10.1016/j.yhbeh.2006.03.017

Bauer, R. T. (2000). Simultaneous hermaphroditism in caridean shrimps: a unique and puzzling sexual system in the Decapoda. *J. Crustacean Biol.* 20, 116–128. doi: 10.1163/1937240x-90000014

Bornhorst, J. A., and Falke, J. J. (2000). Purification of proteins using polyhistidine affinity tags. *Methods Enzymol.* 326, 245–254. doi: 10.1016/s0076-6879(00)26058-26058

Chen, D. M., Liu, F., Zhu, Z. H., Lin, Q., Zeng, C. S., and Ye, H. H. (2019). Ontogenetic development of gonads and external sexual characters of the protandric simultaneous hermaphrodite peppermint shrimp, *Lysmata vittata* (Caridea: Hippolytidae). *PLoS One* 14:e0215406. doi: 10.1371/journal.pone.0215406

Chung, J. S. (2014). An insulin-like growth factor found in hepatopancreas implicates carbohydrate metabolism of the blue crab *Callinectes sapidus*. *Gen. Comp. Endocrinol.* 199, 56–64. doi: 10.1016/j.ygcen.2014.01.012

Fu, C. P., Li, F. J., Wang, L. F., Wu, F. R., Wang, J. M., Fan, X. L., et al. (2020). Molecular characteristics and abundance of insulin-like androgenic gland hormone and effects of RNA interference in *Eriocheir sinensis*. *Anim. Reprod. Sci.* 215:106332. doi: 10.1016/j.anireprosci.2020.106332

Heino, M., and Kaitala, V. (2001). Evolution of resource allocation between growth and reproduction in animals with indeterminate growth. *J. Evol. Biol.* 12, 423–429. doi: 10.1046/j.1420-9101.1999.00044.x

Huang, X. S., Ye, H. H., and Chung, J. S. (2017). The presence of an insulin-like androgenic gland factor (IAG) and insulin-like peptide binding protein (ILPBP) in the ovary of the blue crab, *Callinectes sapidus* and their roles in ovarian development. *Gen. Comp. Endocrinol.* 249, 64–70. doi: 10.1016/j.ygcen.2017.05.001

Jia, X. W., Chen, Y. D., Zou, Z. H., Lin, P., Wang, Y. L., and Zhang, Z. P. (2013). Characterization and expression profile of vitellogenin gene from *Scylla paramamosain*. *Gene.* 520, 119–130. doi: 10.1016/j.gene.2013.02.035

Jiang, Q. L., Lu, B., Lin, D. D., Huang, H. Y., Chen, X. L., and Ye, H. H. (2020). Role of crustacean female sex hormone (CFSH) in sex differentiation in early juvenile mud crabs, *Scylla paramamosain*. *Gen. Comp. Endocrinol.* 289:113383. doi: 10.1016/j.ygcen.2019.113383

Juchault, P. (1999). Hermaphroditism and gonochorism. A new hypothesis on the evolution of sexuality in *Crustacea*. *C. R. Acad. Sci. III Sci. Vie.* 322, 423–427. doi: 10.1016/s0764-4469(99)80078-x

Khalaila, I., Katz, T., Abdu, U., Yehezkel, G., and Sagi, A. (2001). Effects of implantation of hypertrophied androgenic glands on sexual characters and physiology of the reproductive system in the female red claw crayfish, *Cherax quadricarinatus*. *Gen. Comp. Endocrinol.* 121, 242–249. doi: 10.1006/gcen.2001.7607

Kotaka, S., and Ohira, T. (2018). cDNA cloning and in situ localization of a crustacean female sex hormone-like molecule in the kuruma prawn *Marsupenaeus japonicus*. *Fish. Sci.* 84, 53–60. doi: 10.1007/s12562-017-1152-1157

Levy, T., and Sagi, A. (2020). The "IAG-Switch"-A key controlling element in decapod crustacean sex differentiation. *Front. Endocrinol.* 11:651. doi: 10.3389/fendo.2020.00651

Levy, T., Tamone, S. L., Manor, R., Aflalo, E. D., Sklarz, M. Y., Chalifa-Caspi, V., et al. (2020). The IAG-switch and further transcriptomic insights into sexual differentiation of a protandric shrimp. *Front. Mar. Sci.* 7:587454. doi: 10.3389/fmars.2020.587454

Li, S. H., Li, F. H., Sun, Z., and Xiang, J. H. (2012). Two spliced variants of insulin-like androgenic gland hormone gene in the Chinese shrimp, *Fenneropenaeus chinensis*. *Gen. Comp. Endocrinol.* 177, 246–255. doi: 10.1016/j.ygcen.2012.04.010

Liu, A., Liu, J., Liu, F., Huang, Y. Y., Wang, G. Z., and Ye, H. H. (2018). Crustacean female sex hormone from the mud crab *Scylla paramamosain* is highly expressed in prepubertal males and inhibits the development of androgenic gland. *Front. Physiol.* 9:924. doi: 10.3389/fphys.2018.00924

Liu, F., Shi, W. Y., Ye, H. H., Liu, A., and Zhu, Z. H. (2021a). RNAi reveals role of insulin-like androgenic gland hormone 2 (IAG2) in sexual differentiation and growth in hermaphrodite shrimp. *Front. Mar. Sci.* 8:666763. doi: 10.3389/fmars.2021.666763

Liu, F., Shi, W. Y., Ye, H. H., Zeng, C. S., and Zhu, Z. H. (2021b). Insulin-like androgenic gland hormone 1 (IAG1) regulates sexual differentiation in a hermaphrodite shrimp through feedback to neuroendocrine factors. *Gen. Comp. Endocrinol.* 303:113706. doi: 10.1016/j.ygcen.2020.113706

Malecha, S. R., Nevin, P. A., Ha, P., Barck, L. E., Lamadridrose, Y., Masuno, S., et al. (1992). Sex-ratios and sex-determination in progeny from crosses of surgically sex-reversed fresh-water prawns, *Macrobrachium rosenbergii*. *Aquaculture* 105, 201–218. doi: 10.1016/0044-8486(92)90087-90082

Manor, R., Weil, S., Oren, S., Glazer, L., Aflalo, E. D., Ventura, T., et al. (2007). Insulin and gender: an insulin-like gene expressed exclusively in the androgenic gland of the male crayfish. *Gen. Comp. Endocrinol.* 150, 326–336. doi: 10.1016/j.ygcen.2006.09.006

Michalakis, K., Mintziori, G., Kaprara, A., Tarlatzis, B. C., and Goulis, D. G. (2013). The complex interaction between obesity, metabolic syndrome and reproductive axis: a narrative review. *Metab. Clin. Exp.* 62, 457–478. doi: 10.1016/j.metabol.2012.08.012

Nagamine, C., Knight, A. W., Maggenti, A., and Paxman, G. (1980). Masculinization of female *Macrobrachium rosenbergii* (de Man) (Decapoda, Palaemonidae) by androgenic gland implantation. *Gen. Comp. Endocrinol.* 41, 442–457. doi: 10.1016/0016-6480(80)90049-90040

Nguyen, T. V., Cummins, S. F., Elizur, A., and Ventura, T. (2016). Transcriptomic characterization and curation of candidate neuropeptides regulating reproduction in the eyestalk ganglia of the *Australian crayfish*, *Cherax quadricarinatus*. *Sci. Rep.* 6:38658. doi: 10.1038/srep38658

Rosen, O., Manor, R., Weil, S., Gafni, O., Linial, A., Aflalo, E. D., et al. (2010). A sexual shift induced by silencing of a single insulin-like gene in crayfish: ovarian upregulation and testicular degeneration. *PLoS One* 5:e15281. doi: 10.1371/journal.pone.0015281

Shi, W. Y., Liu, F., Liu, A., Huang, H. H., Lin, Q., Zeng, C. S., et al. (2020). Roles of gonad-inhibiting hormone in the protandric simultaneous hermaphrodite peppermint shrimp. *Biol. Reprod.* 103, 817–827. doi: 10.1093/biolre/ioaa111

Subramoniam, T. (2011). Mechanisms and control of vitellogenesis in crustaceans. *Fish. Sci.* 77, 1–21. doi: 10.1007/s12562-010-0301-z

Taketomi, Y., and Nishikawa, S. (1996). Implantation of androgenic glands into immature female crayfish, *Procambarus clarkii*, with masculinization of sexual characteristics. *J. Crustacean Biol.* 16, 232–239. doi: 10.1163/193724096X00027

Thongbuakaew, T., Suwansa-ard, S., Sretarugsa, P., Sobhon, P., and Cummins, S. F. (2019). Identification and characterization of a crustacean female sex hormone in the giant freshwater prawn, *Macrobrachium rosenbergii*. *Aquaculture* 507, 56–68. doi: 10.1016/j.aquaculture.2019.04.002

Tsutsui, N., Kotaka, S., Ohira, T., and Sakamoto, T. (2018). Characterization of distinct ovarian isoform of crustacean female sex hormone in the kuruma prawn *Marsupenaeus japonicus*. *Comp. Biochem. Physiol. A Mol. Integr. Physiol.* 217, 7–16. doi: 10.1016/j.cbpa.2017.12.009

Urtgam, S., Treerattrakool, S., Roytrakul, S., Wongtripop, S., Prommoon, J., Panyima, S., et al. (2015). Correlation between gonad-inhibiting hormone and vitellogenin during ovarian maturation in the domesticated *Penaeus monodon*. *Aquaculture* 437, 1–9. doi: 10.1016/j.aquaculture.2014.11.014

Veenstra, J. A. (2015). The power of next-generation sequencing as illustrated by the neuropeptidome of the crayfish *Procambarus clarkii*. *Gen. Comp. Endocrinol.* 224, 84–95. doi: 10.1016/j.ygcen.2015.06.013

Veenstra, J. A. (2016). Similarities between decapod and insect neuropeptidomes. *PeerJ* 4:e2043. doi: 10.7717/peerj.2043

Ventura, T., Cummins, S. F., Fitzgibbon, Q., Battaglene, S., and Elizur, A. (2014). Analysis of the central nervous system transcriptome of the eastern rock lobster *Sagmariasus verreauxi* reveals its putative neuropeptidome. *PLoS One* 9:e97323. doi: 10.1371/journal.pone.0097323

Ventura, T., Manor, R., Aflalo, E. D., Weil, S., Raviv, S., Glazer, L., et al. (2009). Temporal silencing of an androgenic gland-specific insulin-like gene affecting phenotypical gender differences and spermatogenesis. *Endocrinology* 150, 1278–1286. doi: 10.1210/en.2008-2906

Warrier, S., and Subramoniam, T. (2002). Receptor mediated yolk protein uptake in the crab *Scylla serrata*: crustacean vitellogenin receptor recognizes related mammalian serum lipoproteins. *Mol. Reprod. Dev.* 61, 536–548. doi: 10.1002/mrd.10106

Zhang, D., Sun, M., and Liu, X. (2017). Phase-specific expression of an insulin-like androgenic gland factor in a marine shrimp *Lysmata wurdemanni*: implication for maintaining protandric simultaneous hermaphroditism. *PLoS One* 12:e0172782. doi: 10.1371/journal.pone.0172782

Zmora, N., and Chung, J. S. (2014). A novel hormone is required for the development of reproductive phenotypes in adult female crabs. *Endocrinology* 155, 230–239. doi: 10.1210/en.2013-1603

Conflict of Interest: The authors declare that the research was conducted in the absence of any commercial or financial relationships that could be construed as a potential conflict of interest.

Publisher's Note: All claims expressed in this article are solely those of the authors and do not necessarily represent those of their affiliated organizations, or those of the publisher, the editors and the reviewers. Any product that may be evaluated in this article, or claim that may be made by its manufacturer, is not guaranteed or endorsed by the publisher.

frontiers in Physiology

ORIGINAL RESEARCH
published: 18 February 2022
doi: 10.3389/fphys.2022.805861

RNA Interference Analysis Reveals the Positive Regulatory Role of Ferritin in Testis Development in the Oriental River Prawn, *Macrobrachium nipponense*

Shubo Jin, Hongtuo Fu, Sufei Jiang, Yiwei Xiong, Hui Qiao, Wenyi Zhang, Yongsheng Gong and Yan Wu*

Key Laboratory of Freshwater Fisheries and Germplasm Resources Utilization, Ministry of Agriculture, Freshwater Fisheries Research Center, Chinese Academy of Fishery Sciences, Wuxi, China

OPEN ACCESS

Edited by:
Heinrich Dircksen, Stockholm University, Sweden

Reviewed by:
Gloria Yepiz-Plascencia, Centro de Investigación en Alimentación y Desarrollo, Consejo Nacional de Ciencia y Tecnología (CONACYT), Mexico
Tom Levy, Stanford University, United States

***Correspondence:**
Hongtuo Fu
fuht@ffrc.cn
orcid.org/000-0003-2974-9464

Specialty section:
This article was submitted to Aquatic Physiology, a section of the journal Frontiers in Physiology

Received: *31 October 2021*
Accepted: *25 January 2022*
Published: *18 February 2022*

Citation:
Jin S, Fu H, Jiang S, Xiong Y, Qiao H, Zhang W, Gong Y and Wu Y (2022) RNA Interference Analysis Reveals the Positive Regulatory Role of Ferritin in Testis Development in the Oriental River Prawn, Macrobrachium nipponense. Front. Physiol. 13:805861. doi: 10.3389/fphys.2022.805861

Ferritin plays an essential role in organismic and cellular iron homeostasis in *Macrobrachium nipponense*. In this study, we aimed to investigate the role of ferritin in the sexual development of male *M. nipponense*. According to the qPCR analysis of different tissues and developmental stages, ferritin exhibited high expression levels in the testis and androgenic gland, from post-larval developmental stage 5 (PL5) to PL15, indicating that it may be involved in gonad differentiation and development, especially in male sexual development. *In situ* hybridization and qPCR analysis in various reproductive cycles of the testis indicated that ferritin may play an essential role in spermatogonia development in *M. nipponense*. RNAi analysis revealed that ferritin positively affected mRNA expression of the insulin-like androgenic gland (*Mn-IAG*) and the secretion of testosterone, and thus positively affected testis development in *M. nipponense*. This study highlighted the functions of ferritin in the sexual development of male *M. nipponense* and provided important information for the establishment of a technique to regulate the process of testis development in *M. nipponense*.

Keywords: *Macrobrachium nipponense*, ferritin peptide, male sexual development, RNAi, testosterone

INTRODUCTION

The oriental river prawn, *Macrobrachium nipponense* (Crustacea; Decapoda; and Palaemonidae), is an important commercial species in China (Cai and Shokita, 2006; Salman et al., 2006; Ma et al., 2011), with an annual production of 225,321 tons in 2019 (Zhang et al., 2020). There are significant differences in growth performance of male and female *M. nipponense* in aquaculture systems. Compared to their female counterparts, male *M. nipponense* exhibit better growth performance (Ma et al., 2011). Rapid gonad development has negative effects on the sustainable development of the *M. nipponense* aquaculture industry. A previous study reported that the both testis and ovaries of prawns are mature at 40 days after hatching (Jin et al., 2016). This results in inbreeding between the newborn prawns. Inbreeding leads to multiple generations in the same pond and the degradation

of germplasm qualities, resulting in the prawns with smaller market size, and decreased ability to resist diseases (Fu et al., 2012; Jin et al., 2021a,b). Therefore, studies on the sexual development of male *M. nipponense* have received increased attention in recent years, with the aim of establishing an artificial technique to produce all male progeny on a commercial scale and regulate the process of testis development.

The androgenic gland has become a target tissue for studying male sexual differentiation and development in crustacean species in recent years. The hormones secreted by the androgenic gland have been reported to play positive regulatory roles in the processes driving male sexual differentiation and characteristics, in particular, the promotion of testes development in crustacean species (Sagi et al., 1986, 1990). Insulin-like androgenic gland hormone (*IAG*) is the main gene expressed and analyzed in the androgenic gland (Ventura et al., 2009, 2011; Rosen et al., 2010). It has been shown to play essential roles in promoting male sex determination and sex differentiation in most crustacean species, including *Fenneropenaeus chinensis* (Li et al., 2012), *Scylla paramamosain* (Huang et al., 2014), *Lysmata vittata* (Liu et al., 2021), *Fenneropenaeus merguiensis* (Zhou et al., 2021), and *M. nipponense* (Li et al., 2015a). Silencing of *IAG* in male *M. rosenbergii* by RNA interference (RNAi) may also lead to a complete sex reversal (Ventura et al., 2012). A previous study reported that *IAG* was expressed in the androgenic gland in *M. nipponense* (Ma et al., 2016). Thus, the genes in the androgenic gland have received a lot of attention in recent years and the transcriptome and miRNA library of the androgenic gland have been constructed for *M. nipponense* (Jin et al., 2013, 2015). A series of genes identified in the androgenic gland transcriptome have been analyzed and proven to be involved in the sexual development mechanisms of male *M. nipponense* (Jin et al., 2014, 2018b; Li et al., 2015a; Ma et al., 2016).

Previous studies have found that ferritin regulates cellular and organism-wide iron homeostasis, and thus protects cells from damage by excess iron (Picard et al., 1996; Konijn et al., 1999; Kakhlon et al., 2001; Torti and Torti, 2002). In addition, ferritin has multiple other functions, e.g., in development, cell activation, and angiogenesis (Parthasarathy et al., 2002; Coffman et al., 2008; Alkhateeb and Connor, 2010; Wang et al., 2010). A total of three ferritin subunits were identified in *M. nipponense*, including ferritin, ferritin light-chain subunit, and ferritin heavy-chain subunit. A previous study revealed that ferritin with accession no. KC825355 in GenBank plays an essential role in organismic and cellular iron homeostasis in *M. nipponense* (Sun et al., 2014). However, ferritin was also highly expressed in the androgenic gland, which is predicted to have additional roles in the mechanisms of sexual development in male *M. nipponense* (Jin et al., 2018a).

In this study, we aimed to further analyze the function of ferritin in *M. nipponense*, especially in relation to its role in male sexual development, using Quantitative real-time PCR (qPCR), *in situ* hybridization, and RNAi, combined with histological observations and testosterone measurements. The results of this study highlighted the functions of ferritin in *M. nipponense*, providing a basis for further studies on the mechanism of male sexual development in other crustacean species.

MATERIALS AND METHODS

Ethics Statement

Permission for all experiments involving *M. nipponense* was obtained from the Institutional Animal Care and Use Ethics Committee of the Freshwater Fisheries Research Center, Chinese Academy of Fishery Sciences (Wuxi, China).

The qPCR Analysis

The relative mRNA expression of *Mn-ferritin* was measured using qPCR. Different mature tissues included the testis, androgenic gland, ovary, intestine, hepatopancreas, and heart. The full-sibs population was hatched and cultured, and specimens at different larval and post-larval developmental stages were collected every 5 days during their maturation process. Testes were collected during the reproductive season in July, when the water temperature was $\geq$28°C and the illumination time was $\geq$16 h. Testes were also collected during the non-reproductive season in January, when the water temperature was $\leq$15°C and illumination time was $\leq$12 h. Samples of each tissue or stage were collected from fifty individual prawns. Ten prawns were pooled together to form one biological replicate, in order to minimize the effects of individual differences and five biological replicates were conducted. The procedures of RNA isolation and synthesizing cDNA have been described in detail in previous studies (Jin et al., 2014, 2018b). Briefly, total RNA was extracted from each tissue, using the UNlQ-10 Column TRIzol Total RNA Isolation Kit (Sangon, Shanghai, China) following the manufacturer's protocol. A total of 1 μg total RNA from each tissue was used to synthesize the cDNA template by using the PrimeScript RT reagent Kit (Takara Bio Inc., Japan). The expression level of each tissue was determined using the UltraSYBR Mixture (CWBIO, Beijing, China). All of the qPCR analyses in this study were performed on the Bio-Rad iCycler iQ5 Real-Time PCR System (Bio-Rad, Hercules, CA, United States), which was used to carry out the SYBR Green RT-qPCR assay. All qPCR reactions were run in three technical replicates. **Table 1** lists the primers used for qPCR analysis, including the eukaryotic translation initiation factor 5A (EIF 5A), which was identified as a suitable reference gene for PCR analysis in *M. nipponense* (Hu et al., 2018). The relative mRNA expressions of *Mn-ferritin* were calculated, based on the $2^{-\Delta\Delta CT}$ comparative CT method (Livak and Schmittgen, 2001).

In situ Hybridization

The mRNA locations of *Mn-ferritin* were analyzed by *in situ* hybridization. Paraformaldehyde (4%) (Sangon, Shanghai, China) was used to fix the tissue samples until the experiment was carried out. The androgenic gland and hepatopancreas were sampled during the reproductive season (28°C), while testes were collected from both of the reproductive season (28°C) and non-reproductive season (15°C). Procedures of primer design and *in situ* hybridization have been described in detail in previous studies (Jin et al., 2018b; Li et al., 2018). Briefly, Primer 5 software was used to design the anti-sense and sense probes with a DIG tag for the *in-situ* hybridization

TABLE 1 | Universal and specific primers used in this study.

Primer name	Nucleotide sequence (5′→3′)	Purpose	GenBank
Fer-RTF	CCGAAATCCGCCAGAACTAC	FWD primer for ferritin expression	KC825355
Fer-RTR	GCTTATCGGCATGCTCTCTC	RVS primer for ferritin expression	
Fer anti-sense probe	GCTGGCATACAATTCCATGTTGATCTGCTTGTTAATG	Probe for ferritin ISH analysis	
Fer sense probe	CATTAACAAGCAGATCAACATGGAATTGTATGCCAGC	Probe for ferritin ISH analysis	
Fer RNAi-F	TAATACGACTCACTATAGGGTGCTCTTCCTGGTATGTCCC	FWD primer for RNAi analysis	
Fer RNAi-R	TAATACGACTCACTATAGGGCCAAGCTCCTTGATGGACTC	RVS primer for RNAi analysis	
EIF-F	CATGGATGTACCTGTGGTGAAAC	FWD primer for EIF expression	MH540106
EIF-R	CTGTCAGCAGAAGGTCCTCATTA	RVS primer for EIF expression	

study, based on the cDNA sequence of *Mn-ferritin*. **Table 1** lists the primers used for *in situ* hybridization analysis, and the primers with DIG signals were synthesized by Shanghai Sangon Biotech Company. The anti-sense probe and sense probe were prepared for the experimental group and the control group, respectively. All of the collected testes (15 and 28°C), androgenic glands (28°C) and hepatopancreas (28°C) were embedded by paraffin. The *in situ* hybridization study was performed on 4 μm thick sections of paraffin-embedded tissues using the ZytoFast PLUS CISH implementation kit (ZytoVision GmBH, Bremerhaven, Germany), following the manufacturer's protocol. The sections were incubated in 3% H_2O_2 for 10 min. After rinsing in deionized water (DW), target retrieval was achieved using 0.5 mg/ml pepsin digestion in a humidity chamber for 10 min. The slides were incubated in EDTA solution at 95°C for 15 min after being washed in DW. The slides were then washed in DW, drained off, and 20 μL of CISH anti-sense probe and sense probe were poured over each slide. Denaturation was carried out at 75°C for 5 min, followed by hybridization at 37°C for 60 min in the ThermoBrite TM hybridization chamber (Vysis Inc, Downers Grove, IL, United States). Tris-buffered-saline (TBS) washing was carried out at 55°C for 5 min, and then at room temperature for five min. Mouse-anti-DIG (ZytoVision GmBH, Bremerhaven, Germany) was dropped over each slide, and incubated in a humidity chamber at 37°C for 30 min. Three washings were carried out with TBS, each lasting for 1 min, before and after incubating slides in anti-mouse-HRP-polymer for 30 min at room temperature. The 3,3′-diaminobenzidine (DAB) solution was prepared as per guidelines (ZytoFast PLUS CISH; ZytoVision GmbH) and 50 μL was poured over each slide for 10 min at room temperature. After washing, hematoxylin–eosin was used for counterstaining (see below for details). Slides were dehydrated in graded ethanol solutions, air dried and mounted with a mixture of distyrene, plasticizer, and xylene (DPX). Slides were examined under a light microscope.

RNA Interference Analysis

RNA interference was performed to analyze the novel regulatory roles of ferritin in the mechanism of sexual development in male *M. nipponense*. A specific RNAi primer with a T7 promoter site was designed in the open reading frame of *Mn-ferritin*, using Snap Dragon tools[1] (**Table 1**). The *Mn-ferritin* dsRNA was synthesized using the Transcript Aid^{TM} T7 High Yield Transcription kit (Fermentas Inc., Burlington, ON, Canada), based on the manufacturer's protocol. Six hundred healthy, mature, male *M. nipponense* with a bodyweight of 2.11–2.78 g were collected approximately 5 months after hatching from Tai Lake in Wuxi, China (120°13′44″E, 31°28′22″N). These male prawns were randomly divided into the RNAi group and 0.9% saline group with each group containing 300 prawns; 0.9% saline group was considered as the negative control. As described in a previous study (Jiang et al., 2014; Li et al., 2018), prawns from the RNAi group were injected with 4 μg/g *Mn-ferritin* dsRNA. Prawns from the control group were injected with an equal volume of 0.9% saline, according to the prawn's body weight. Androgenic gland samples were collected from both the control group and the RNAi group on days 1, 7, and 14, after 0.9% saline and *Mn-ferritin* dsRNA injection, and the *Mn-ferritin* mRNA expression was measured by qPCR, permitting confirmation of silencing efficiency. The androgenic gland samples were collected from five individual prawns and pooled together to form a biological replicate, and five biological replicates were performed. The mRNA expression of *Mn-IAG* was measured using the same cDNA templates in order to analyze the regulatory relationship between *Mn-ferritin* and *Mn-IAG*.

Testosterone Measurement

Testes were collected from the both control group and the RNAi group 1, 7, and 14 days after the injection of 0.9% saline and *Mn-ferritin* dsRNA, and stored at −20°C. Testes were collected from forty individual prawns at each time point in both control and RNAi groups. Eight prawns were pooled together to form one biological replicate, in order to produce a total tissue sample weight of 0.2 g, and five biological replicates were performed. The testosterone was extracted from the testes by adding 5 mL 100% methyl alcohol and fully grinding the sample. The ground samples were kept at 4°C for 4 h and centrifuged at 3,000 rpm for 5 min. The supernatant was collected and directly used to measure the content of testosterone. The testosterone concentration in triplicate samples was measured using an Access 2 Immunoassay System (Beckman Coulter, Inc., Brea, CA, United States) (Jin et al., 2019).

Hematoxylin and Eosin Staining

Hematoxylin and eosin staining was used to measure the morphological differences of the testis between the control group

[1]https://www.flyrnai.org/cgi-bin/RNAi_find_primers.pl

and RNAi group. The procedure of HE staining has been well described in previous studies (ShangGuan et al., 1991; Ma et al., 2006). Briefly, the tissues were first dehydrated by using 50, 70, 80, 95, and 100% ethanol. The tissues were then made transparent and embedded using alcohol: xylene (1:1), xylene, xylene: wax (1:1), and wax. The embedded tissues were sectioned to a thickness of 5 μm using a slicer (Leica, Wetzlar, Germany), and placed on a slide. The slides were then stained with HE for 3–8 min. The slides were observed under an Olympus SZX16 microscope (Olympus Corporation, Tokyo, Japan).

Statistical Analysis

SPSS Statistics 23.0 (IBM, Armonk, NY, United States) was used to conduct all statistical analyses. The test of homogeneity of variances was performed prior to ANOVA analysis and *t*-test (Sig. >0.05). Meanwhile, a linear regression analysis was performed on each set of data. The mean residual of each group data is close to 0, and the residual deviation is close to 1 for the linear regression analysis, indicating that the residuals of the data are normally distributed and can be analyzed. Statistical differences were identified by ANOVA analysis of variance followed by the least significant difference and Duncan's multiple range tests. The statistical difference between the control group and the RNAi group on the same day was assessed using the paired *t*-test. Quantitative data were expressed as mean ± standard deviation. A *P*-value < 0.05 was considered to be statistically significant.

RESULTS

Expression Analysis in Different Tissues

The physiological function of *Mn-ferritin* was reflected by tissue distribution in *M. nipponense*, verified by qPCR (**Figure 1A**). According to qPCR analysis, *Mn-ferritin* showed the highest expression level in the hepatopancreas ($P < 0.05$), followed by the testis and androgenic gland. The intestine had the lowest expression level. The mRNA expressions of *Mn-ferritin* in the testis and androgenic gland were over five times higher than that of the intestine ($P < 0.05$).

Expression Analysis in Developmental Stages

During the different developmental stages, *Mn-ferritin* expression was generally higher during the post-larval developmental stages than the larval developmental stages. *Mn-ferritin* expression remained stable during the larval developmental stages, with no significant difference in expression levels ($P > 0.05$). *Mn-ferritin* expression peaked during the post-larval developmental stage (PL) at PL5 ($P < 0.05$) and remained at a high level until PL15 (**Figure 1B**). *Mn-ferritin* expression level in the testis of the non-reproductive season was 2.43-fold higher than that in the testis of the reproductive season ($P < 0.05$) (**Figure 1C**).

In situ Hybridization Analysis

In situ hybridization was used to determine the mRNA locations of *Mn-Ferritin* in different tissues. According to the HE staining, the cell types in hepatopancreas were secretory cells, basement membrane, lumen, storage cells and transferred vacuoles, and strong DIG signals were also observed in these cells (**Figure 2**). Sperm was the dominant cell type in the testis of the reproductive season, as well as a small number of spermatogonia and spermatocytes. However, the dominant cell types in the testis of the non-reproductive season were spermatogonia and spermatocytes. The DIG signals in the testis of the non-reproductive season were stronger than that in the reproductive season. Androgenic gland cells and funicular structures were observed in the androgenic gland (**Figure 2**). Strong DIG signals

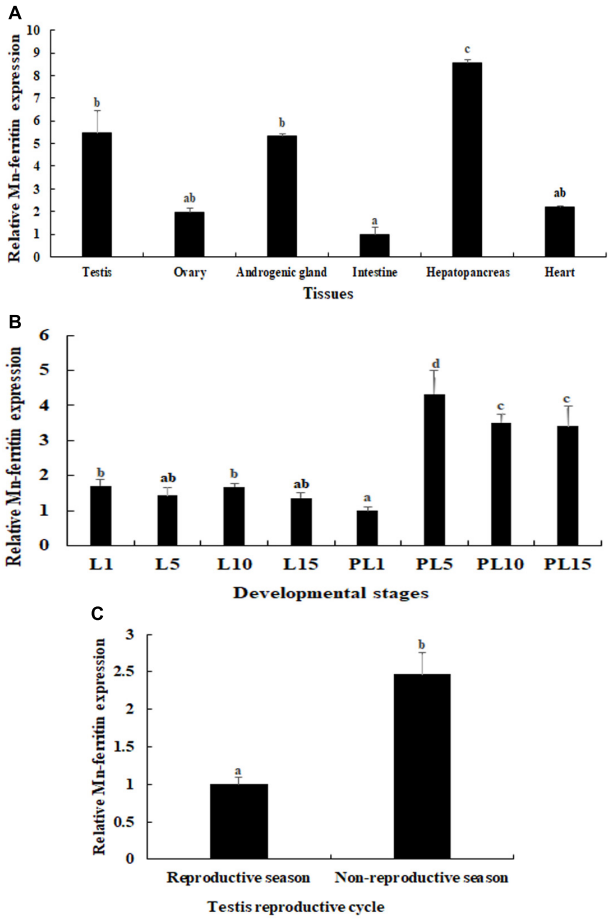

FIGURE 1 | qPCR analysis of *Mn-ferritin* in different tissues and developmental stages. The amount of *Mn-ferritin* mRNA was normalized to the *EIF* transcript level. Data are shown as mean ± SD (standard deviation) of tissues from five biological replicates. Letters indicate expression differences between different samples. Highest expression level of *Mn-ferritin* was observed in the hepatopancreas, followed by the testis and androgenic gland. *Mn-ferritin* expression was generally higher during the post-larval developmental stages than the larval developmental stages, and the expressions remained at a high level from PL5 to PL15. *Mn-ferritin* expression level in the testis of the non-reproductive season was significantly higher than that in the testis of the reproductive season. **(A)** Expression characterization in different tissues. **(B)** Expression characterization in different developmental stages. **(C)** Expression characterization in different reproductive seasons of testis.

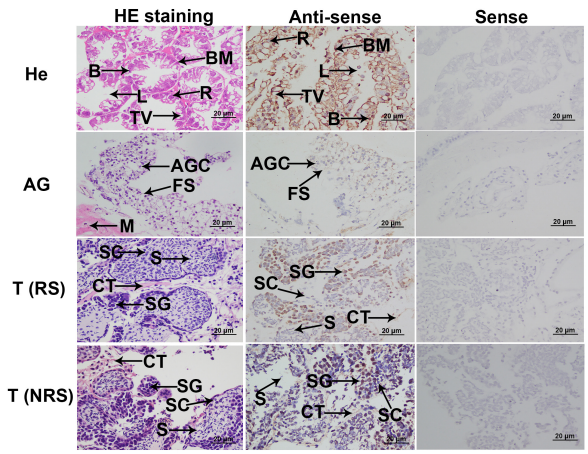

FIGURE 2 | *In situ* hybridization analysis of ferritin in *M. nipponense*. *In situ* hybridization analyses of ferritin were performed in hepatopancreas, testis, and androgenic gland. AG, androgenic gland; AGC, androgenic gland cells; B, secretory cells of type B; BM, basement membrane; CT, connective tissue; FS, funicular structure; He, hepatopancreas; L, lumen; M, muscle; R, storage cells of type R; T (NRS), testis of the non-reproductive season; T (RS), testis of the reproductive season; TV, transferred vacuoles; S, sperm; SC, spermatocyte; SG, spermatogonia. Scale bars = 20 μm. The positively stained cells with DIG signals in antisense labels are characterized by "brown color". Strong DIG signals were observed in all cell types of the hepatopancreas. Strong DIG signal was only observed in the spermatogonia in the testis of the non-reproductive season and reproductive season. Strong DIG signal was also observed in the funicular structure, surrounding the androgenic gland cells.

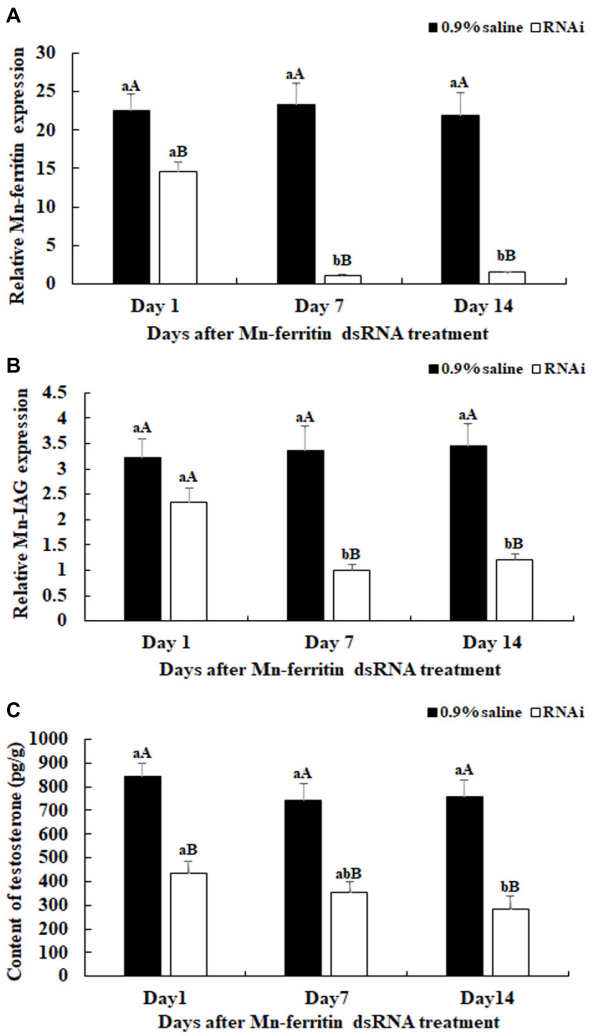

FIGURE 3 | Expression characterization of *Mn-ferritin* and *Mn-IAG*, and measurement of the contents of testosterone at different days after *Mn-ferritin* dsRNA injection. The amount of *Mn-ferritin* and *Mn-IAG* mRNA was normalized to the *EIF* transcript level. Data are shown as mean ± SD (standard deviation) of tissues from five biological replicates. Lowercases indicated significant expression difference among different time points in the same treated group and capital letters indicated the significant difference between the RNAi group and control group on the same day after treatment ($P < 0.05$). The *Mn-ferritin* expressions, *Mn-IAG* expressions, and the contents of testosterone showed slight differences on different days after the injection of 0.9% saline ($P > 0.05$). However, the *Mn-ferritin* expressions, *Mn-IAG* expressions, and the contents of testosterone were significantly decreased on different days after the injection of *Mn-ferritin* dsRNA, and showed significant differences on days 7 and 14 ($P < 0.01$), compared to those of 0.9% saline injection. **(A)** Expression characterization of *Mn-ferritin* after *Mn-ferritin* dsRNA injection. **(B)** Expression characterization of *Mn-IAG* after *Mn- ferritin* dsRNA injection. **(C)** Measurement of the contents of testosterone after *Mn-ferritin* dsRNA injection.

for *Mn-ferritin* were only observed in spermatogonia in the testis of *M. nipponense*, revealed by *in situ* hybridization analysis. No DIG signals were observed in spermatocytes and sperm. In the androgenic gland, no DIG signal was directly observed in the androgenic gland cells. In addition, strong DIG signals were observed in the funicular structure surrounding the androgenic gland cells (**Figure 2**). No DIG signals were observed when the sense RNA probe was used.

RNA Interference Analysis

This study aimed to analyze the potentially novel functions of *Mn-ferritin* during sexual development in male *M. nipponense* using RNAi. Male prawns were used for RNAi analysis. qPCR analysis revealed that *Mn-ferritin* expression remained at a stable level on different days after the treatment of 0.9% saline ($P > 0.05$). However, *Mn-ferritin* expressions were dramatically decreased after the treatment with *Mn-ferritin* dsRNA. *Mn-ferritin* expressions decreased over 90% at day 7 and day 14 after the *Mn-ferritin* dsRNA injection, compared with that of the 0.9% saline injection on the same day ($P < 0.01$) (**Figure 3A**).

Mn-IAG expression was measured using the same cDNA template after the injection of *Mn-ferritin* dsRNA. The qPCR analysis revealed that there were no significant differences in *Mn-IAG* expression on different days after the injection of 0.9% saline ($P > 0.05$). However, the *Mn-IAG* expressions in the RNAi group decreased with decreasing *Mn-Ferritin*. The *Mn-IAG* expression on day 1 in the RNAi group only decreased by 25%, compared with the injection of 0.9% saline on the same day. However, expression levels decreased by over 60% on days 7 and 14 and showed significant differences with the injection of 0.9% saline on the same day ($P < 0.01$) (**Figure 3B**).

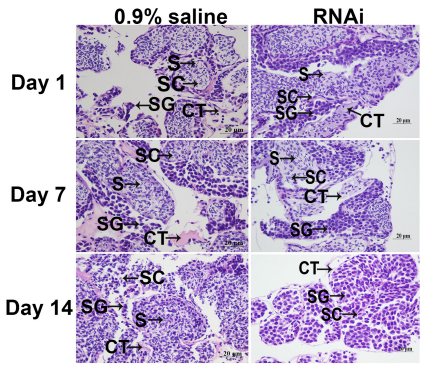

FIGURE 4 | Histological observations of testis between 0.9% saline and *Mn-ferritin* dsRNA treated group by HE staining. Sperm was the dominant cell type in the testis of 0.9% saline group, while the number of sperm gradually decreased from day 1 to 14 after the *Mn-ferritin* dsRNA injection. CT, connective tissue; S, sperm; SC, spermatocyte; SG, Spermatogonia. Scale bars = 20 μm.

Testosterone levels were measured on days 1, 7, and 14 after *Mn-ferritin* dsRNA injection. Testosterone levels significantly decreased (up to 60%) on days 7 and 14 in the RNAi group, compared with that of 0.9% saline injection on the same day ($P < 0.01$) (**Figure 3C**).

Histological Observations

There were no significant differences in the testis on different days in the control group. Sperm cells were the dominant cell type in the testis of the 0.9% saline injection. However, the number of sperm gradually decreased from day 1 to 14 after the *Mn-ferritin* dsRNA injection. The numbers of spermatogonia and spermatocytes were much higher than the number of sperm on day 7 in the RNAi group, and sperm was rarely recorded on day 14 in the RNAi group (**Figure 4**).

DISCUSSION

Ferritin has been confirmed to be involved in multiple physiological function regulation, such as development, cell activation, and angiogenesis (Parthasarathy et al., 2002; Coffman et al., 2008; Alkhateeb and Connor, 2010; Wang et al., 2010). Recent studies showed that it was differentially expressed in the proteomic profiling analysis of the androgenic gland between *M. nipponense* in reproductive season and non-reproductive season (Jin et al., 2018a). In addition, ferritin also showed a higher expression level in the androgenic gland than that of the testis and ovaries, verified by qPCR (Jin et al., 2018a). Thus, ferritin was predicted to be involved in the mechanism of male sexual development in *M. nipponense*, due to the positive regulatory role of the androgenic gland in male sexual development in crustacean species (Jin et al., 2018a). In the present study, we aimed to further investigate the potentially novel functions of ferritin in the mechanism of male sexual development of *M. nipponense*.

The tissue distributions of ferritin showed different expression patterns in various species. Ferritin exhibited the highest expression in the hemocytes of *L. vannamei* (Hsieh et al., 2006), while *Pacifastacus leniusculus* had the highest expression levels of ferritin in the hepatopancreas (Huang et al., 1996). In the current study, ferritin also showed the highest expression level in the hepatopancreas of *M. nipponense*, followed by the testis and the androgenic gland, whereas expression in the ovary was relatively low. Similar results were also obtained in *M. rosenbergii* (Qiu et al., 2008). However, the prawn hepatopancreas was not responsive to iron injections. Thus, the high expression of ferritin in the hepatopancreas could be regulated at the post-transcriptional level (Huang et al., 1999). Previous studies revealed that ferritin also showed the highest expression levels in the hepatopancreas, and the levels were upregulated after iron and pathogen challenge in *M. nipponense*, indicating that ferritin played essential roles in organismic and cellular iron homeostasis of *M. nipponense*, protecting the cells from damage by excess iron (Sun et al., 2014). In addition, the expressions of *Mn-ferritin* were higher in the testis and the androgenic gland than the other tested tissues ($P < 0.05$), except hepatopancreas in this study. This indicates that ferritin may have additional functions in the mechanism of male sexual development in *M. nipponense*, based on the essential roles of the testis and the androgenic gland on male sexual development in crustacean species. Furthermore, this indicates that iron homeostasis may mediate gonad development in *M. nipponense*. The *Mn-ferritin* expression in the testis was slightly higher than that in the androgenic gland in this study ($P > 0.05$), which is different from the previous study. A reasonable explanation for the difference is that the testis development is continuous. Thus, the cell numbers of spermatogonium, spermatocyte, and sperm in the testis of this study may be different from those in the previous study.

The ferritin expression has shown dramatic differences during different developmental stages of aquatic species. During continuous developmental stages, ferritin was expressed in the zoea stage, as well as the megalopa and juvenile crab I stage in *Scylla paramamosain* (Zhang et al., 2011). The ferritin of *Exopalaemon carinicauda* was rarely expressed at the gastrula and zoea stage, whereas it was significantly upregulated from the egg protozoea stage, and showed the highest expression level at the post-larvae stages (Zhang et al., 2015). In the present study, the expression level of ferritin remained stable and low during the larval developmental stages of *M. nipponense*, compared to those of the post-larval developmental stages. During the post-larval developmental stages, *Mn-ferritin* expression increased dramatically, peaked at PL5, and remained at a high level until PL15. *Mn-ferritin* exhibited higher expression levels during the post-larval developmental stages than the larval developmental stages. Histological observations during the larval and post-larval developmental stages of *M. nipponense* have proven that the sex-differentiation sensitive period of *M. nipponense* is from PL7 to PL22 (Jin et al., 2016), during which time the androgenic gland, testis, and ovary differentiated and matured. The dramatically high expression levels from PL5 to PL15 indicated that ferritin may play vital roles in gonad differentiation and development in *M. nipponense*.

The *in situ* hybridization analysis of ferritin has been reported for several species. A ferritin homolog is ubiquitously expressed

in *Branchiostoma belcheri* (Li et al., 2008). Ferritin mRNA is highly expressed in the mantle fold of *Pinctada fucata* (Zhang et al., 2003). L-ferritin mRNA was observed to be upregulated in iron-loaded rats. L-ferritin mRNA was localized in the colonic crypt, villus epithelial cells, small intestinal crypt, and surface epithelial cells (Jeffrey et al., 1996). In the present study, strong DIG signals for ferritin were observed in all cell types in the hepatopancreas, indicating that the hepatopancreas was the main organ for iron homeostasis in *M. nipponense*. Interestingly, strong DIG signals were only detected in spermatogonia in the testis of both reproductive season and non-reproductive season, indicating that ferritin may promote spermatogonia development or activate testis development. DIG signals in the testes from the non-reproductive season were stronger than those from the reproductive season. qPCR analysis revealed that *Mn-ferritin* in the testes of the non-reproductive season was higher than in those of the reproductive season, which is consistent with the *in situ* hybridization analysis. Histological observations revealed that the main cell type in the testis of the reproductive season was sperm, while spermatogonia and spermatocytes were the dominant cell type in the testis of the non-reproductive season (Jin et al., 2020). This result further confirmed that ferritin promoted spermatogonia development. Our data also showed that strong DIG signals were detected in the funicular structure surrounding the androgenic gland cells, while no signal was directly detected in the androgenic gland cells. Previous research indicated that the androgenic gland development began with the formation of the funicular structure, then androgenic gland cells were formed and filled the funicular structure (Jin et al., 2016). The *in situ* hybridization of ferritin in the androgenic gland of *M. nipponense* suggested ferritin played essential roles in the development of the funicular structure, most likely supporting the formation of androgenic gland cells.

RNA interference was efficiently used to analyze the gene functions through knockdown of the gene expression of target genes, which has been widely used in *M. nipponense* (Jiang et al., 2014; Li et al., 2015a, 2018). In this study, *Mn-ferritin* expression levels on days 7 and 14 in the RNAi group were significantly lower than the control group on the same day, indicating the dsRNA can efficiently inhibit *Mn-ferritin* expression. We also found that, after the injection of *Mn-ferritin* dsRNA, the *Mn-IAG* expressions decreased with decreasing *Mn-ferritin* expression, indicating that ferritin positively regulated *IAG* expression in *M. nipponense*. *IAG* has been reported to positively promote the male differentiation and development in crustacean species (Ventura et al., 2009, 2011). RNAi of *IAG* showed a significant inhibitory effect on male sexual differentiation and development of secondary sexual characteristics, including the formation of spermatogenesis in *M. rosenbergii* (Ventura et al., 2012). *IAG* has been proven to be expressed in the androgenic gland of *M. nipponense* (Ma et al., 2016). Furthermore, the expressions of *IAG* were regulated by the expressions of crustacean hyperglycemic hormone, gonad inhibiting hormone, and molting inhibiting hormone in *M. nipponense* (Li et al., 2015b). Our data also revealed that the testosterone levels in the RNAi group were lower than that of control group on the same day. Testosterone has been proven to result in sex reversal in *Oreochromis mossambicus* (Cao et al., 1994), allogynogenetic crucian carp (*Carassius auratus*) (Lou et al., 1994; Zhang et al., 2000), *Xiphophorus hellerii* (Han et al., 2010) and the grouper *Epinephelus akaara* (Li et al., 2006). In addition, testosterone promotes the development of testes and sperm in *Eriocheir sinensis*, and is involved in early gonad differentiation and development in *M. nipponense* (Jin et al., 2016). The positive regulatory roles between the expression of ferritin and *IAG*, and the secretion of testosterone indicated that ferritin was involved in the mechanism of male sexual development in *M. nipponense*. Histological observations of testis indicated that the number of sperm decreased dramatically after injection of *Mn-ferritin* dsRNA. Sperm was rarely found on day 14 after the injection of *Mn-ferritin* dsRNA. This indicates that ferritin was involved in the regulation of testis development in *M. nipponense* by inhibiting the expression of *Mn-IAG* and the secretion of testosterone, indicating iron homeostasis was involved in the process of testis development in *M. nipponense*.

CONCLUSION

We proved that ferritin played an essential role in the sexual development of male *M. nipponense*. Ferritin exhibited a positive regulation in *M. nipponense* testis development by regulating *Mn-IAG* expression and the secretion of testosterone, indicating that iron homeostasis was also involved in the testis development of *M. nipponense*. The present study provided an essential basis for the future establishment of novel techniques to regulate testis development in *M. nipponense*.

DATA AVAILABILITY STATEMENT

The original contributions presented in the study are included in the article/supplementary material, further inquiries can be directed to the corresponding author/s.

ETHICS STATEMENT

The animal study was reviewed and approved by the Institutional Animal Care and Use Ethics Committee of the Freshwater Fisheries Research Center, Chinese Academy of Fishery Sciences (Wuxi, China). Written informed consent was obtained from the owners for the participation of their animals in this study.

AUTHOR CONTRIBUTIONS

SBJ designed and wrote the manuscript. HF supervised the experiment. SFJ provided the experimental prawns. YX performed the qPCR analysis. HQ performed the *in situ* hybridization analysis. WZ performed the RNAi analysis. YG performed the histological observations. YW revised the manuscript. All authors contributed to the article and approved the submitted version.

FUNDING

This research was supported by grants from the Central Public-Interest Scientific Institution Basal Research Fund, CAFS (2021JBFM02 and 2020TD36), National Key R&D Program of China (2018YFD0900201), Jiangsu Agricultural Industry Technology System (JATS[2020]461), China Agriculture Research System-48 (CARS-48), and New Cultivar Breeding Major Project of Jiangsu Province (PZCZ2 01745).

REFERENCES

Alkhateeb, A. A., and Connor, J. R. (2010). Nuclear ferritin: a new role for ferritin in cell biology. *Biochim. Biophys. Acta* 1800, 793–797. doi: 10.1016/j.bbagen.2010.03.017

Cai, Y., and Shokita, S. (2006). Report on a collection of freshwater shrimps (Crustacea: Decapoda: Caridea) from the Philippines, with descriptions of four new species. *Raffles Bull. Zool.* 54, 245–270.

Cao, L. Q., Tao, Y. G., and Tan, H. Z. (1994). Studies on unisexualization in Red Tilapia. *J. Fish. China* 18, 75–80.

Coffman, L. G., Brown, J. C., Johnson, D. A., Parthasarathy, N., D'Agostino, R. B. Jr., Lively, M. O., et al. (2008). Cleavage of high-molecular-weight kininogen by elastase and tryptase is inhibited by ferritin. *Am. J. Physiol. Lung Cell. Mol. Physiol.* 294, L505–L515. doi: 10.1152/ajplung.00347.2007

Fu, H. T., Jiang, S. F., and Xiong, Y. W. (2012). Current status and prospects of farming the giant river prawn (*Macrobrachium rosenbergii*) and the oriental river prawn (*Macrobrachium nipponense*) in china. *Aquac. Res.* 43, 993–998. doi: 10.1111/j.1365-2109.2011.03085.x

Han, J., Xu, Y., Yu, Y. M., Xu, L. N., and Fang, Z. Q. (2010). Effects of 17 alpha-methyltestosterone on the reversal of male resistance in Viviparous Swordtail Fish (*Xiphophorus helleri*). *Acta Lab. Anim. Sci. Sin.* 18, 484–488.

Hsieh, S. L., Chiu, Y. C., and Kuo, C. M. (2006). Molecular cloning and tissue distribution of ferritin in Pacific white shrimp (*Litopenaeus vannamei*). *Fish Shellfish Immunl.* 21, 279–283. doi: 10.1016/j.fsi.2005.12.003

Hu, Y. N., Fu, H. T., Qiao, H., Sun, S. M., Zhang, W. Y., Jin, S. B., et al. (2018). Validation and evaluation of reference genes for Quantitative real-time PCR in *Macrobrachium nipponense*. *Int. J. Mol. Sci.* 19:2258. doi: 10.3390/ijms19082258

Huang, T. S., Law, J. H., and Soderhall, K. (1996). Purification and cDNA cloning of ferritin from the hepatopancreas of the freshwater crayfish *Pacifastacus leniusculus*. *Eur. J. Endocrinol.* 236, 450–456. doi: 10.1111/j.1432-1033.1996.00450.x

Huang, T. S., Melefors, O., Lind, M. I., and Soderhall, K. (1999). An atypical iron-responsive element (IRE) within crayfish ferritin mRNA and an iron regulatory protein 1 (IRP1)-like protein from crayfish hepatopancreas. *Insect Biochem. Mol. Biol.* 29, 1–9. doi: 10.1016/s0965-1748(98)00097-6

Huang, X. S., Ye, H. H., Huang, H. Y., Yang, Y. N., and Gong, J. (2014). An insulin-like androgenic gland hormone gene in the mud crab, *Scylla paramamosain*, extensively expressed and involved in the processes of growth and female reproduction. *Gen. Comp. Endocrinol.* 204, 229–238. doi: 10.1016/j.ygcen.2014.06.002

Jeffrey, G. P., Basclain, K. A., and Allen, T. L. (1996). Molecular regulation of transferrin receptor and ferritin expression in the rat gastrointestinal tract. *Gastroenterology.* 110, 790–800. doi: 10.1053/gast.1996.v110.pm8608889

Jiang, F. W., Fu, H. T., Qiao, H., Zhang, W. Y., Jiang, S. F., Xiong, Y. W., et al. (2014). The RNA interference regularity of transformer-2 gene of oriental river Prawn *Macrobrachium nipponense*. *Chin. Agric. Sci. Bul.* 30, 32–37.

Jin, S. B., Fu, H. T., Jiang, S. F., Xiong, Y. W., Qiao, H., Zhang, W. Y., et al. (2015). Identification of androgenic gland microRNAs and their targeted genes for discovery of sex-related microRNAs in oriental river prawn, *Macrobrachium nipponense*. *Genet. Mol. Res.* 14, 18396–18406. doi: 10.4238/2015.December.23.27

Jin, S. B., Fu, H. T., Zhou, Q., Sun, S. M., Jiang, S. F., Xiong, Y. W., et al. (2013). Transcriptome analysis of androgenic gland for discovery of novel genes from the Oriental River Prawn, *Macrobrachium nipponense*, using Illumina Hiseq 2000. *PLoS One* 8:e76840. doi: 10.1371/journal.pone.0076840

Jin, S. B., Hu, Y. N., Fu, H. T., Jiang, S. F., Xiong, Y. W., Qiao, H., et al. (2019). Potential functions of gem-associated protein 2-like isoform X1 in the Oriental River Prawn *Macrobrachium nipponense*: cloning, qPCR, *In Situ* Hybridization, and RNAi Analysis. *Int. J. Mol. Sci.* 20:3995. doi: 10.3390/ijms20163995

Jin, S. B., Hu, Y. N., Fu, H. T., Sun, S. M., Jiang, S. F., Xiong, Y. W., et al. (2020). Analysis of testis metabolome and transcriptome from the oriental river prawn (*Macrobrachium nipponense*) in response to different temperatures and illumination times. *Comp. Biochem. Phys. D* 34:100662. doi: 10.1016/j.cbd.2020.100662

Jin, S. B., Jiang, S. F., Xiong, Y. W., Qiao, H., Sun, S. M., Zhang, W. Y., et al. (2014). Molecular cloning of two tropomyosin family genes and expression analysis during development in oriental river prawn, *Macrobrachium nipponense*. *Gene* 546, 390–397. doi: 10.1016/j.gene.2014.05.014

Jin, S. B., Zhang, Y., Guan, H. H., Fu, H. T., Jiang, S. F., Xiong, Y. W., et al. (2016). Histological observation of gonadal development during post-larva in oriental river prawn, *Macrobrachium nipponense*. *Chin. J. Fish.* 29, 11–16.

Jin, S. B., Hu, Y. N., Fu, H. T., Jiang, S. F., Xiong, Y. W., Qiao, H., et al. (2021a). Identification and characterization of the succinate dehydrogenase complex iron sulfur subunit B gene in the Oriental River Prawn, *Macrobrachium nipponense*. *Front. Genet.* 12:698318. doi: 10.3389/fgene.2021.698318

Jin, S. B., Fu, H. T., Sun, S. M., Jiang, S. F., Xiong, Y. W., Gong, Y. S., et al. (2018b). iTRAQ-based quantitative proteomic analysis of the androgenic glands of the oriental river prawn, *Macrobrachium nipponense*, during nonreproductive and reproductive seasons. *Comp. Biochem. Phys. D* 26, 50–57. doi: 10.1016/j.cbd.2018.03.002

Jin, S. B., Fu, H. T., Jiang, S. F., Xiong, Y. W., Sun, S. M., Qiao, H., et al. (2018a). Molecular cloning, expression, and *in Situ* Hybridization analysis of forkhead box protein L2 during development in *Macrobrachium nipponense*. *J. World Aquacul. Soc.* 49, 429–440.

Jin, S. B., Hu, Y. N., Fu, H. T., Jiang, S. F., Xiong, Y. W., Qiao, H., et al. (2021b). Identification and Characterization Of The Pyruvate Dehydrogenase E1 gene in the Oriental River Prawn, *Macrobrachium nipponense*. *Front. Endocrinol.* 12:752501. doi: 10.3389/fendo.2021.752501

Kakhlon, O., Gruenbaum, Y., and Cabantchik, Z. I. (2001). Repression of the heavy ferritin chain increases the labile iron pool of human K562 cells. *Biochem. J.*356, 311–316. doi: 10.1042/0264-6021:3560311

Konijn, A. M., Glickstein, H., Vaisman, B., Meyron-Holtz, E. G., Slotki, I. N., and Cabantchik, Z. I. (1999). The cellular labile iron pool and intracellular ferritin in K562 cells. *Blood* 94, 2128–2134.

Li, F., Qiao, H., Fu, H. T., Sun, S. M., Zhang, W. Y., Jin, S. B., et al. (2018). Identification and characterization of opsin gene and its role in ovarian maturation in the oriental river prawn *Macrobrachium nipponense*. *Comp. Biochem. Phys. B* 218, 1–12. doi: 10.1016/j.cbpb.2017.12.016

Li, G. L., Liu, X. C., and Lin, H. R. (2006). Effects of 17α-methyltestosterone on sex reversal in red-spotted grouper, *Epinephelus akaara*. *J Fish China* 30, 145–150.

Li, M., Saren, G. W., and Zhang, S. C. (2008). Identification and expression of a ferritin homolog in amphioxus *Branchiostoma belcheri*: evidence for its dual role in immune response and iron metabolism. *Comp. Biochem. Phys. B* 150, 263–270. doi: 10.1016/j.cbpb.2008.03.014

Li, S. H., Li, F. H., Sun, Z., and Xiang, J. H. (2012). Two spliced variants of insulin-like androgenic gland hormone gene in the Chinese shrimp, *Fenneropenaeus chinensis*. *Gen. Comp. Endocrinol.* 177, 246–255. doi: 10.1016/j.ygcen.2012.04.010

Li, F. J., Bai, H. K., Xiong, Y. W., Fu, H. T., Jiang, F. W., Jiang, S. F., et al. (2015a). Molecular characterization of insulin-like androgenic gland hormone-binding protein gene from the oriental river prawn *Macrobrachium nipponense* and investigation of its transcriptional relationship with the insulin-like androgenic gland hormone gene. *Gen. Comp. Endocr.* 216, 152–160. doi: 10.1016/j.ygcen.2014.12.007

Li, F. J., Bai, H. K., Zhang, W. Y., Fu, H. T., Jiang, F. W., Liang, G. X., et al. (2015b). Cloning of genomic sequences of three crustacean hyperglycemic hormone superfamily genes and elucidation of their roles of regulating insulin-like androgenic gland hormone gene. *Gene.* 561, 68–75. doi: 10.1016/j.gene.2015.02.012

Liu, F., Shi, W., Ye, H., Liu, A., and Zhu, Z. (2021). RNAi reveals role of insulin-like androgenic gland hormone 2 (IAG2) in sexual differentiation and growth in hermaphrodite shrimp. *Front. Mar. Sci.* 8:666763.

Livak, K. J., and Schmittgen, T. D. (2001). Analysis of relative gene expression data using real-time quantitative PCR and the 2-ΔΔCT method. *Methods* 25, 402–408.

Lou, Y. D., Song, T. F., Wang, Y. M., Wei, H., Wu, M. C., Xu, H. M., et al. (1994). Studies on sex control in allogynogenetic crucian carp. *J Fish China* 3, 169–176.

Ma, K. Y., Feng, J. B., Lin, J. Y., and Li, J. L. (2011). The complete mitochondrial genome of *Macrobrachium nipponense*. *Gene* 487, 160–165. doi: 10.1016/j.gene.2011.07.017

Ma, K. Y., Li, J. L., and Qiu, G. F. (2016). Identification of putative regulatory region of insulin-like androgenic gland hormone gene (IAG) in the prawn *Macrobrachium nipponense* and proteins that interact with IAG by using yeast two-hybrid system. *Gen. Comp. Endocr.* 229, 112–118. doi: 10.1016/j.ygcen.2016.03.019

Ma, X. K., Liu, X. Z., Wen, H. S., Xu, Y. J., and Zhang, L. J. (2006). Histological observation on gonadal sex differentiation in Cynoglossus semilaevis Günther. *Mar. Fish. Res.* 27, 55–61.

Parthasarathy, N., Torti, S. V., and Torti, F. M. (2002). Ferritin binds to light chain of human Hkininogen and inhibits kallikrein-mediated bradykinin release. *Biochem. J.* 365, 279–286. doi: 10.1042/BJ20011637

Picard, V., Renaudie, F., Porcher, C., Hentze, M. W., Grandchamp, B., and Beaumont, C. (1996). Overexpression of the ferritin H subunit in cultured erythroid cells changes the intracellular iron distribution. *Blood* 87, 2057–2064. doi: 10.1182/blood.v87.5.2057.bloodjournal8752057

Qiu, G. F., Zheng, L., and Liu, P. (2008). Transcriptional regulation of ferritin mRNA levels by iron in the freshwater giant Prawn, *Macrobrachium rosenbergii*. *Comp. Biochem. Phys. B* 150, 320–325. doi: 10.1016/j.cbpb.2008.03.016

Rosen, O., Manor, R., Weil, S., Gafni, O., Linial, A., Aflalo, E. D., et al. (2010). A sexual shift induced by silencing of a single insulin-like gene in crayfish: ovarian upregulation and testicular degeneration. *PLoS One* 5:e15281. doi: 10.1371/journal.pone.0015281

Sagi, A., Cohen, D., and Milner, Y. (1990). Effect of androgenic gland ablation on morphotypic differentiation and sexual characteristics of male freshwater prawns, *Macrobrachium rosenbergii*. *Gen. Comp. Endocr.* 77, 15–22. doi: 10.1016/0016-6480(90)90201-v

Sagi, A., Cohen, D., and Wax, Y. (1986). Production of *Macrobrachium rosenbetgii* in momosex population: yield characteristes under intensive monoculture conditions in cages. *Aquaculture.* 51, 265–275.

Salman, S. D., Page, T. J., Naser, M. D., and Yasser, A. G. (2006). The invasion of *Macrobrachium nipponense* (De Haan, 1849) (Caridea: Palaemonidae) into the southern Iraqi marshes. *Aquat. Invasions* 1, 109–115.

ShangGuan, B. M., Liu, Z. Z., and Li, S. Q. (1991). Histological Studies on Ovarian Development in *Scylla serrata*. *J. Fish. Sci. China* 15, 96–103.

Sun, S. M., Gu, Z. M., Fu, H. T., Zhu, J., Xuan, F. J., and Ge, X. P. (2014). Identification and characterization of a *Macrobrachium nipponense* ferritin subunit regulated by iron ion and pathogen challenge. *Fish Shellfish Immunol.* 40, 288–295. doi: 10.1016/j.fsi.2014.07.002

Torti, F. M., and Torti, S. V. (2002). Regulation of ferritin genes and protein. *Blood* 99, 3505–3516. doi: 10.1182/blood.v99.10.3505

Ventura, T., Manor, R., Aflalo, E. D., Weil, S., Khalaila, I., Rosen, O., et al. (2011). Expression of an androgenic gland-specific insulin-like peptide during the course of prawn sexual and morphotypic differentiation. *ISRN Endocrinol.* 2011:476283. doi: 10.5402/2011/476283

Ventura, T., Manor, R., Aflalo, E. D., Weil, S., Raviv, S., Glazer, L., et al. (2009). Temporal silencing of an androgenic gland-specific insulin-like gene affecting phenotypical gender differences and spermatogenesis. *Endocrinology* 150, 1278–1286. doi: 10.1210/en.2008-0906

Ventura, T., Manor, R., Aflalo, E. D., Weil, S., Rosen, O., and Sagi, A. (2012). Timing sexual differentiation: full functional sex reversal achieved through silencing of a single insulin-like gene in the prawn, *Macrobrachium rosenbergii*. *Biol. Reprod.* 86:90. doi: 10.1095/biolreprod.111.097261

Wang, W., Knovich, M. A., Coffman, L. G., Torti, F. M., and Torti, S. V. (2010). Serum ferritin: past, present and future. *BBA Gen. Subjects* 1800, 760–769. doi: 10.1016/j.bbagen.2010.03.011

Zhang, D., Jiang, K. J., Zhang, F. Y., Ma, C. Y., Shi, Y. H., Qiao, Z. G., et al. (2011). Isolation and characterization of a ferritin cDNA from the Mud Crab *Scylla paramamosain*. *J. Crustacean Biol.* 31, 345–351.

Zhang, J. Q., Gui, T. S., Wang, J., and Xiang, J. H. (2015). The ferritin gene in ridgetail white prawn *Exopalaemon carinicauda*: cloning, expression and function. *Int. J. Mol. Sci.* 72, 320–325. doi: 10.1016/j.ijbiomac.2014.08.036

Zhang, P. Y., Hu, W., Wang, Y. P., and Zhu, Z. Y. (2000). Methyltestosterone induction of sex reversal in allogynogenetic crucian carp. *Hereditas* 22, 25–27.

Zhang, X. L., Cui, L. F., Li, S. M., Liu, X. Z., Han, X., Jiang, K. Y., et al. (2020). "Bureau of fisheries, Ministry of Agriculture, P.R.C. Fisheries Economic Statistics," in *China Fishery Yearbook*, eds X. J. Yu, L. J. Xu, F. X. Wu, D. D. Song, and H. Q. Gao (Beijing: China Agricultural Press), 24.

Zhang, Y., Meng, Q. X., Jiang, T. M., Wang, H. Z., Xie, L. P., and Zhang, R. Q. (2003). A novel ferritin subunit involved in shell formation from the pearl oyster (*Pinctada fucata*). *Comp. Biochem. Phys. B* 135, 43–54. doi: 10.1016/s1096-4959(03)00050-2

Zhou, T. T., Wang, W., Wang, C. G., Sun, C. B., Shi, L. L., and Chan, S. F. (2021). Insulin-like androgenic gland hormone from the shrimp *Fenneropenaeus merguiensis*: expression, gene organization and transcript variants. *Gene* 782:145529. doi: 10.1016/j.gene.2021.145529

Conflict of Interest: The authors declare that the research was conducted in the absence of any commercial or financial relationships that could be construed as a potential conflict of interest.

frontiers | Frontiers in Marine Science

ORIGINAL RESEARCH
published: 02 June 2022
doi: 10.3389/fmars.2022.880235

Acceleration of Ovarian Maturation in the Female Mud Crab With RNA Interference of the Vitellogenesis-Inhibiting Hormone (VIH)

*Supawadee Duangprom[1], Jirawat Saetan[2], Teva Phanaksri[1], Sineenart Songkoomkrong[1], Piyaporn Surinlert[1], Montakan Tamtin[3], Prasert Sobhon[4] and Napamanee Kornthong[1]**

[1] Chulabhorn International College of Medicine, Thammasat University, Rangsit Campus, Pathumthani, Thailand, [2] Division of Health and Applied Sciences, Faculty of Science, Prince of Songkla University, Hat Yai, Songkhla, Thailand, [3] Coastal Aquaculture Research and Development Regional Center 2 (Samut Sakhon), Department of Fisheries, Ministry of Agriculture and Cooperatives, Samut Sakhon, Thailand, [4] Department of Anatomy, Faculty of Science, Mahidol University, Bangkok, Thailand

OPEN ACCESS

Edited by:
Haihui Ye,
Jimei University, China

Reviewed by:
Xi Xie,
Ningbo University, China
Hanafiah Fazhan,
Shantou University, China

***Correspondence:**
Napamanee Kornthong
napamaneenatt@gmail.com

Specialty section:
This article was submitted to Aquatic Physiology, a section of the journal Frontiers in Marine Science

Received: 21 February 2022
Accepted: 19 April 2022
Published: 02 June 2022

Citation:
Duangprom S, Saetan J, Phanaksri T, Songkoomkrong S, Surinlert P, Tamtin M, Sobhon P and Kornthong N (2022) Acceleration of Ovarian Maturation in the Female Mud Crab With RNA Interference of the Vitellogenesis-Inhibiting Hormone (VIH). Front. Mar. Sci. 9:880235. doi: 10.3389/fmars.2022.880235

In the present study, double strand RNA technology (dsRNA) was used to inhibit transcripts of vitellogenesis-inhibiting hormone (VIH) that mainly synthesized and secreted from the central nervous system in *Scylla olivacea* females. The results presented in this study clearly demonstrate the potential dsRNA-VIH was highly effective to inhibit VIH in the eyestalks of females injected with dsRNA-VIH on the 3rd, 7th and 14th day, respectively. The dsRNA-VIH injections were performed at 14-day intervals, a single dsRNA dose of 0.6 μg/gram body weight was enough to suppress *VIH* expression until 14th day after injection. The dsRNA-VIH injection significantly increased gonad-somatic index (GSI) and hemolymph vitellin level at day 14 and 28 when compared with control groups. The histological observation found that the number of oocyte step 4 in dsRNA-VIH group was significantly higher than that of the control group. Also, dsRNA-VIH has stimulatory function on other reproduction-related genes such as the *ScyoI-PGES* and *ScyoI-ESULT* that both genes gradually increased their expressions in brain and ventral nerve cord. In conclusion, the silence of *VIH* gene could reduce the production of *VIH* from eyestalk and brain that affected other downstream genes related to ovarian maturation in the mud crab.

Keywords: vitellogenesis-inhibiting hormone (VIH), double strand RNA, *Scylla olivacea*, ovarian maturation, reproductive-related genes

INTRODUCTION

The vitellogenesis-inhibiting hormone (VIH), also known as gonad-inhibiting hormone (GIH), is produced and secreted by neuroendocrine cells of the X-organ-sinus gland complex (XO-SG) in the eyestalk of various crustaceans (Treerattrakool et al., 2011; Feijo et al., 2016). This peptide hormone is a member of crustacean hyperglycemic hormone (CHH) family which their candidates include the CHH, GIH/VIH, molt-inhibiting hormone (MIH), and mandibular organ-inhibiting hormone

(MOIH) (Kegel et al., 1989; Hsu et al., 2006; Webster et al., 2012). Commonly, the CHH family peptides, as well as the VIH, contain six cysteine residues forming three intramolecular disulfide bonds in their molecules (Lacombe et al., 1999; Webster et al., 2012). Functional studies of this peptide hormone family revealed diverse physiological involvements in crustaceans include metabolism, osmoregulation, molting, and reproduction (Chen et al., 2014). Considering the VIH function, it was mostly recognized as a potent negative regulator of crustacean reproduction (Chen et al., 2014). It has been reported that VIH diminished the synthesis of vitellogenin (VTG) from the ovary (Tsukimura, 2015). The characterization of VIH have been reported in several crustacean species such as *Penaeus monodon*, *Rimicaris kairei*, *Litopenaeus vannamei, Scylla paramamosain* and *Scylla olivacea* (Treerattrakool et al., 2008; Qian et al., 2009; Chen et al., 2014; Liu et al., 2018; Kornthong et al., 2019). The white leg shrimp, *L. vannamei*, presented high rate of ovarian maturation (Kang et al., 2014) and increased hepatopancreatic VTG expression (Chen et al., 2014) after the eyestalk ablation. Moreover, dsRNA-mediated *GIH* silencing have been reported to increase ovarian maturation and eventual spawning in both domesticated and wild female broodstock, particularly with a comparable effect to eyestalk ablation in wild shrimp in *P. monodon* (Treerattrakool et al., 2011).

Ovarian maturation period of mud crabs (*Scylla* spp.) is a time-consuming process which takes approximately 55-60 days depending on the environmental conditions, i.e., hormonal control, water salinity, natural diet, biochemical compositions, and enzyme activities (Nagaraju, 2011; Amin-Safwan et al., 2016; Azra and Ikhwanuddin, 2016; Hidir et al., 2018; Muhd-Farouk et al., 2019; Hidir et al., 2021). The vitellin (Vn), a set of multiple cleaved products of VTG, is a key molecule of crustacean yolk proteins that plays a significant role in the embryonic development (Volz et al., 2002; Quackenbush, 2015). In the *Scylla serrata*, vitellogenesis takes place in both hepatopancreas and ovary while the cleaved Vn subunits being processed in hepatopancreas, and hemolymph was sequestered by the growing oocytes (Rani and Subramoniam, 1997; Subramoniam, 2011). Therefore, various researchers have suggested that Vn is the major egg yolk protein and a high density lipoglycoprotein frequently associated with carotenoid pigments and the common form of yolk stored in oocytes and a nutrient source for developing embryos. In many species, VTG, the precursor molecule to Vn, is transported through the hemolymph to developing oocytes in the marine shrimp *Penaeus semisulcatus* (Avarre et al., 2003). Previous studies have found that high hemolymph VTG levels result to late ovarian development as histologically demonstrated by the vitellogenic oocytes become larger and they are filled with yolk globules in *Pandalus hypsinotus* and *Marsupenaeus japonicus* (Okumura et al., 2004; Okumura, 2007).

Normal processes of crab reproduction consume long period to complete its cycle. The eyestalk ablation, therefore, was introduced to remove the reproductive inhibiting hormones in crustaceans, including CHH peptide family-the VIH and MIH (Okumura and Aida, 2001; Nagaraju, 2011; Kang et al., 2014). By microarray analysis, ablation of eyestalk positively increased the vitellogenesis, ovarian weight as well as altered gene expressions that participate in reproduction, immune response and calcium signaling transduction in the *Penaeus monodon* (Uawisetwathana et al., 2011). Therefore, this procedure has been used for ripening ovarian development and maturation of many crustaceans i.e., the *P. monodon*, *Procambarus clarkia* and *M. japonicus* (Tan-Fermin, 1991; Okumura et al., 2007; Guan et al., 2017). Recent study also showed that eyestalk ablation in the freshwater crab, *Barytelphusa lugubris*, was able to induce breeding by rapid ripening the ovary and shortening the molting cycle (Rana, 2018). Besides, an alternative technique to eyestalk ablation by neuropeptide and hormone administration such as the serotonin (5-HT) and dopamine antagonist was also noted (Alfaro-Montoya et al., 2004).

The dsRNA technique has been used to silence the hormonal target transcripts by RNA interference (Alfaro-Montoya et al., 2004; Treerattrakool et al., 2011; Kang et al., 2021). This method post-transcriptionally silenced the target gene using specific dsRNA (Meister and Tuschl, 2004; Pak and Fire, 2007; Kang et al., 2019; Kang et al., 2021). The administration of dsRNA to silence *P. monodon GIH* gene was reported giving the known function of GIH in inhibiting *VTG* gene expression (Treerattrakool et al., 2008). In addition, the injections of dsRNA of *CHH1* and *MIH1* reduced the hemolymph glucose level and days of molting period in the *P. monodon*. The dsRNA of *GIH* gene application also promoted the *VTG* gene expression in the same species (Sukumaran et al., 2017). Although eyestalk ablation in crab is quite limited since it provides physiological abnormalities and low survival rate (Sroyraya et al., 2010). Using dsRNA to silence the *VIH* gene is therefore an alternative method to stimulate vitellogenesis and ovarian maturation in the female *S. olivacea*.

Therefore, in this study we successfully used specific dsRNA to knockdown the *VIH* transcript of *S. olivacea* and demonstrated its effects in temporary silencing *VIH* gene. In addition, the dsRNA-VIH could significantly increase Vn level in hemolymph and enhance ovarian maturation as well as promote some reproduction-related gene expression in the central nervous system of the female mud crab.

MATERIAL AND METHODS

Animals

The female mud crabs, *S. olivacea*, were cultured in Coastal Aquaculture Research and Development Regional Center 2, Samut Sakhon, Thailand. Identification of maturity stage of each crab was followed the previous study (Overton and Macintosh, 2002). All procedures on experimental animals were approved by Animal Care and Use Committee of Thammasat University, National Research Council of Thailand (NRCT), Protocol Number 020/2561 in which all efforts were made to minimize the suffering of animals. Crabs were

maintained in the concrete tanks filled with approximately 1000 L natural seawater (30 ppt) at 26-28°C, under a 12 h light and 12 h dark photoperiod. Crabs were fed twice daily (at 8:00 AM and 4:00 PM) with commercial fresh food throughout this study. The intermolt female mud crabs (n = 60) with average weight of 45-55 g were used in the dsRNA optimization assay. The mature female mud crabs at the same molting stage with average weight of 135-145 g, together with gonadsomatic index (GSI) less than 0.2, and the distance between the two tips of the 9th spine of anterolateral carapace approximately 85-92 mm (Ghazali et al., 2017; Amin-Safwan et al., 2018), were used to study the prolonged inhibitory effect of *VIH* knockdown and effect of dsRNA on ovarian maturation.

Construction of Recombinant Plasmids

To engineer the recombinant plasmid for dsRNAs expression, the DNA fragments corresponding to *VIH* sequence (380 bp) with loop sequence (580 bp) were amplified from pUC57 containing synthetic *VIH* gene (GenBank accession no. MH882453). The enhanced green fluorescent protein (EGFP) fragments with loop (570 bp) and without loop sequences (380 bp) were amplified by PCR using pUC-EGFP as the template. The specific primers used in this study were shown in **Table 1**. The PCR condition was set as follows: 95°C for 5 min, 35 cycles of 95°C for 30 s, 55°C for 30 s and 72°C for 1 min, followed by final extension at 72°C for 5 min. The PCR fragments (fragment with and without loop sequences) of *VIH* or *EGFP* were cloned into pET17b at *Xba*I and *Xho*I sites. The DNA fragments with and without loop sequence of each gene were linked together by using *Hind*III site to generate opposite direction. The ligated product was introduced into *Escherichia coli* DH5α for propagating the plasmids. The recombinant plasmids were digested with *Xba*I and *Xho*I and then confirmed the sequences by DNA sequencing. For template of dsRNAs production *in vitro*, both stem loop fragments were excised from pET17b and cloned into pDrive cloning vector at the *Xba*I and *Xho*I sites.

Production of DsRNA-VIH and DsRNA-EGFP

For *in vitro* dsRNA production, *Xho*I-linearized recombinant plasmids were used as the templates to produce the dsRNAs using SP6 RiboMAX^{TM} Express Large-Scale RNA Production System (Promega, USA) kit according to the manufacturer's protocol. The remaining template was removed by RQ1 RNase-free DNase (Promega, USA) treatment at 37°C for 15 min and dsRNA was extracted by TriPure Isolation reagent (Roche, Germany) as described by manufacturer's protocol. dsRNA pellet was solubilized by 150 mM NaCl and characterized by RNase III and RNase A digestion. dsRNA was verified the integrity by agarose gel electrophoresis and estimated the concentration by Nanodrop.

Dose Optimization of Double-Stranded RNAs (DsRNAs) and Prolonged Inhibitory Effect of DsRNAs

After acclimatization for 14 days, thirty-five crabs were divided equally into 7 groups (n = 5 each); (1) Vehicle control group, in which the animals were administered with 100 µl of 0.9% normal saline (NSS); (2-4) dsRNA-VIH groups in which the animals were administered with 100 µl of dsRNA-VIH at 0.2, 0.4, 0.6 µg/g BW dissolved in 0.9% normal saline; (5-7) dsRNA-EGFP groups in which the animals were administered with 100 µl of dsRNA-EGFP at 0.2, 0.4, 0.6 µg/g BW dissolved in 0.9% normal saline. Administration was performed intramuscularly at the base of the fifth walking leg. Animals were sacrificed at 24 h post injection, then the eyestalk and brain from individuals were collected for determining the *VIH* and *EGFP* genes expression. Prolonged inhibition effect of the dsRNAs was verified by the *VIH* and *EGFP* genes expression in both organs after 3rd day, 7th day and 14th day post injection.

VIH Gene Expression Analysis by Reverse Transcription-Polymerase Chain Reaction (RT-PCR)

Total RNA was extracted from eyestalk and brain using TriPure Isolation reagent (Roche, Germany), following the

TABLE 1 | Primers used for recombinant plasmids construction, RT-PCR and Real-time PCR.

Primer name	Size	Sequences
SO-dsVIH (580)-F (Xba)	580 bp	5′ACTGTCTAGAGATTTTTGTTCCTGTTCTGCATC 3′
SO-dsVIH (580)-R (Hin)		5′ATCGAAGCTTAGAAATGTCTCCTATTGGTGAGT 3′
SO-dsVIH-F (Xho)	380 bp	5′ATCGCTCGAGGATTTTTGTTCCTGTTCTGCATC 3′
SO-dsVIH-R2 (Hin)		5′ATCGAAGCTTACCCATTGCATCAGTTCCTTC 3′
dsEGFP-F (Xba)	570 bp	5′ACTGTCTAGAATGGTGAGCAAGGGCGAGGA 3′
dsEGFP-R (Hin)		5′ATCGAAGCTTGCCGATGGGGGTGTTCTGCT3′
dsEGFP-F (XhoI)	380 bp	5′ATCGCTCGAGATGGTGAGCAAGGGCGAGGA 3′
dsEGFP-R2 (Hin)		5′ATCGAAGCTTTTCAGCTCGATGCGGTTCACC 3′
β-actin-F	150 bp	5'GAGCGAGAAATCGTTCGTGACAT3'
β-actin-R		5'CCCATGGTGATGACCTGGCCGT3'
VIHq-F	153 bp	5'CACGTGGTGCATCAGCGCGA 3'
VIHq-R		5'GTACCGTCGTCAGCATGAGGGCG3'
PGE specific F:	166 bp	5'GCTGCTCGGTGTGGGTTTCGGT3'
PGE specific R:		5'GCAGCAAAATGGGCATGTCTGGTAC3'
ESULT-F	256 bp	5' GCGTGGCAGAAGAGGCACCA 3'
ESULT-R		5' TCCAGTCTCCCGTCTTGCCCT 3'

manufacturer's protocol, and kept at -80°C until use. The purity and quantity of RNA were measured by using a nanodrop spectrophotometer. Total RNA (2 μg) were synthesized the first-strand cDNA synthesis using QuantiNova Reverse Transcription Kit (Qiagen, Germany), following the manufacturer's protocol. To determine the inhibition effect of dsRNA-VIH and dsRNA-EGFP, the *VIH* gene expression was performed using VIHq-F and VIHq-R primers (**Table 1**). Thermocycling condition was set as follows: One cycle at 95°C for 5 minutes followed by 30 seconds at 94°C, 45 seconds at 55°C, and 30 seconds at 72°C for 35 cycles and a final extension of 10 minutes at 72°C. The PCR product was analyzed by electrophoresis with 1.5% agarose gels. The amplification of *β-actin* was used as internal control.

Effect of DsRNA-VIH on Ovarian Maturation Determining by Gonad Somatic Index (GSI) and Histological Analysis

Ninety crabs were divided equally into 3 groups (n = 30 each); (1) Vehicle control group in which the animals were administered with 100 μl of 0.9% normal saline (NSS); (2) dsRNA-VIH groups in which the animals were administered with 100 μl of dsRNA-VIH at 0.6 μg/g BW dissolved in 0.9% normal saline; (3) dsRNA-EGFP groups in which the animals were administered with 100 μl of dsRNA-EGFP at 0.6 μg/g BW dissolved in 0.9% normal saline. The injections were performed at day 0 and 14 of the experimental period, and ten crabs from each group were randomly collected and sacrificed at day 0, 14 and 28. Gonadal development was examined, based on external morphology (Stewart et al., 2007; Islam et al., 2010; Ghazali et al., 2017; Hidir et al., 2018) and routine histology (Saetan et al., 2017). To validate the histological differences between groups, the numbers of Oc1-Oc4 taken from ovary samples of day 0, 14 and 28 were randomly selected for four fields of non-consecutive sections (at a magnification of x200) taken from each crab (n=3). The sections were viewed and photographed under a Leica compound microscope equipped with a digital camera (Leica, Germany). Data on gonadosomatic index (GSI) was collected following the previous described protocol (Tinikul et al., 2016; Saetan et al., 2017). The eyestalk, brain, and ventral nerve cord (VNC) were collected for subsequent molecular analysis and the hemolymph was collected for Vn level measurement.

Standard Preparation of *S. olivacea* Vn

Different stages of *S. olivacea* ovaries (5 crabs each stage) were homogenized in 0.5 M Tris-HCl buffer containing 0.5 M NaCl, pH 7.5, at 4°C. Each homogenate was then centrifuged at 10,000 x g, for 30 min at 4°C, and the supernatant was retained for further purification. Western blot was used to test the specificity of anti-Vn which was raised against the *M. rosenbergii* Vn (anti-MrVn) in our laboratory (Soonklang et al., 2012). The 30 μg of ovarian total protein from stage 1 to stage 4 ovaries of ovary were loaded and run through the 12% tris-glycine gels for SDS polyacrylamide gel electrophoresis. Separated proteins were transferred to 0.45 μm nitrocellulose membrane and the membranes were blocked in 5% skim milk diluted in 0.1 M TBS containing 0.1% tween 20 (TBST) for 1 h and then were incubated in anti-MrVn (1:1000) diluted in blocking solution at 4°C for an overnight. After washing, the membranes were probed with the horseradish peroxidase (HRP)-conjugated goat anti-rabbit IgG (1:5000) (Abcam, USA) at room temperature for 1 h. The immunoreactive protein bands were visualized by adding the ECL chemiluminescence substrate (Thermo Fisher Scientific Inc., Pittsburgh, PA) and all bands were finally visualized by Amersham Imager (GE Healthcare, Sweden).

To separate the Vn and use as standard in ELISA, the early- and late-stage 4 ovarian extracts were pooled and concentrated by ultrafiltration through the molecular weight-cut off concentrator (Ultra-30kDa, Amicon), followed by a final buffer exchange with 50-mM Tris-HCl buffer, pH 7.5, at 4 °C. The concentrated extract was then fractionated by fast protein liquid chromatography (FPLC) (GE Healthcare, Sweden) on an ion exchange column (HiScreen^{TM} Q HP columns, 100mm x 7.7 mm i.d., GE Healthcare, Sweden) equilibrated with 50-mM Tris-HCl buffer, pH 7.5, as described by (Chen and Kuo, 1998). The percentage of solution A (Tris-HCl) was gradually decreased from 100 to 0, while the percentage of solution B, elution buffer (Tris-HCl + 1N NaCl) was gradually increased from 0 to 100 at a flow rate of 1 mL/min, for 35 min with absorbencies monitored at 280 nm and 474 nm (Chen and Kuo, 1998). Presence of the *S. olivacea* Vn in each fraction was tested by dot blot. One hundred nanogram of each fraction collected from 22nd to 28th min was dotted onto a 0.45 μm PVDF membrane (Merck, Darmstadt, Germany). The membranes were blocked for non-specificity by incubating with 5% skim milk in TBST for 1 h at room temperature. The membranes were then incubated with anti-MrVn, at a 1:1000 dilution, for overnight at 4°C. Horseradish peroxidase (HRP)-conjugated goat anti-rabbit IgG (Abcam, USA) was applied, at a 1:5,000 dilution, for 1 h at room temperature. An enhanced chemiluminescence kit (Thermo Fisher Scientific Inc., Pittsburgh, PA) was used to develop the membranes and the result was detected and photographed by Amersham Imager (GE Healthcare, Sweden).

Effect of DsRNA-VIH on Ovarian Maturation Determining by Vn Level in Hemolymph

The hemolymph Vn level of female *S. olivacea* was determined by an indirect ELISA (Tinikul et al., 2016; Saetan et al., 2017) with some modifications. Hemolymph was collected from the base of the fifth walking leg and transferred into a vial containing anticoagulant solution [0.45 M NaCl, 0.1 M glucose, 30 mM tri-sodium citrate, 26 mM citric acid and 10 mM EDTA (pH4.6)] at equal volume as hemolymph. The mixture was separated by centrifugation at 9000 x g, 4°C, 10 min and the supernatants were frozen at -20°C. One hundred microliters of all supernatant, and our purified Vn with known concentration, were diluted in coating buffer (15 mM Na_2CO_3 and 35 mM $NaHCO_3$, pH 9.6) and coated on 96 well ELISA plate for overnight at 4°C. Each well was subsequently washed three times with 0.01 M PBS containing 0.05% tween 20 (PBST) and blocked non-specific binding with 0.25% bovine serum albumin (BSA) in PBST, at 37°C for 30 minutes. The primary antibody (anti-MrVn) diluted at 1:2000 in blocking buffer was

applied and incubated at 37°C for 2 h. The goat anti-rabbit IgG-HRP (Abcam, USA) diluted at 1:10000 in blocking buffer was added to each well and incubated at 37°C for 1 h. The plate was then washed in triplicate and the color was developed by adding TMB substrate for 15 min. The reaction was stopped by adding 1 N HCl. Then, the absorbance was measured by microplate spectrophotometer (Thermo Fisher, USA) at a wavelength of 450 nm. Calculation of the Vn level of each sample was based on the standard curve of purified Vn. Determination of hemolymph Vn level was performed in triplicate.

Relative Abundance of Reproductive-Related Genes Expression Following DsRNA-VIH Administration

To study the effect of dsRNA-VIH on gene expression, the *S. olivacea* reproduction genes were selected from previous reports (Kornthong et al., 2014; Duangprom et al., 2018). The brain and ventral nerve cord (VNC) were collected from day 0, 7 and 14 of the experimental periods. The cDNAs were then prepared as described in the previous section of this manuscript. Real-time PCR for amplification of reproduction related genes, including *S. olivacea prostaglandin E synthase* (*Scyol-PGES)* and *S. olivacea estrogen sulfotransferase (Scyol-ESULT)* was performed in duplicate for each sample (n = 10 per group). Amplifications were conducted on a CFX-96 (Bio-Rad, USA) using iTaq Universal SYBR Green Supermix (Bio-Rad, USA). *Scyol-PGES* and *Scyol-ESULT* primers were shown in **Table 1**. Relative expression of *Scyol-PGES* and *Scyol-ESULT* against *β-actin* expression and a variance between individual treatments were performed, calculated, and statistically analyzed followed the methods described in (Kornthong et al., 2013; Kornthong et al., 2014; Duangprom et al., 2017; Duangprom et al., 2018).

Statistical Analysis

Values of the GSI, hemolymph Vn and relative gene expression levels of *Scyol-PGES* and *Scyol-ESULT* genes to *β*-actin, in different sample groups were tested by one-way analysis of variance (ANOVA) followed by Tukey test. All tests were performed using GraphPad Prism 9.0 software for Windows (GraphPad Software, USA). Mean values were identified as significantly different if the *p*-value was less than 0.05.

RESULTS

Determination of DsRNA-VIH and DsRNA-EGFP Production

The coding sequence of *S. olivacea VIH* (MH882453; nucleotide 167 to 537) were used as the template for dsRNA-VIH production. To determine the quality of dsRNA, a large fragment of the dsRNA-VIH (380 bp) genes and dsRNA-EGFP (380 bp) were amplified using RT-PCR. After purification, the non-digested, RNase A-digested and RNase III-digested dsRNAs were visualized by agarose gel electrophoresis (**Figure 1**). The non-digested dsRNA-VIH and dsRNA-EGFP were shown approximately 1200 bp in lane 1 and 4 (**Figure 1**), while those of RNase A-digested dsRNA-VIH and dsRNA-EGFP were shown approximately 600 bp in lane 2 and 5 (**Figure 1**). Lastly, there was no band detected for both RNase III-digested dsRNA-VIH and dsRNA-EGFP (**Figure 1**, lane 3 and 6).

Dose-Dependent Study of the DsRNA Induced *VIH* Knockdown and Prolonged Inhibitory Effect of *VIH* Knockdown

To determine the potent dose of dsRNA-VIH in sequestering the *S. olivacea* VIH expression, we administrated different doses of 0.2, 0.4, and 0.6 μg/g BW for the dsRNA-VIH and those of 0.2, 0.4 and 0.6 μg/g BW for dsRNA-EGFP and vehicle control (NSS) for injecting the female mud crabs. At 24 h post-injection, the VIH expressions of eyestalk and brain were inhibited by the 0.6 μg/g BW of dsRNA-VIH (**Figures 2A, B**). On the contrary, 0.2 and 0.4 μg/g BW of dsRNA-VIH failed to inhibit the VIH expressions in both organs (**Figures 2A, B**). According to these, the 0.6 μg/g BW of dsRNA-VIH was retained for further experiments. The selected dose of 0.6 μg/g BW dsRNA-VIH successfully displayed the prolonged inhibitory effect of *VIH* knockdown in the eyestalk for 3-, 7- and 14-days post-injection (**Figure 3**). However, at day 14 one of three crab was able to express VIH again while the remaining two ones were not (**Figure 3**). The irrelevant dsRNA-EGFP and vehicle control (NSS) had no effect on VIH inhibition (**Figures 2A, B**, and **3**).

Validation of the Anti-MrVn and Standard Vn Preparation

To determine the antibody reactivity between anti-MrVn and *S. olivacea* Vn, the western blot analysis was performed. The anti-MrVn was able to depict 2 molecular subunits of Vn comprising the 85 kDa and 105 kDa respectively. In stage 1 of ovary, the Vn subunits were not appeared. In stage 2-3 of ovary, the two subunits of Vn were slightly observed while they were mostly

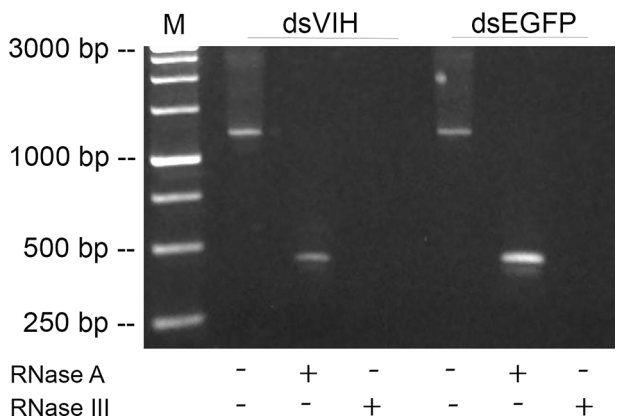

FIGURE 1 | Visualization of the dsRNA production. Lane M was the 3kb DNA ladder marker. Lanes 1 and 4 were shown approximately 1200 bp of non-digested dsRNA-VIH and dsRNA-EGFP. Lanes 2 and 5 were shown approximately 600 bp of RNase A-digested dsRNA-VIH and dsRNA-EGFP. Lanes 3 and 6 were the RNase III-digested dsRNA-VIH and dsRNA-EGFP revealed no product detected.

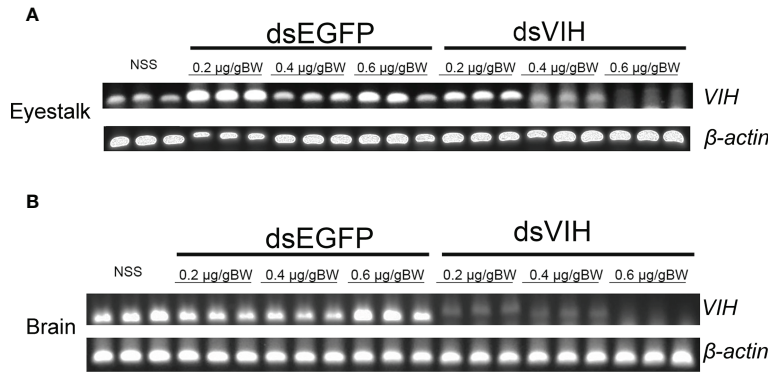

FIGURE 2 | Dose-dependent effects of dsRNA-VIH, dsRNA-EGFP, and vehicle control (NSS) in sequestering the *VIH* gene expression in **(A)** eyestalk and **(B)** brain. In both organs, the most potent dose of dsRNA-VIH to inhibit the *VIH* gene expression was 0.6 µg/g BW. No inhibitory effect on *VIH* gene expression was observed by the injection of either the dsRNA-EGFP and vehicle control (NSS).

intensely expressed in the stage 4 of ovary (**Figure 4A**). Fractionation of the *S. olivacea* Vn by ion exchange FPLC and dot blot with MrVn antibody revealed the immunoreactivity in the fractions of 24-28 min (**Figure 4B**) Therefore, these fractions were combined, measured the concentration and used as standard Vn in ELISA.

Effect of DsRNA-VIH on Ovarian Development of the *S. olivacea*

At day 14 and day 28 post injection, the ovarian development was determined by GSI value and hemolymph Vn level. The dsRNA-VIH treated crabs significantly produced higher GSI compared with the control group (**Figure 5A**). Moreover, the

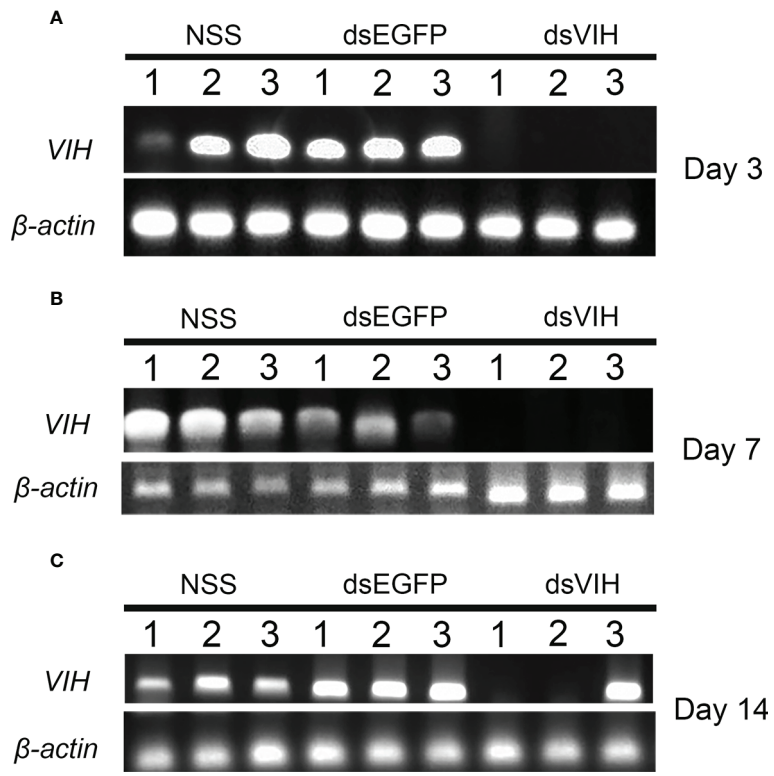

FIGURE 3 | Prolonged effect of the 0.6 µg/g BW of dsRNA-VIH on inhibiting the eyestalk *VIH* gene expression at day 3 **(A)**, day 7 **(B)** and day 14 **(C)** post-injection. No inhibitory effect on *VIH* gene expression was observed by the injection of either the dsRNA-EGFP and vehicle control (NSS).

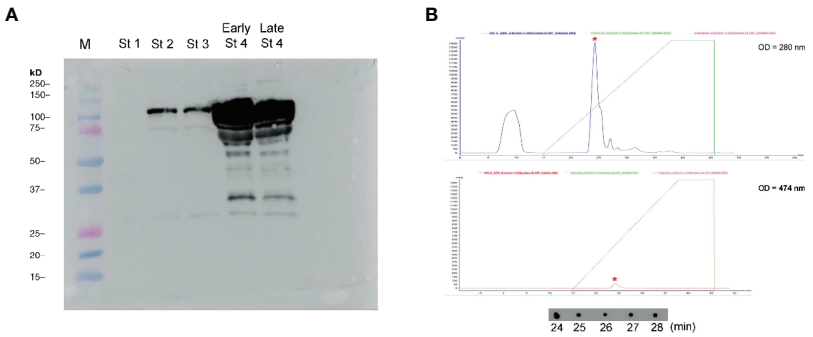

FIGURE 4 | **(A)** Validation of anti-MrVn in probing the Vn subunits of the *S. olivacea*, lane M referred to molecular ladder, St1-Late St4 referred to the ovary samples taken from stage 1 to late stage 4, respectively. **(B)** Chromatogram of ovarian extract of *S. olivacea* as fractionated by ion exchange FPLC on a HiScreen™ Q HP columns and monitored at wavelengths of 280 nm and 474 nm, respectively. Asterisk showed the immunoreactive peak whose fractions (24-28 min) were confirmed by dot blot with anti-MrVn.

hemolymph Vn level of the dsRNA-VIH treated crabs at day was significantly greater than that of the control crabs at the same day of comparison (**Figure 5B**).

Moreover, the histology of ovaries was observed at day 0, day 14 and day 28 of the experimental period. The histology of *S. olivacea* ovary, including oogonia and four steps of developing oocyte (Oc1-Oc4) was analyzed according to the previous reports (Stewart et al., 2007; Saetan et al., 2017). At day 0, ovaries in dsRNA-VIH and 0.9% normal saline (NSS) injected groups, showed three steps of oocyte (Oc1-Oc3) and oogonia (Og). The number of each stage of oocyte was similar between these two groups. (**Figures 6A, B**). At day 14, the NSS injected group showed Oc1-Oc3 in the ovaries, while the dsRNA-VIH injected group showed Oc4 that are fully mature oocyte (**Figures 6C, D**). At day 28, the NSS injected group showed Oc4 and some of Oc1-Oc2 in the ovaries, while the dsRNA-VIH injected group showed only Oc4 in the ovaries (**Figures 6E, F**). The number of Oc4 observed in the ovaries of dsRNA-VIH injected groups were significantly higher than those observed in the ovaries of females injected with NSS on the day 14, and 28 (**Figures 6G–I**).

Effect of DsRNA-VIH on the Upregulation of Reproductive-Related Genes

To study the effect of dsRNA-VIH, relative abundances of the *S. olivacea prostaglandin E synthase* (*Scyol-PGES)* and *S. olivacea estrogen sulfotransferase (Scyol-ESULT)* transcripts in brain and ventral nerve cord (VNC) were validated. The relative abundances of these two genes were normalized using abundance of *β-actin* transcript for both treatment and control groups. After dsRNA-VIH administration at day 7, relative abundance of the *Scyol-PGES* in the brain and VNC was greater when compared with those expressed in control crabs (**Figures 7A, B**). The relative abundance of *Scyol-ESULT* of dsRNA-VIH group in the brain and VNC were also significantly greater than those of control group at day 7 and day 14 post-injection (**Figures 7C, D**).

DISCUSSION

In this study, we demonstrated the use of dsRNA-VIH to promote ovarian development in the *Scylla olivacea*. As the reproduction of crustaceans was naturally promoted by groups of neurotransmitter (NT)/neurohormone (NH) i.e., the

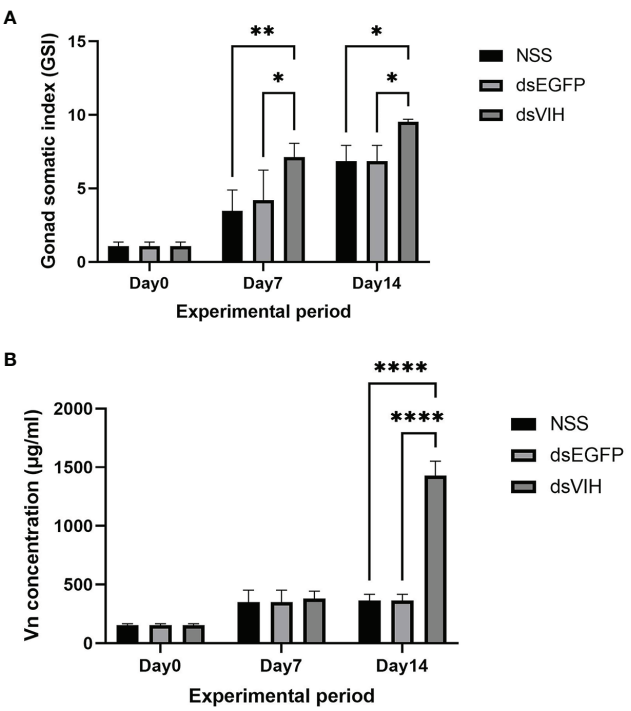

FIGURE 5 | The effects of dsRNA-VIH on **(A)** GSI and **(B)** hemolymph Vn level of the dsRNA-VIH treated crabs and control crabs at day 14 and day 28 post-injection. Bars represented the standard error of the mean (SEM). *$p < 0.05$ **$p < 0.005$, and ****$p < 0.0001$.

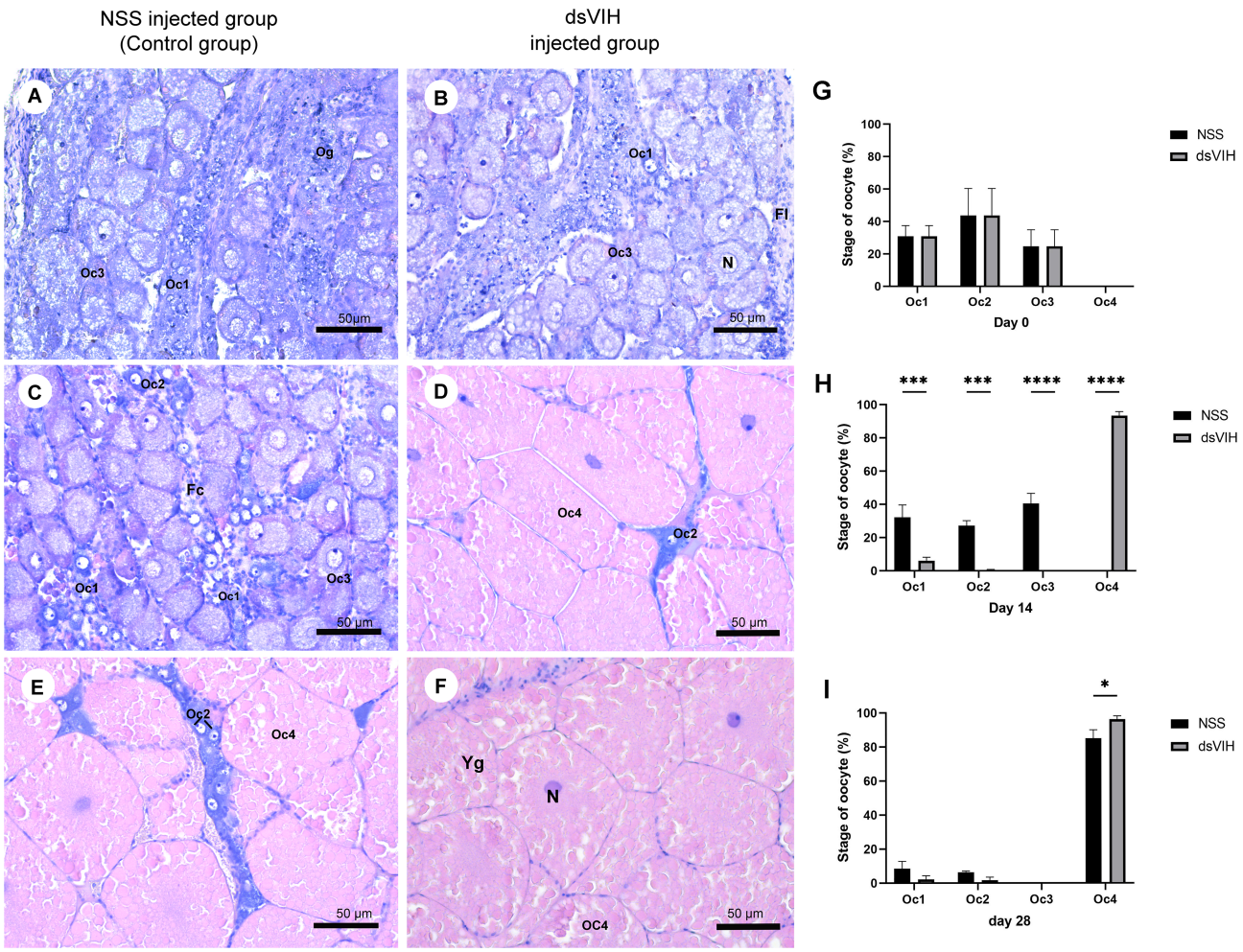

FIGURE 6 | Histological analysis of the ovaries of dsRNA-VIH and NSS treated crabs. A representative sample from each group is shown. **(A, B)** At day 0, ovaries in both group showed oogonia (Og) and three steps of oocyte (Oc1-Oc3) **(C, D)** At day 14, NSS injected group and dsRNA-VIH injected group showed Oc1 that clearly displayed euchromatic nucleus, Oc2 that was oval and was surrounded by follicular cells, Oc3 that was oval and it contained mostly euchromatin and prominent nucleolus with small lipid droplets in cytoplasm, and Oc4 that was fully mature oocyte with large spherical ovoid shape and heavy lipid droplets in cytoplasm. **(E, F)** At day 28, the dsRNA-VIH injected group showed more Oc4 than that of the NSS injected group while the latter also showed some pre-mature stage (Oc1-Oc2). **(G–I)** Quantification of the oocyte stage on day 0, 14 and 28. Asterisks indicate significant differences compared to the NSS injected group and dsRNA-VIH injected group with $^{*}p < 0.05$, $^{***}p < 0.001$, $^{****}p < 0.0001$. Oocyte developmental features are indicated as Yg, yolk granule oocyte; Oc, oocyte, Og, oogania; Fc, foccicle cell; N, nucleus.

serotonin (Tinikul et al., 2016), the GnRH-like peptide (Guan et al., 2014; Bao et al., 2015), the RPCH (Zeng et al., 2016; Jayasankar et al., 2020) while it was together suppressed by some particular NT/NH, i.e., the dopamine (Alfaro-Montoya et al., 2004; Tinikul et al., 2016), oxytocin/vasopressin-like peptide (Saetan et al., 2018; Lin et al., 2020; Saetan et al., 2021) and the VIH (Kang et al., 2021). In the mud crab, the *VIH* gene was characterized and demonstrated its expression in the eyestalk, brain, and ventral nerve cord (VNC) (Kornthong et al., 2019) while this gene expressed specifically in the eyestalk of the *S. paramamosain* (Liu et al., 2018). The expression of *VIH* gene detected in eyestalk, brain, VNC as well as in other peripheral organs was also mentioned in the *L. vannamei* (Chen et al., 2014). Since there is no direct evidence of VIH in inhibiting vitellogenesis in this species, however, the VIH inhibited hepatopancreas vitellogenesis was reported in the *L. vannamei* (Chen et al., 2014). Referring the common practice for enhancing crustacean reproduction, as reported in the *L. vannamei* (Chen et al., 2014; Kang et al., 2014; Feijo et al., 2016), *Penaeus monodon* (Treerattrakool et al., 2008) and *Barytelphusa lugubris* (Rana, 2018), is the unilateral eyestalk ablation which resembled the removal of eyestalk GIH/VIH synthesis and release, this practice may cause significant hormonal imbalance and severe injury to the animal that affect the quantity and quality of larvae (Okumura, 2007; Uawisetwathana et al., 2011). Hence, based on the *S. olivacea* VIH sequence (GenBank accession no. MH882453.1), we successfully produced the dsRNA-VIH with expectation to silence the endogenous

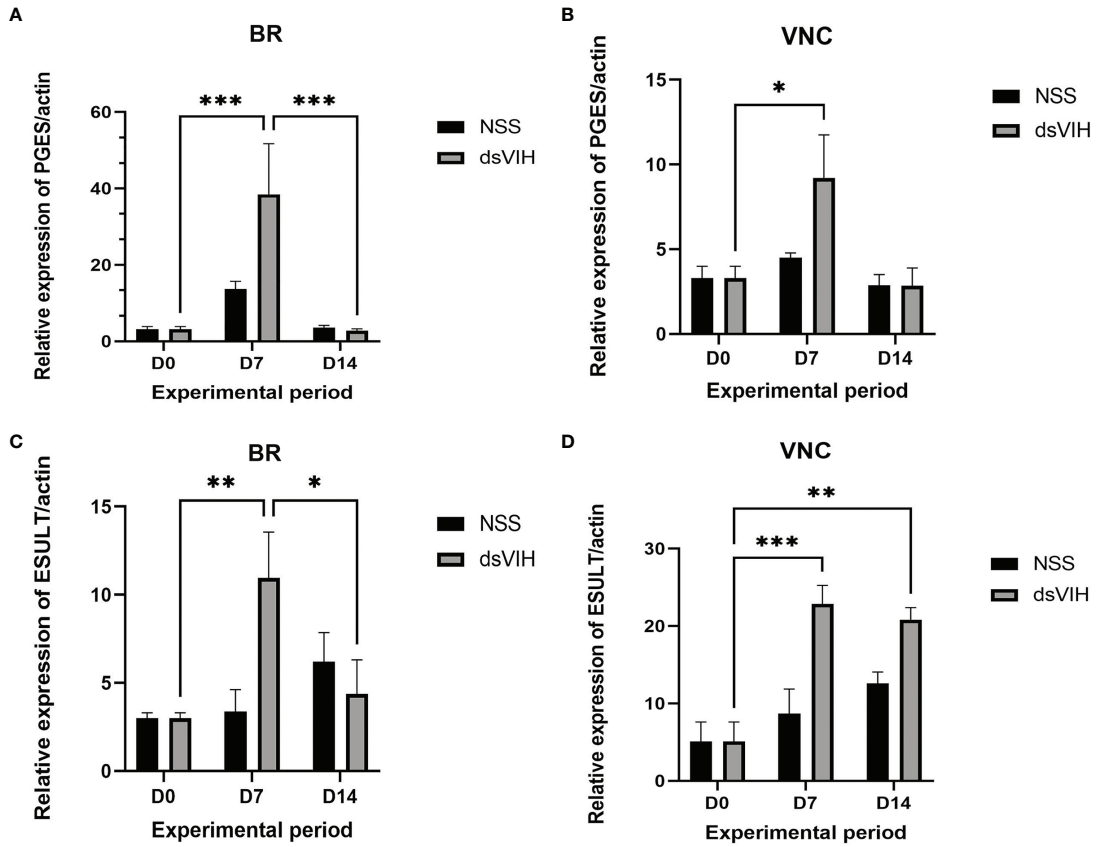

FIGURE 7 | Effect of dsRNA-VIH on the *Scyol-PGES* and *Scyol-ESULT* transcript abundances using quantitative RT-PCR. **(A, B)** The histograms showed the level of *Scyol-PGES* which significantly expressed higher in brain and VNC after dsRNA-VIH administration for 7 days. **(C, D)** The histograms showed the level of *Scyol-ESULT* which significantly expressed higher in brain and VNC after dsRNA-VIH administration for 7 and 14 days. BR, brain; VNC, ventral nerve cord. Bars represent the standard error of the mean (SEM). $^{*}p < 0.05$, $^{**}p < 0.005$ and $^{***}p < 0.0005$.

eyestalk and brain *VIH* expression that in turn helped promoting mud crab reproduction without torturing the animals and hence, can sustainably employ them in aquaculture.

As the *VIH* in *S. olivacea* was demonstrated to express in the eyestalk, brain and VNC, and the treatment of dopamine was found to promote the eyestalk *VIH* gene expression in this species (Kornthong et al., 2019). In this study, injection of dsRNA-VIH potentially inhibited the eyestalk and brain *VIH* transcripts for 24 h, with prolonged effect for 3 to 14 days for eyestalk *VIH* suppression. In *P. monodon*, the dsRNA-GIH, once being applied into the animal, could suppress the *GIH* gene expression for 24 h to 60 h (Sukumaran et al., 2017). The use of RNAi against the *GIH* in the same species displayed longer suppressing effect up to 30 days post-injection (Treerattrakool et al., 2011). Moreover, in *L. vannamei* injection of the various dsRNA-VIHs to the animals could suppress multiple VIH candidates for 10 to 30 days (Kang et al., 2019; Kang et al., 2021). Since the suppressing effect of dsRNA-VIH on its target gene was varied among species, however, it could say that the dsRNA-VIH produced in this study was efficient to silence the *VIH* transcript in mud crab.

The effect of dsRNA-VIH on the *VTG* expression was assumed by the stage of ovarian maturation and level of hemolymph Vn. The VTG, a key protein of yolk protein, has been used as indicator for determining ovarian maturation in many crustaceans (Soonklang et al., 2012; Guan et al., 2014), in this study, we fractionated the Vn from crab ovary and used it as standard protein in our Vn indirect-ELISA (Tinikul et al., 2016; Saetan et al., 2017). However, the anti-MrVn which was produced against the Vn of *Macrobrachium rosenbergii* was used (Soonklang et al., 2012). We, therefore, validated the antibody specificity by probing it against the *S. olivacea* ovarian proteins. The anti-MrVn was able to depict 2 Vn subunits which sizes were about 85 and 111 kDa and this result corresponded with previous report of 2 Vn subunits in the *S. olivacea* (Chen et al., 2007). Moreover, the well-organized standard curve of Vn in ELISA (data not shown) also conformed the ability of anti-MrVn to effectively probe the mud crab Vn in our study.

A single dose of 0.6 μg/g BW of dsRNA-VIH was enough to suppress *VIH* gene expression, without the repeat injection of dsRNA-VIH until day 14 after injection. Expectedly, the dsRNA-VIH injected crabs significantly had higher GSI value at day 28

with ovarian histology showing more mature oocytes. As similar with Vn level, the dsRNA-VIH injected crabs significantly had higher Vn level in hemolymph at day 28 compared to the control group. This was in concerted with other studies that the dsRNA-VIH injection can trigger vitellogenesis and ovarian maturation for example, in the *P. monodon* (Treerattrakool et al., 2008); *L. vannamei* (Feijo et al., 2016) and *M. rosenbergii* (Cohen et al., 2021). In contrast, the dsRNA-VIH injected in *L. vannamei* showed no significant elevation of either hemolymph Vg or ovarian Vg transcripts (Kang et al., 2019; Kang et al., 2021), while the authors suggested that the synthesized VIH was probably kept in the eyestalk and released during the time the *VIH* gene was silenced (Kang et al., 2021). In addition, we purposed that the dsRNA-VIH itself might not fully exert the stimulatory effects on *S. olivacea* reproduction in this time since other unidentified factors might probably affect. Removal of VIH by dsRNA-VIH might change their expression thresholds that in turn possibly decelerated some reproductive parameters in the *S. olivacea*. However, combination of dsRNA-VIH with other known stimulating agents, i.e., serotonin (Tinikul et al., 2016); or spiperone (Alfaro-Montoya et al., 2004) might be more effective in promoting female mud crab reproduction.

The *S. olivacea prostaglandin E synthase* (*Scyol-PGES)* and *S. olivacea estrogen sulfotransferase (Scyol-ESULT)* were identified in our previous studies (Kornthong et al., 2014; Duangprom et al., 2018). The *PGES* functioned in biogenesis of PGE_2 which was reported in participating ovarian maturation in many crustaceans (Sarojini et al., 1988; Reddy et al., 2004; Sumpownon et al., 2015). The *Scyol-PGES* was highly expressed in stage 4 ovary and abundantly found in the small- and medium-sized neurons of the brain (Duangprom et al., 2018). In this study, the absence of *VIH* by our dsRNA-VIH administration enhanced the expression of *Scyol-PGES* in brain and VNC at day 7 post-injection. These findings provide the first insight into a relationship between the *VIH* and *Scyol-PGES* in a crustacean related with ovarian maturation. As well, the dsRNA-VIH could enhance expression of the *Scyol-ESULT* which presumably functioned in solubility of estradiol in hemolymph (Cole et al., 2010). The ESULT plays an essential role by adding a sulfate group to estradiol which play role in gonadal maturation in the *S. serrata* and *P. monodon* (Quinitio et al., 1994; Warrier et al., 2001). Therefore, this gene has also been a potential candidate for reproduction in mud crab and the *Scyol-ESULT* expressed in the brain and VNC was negatively regulated by the *VIH*. Since the direct connection between *VIH* and these two genes was not reported yet in any crustaceans, however, it can be assumed that the lack of VIH by the dsRNA-VIH turned other stimulating molecules, i.e., serotonin, to positively regulated the expression of these two genes, and probably of others. For example, the serotonin injection was able to increase the *Scyol-ESULT* expression in both brain and ovary of the mud crab (Kornthong et al., 2014). Since the serotonin injection had no effect on the *VIH* expression in the same species (Kornthong et al., 2019), we could therefore not set any direct link between these two molecules in the mud crab.

In conclusion, the present study was successful in synthesizing the dsRNA-VIH for applying in the *S. olivacea*. The dsRNA-VIH was proved to last inhibit the VIH synthesis in eyestalk and brain of the mud crabs. Injection of the dsRNA-VIH at the dose of 0.6 μg/gram body weight to the crabs could promote many reproductive parameters as well as the expression of *Scyol-PGES* and *Scyol-ESULT* which reflected the effectiveness of dsRNA-VIH. However, to get better reproductive stimulation, the combination of the dsRNA-VIH with other stimulating neuropeptides/neurohormones was suggested.

DATA AVAILABILITY STATEMENT

The datasets presented in this study can be found in online repositories. The names of the repository/repositories and accession number(s) can be found in the article/**Supplementary Material**.

AUTHOR CONTRIBUTIONS

SD, TP, SS, JS, MT and NK designed experiment, analyzed data and wrote manuscript. SD, SS, TP, PSu, and MT performed experiments. SD, JS, PSo, and NK conceptual designed the experiment, provided experimental tools and made manuscript revisions. All authors contributed to the article and approved the submitted version.

FUNDING

This work was supported by Thammasat University Research Unit in Biotechnology and its application of aquatic animals. The authors also gratefully acknowledge the financial support provided by Thammasat University under the TU Research scholar (Grant No. TUGT5/2562) and Thai Government Research Fund (Integrated Research and Innovation Fund) through Thammasat University, Contract No. 38/2562.

ACKNOWLEDGMENTS

The authors are especially grateful to Thammasat University Research Unit in Biotechnology and its application of aquatic animals, Thammasat University under the TU Research scholar and Thai Government Research Fund (Integrated Research and Innovation Fund) through Thammasat University. The authors also gratefully thank Center of Scientific Equipment for Advanced Research, Office of Advanced Science and Technology, Thammasat University and Coastal Aquaculture Research and Development Regional Center 2, Samut Sakhon, Thailand for support the research instrument and crab culture area in this work.

SUPPLEMENTARY MATERIAL

The Supplementary Material for this article can be found online at: https://www.frontiersin.org/articles/10.3389/fmars.2022.880235/full#supplementary-material

REFERENCES

Alfaro-Montoya, J., Zúñiga Calero, G., and Komen, H. (2004). Induction of Ovarian Maturation and Spawning by Combined Treatment of Serotonin and a Dopamine Antagonist, Spiperone in *Litopenaeus Stylirostris* and *Litopenaeus Vannamei*. *Aquaculture* 236, 511–522. doi: 10.1016/j.aquaculture.2003.09.020

Amin-Safwan, A., Harman, M. F., Mardhiyyah, M., Nadirah, M., and Ikhwanuddin, M. (2018). Does Water Salinity Affect the Level of 17β-Estradiol and Ovarian Physiology of Orange Mud Crab, *Scylla Olivacea* (Herbst 1796) in Captivity? *J. King Saud Univ. Sci.* 31, 827–835. doi: 10.1016/j.jksus.2018.08.006

Amin-Safwan, A., Muhd-Farouk, H., Nadirah, M., and Ikhwanuddin, M. (2016). Effect of Water Salinity on the External Morphology of Ovarian Maturation Stages of Orange Mud Crab, Scylla Olivacea (Herbst 1796) in Captivity. *Pak. J. Biol. Sci.* 19, 219–226. doi: 10.3923/pjbs.2016.219.226

Avarre, J.-C., Michelis, R., Tietz, A., and Lubzens, E. (2003). Relationship Between Vitellogenin and Vitellin in a Marine Shrimp (*Penaeus Semisulcatus*) and Molecular Characterization of Vitellogenin Complementary Dnas1. *Biol. Reprod.* 69, 355–364. doi: 10.1095/biolreprod.102.011627

Azra, M. N., and Ikhwanuddin, M. (2016). A Review of Maturation Diets for Mud Crab Genus Scylla Broodstock: Present Research, Problems and Future Perspective. *Saudi J. Biol. Sci.* 23, 257–267. doi: 10.1016/j.sjbs.2015.03.011

Bao, C., Yang, Y., Huang, H., and Ye, H. (2015). Neuropeptides in the Cerebral Ganglia of the Mud Crab, *Scylla Paramamosain*: Transcriptomic Analysis and Expression Profiles During Vitellogenesis. *Sci. Rep.* 5, 17055. doi: 10.1038/srep17055

Chen, H.-Y., Ho, S.-H., Chen, T.-I., Soong, K., Chen, I. M., and Cheng, J.-H. (2007). Identification of a Female-Specific Hemocyanin in the Mud Crab, *Scylla Olivacea* (Crustacea: Portunidae). *Zool. Stud.* 46, 194–202.

Chen, Y.-N., and Kuo, C. (1998). Purification and Characterization of Vitellin From the Freshwater Giant Prawn, *Macrobrachium Rosenbergii*. *Zool. Stud.* 37, 126–136.

Chen, T., Zhang, L. P., Wong, N. K., Zhong, M., Ren, C. H., and Hu, C. Q. (2014). Pacific White Shrimp (*Litopenaeus Vannamei*) Vitellogenesis-Inhibiting Hormone (VIH) is Predominantly Expressed in the Brain and Negatively Regulates Hepatopancreatic Vitellogenin (VTG) Gene Expression. *Biol. Reprod.* 90, 47. doi: 10.1095/biolreprod.113.115030

Cohen, S., Ilouz, O., Manor, R., Sagi, A., and Khalaila, I. (2021). Transcriptional Silencing of Vitellogenesis-Inhibiting and Molt-Inhibiting Hormones in the Giant Freshwater Prawn, *Macrobrachium Rosenbergii*, and Evaluation of the Associated Effects on Ovarian Development. *Aquaculture* 538, 736540. doi: 10.1016/j.aquaculture.2021.736540

Cole, G. B., Keum, G., Liu, J., Small, G. W., Satyamurthy, N., Kepe, V., et al. (2010). Specific Estrogen Sulfotransferase (SULT1E1) Substrates and Molecular Imaging Probe Candidates. *Proc. Natl. Acad. Sci. U.S.A.* 107, 6222–6227. doi: 10.1073/pnas.0914904107

Duangprom, S., Ampansri, W., Suwansa-Ard, S., Chotwiwatthanakun, C., Sobhon, P., and Kornthong, N. (2018). Identification and Expression of Prostaglandin E Synthase (PGES) Gene in the Central Nervous System and Ovary During Ovarian Maturation of the Female Mud Crab, *Scylla Olivacea*. *Anim. Reprod. Sci.* 198, 220–232. doi: 10.1016/j.anireprosci.2018.09.022

Duangprom, S., Kornthong, N., Suwansa-ard, S., Srikawnawan, W., Chotwiwatthanakun, C., and Sobhon, P. (2017). Distribution of Crustacean Hyperglycemic Hormones (CHH) in the Mud Crab (*Scylla Olivacea*) and Their Differential Expression Following Serotonin Stimulation. *Aquaculture* 468, 481–488. doi: 10.1016/j.aquaculture.2016.11.008

Feijo, R. G., Braga, A. L., Lanes, C. F., Figueiredo, M. A., Romano, L. A., Klosterhoff, M. C., et al. (2016). Silencing of Gonad-Inhibiting Hormone Transcripts in *Litopenaeus Vannamei* Females by Use of the RNA Interference Technology. *Mar. Biotechnol. (NY)* 18, 117–123. doi: 10.1007/s10126-015-9676-2

Ghazali, A., Mat Noordin, N., Abol-Munafi, A. B., Azra, M. N., and Ikhwanuddin, M. (2017). Ovarian Maturation Stages of Wild and Captive Mud Crab, *Scylla Olivacea* Fed With Two Diets. *Sains Malays.* 46, 2273–2280. doi: 10.17576/jsm-2017-4612-03

Guan, Z.-B., Shui, Y., Liao, X.-R., Xu, Z.-H., and Zhou, X. (2014). Primary Structure of a Novel Gonadotropin-Releasing Hormone (GnRH) in the Ovary of Red Swamp Crayfish *Procambarus Clarkii*. *Aquaculture* 418-419, 67–71. doi: 10.1016/j.aquaculture.2013.10.010

Guan, Z.-B., Yi, H.-X., Zhao, H., Shui, Y., Cai, Y.-J., and Liao, X.-R. (2017). Cell Division Cycle 2 Participates in Eyestalk Ablation-Induced Ovarian Maturation of *Procambarus Clarkii*. *Aquaculture* 468, 115–119. doi: 10.1016/j.aquaculture.2016.10.009

Hidir, A., Aaqillah-Amr, M. A., Azra, M. N., Shahreza, M. S., Abualreesh, M. H., Peng, T. H., et al. (2021). Sexual Dimorphism of Mud Crab, Genus Scylla Between Sexes Based on Morphological and Physiological Characteristics. *Aquac. Res.* 52, 5943–5961. doi: 10.1111/are.15497

Hidir, A., Aaqillah-Amr, M. A., Noordiyana, M. N., and Ikhwanuddin, M. (2018). Diet and Internal Physiological Changes of Female Orange Mud Crabs, *Scylla Olivacea* (Herbst 1796) in Different Ovarian Maturation Stages. *Anim. Reprod. Sci.* 195, 216–229. doi: 10.1016/j.anireprosci.2018.05.026

Hsu, Y. W., Messinger, D. I., Chung, J. S., Webster, S. G., de la Iglesia, H. O., and Christie, A. E. (2006). Members of the Crustacean Hyperglycemic Hormone (CHH) Peptide Family are Differentially Distributed Both Between and Within the Neuroendocrine Organs of Cancer Crabs: Implications for Differential Release and Pleiotropic Function. *J. Exp. Biol.* 209, 3241–3256. doi: 10.1242/jeb.02372

Islam, M. S., Kodama, K., and Kurokora, H. (2010). Ovarian Development of the Mud Crab *Scylla Paramamosain* in a Tropical Mangrove Swamps, Thailand. *J. Sci. Res.* 2, 380–389. doi: 10.3329/jsr.v2i2.3543

Jayasankar, V., Tomy, S., and Wilder, M. N. (2020). Insights on Molecular Mechanisms of Ovarian Development in Decapod Crustacea: Focus on Vitellogenesis-Stimulating Factors and Pathways. *Front. Endocrinol.* 11. doi: 10.3389/fendo.2020.577925

Kang, B. J., Bae, S.-H., Suzuki, T., Niitsu, S., and Wilder, M. N. (2019). Transcriptional Silencing of Vitellogenesis-Inhibiting Hormone (VIH) Subtype-I in the Whiteleg Shrimp, *Litopenaeus Vannamei*. *Aquaculture* 506, 119–126. doi: 10.1016/j.aquaculture.2019.03.028

Kang, B. J., Okutsu, T., Tsutsui, N., Shinji, J., Bae, S. H., and Wilder, M. N. (2014). Dynamics of Vitellogenin and Vitellogenesis-Inhibiting Hormone Levels in Adult and Subadult Whiteleg Shrimp, *Litopenaeus Vannamei*: Relation to Molting and Eyestalk Ablation. *Biol. Reprod.* 90, 12. doi: 10.1095/biolreprod.113.112243

Kang, B. J., Sultana, Z., and Wilder, M. N. (2021). Assessment of the Effects of Double-Stranded Rnas Corresponding to Multiple Vitellogenesis-Inhibiting Hormone Subtype I Peptides in Subadult Female Whiteleg Shrimp, *Litopenaeus Vannamei*. *Front. Endocrinol.* 12. doi: 10.3389/fendo.2021.594001

Kegel, G., Reichwein, B., Weese, S., Gaus, G., Peter-Katalinic, J., and Keller, R. (1989). Amino Acid Sequence of the Crustacean Hyperglycemic Hormone (CHH) From the Shore Crab, *Carcinus Maenas*. *FEBS Lett.* 255, 10–14. doi: 10.1016/0014-5793(89)81051-8

Kornthong, N., Chotwiwatthanakun, C., Chansela, P., Tinikul, Y., Cummins, S. F., Hanna, P. J., et al. (2013). Characterization of Red Pigment Concentrating Hormone (RPCH) in the Female Mud Crab (*Scylla Olivacea*) and the Effect of 5-HT on its Expression. *Gen. Comp. Endocrinol.* 185, 28–36. doi: 10.1016/j.ygcen.2013.01.011

Kornthong, N., Cummins, S. F., Chotwiwatthanakun, C., Khornchatri, K., Engsusophon, A., Hanna, P. J., et al. (2014). Identification of Genes Associated With Reproduction in the Mud Crab (*Scylla Olivacea*) and Their Differential Expression Following Serotonin Stimulation. *PloS One* 9, e115867. doi: 10.1371/journal.pone.0115867

Kornthong, N., Duangprom, S., Suwansa-Ard, S., Saetan, J., Phanaksri, T., Songkoomkrong, S., et al. (2019). Molecular Characterization of a Vitellogenesis-Inhibiting Hormone (VIH) in the Mud Crab (*Scylla Olivacea*) and Temporal Changes in Abundances of VIH mRNA Transcripts During Ovarian Maturation and Following Neurotransmitter Administration. *Anim. Reprod. Sci.* 208, 106122. doi: 10.1016/j.anireprosci.2019.106122

Lacombe, C., Greve, P., and Martin, G. (1999). Overview on the Sub-Grouping of the Crustacean Hyperglycemic Hormone Family. *Neuropeptides* 33, 71–80. doi: 10.1054/npep.1999.0016

Lin, D., Wei, Y., and Ye, H. (2020). Role of Oxytocin/Vasopressin-Like Peptide and Its Receptor in Vitellogenesis of Mud Crab. *Int. J. Mol. Sci.* 21, 2297. doi: 10.3390/ijms21072297

Liu, C., Jia, X., Zou, Z., Wang, X., Wang, Y., and Zhang, Z. (2018). VIH From the Mud Crab is Specifically Expressed in the Eyestalk and Potentially Regulated by

Transactivator of Sox9/Oct4/Oct1. *Gen. Comp. Endocrinol.* 255, 1–11. doi: 10.1016/j.ygcen.2017.09.018

Meister, G., and Tuschl, T. (2004). Mechanisms of Gene Silencing by Double-Stranded RNA. *Nature* 431, 343–349. doi: 10.1038/nature02873

Muhd-Farouk, H., Nurul, H. A., Abol-Munafi, A. B., Mardhiyyah, M. P., Hasyima-Ismail, N., Manan, H., et al. (2019). Development of Ovarian Maturations in Orange Mud Crab, Scylla Olivacea (Herbst 1796) Through Induction of Eyestalk Ablation and Methyl Farnesoate. *Arab. J. Basic Appl. Sci.* 26, 171–181. doi: 10.1080/25765299.2019.1588197

Nagaraju, G. P. C. (2011). Reproductive Regulators in Decapod Crustaceans: An Overview. *J. Exp. Biol.* 214, 3–16. doi: 10.1242/jeb.047183

Okumura, T. (2007). Effects of Bilateral and Unilateral Eyestalk Ablation on Vitellogenin Synthesis in Immature Female Kuruma Prawns, *Marsupenaeus Japonicus*. *Zoolog. Sci.* 24, 233–240. doi: 10.2108/zsj.24.233

Okumura, T., and Aida, K. (2001). Effects of Bilateral Eyestalk Ablation on Molting and Ovarian Development in the Giant Freshwater Prawn, *Macrobrachium Rosenbergii*. *Fish. Sci.* 67, 1125–1135. doi: 10.1046/j.1444-2906.2001.00370.x

Okumura, T., Yamano, K., and Sakiyama, K. (2007). Vitellogenin Gene Expression and Hemolymph Vitellogenin During Vitellogenesis, Final Maturation, and Oviposition in Female Kuruma Prawn, *Marsupenaeus Japonicus*. *Comp. Biochem. Physiol. Part A Mol. Integr. Physiol.* 147, 1028–1037. doi: 10.1016/j.cbpa.2007.03.011

Okumura, T., Yoshida, K., and Nikaido, H. (2004). Ovarian Development and Hemolymph Vitellogenin Levels in Laboratory-Maintained Protandric Shrimp, *Pandalus Hypsinotus*: Measurement by a Newly Developed Time-Resolved Fluoroimmunoassay (TR-FIA). *Zoolog. Sci.* 21, 1037–1047. doi: 10.2108/zsj.21.1037

Overton, J. L., and Macintosh, D. J. (2002). Estimated Size at Sexual Maturity for Female Mud Crabs (Genus Scylla) From Two Sympatric Species Within Ban Don Bay, Thailand. *J. Crust. Biol.* 22, 790–797. doi: 10.1163/20021975-99990293

Pak, J., and Fire, A. (2007). Distinct Populations of Primary and Secondary Effectors During RNAi in *C. Elegans*. *Science* 315, 241–244. doi: 10.1126/science.1132839

Qian, Y.-Q., Dai, L., Yang, J.-S., Yang, F., Chen, D.-F., Fujiwara, Y., et al. (2009). CHH Family Peptides From an 'Eyeless' Deep-Sea Hydrothermal Vent Shrimp, Rimicaris Kairei: Characterization and Sequence Analysis. *Comp. Biochem. Physiol. B Biochem. Mol. Biol.* 154, 37–47. doi: 10.1016/j.cbpb.2009.04.013

Quackenbush, L. S. (2015). Yolk Synthesis in the Marine Shrimp, *Penaeus Vannamei*. *Am. Zool.* 41, 458–464. doi: 10.1093/icb/41.3.458

Quinitio, E. T., Hara, A., Yamauchi, K., and Nakao, S. (1994). Changes in the Steroid Hormone and Vitellogenin Levels During the Gametogenic Cycle of the Giant Tiger Shrimp, Penaeus Monodon. *Comp. Biochem. Physiol. Part C: Pharmacol. Toxicol. Endocrinol.* 109, 21–26. doi: 10.1016/0742-8413(94)00044-B

Rana, S. K. (2018). Eye Stalk Ablation of Freshwater Crab, *Barytelphusa Lugubris*: An Alternative Approach of Hormonal Induced Breeding. *Int. J. Pure Appl. Zool.* 6, 30–34.

Rani, K., and Subramoniam, T. (1997). Vitellogenesis in the Mud Crab *Scylla Serrata*—an *in Vivo* Isotope Study. *J. Crust. Biol.* 17, 659–665. doi: 10.1163/193724097x00080

Reddy, P. S., Reddy, P. R., and Nagaraju, G. P. (2004). The Synthesis and Effects of Prostaglandins on the Ovary of the Crab *Oziotelphusa Senex Senex*. *Gen. Comp. Endocrinol.* 135, 35–41. doi: 10.1016/j.ygcen.2003.08.002

Saetan, J., Kornthong, N., Duangprom, S., Phanthong, P., Kruangkum, T., and Sobhon, P. (2021). The Oxytocin/Vasopressin-Like Peptide Receptor mRNA in the Central Nervous System and Ovary of the Blue Swimming Crab, *Portunus Pelagicus*. *Comp. Biochem. Physiol. Part A Mol. Integr. Physiol.* 258, 110983. doi: 10.1016/j.cbpa.2021.110983

Saetan, J., Kruangkum, T., Phanthong, P., Tipbunjong, C., Udomuksorn, W., Sobhon, P., et al. (2018). Molecular Cloning and Distribution of Oxytocin/Vasopressin-Like mRNA in the Blue Swimming Crab, *Portunus Pelagicus*, and its Inhibitory Effect on Ovarian Steroid Release. *Comp. Biochem. Physiol. Part A Mol. Integr. Physiol.* 218, 46–55. doi: 10.1016/j.cbpa.2018.01.012

Saetan, J., Senarai, T., Thongbuakaew, T., Kruangkum, T., Chansela, P., Khornchatri, K., et al. (2017). The Presence of Abalone Egg-Laying Hormone-Like Peptide in the Central Nervous System and Ovary of the Blue Swimming Crab, *Portunus Pelagicus*, and its Effect on Ovarian Maturation. *Aquaculture* 479, 412–422. doi: 10.1016/j.aquaculture.2017.06.007

Sarojini, R., Jayalakshmi, K., Rao, S. S., and Nagabhushanam, R. (1988). Stimulation of Oogenesis in the Freshwater Prawn, *Macrobrachium Lamerri* by Prostagalndin E2 and Follicle Stimulating Hormone. *Indian J. Fish* 25, 283–287.

Soonklang, N., Wanichanon, C., Stewart, M. J., Stewart, P., Meeratana, P., Hanna, P. J., et al. (2012). Ultrastructure of Differentiating Oocytes and Vitellogenesis in the Giant Freshwater Prawn, *Macrobrachium Rosenbergii* (De Man). *Microsc. Res. Tech.* 75, 1402–1415. doi: 10.1002/jemt.22081

Sroyraya, M., Chotwiwatthanakun, C., Stewart, M. J., Soonklang, N., Kornthong, N., Phoungpetchara, I., et al. (2010). Bilateral Eyestalk Ablation of the Blue Swimmer Crab, *Portunus Pelagicus*, Produces Hypertrophy of the Androgenic Gland and an Increase of Cells Producing Insulin-Like Androgenic Gland Hormone. *Tissue Cell.* 42, 293–300. doi: 10.1016/j.tice.2010.07.003

Stewart, M., Soonklang, N., Stewart, P., Hanna, P., Wanichanon, C., Parratt, A., et al. (2007). Histological Studies of the Ovaries of Two Tropical Portunid Crabs, *Portunus Pelagicus* (L.) and *Scylla Serrata* (F.). *Inver. Reprod. Dev.* 50, 85–97. doi: 10.1080/07924259.2007.9652231

Subramoniam, T. (2011). Mechanisms and Control of Vitellogenesis in Crustaceans. *Fish. Sci.* 77, 1–21. doi: 10.1007/s12562-010-0301-z

Sukumaran, V., Reshmi, C., Jose, S., Peter, R., Kk, V., Philip, R., et al. (2017). Crustacean Hyperglycemic Hormone Family Gene Silencing in *Penaeus Monodon* Mediated Through dsRNA Synthesized In Vitro From Genomic and Cdna. *Indian J. Biotechnol.* 16, 37–43.

Sumpownon, C., Engsusophon, A., Siangcham, T., Sugiyama, E., Soonklang, N., Meeratana, P., et al. (2015). Variation of Prostaglandin E2 Concentrations in Ovaries and its Effects on Ovarian Maturation and Oocyte Proliferation in the Giant Fresh Water Prawn, *Macrobrachium Rosenbergii*. *Gen. Comp. Endocrinol.* 223, 129–138. doi: 10.1016/j.ygcen.2015.04.019

Tan-Fermin, J. D. (1991). Effects of Unilateral Eyestalk Ablation on Ovarian Histology and Oocyte Size Frequency of Wild and Pond-Reared *Penaeus Monodon* (Fabricius) Broodstock. *Aquaculture* 93, 77–86. doi: 10.1016/0044-8486(91)90206-M

Tinikul, Y., Poljaroen, J., Tinikul, R., and Sobhon, P. (2016). Changes in the Levels, Expression, and Possible Roles of Serotonin and Dopamine During Embryonic Development in the Giant Freshwater Prawn, *Macrobrachium Rosenbergii*. *Gen. Comp. Endocrinol.* 225, 71–80. doi: 10.1016/j.ygcen.2015.09.018

Treerattrakool, S., Panyim, S., Chan, S. M., Withyachumnarnkul, B., and Udomkit, A. (2008). Molecular Characterization of Gonad-Inhibiting Hormone of *Penaeus Monodon* and Elucidation of its Inhibitory Role in Vitellogenin Expression by RNA Interference. *FEBS J.* 275, 970–980. doi: 10.1111/j.1742-4658.2008.06266.x

Treerattrakool, S., Panyim, S., and Udomkit, A. (2011). Induction of Ovarian Maturation and Spawning in *Penaeus Monodon* Broodstock by Double-Stranded RNA. *Mar. Biotechnol. (NY)* 13, 163–169. doi: 10.1007/s10126-010-9276-0

Tsukimura, B. (2015). Crustacean Vitellogenesis: its Role in Oocyte Development1. *Am. Zool.* 41, 465–476. doi: 10.1093/icb/41.3.465

Uawisetwathana, U., Leelatanawit, R., Klanchui, A., Prommoon, J., Klinbunga, S., and Karoonuthaisiri, N. (2011). Insights Into Eyestalk Ablation Mechanism to Induce Ovarian Maturation in the Black Tiger Shrimp. *PloS One* 6, e24427. doi: 10.1371/journal.pone.0024427

Volz, D. C., Kawaguchi, T., and Chandler, G. T. (2002). Purification and Characterization of the Common Yolk Protein, Vitellin, From the Estuarine Amphipod *Leptocheirus Plumulosus*. *Prep. Biochem. Biotechnol.* 32, 103–116. doi: 10.1081/PB-120004123

Warrier, S. R., Tirumalai, R., and Subramoniam, T. (2001). Occurrence of Vertebrate Steroids, Estradiol 17beta and Progesterone in the Reproducing Females of the Mud Crab Scylla Serrata. *Comp. Biochem. Physiol. A Mol. Integr. Physiol.* 130, 283–294. doi: 10.1016/s1095-6433(01)00385-3

Webster, S. G., Keller, R., and Dircksen, H. (2012). The CHH-superfamily of Multifunctional Peptide Hormones Controlling Crustacean Metabolism, Osmoregulation, Moulting, and Reproduction. *Gen. Comp. Endocrinol.* 175, 217–233. doi: 10.1016/j.ygcen.2011.11.035

Zeng, H., Bao, C., Huang, H., Ye, H., and Li, S. (2016). The Mechanism of Regulation of Ovarian Maturation by Red Pigment Concentrating Hormone in

the Mud Crab *Scylla Paramamosain*. *Anim. Reprod. Sci.* 164, 152–161. doi: 10.1016/j.anireprosci.2015.11.025

Conflict of Interest: The authors declare that the research was conducted in the absence of any commercial or financial relationships that could be construed as a potential conflict of interest.

Publisher's Note: All claims expressed in this article are solely those of the authors and do not necessarily represent those of their affiliated organizations, or those of the publisher, the editors and the reviewers. Any product that may be evaluated in this article, or claim that may be made by its manufacturer, is not guaranteed or endorsed by the publisher.

frontiers | Frontiers in Marine Science

ORIGINAL RESEARCH
published: 15 July 2022
doi: 10.3389/fmars.2022.940303

Embryo Development and Effects of Temperature, Salinity, and Light Intensity on Egg Hatching of Calanoid Copepod Bestiolina amoyensis (Calanoida: Paracalanidae)

Shuhong Wang[1,2,3*], *Lin Wang*[1,2], *Yuyue Wang*[1,2], *Yun Chen*[1,2], *Jinmin Chen*[1,2] *and Nan Chen*[1,2]

[1] Fisheries College, Jimei University, Xiamen, China, [2] Ornamental Aquarium Engineering Research Centre in University of Fujian Province, Xiamen, China, [3] Key Laboratory of Healthy Mariculture for the East China Sea, Ministry of Agriculture and Rural Affairs, Xiamen, China

Bestiolina amoyensis distributes in subtropical inshore waters across the Pacific Ocean, with a relatively long reproductive lifespan and high intrinsic population increase rate compared with other small paracalanid species, which makes it a good candidate to develop culture techniques for hatchery larval rearing. However, the reproductive biology of this subtropical broadcast spawning species is still largely unknown. The present investigation provides the first published data on the embryo development and effects of different light intensities (0, 500, and 1,000 lx), temperatures (16°C, 18°C, 20°C, 22°C, 24°C, 26°C, 28°C, 30°C, 32°C, and 34°C), and salinities (22, 24, 26, 28, 30, 32, and 34 psu) on hatching success rates of *B. amoyensis*. The same batch of eggs were collected from gravid females to observe their embryonic development and incubated under designed light intensities, temperatures, and salinities. Results showed that the whole embryonic development of *B. amoyensis* lasted, on average, 6 h and 40 min at 26°C, and egg hatching time of *B. amoyensis* shortened exponentially with the increasing temperature. The highest egg hatching rate (100%) was recorded from the 0-lx treatment, indicating that the dark condition was favorable for the egg incubation of *B. amoyensis*. The optimum temperature and salinity range for the hatching success of *B. amoyensis* was 22°C–30°C (above 94%) and 22–34 psu salinity (above 88%), respectively, indicating that *B. amoyensis* had wide adaptability to temperature and salinity. Light and too low or high temperature leads to abnormal embryonic development and malformed nauplii. The relatively wide adaptability to temperature and salinity and fast embryo development also suggests that *B. amoyensis* was a good candidate as live feed for hatchery larval rearing.

Keywords: hatching time, egg hatching rate, hatching success, live feed, Calanoida

OPEN ACCESS

Edited by:
Chaoshu Zeng,
James Cook University,
Australia

Reviewed by:
Per Meyer Jepsen,
Roskilde University, Denmark
Yen-Ju Pan,
National Taiwan Ocean
University, Taiwan

***Correspondence:**
Shuhong Wang
shwang@jmu.edu.cn

Specialty section:
This article was submitted to Aquatic Physiology, a section of the journal Frontiers in Marine Science

Received: *10 May 2022*
Accepted: *09 June 2022*
Published: *15 July 2022*

Citation:
Wang S, Wang L, Wang Y, Chen Y, Chen J and Chen N (2022) Embryo Development and Effects of Temperature, Salinity, and Light Intensity on Egg Hatching of Calanoid Copepod Bestiolina amoyensis (Calanoida: Paracalanidae). Front. Mar. Sci. 9:940303. doi: 10.3389/fmars.2022.940303

1 INTRODUCTION

Planktonic copepods are natural and preferable feeds for fish and invertebrate larvae in marine environment and are widely used as live feed in marine larviculture hatcheries (Drillet et al., 2011; Santhanam et al., 2019; Fernández-Ojeda et al., 2021; Pan et al., 2022), especially some species of paracalanid family, such as *Parvocalanus carssirostris* (Alajmi & Zeng, 2015; Kline & Laidley, 2015;

Valencia et al., 2022), *Bestiolina similis* (McKinnon et al., 2003; Camus et al., 2009; VanderLugt et al., 2009; Camus & Zeng, 2010; Camus et al., 2021), and *Bestiolina amoyensis* (Wang et al., 2021). Small body size and the herbivorous characteristics make them good candidates as larvae prey for fish larvae with small mouth gape (Wang et al., 2021).

Calanoid copepods are generally well adapted to seasonal fluctuations in temperature and salinity under natural conditions (Miller & Marcus, 1994; Engel & Hirche, 2004; Marcus, 2005). Examples are *Eurytemora affinis* (Roddie et al., 1984; Nagaraj, 1992; Devreker et al., 2009; Souissi et al., 2016; Karlsson et al., 2018) and a number of *Acartia* congeners (Gaudy et al, 2000; Castro-Longoria, 2003; Chinnery & Williams, 2004; Milione & Zeng, 2008; Choi et al., 2021; Choi et al., 2022); these estuarine and coastal calanoid copepods are more widely adapted to temperature and salinity than pelagic species, which makes them more suitable for culture as live feed. For most of Paracalanidae species, information about reproduction is still very limited, and the functional response of reproductive success (i.e., egg production and hatching) to salinity and/or temperature only have been studied in a handful species, such as *Paracalanus parvus* (Jang et al., 2013). In addition, light is one of the most significant ecological factors influencing many biological functions of organisms (Hairston & Kearns, 1995; Chinnery & Williams, 2004; Radhakrishnan et al., 2020), but there are few studies that focus on the functional response of copepods to light intensity and/or periodicity (Peck & Holste, 2006, Peck et al., 2008; Radhakrishnan et al., 2020; Wang et al., 2021). Therefore, it is necessary to further study the effects of environmental factors on the reproductive success of copepods in order to optimize the culture conditions and maintain a relative high population density.

The embryonic development study of Crustaceans can be retracted to the nineteenth century, but it mainly focus on the species of Decapoda. Copepods have always received very little attention (Loose & Scholtz, 2019). Few available copepod embryonic studies were mainly on species with large eggs (>100 μm) (Marshall & Orr, 1954; Marshall and Orr, 1955; Conover, 1967; Gao, 2014; Loose & Scholtz, 2019) or resting eggs (Marshall & Orr, 1954; Marshall and Orr, 1955; Chen, 2014; Nilsson & Hansen, 2018). Small size copepods usually have a tiny egg (50–90 m in diameter) and covering with a very complicated chitin shell, which make the observation became difficult. We still know very little about the embryonic development of copepods nowadays.

Bestiolina amoyensis distributes in subtropical coastal and estuarine waters, which is easily cultured in laboratory (Wang et al., 2021) and hence is recommended as one of the promising live feed candidates. Previous studies have quantified the effects of food concentration and photoperiod on the reproductive performance of *B. amoyensis*, including egg production and female life expectancy (Wang et al., 2021). Clarifying the embryonic development of *B. amoyensis* not only could improve the basic understanding about ontogenesis of crustaceans but also could enhance the intensive culture techniques as a live feed. For some fish larvae with a small gape, they only could use Nauplii I copepods as the first feed. Farmers could predict the exact time when Nauplii I copepods could be collected for fish feeding. Therefore, the embryonic development process was investigated at 26°C, and the hatching time at different temperatures was evaluated. In an effort to optimize the incubation conditions for egg hatching and embryonic development of *B. amoyensis*, three experiments were conducted to quantify egg hatching success: (1) under different light intensities, (2) at different temperatures, and (3) at different salinities.

2 MATERIALS AND METHODS

2.1 *B. amoyensis* Stock Culture

Bestiolina amoyensis was obtained from Ornamental Aquarium Engineering Research Centre of Jimei University, Xiamen, China. It was scaled up and kept in several 18-L containers filled with 0.01-μm filtered seawater and with gentle aeration. For stock culture conditions, *B. amoyensis* was fed daily with microalgae *Isochrysis* spp. at a concentration of 1×10^5 cells ml^{-1}, and the temperature and salinity were maintained at 26 ± 1°C and 28 ± 1 psu, respectively. Light intensity was 500 lx with a light/dark cycle of 12 h:12 h (Wang et al, 2021).

2.2 Experimental Design and Setup

A series of experiments were carried out to explore the embryonic development of *B. amoyensis* and assess the effects of temperature, salinity, and light intensity on the hatching of embryos.

2.2.1 Embryogenesis of *B. amoyensis*

The mature male/female ratio was designed to be 2:1 to make sure the mating success and placed into six-well cell culture plates with 28 ± 1 psu seawater, and the concentration of microalgae *Isochrysis* spp. was 1×10^5 cells ml^{-1}. Plates with paired adults were placed into an incubator with constant temperature (26 ± 1°C) and a light/dark cycle of 0L:24D. After 20–30 min of dark culture in the incubator, newly spawned fertilized eggs were collected under a microscope using a glass pipette with an arc tip.

Embryo development experiments were performed with 90 replicates (two to three eggs from the same batch per replicate). Eggs were transferred to 35 mm in diameter NEST® glass-bottom cell culture dishes, containing filtered seawater of the same salinity. Eggs were incubated at 26 ± 1°C for embryonic development under dark conditions.

The frequency of embryo observation was determined by pre-experiments as a way to calculate the percentage of specific stages within a set time. Microscopic observations were made at 5-min intervals for 40 min after spawning and at 30-min intervals for the next 90 min. Microscopic observations were made at 1-h intervals after 2 h and 10 min of spawning and at 30-min intervals after 5 h and 10 min of spawning. Median development time of a specific stage was defined as the period when 50% of the species had passed into that stage (Landry, 1975).

2.2.2 Hatching Time Experiment

This experiment was designed with five temperatures of 22°C, 24°C, 26°C, 28°C, and 30°C. With 30 replicates (two to three eggs from the same batch per replicate) per treatment, a total

of 150 NEST® glass-bottom cell culture dishes were set up. Eggs were incubated at designed temperatures under dark conditions. After 3 h of incubation per treatment, microscopic observations were made every 30 min, recording the incubation time until all eggs had hatched. The relationship between hatching time (D; h) and temperature (T; °C) in small copepods was fitted to Bělehrádek's function (McLaren et al, 1969; Lee et al, 2003):

$$D = A\left(T - \alpha\right)^{B}$$

where A, B, and α are fitted constants.

2.2.3 Spawning Rhythm Experiment

To study the daily egg spawning rhythm of *B. amoyensis*, 36 replicates were set up, each with one pair of adults, and the paired adults were placed into six-well cell culture plates, one pair per well, and feed microalgae *Isochrysis* spp. at a concentration of 1×10^5 cells ml^{-1}; the temperature and salinity were maintained at 26 ± 1°C and 28 ± 1 psu, respectively. Light intensity was 500 lx with a light/dark cycle of 12 h:12 h. Spawning rhythm experiment of *B. amoyensis* within 24 h was started at 8:00 a.m. The plates were examined microscopically at 2-h intervals, and the eggs were sucked out with an aforementioned arc pipette, the spawning time, and the number of eggs were recorded.

2.2.4 Egg Hatching Rate

Three environmental factors affecting incubation were set up, namely, light intensity, temperature, and salinity. Three light intensity treatments were 0, 500, and 1,000 lx, with a total of 45 replicates for each treatment (two to three eggs from the same batch per replicate), and eggs were collected in the same way as described previously. Salinity and temperature were the same as the stock culture (i.e., 26 ± 1°C, 28 ± 1 psu). Similarly, 10 temperature treatments of 16°C, 18°C, 20°C, 22°C, 24°C, 26°C, 28°C, 30°C, 32°C, and 34°C were set up, each with 45 replicates per treatment (two to three eggs from the same batch per replicate), incubated at the same salinity as the stock culture (28 ± 1 psu). In addition, seven salinity treatments of 22, 24, 26, 28, 30, 32, and 34 psu were set up with a total of 45 replicates, incubated at the same temperature as the stock culture (26 ± 1°C). The effect of temperature and salinity on incubation were conducted in dark conditions. The egg hatching rates (EHRs) of *B. amoyensis* under different designed regimes are presented in two categories: "Proportion of Hatching Normal Nauplii," which included normal nauplii, and "Proportion of Hatching Abnormal Nauplii," which included deformed nauplii (with twisted and distorted appendages and body). All eggs were kept in designed culture conditions for 24 h of observation until hatched. Unhatched eggs were moved into 26 ± 1°C, 28 ± 1 psu, dark condition after 24 h of experiment, and culturing was continued for another 24 h to make sure of the status of the egg.

2.3 Data Collection and Analysis

Data from all experiments were analyzed using one-way ANOVA. All data were tested for normality (Shapiro–Wilk test) and homogeneity of variance (Levene's test) prior to analysis of ANOVA. When significant differences ($p<0.05$) were found, Tukey's multiple comparisons test was performed to determine significant differences among treatments ($p<0.05$).

3 RESULTS

3.1 Embryo Morphology of *B. amoyensis*

The whole embryonic development of *B. amoyensis* lasted, on average, 6 h and 40 min at 26°C. It was classified into seven main stages: fertilized eggs, cleavage stage, grastrulation, no structure visible, limb bud, early nauplii, and hatching. Percentages of

TABLE 1 | Percentages of embryonic stages during the embryo development of *B. amoyensis* (N=90).

Time	Embryonic stages										
	S1	**S2**	**S3**	**S4**	**S5**	**S6**	**G**	**NS**	**LB**	**EN**	**FN**
5 min	100%										
10 min	90%	10%									
15 min		90%	10%								
20 min			80%	20%							
25 min			35%	55%	10%						
30 min				70%	30%						
35 min					90%	10%					
40 min					45%	55%					
1 h 10 min						100%					
1 h 40 min						45%	55%				
2 h 10 min							100%				
3 h, 10 min							100%				
4 h, 10 min								100%			
5 h 10 min									100%		
5 h 40 min										100%	
6 h 10 min										45%	55%
6 h 40 min											100%

Embryogenesis was divided into following stages: fertilized egg (S1), 2-cell stage (S2), 4-cell stage (S3), 8-cell stage (S4), 16-cell stage (S5), multicellular stage (S6), grastrula stage (G), no structure visible (NS), limb bud stage (LB), early nauplii (EN), and final nauplii just before hatching (FN).

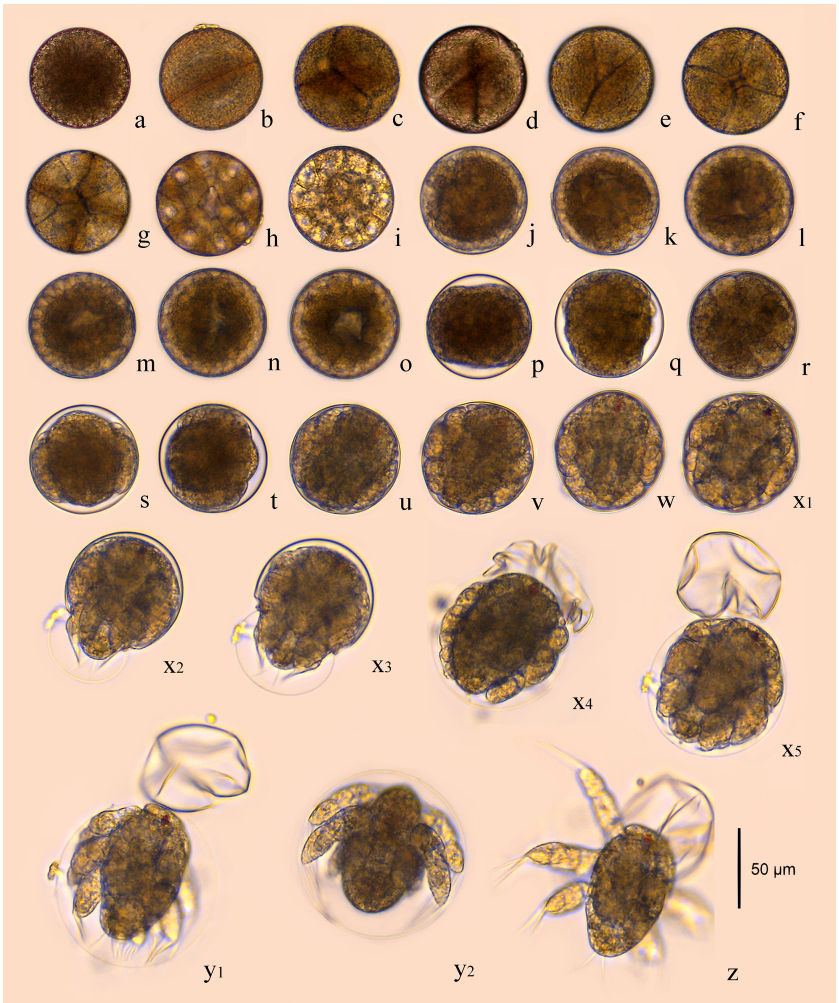

FIGURE 1 | Embryonic development of *B. amoyensis*. **(A)**, fertilized eggs; **(B)**, 2-cell stage; **(C–E)**, 4-cell stage; **(F)**, 8-cell stage; **(G)**, 16-cell stage; **(H–I)**, multicellular phase; **(J–O)**, grastrula stage; **(P–Q)**, no structure visible; **(R–T)**, limb bud stage; **(U–W)**, the early stage of nauplii; **(X1–X5)**, the rupture stage of outer membrane; **(Y1–Y2)**, the rupture stage of inner membrane; **(Z)**, the first stage of nauplii.

embryonic stages during the embryo development of *B. amoyensis* was shown in **Table 1**.

3.1.1 Fertilized Eggs

The fertilized egg was about 71.74 μm in diameter, brownish yellow in color, and has two layers of membrane. The eggs, which sank to the bottom of the container after being laid, were long and elliptical in shape, very similar to the long strips shape of fecal pellet. They quickly absorbed water and became ellipsoidal in shape, turning into near-spherical shape a few minutes later (**Figure 1A**).

3.1.2 Cleavage Stage

The cleavage of *B. amoyensis* was total and equal to adequal. After the onset of oogenesis, the fertilized egg cells underwent mitosis in sequence, with the cleavage furrow clearly visible at each stage. The number of cells was increasing, and the nuclei were arranged in columns, showing the typical features of radial cleavage (**Figures 1B–I**).

The first cleavage occurred about 15 min (majority of 90%, **Figure 1B**) after the egg was deposited, followed by 4-cell, 8-cell, 16-cell, and multicellular stage at about 20, 25, 35, and 40 min after, respectively (majority of 80%, 55%, 90%, and 55%, **Figures 1C–I**). The first, second, and fourth cleavage divisions were meridional, while the third cleavage was equatorial and oriented perpendicularly to the previous cleavage. "I-section shaped" (**Figure 1C**), "X-section shaped" (**Figure 1D**), and "Herringbone" (**Figure 1E**) division furrow of second cleavage were obvious from different angles of view, while the division furrow of 8- and 16-cell resembled "cross-shaped" (**Figure 1F**) and "*" shaped (**Figure 1G**).

3.1.3 Gastrulation

The gastrulae were formed 1 h and 40 min after oviposition (majority of 55%, **Figures 1J–O**) when translucent area appeared at the edge of the egg, and the cells were continuously invaginated to form the archenteric cavity.

3.1.4 No Structure Visible

The stage of no structure visible was formed 4 h and 10 min after oviposition (100%, **Figures 1P, Q**), and the internal structure of the embryo was variable, with numerous transparent areas appearing on both sides (**Figures 1P, Q**).

3.1.5 Limb Bud Stage

The embryo developed into the early limb bud stage 1 h after of the stage of no structure visible, and the limb primordia was initially distinguishable, outlined with lateral invaginations between the three pairs of limbs in horizontal view (**Figure 1R**). At the late stage of limb bud, tubular structures were seen at the distal end of the limb (**Figures 1S, T**).

3.1.6 The Early Stage of Nauplii

The embryo assumed the typical nauplii configuration about 30 min after the limb bud stage. At this stage, a large amount of red pigment gathered toward the anterior end of the embryo, forming a red eyespot, with obvious segmentation of the appendages and a clear endwise furrow between the body and the appendages (**Figures 1U–W**).

3.1.7 Hatching Stage

This stage was formed 6 h and 10 min after oviposition (majority of 55%) and could be divided into the rupture stage of outer and inner membranes.

3.1.8 The Rupture Stage of Outer Membrane

This stage could be recognized by the intermittent twitch of appendages and the concentrations of muscles. The nauplii twitched on an average frequency of three to four times per minute initially. This twitching process could last for about 20–30 min, and it was not at a consistent speed; sometimes it twitched strongly, sometimes it stopped twitching. The frequency of twitching accelerated to once per 1 or 2 s near the rupture stage of the outer membrane (**Figure 1X**). The embryo ruptured the outer membrane from the posterior end (**Figure 1X2**). The transparent outer membrane slid and shrank backward, and the inner membrane, which enclosed the fully developed nauplii, extruded from the outer membrane, which took about 10 s (**Figures 1X3–X5**).

3.1.9 The Rupture Stage of Inner Membrane

The inner membrane was thinner and more transparent than the outer membrane. The appendages of nauplii stretched out and the inner membrane expanded; subsequently, the nauplii rapidly ruptured membrane from the anterior end of the body 70 s after the rupture of the outer membrane (**Figures 1Y1, Y2**). The nauplii remained stationary for about 10 s after hatching and then began to do skipping movements (**Figure 1Z**).

3.2 Effects of Temperature on Egg Hatching Time

The time required for hatching of viable eggs (exceed 50%) at various temperatures are shown in **Figure 2**. A Bělehrádek's function was applied to describe the relationship between egg hatching time and the water temperature. By fitting the data between 22°C and 30°C, the following equation was derived:

$$D = 24.01\left(T - 16.92\right)^{-0.61}$$

The physiological relationship between temperature and development time was obvious: water temperature significantly affected egg development time of *B. amoyensis* ($p < 0.001$, one-way ANOVA), and egg hatching time of *B. amoyensis* shortened exponentially with increasing temperature.

3.3 Spawning Rhythm

The fluctuations of egg production of *B. amoyensis* from 8:00 a.m. to next day 8:00 a.m. are shown in **Figure 3**. Copepods kept spawning during the 24 h of the whole experiment. Females usually spawn two eggs at a time, sometimes up to four, and the eggs are arranged in pairs. The maximum egg production was 44 eggs female^{-1} day^{-1}, and the minimum egg production was 24 eggs female^{-1} day^{-1}, with an average egg production of 33 eggs female^{-1} day^{-1}. The peak of egg production of *B. amoyensis*

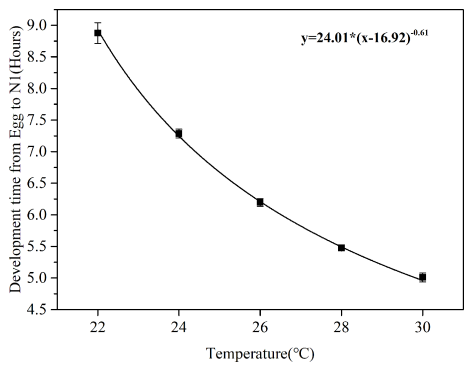

FIGURE 2 | Correlation curves between egg development time (D) and water temperature (T) in *B. amoyensis* (N=30). Data are presented as mean± standard error (SE).

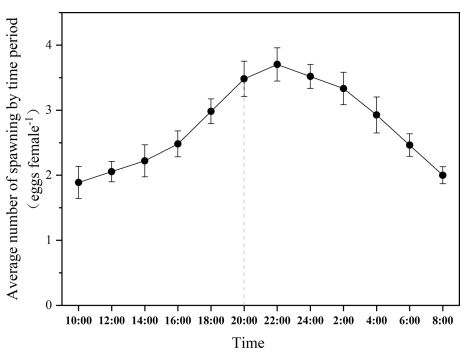

FIGURE 3 | The daily spawning rhythm of *B. amoyensis*. Data are presented as mean± standard error (SE). The dotted line is the point in time when the dark period is entered.

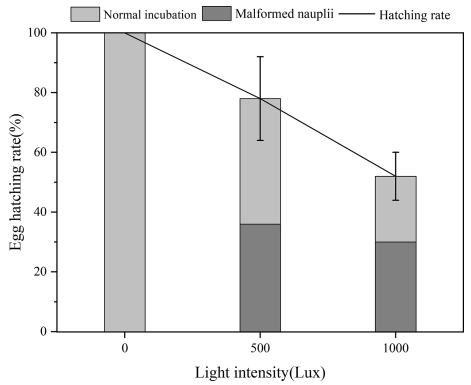

FIGURE 4 | Egg hatching rate of *B. amoyensis* incubated at three different light intensities (N=45). Data are presented as mean ± standard error (SE).

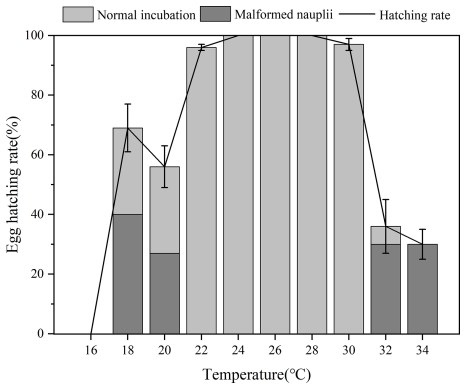

FIGURE 5 | Egg hatching rate of *B. amoyensis* incubated at different temperatures(N=45). Data are presented as mean± standard error (SE).

presented after 2 h of dark; more than 54% of eggs spawn during dark period (p<0.001).

3.4 Effects of Light Intensity, Temperature, and Salinity on Egg Hatching Rate

3.4.1 Effects of Light Intensity on Egg Hatching Rate

The EHRs of *B. amoyensis* are presented in **Figure 4**. Significant differences were detected under different light intensities, and the EHR of *B. amoyensis* decreased with increasing light intensity. The data were used to show the overall egg hatching rate, the rate of hatching normal nauplii, and deformed nauplii (p< 0.05, one-way ANOVA).

There was >50% success in EHR across all treatments, and the highest EHR (100%) was recorded for the dark treatment, which was significantly higher (p< 0.01) than that of the 1,000 lx treatment. Malformed nauplii, which usually could not survive, were observed at both two treatments of 500 and 1,000 lx, and the ratio of malformed nauplii was 36% and 30%, respectively, which indicated that these two light intensities were detrimental to egg hatching of *B. amoyensis* and dark condition was favorable for the egg incubation of *B. amoyensis*. The percentage of normal nauplii from the 500 lx group was 42%, while in the 1,000 lx group, it was 22%. The unhatched embryos stopped developing and presented an abnormal shape, which were obviously dead.

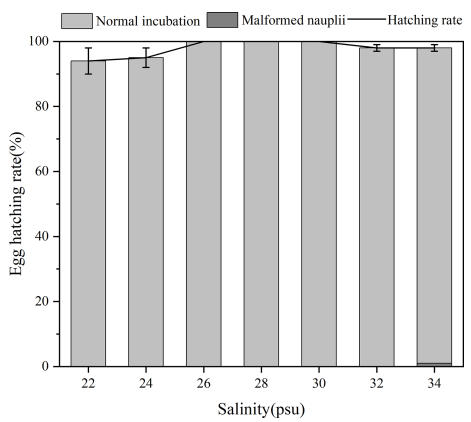

FIGURE 6 | Egg hatching rate of *B. amoyensis* incubated at seven different salinities (N=45). Data are presented as mean± standard error (SE).

3.4.2 Effects of Temperature on Egg Hatching Rate

Temperature significantly affected egg incubation (p< 0.01, one-way ANOVA). Hatching success of *B. amoyensis* eggs incubated at different temperatures was highest at a range of 24–28°C (**Figure 5**), with 100% of eggs hatched in all replicates, followed by 97% and 96% at 30°C and 22°C, respectively.

Hatching percentages from 32°C (36%) and 34°C (30%) were significantly lower than that of other treatments (p< 0.01). Hatching success also was significantly lower (p< 0.01) from three temperatures lower than 22°C, which was 56%, 69%, and 0% at 20°C, 18°C, and 16°C, respectively (**Figure 5**). These results suggested that too low and too high temperatures would decrease EHR and lead to malformed nauplii. Hatching success at 22°C–30°C was above 94% for all (**Figure 5**), and no statistical differences were found among them, which indicated that this temperature range was optimum for the egg incubation of *B. amoyensis*. The percentage of malformed nauplii from 18°C, 20°C, 32°C, and 34°C was 40%, 20%, 30%, and 30%, respectively, while no malformed nauplii was found in the treatments of 22°C, 24°C, 26°C, and 28°C. The ratio of normal nauplii from 18°C, 20°C, 32°C, and 34°C was 29%, 29%, 6%, and 0%, respectively. Embryo development of the unhatched eggs stopped, and the abnormal shape obviously indicated that they were already dead.

3.4.3 Effects of Salinity on Egg Hatching Rate

Hatching success was not significantly different among the six salinity treatments (p > 0.05, one-way ANOVA), which were all above 88% and the hatching success reached 100% at 26–30 psu salinity treatments (**Figure 6**). Although a few malformed nauplii were hatched at salinity of 34 psu, the hatching rate from that salinity was still high and that of all replicates was above 96%. These results indicated that *B. amoyensis* eggs could hatch well within a salinity range of 22–34 psu.

4 DISCUSSION

Bestiolina amoyensis has a small egg (<75 μm) compared to other free-spawning copepods, such as *Calanus* spp., whose eggs are about 145–340 μm in diameter (Marshall and Orr, 1954; Marshall and Orr, 1955; Conover, 1967); that of *Acartia* spp. are about 77–78 μm (Marshall & Orr, 1954; Marshall and Orr, 1955; Nilsson & Hansen, 2018). *Bestiolina amoyensis* also has a demersal egg, which quickly sinks into the water after spawning, and the sinking egg facilitated its collection from the bottom of the culture vessel and the embryonic observation.

The embryonic development of copepods starts from the nuclear division of fertilized egg to the hatching of the first stages of nauplii, which are generally divided into different stages according to the external morphological features of embryos at different development process, such as blastomere division, the appearance of appendages, and the formation of the compound eyes and other organs. Similar to free-spawning calanoid copepods such as *Calanus finmarchicus* (Marshall & Orr, 1954; Marshall and Orr, 1955), *Parvocalanus carssirostris* (Yang, 1977), *Centropages tenuiremis* (Gao, 2014), *Sinocalanus tenellus* and *Acartia* spp. (Chen, 2014), and *A. tonsa* (Nilsson & Hansen, 2018), the embryonic development of *B. amoyensis* was divided into seven stages: newly laid eggs, cleavage stages (2-cell stage, 4-cell stage, 8-cell stage 16-cell stage, and multicellular stage), grastrulation, no structure visible, limb bud stage, early stage of nauplii, and hatching.

The early cleavage stages of copepods, although with more or less stereotyped patterns of blastomere divisions, have been largely neglected in copepod embryology (Loose and Scholtz, 2019). The cleavage of free-living copepods is total and equal to adequal (Loose and Scholtz, 2019), such as *Calanus helgolandicus* (Poulet et al., 1995), *C. finmarchicus*, *C. pacificus*, *C. marshallae*, *Metridia* spp. (Zirbel et al., 2007), *A. tonsa* (Nilsson and Hansen, 2018), and *Skistodiaptomus* spp. (Loose and Scholtz, 2019). Yang (1977) showed that the first and second cleavage of *P. carssirostris* were meridional, and the third cleavage was equatorial. Loose and Scholtz (2019) showed that the first and second cleavages of *Skistodiaptomus* spp. are both meridional; the third cleavage is equatorial, forming a total of four smaller and four larger blastomeres; and the fourth and fifth cleavage are asynchronous. The cleavage of *B. amoyensis* is similar to the above-mentioned free-spawning copepod in that the first cleavages are meridional, bisecting the two blastomeres, which are approximately equal in size. Furthermore, the second cleavages are meridional, the third cleavage is equatorial, the fourth cleavages are meridional, and the fifth cleavages are difficult to distinguish under light microscopy due to the small size of the blastomere.

The early cleavage stage of *B. amoyensis* developed very fast at 26°C. It took 30 min from spawning to the fourth cleavage stage, which was very similar with *P. carssirostris*, in which it took 28 min from newly laid eggs to the fourth cleavage stage at 29°C–30°C (Yang, 1977). The duration of the 2-, 4-, 8-, and 16-cell stages of *B. amoyensis* was short and almost isochronous, taking about 5 min each at 26°C. In addition, the two-, four-, and eight-cell stages of early cleavage in *C. tenuiremis* at 20°C also approximated isochronous development, which was 0.8, 1.0, and 0.9 h, respectively (Gao, 2014). These results indicated that, to some extent, the duration of the early cleavage stage of copepods may be approximately isochronous. The relative long early cleavage duration of *C. tenuiremis* mainly related to the much lower embryo incubation temperature, which was 20°C for *C. tenuiremis*, while for *B. amoyensis* and *P. carssirostris*, the incubation temperature was 26°C and 29°C–30°C, respectively.

Some studies stained embryonic nucleus to observe the cleavage (Poulet et al., 1995; Nilsson & Hansen, 2018; Loose & Scholtz, 2019), while those copepods typically had either large eggs or hard eggshells, facilitating the manipulation of the staining process. We tried hard to stain the embryo of *B. amoyensis* but failed. The relatively small (<75 μm) size and the thin egg membranes made it very difficult to manipulate and easy to lose during the staining process. In addition, the eggs of *Parvocalanus aculeatus* and *P. parvus* not only have a thin egg membrane that is easily ruptured but also are transparent, which make the observation difficult. These might be the reasons why the study of copepod embryology is somewhat neglected.

It is noteworthy that the nauplius of almost all species started twitching shortly before hatching (Marshall & Orr, 1954; Marshall and Orr, 1955). Although the eggs of numerous copepods hatched in much the same way (Marshall & Orr, 1954; Marshall and Orr, 1955), studies and specific descriptions of copepod hatching need to be refined, and even further studies are needed to determine whether the hatching patterns are the same. Marshall & Orr (1954) stated that in free-spawning copepods such as *Calanus* spp., *Metridia* spp., and *Acartia* spp., the embryonic inner membrane was completely separated from the outer membrane. Several studies (Marshall & Orr, 1954; Marshall and Orr, 1955; Yang, 1977; Chen, 2014) indicated that copepod eggs had both inner and outer membranes. Separation of the outer membrane from the inner membrane was also observed in *B. amoyensis*, and the inner membrane was bulged out of the outer membrane. This is similar to the description of the incubation process by Davis (1959), who examined the freshwater copepod *Diaptomus asblandi*, *Diaptomus siciloides*, *Cyclops bicuspidatus*, and *Mesocyclops edax*, where the outer membrane was ruptured by pressure from the inner membrane, while the inner membrane was expanded by the osmotic entry of water.

It had been observed that the nauplii of *B. amoyensis*, *B. similis*, and *P. carssirostris* all broke the outer membrane from the tail end during hatching, which was consistent with the description by Marshall and Orr (1954), who proposed that the nauplius usually extrudes from the head or tail end during the process of rupturing the outer membrane. Marshall and Orr (1954) also found that although some nauplii also could extrude out from lateral side of the limbs occasionally, it usually leads to hatching failure. When nauplii just got rid of inner membranes, they often did not start swimming immediately; they usually remained stationary for 10–20 s and then swam off (Marshall & Orr, 1954; Marshall and Orr, 1955), and this phenomenon was also observed in *B. amoyensis*.

In an environment where food is not a limiting factor, the temperature is the main environmental factor regulating

the development time of copepods (Ban, 1994; Anzueto-Sánchez et al., 2014), and temperature changes could increase or decrease the hatching time of eggs (Castro-Longoria, 1998; Chinnery & Williams, 2004). Previous investigations indicated that the development time of copepod decreased with increasing temperature (Ozaki & Ikeda, 1997; Chinnery & Williams, 2004), as does the hatching time of *B. amoyensis* eggs, which shortened progressively as temperature increased at a range of 22°C–30°C.

Light is one of the most important structuring factors for life in aquatic biology (Radhakrishnan et al., 2020). There are some evidence suggesting that subitanous and/or dormant eggs of various invertebrates (e.g., crustaceans, insects, and rotifers) can exhibit photoreception (Hagiwara & Hino, 1989; Itoh & Sumi, 2000; Blackmer et al., 2002). Photic stimulations represent important extrinsic factors controlling aspects of reproduction in many marine invertebrates (Moraitou-Apostolopoulou & Verriopoulos, 1982). A majority of studies reported that light could induce hatching in aquatic invertebrates (Takahashi, 1977; Mitchell, 1990; Hagiwara et al.,1995; Murugan & Dumont, 1995). Conversely, the present results indicated that too much light (500 and 1,000 lx) inhibited the hatching of *B. amoyensis* eggs. Hagemann et al. (2016) also found a highly negative effect of light on EHR of cold storage eggs of *A. tonsa* and noted that light hindered the oxygen diffusion across the eggshell, resulting in a high bacterial load that prevented the eggs from hatching. Although the exact cause of the negative effects of light on EHR of *B. amoyensis* still needs further experiment, the present hindrance to the hatching of *B. amoyensis* eggs might be related to its nocturnal spawning rhythm. Marine calanoid copepods had a distinct diurnal spawning rhythm, and *Calanus* spp. (Harding et al., 1951) and *P. crassirostris* (Sun, 2008) were mostly nocturnal. The daily spawn rhythms of *B. amoyensis* (500 lx, 12L:12D) were observed. The peak of egg production of *B. amoyensis* presented after 2 h of dark; more than 54% of eggs spawned during dark conditions ($p<0.001$). We also cultured *B. amoyensis* under light intensity of 4,000–5,000 lx and found that over 90% of the eggs produced during dark period. These characteristics indicated that *B. amoyensis* was a nocturnal spawning species, and high levels of light intensities (500 and 1,000 lux in the present experiment) were detrimental for its embryo development. Unfortunately, there is very little reference involving the effects of light intensity on embryonic development of crustacean. Liang and Chen (2010) reported that *Panulirus ornatus* eggs should incubated in a light intensity<200 lx; lots of malformation were observed when light intensity was higher than 500 lx. Further study is needed to explore the effect of light on the malformation.

Unlike *Acartia* species, whose eggs are hard and with an opaque egg outer membrane, *B. amoyensis* has transparent and thin egg membrane. Considering the mode of action of light, it could act directly on germ cells by passing through the integument in transparent or translucent organisms (Moraitou-Apostolopoulou & Verriopoulos, 1982). Most marine copepods including *B. amoyensis*, *B. similis*, *P. parvus*, *Calanus* spp. (Marshall & Orr, 1954; Marshall and Orr, 1955), and *P. carsirostris* (Yang, 1977) have transparent egg membranes and nocturnal spawning habits, and thus, the effects of light on their hatching could be direct. If such nocturnally laid eggs are incubated under light conditions, the light might directly affect the embryo through the transparent egg membrane, altering the rhythm of long-adapted dark incubation, which placed the embryo in a state of stress, further leading to abnormal embryonic development and malformed nauplii. This would account why more than 30% malformed *B. amoyensis* nauplii were recorded under 500 and 1,000 lx of light intensity. Meanwhile, light condition, i.e., photoperiod and light intensity, can be easily manipulated with minimal costs in larviculture (Chinnery & Williams, 2003). For *B. amoyensis*, farmers could incubate the eggs during the night, which ensures that large numbers of nauplii could be collected the next daytime to timely meet the prey requirements of marine fish larvae.

Temperature and salinity are the two most important environmental parameters affecting the seasonal and spatial distribution of marine copepods in the wild (Miller & Marcus, 1994). Copepods like *P. crassirostris*, *A. clausi*, and *P. parvus* (Li et al., 2001; Yang, 2007; Lian et al., 2018), living in nearshore and warm water areas, are a group of high temperature and low salinity species; surface water temperatures of their natural waters are generally >20°C (Sun et al., 2014), and the distribution salinity range are approximately within 20–31.7 psu (Huang & Zheng, 1984). *Bestiolina amoyensis* usually lives in coastal and estuarine waters (Wang et al., 2021), where it adapts to a temperature range of 14°C–29.5°C and a salinity range of 16.6–30.7 psu in nature. Larger numbers of *B. amoyensis* were reported when salinity was higher than 25 psu (Li & Huang, 1984). The hatching success of *B. amoyensis* at 22°C–30°C, i.e., within the acclimation temperature range of their natural distribution area, was above 94% in the present experiment. Moreover, the hatching success reached 100% at salinities of 26–30 psu, which was consistent with the larger distribution populations at salinity >25 psu (Li & Huang, 1984). All of the above indicate that *B. amoyensis* is a nearshore and warm-water species.

Temperature and salinity exceeding suitable range caused malformation of nauplii of *B. amoyensis*. Planktonic copepods maintain large free amino acid pools, such as *C. finmarchicus* (Cowey & Corner, 1963) and *A. tonsa* (Alzara, 1968; Farmer & Reeve, 1978), and catabolism of free amino acids is important in the regulation of cellular osmotic pressure exposed to low and high salinity (Farmer & Reeve, 1978). Previous research also indicated that prolonged exposure to salinity and temperature stress enhanced protein absence (Gonzalez & Bradley, 1994; Kimmel & Bradley, 2001). Free amino acid would be catabolized to cope with the temperature and salinity stress and increase the consumption of protein, which might lead to abnormal embryonic development and malformed nauplii.

5 CONCLUSION

The embryonic development process of *B. amoyensis* is similar to other calanoid copepods including seven sequential stages: fertilized eggs, cleavage stage, gastrulation, no structure visible stage, limb bud stage, early nauplii, and hatching. The egg hatching time of *B. amoyensis* shortened exponentially with the increasing

temperature. The optimum light intensity, temperature, and salinity ranges for the egg hatching of *B. amoyensis* was 0 lx, 22°C–30°C, and 22–34 psu, respectively.

DATA AVAILABILITY STATEMENT

The original contributions presented in the study are included in the article/supplementary material. Further inquiries can be directed to the corresponding author.

AUTHOR CONTRIBUTIONS

SW and LW conceived the original idea of this study and designed the experiments. LW conducted the experiments and collected the data. LW, SW, and YC performed the data analyses. LW and YW wrote the draft of the article and revised it with SW. SW supervised the research. All authors contributed to the article and approved the submitted version.

FUNDING

This work was contribution to the Regional Demonstration Project of the 13th Five-Year Plan of Marine Economy Innovation & Development in Xiamen (funded by the State Oceanic Administration, People's Republic of China, grant no. 16PZY002SF18).

ACKNOWLEDGMENTS

We thank researcher Changshou Zhu from Fujian Institute of Oceanography for professionally guiding the identification of *B. amoyensis*.

REFERENCES

Alajmi, F. and Zeng, C. (2015). Evaluation of Microalgal Diets for the Intensive Cultivation of the Tropical Calanoid Copepod, *Parvocalanus Crassirostris*. *Aquac. Res.* 46, 1025–1038. doi: 10.1111/are.12254

Alzara, L. (1968). *Survey of Free Amino Acids in Copepod Populations* (Kingston: University of Rhode Island), 97 pp.

Anzueto-Sánchez, M. A., Barón-Sevilla, B., Cordero-Esquivel, B. and Celaya-Ortega, A. (2014). Effects of Food Concentration and Temperature on Development, Growth, Reproduction and Survival of the Copepod *Pseudodiaptomus Euryhalinus*. *Aquac. Int.* 22, 1911–1923. doi: 10.1007/s10499-014-9791-5

Ban, S. (1994). Effect of Temperature and Food Concentration on Post-Embryonic Development, Egg Production and Adult Body Size of Calanoid Copepod *Eurytemora Affinis*. *J. Plankton Res.* 16, 721–735. doi: 10.1093/plankt/16.6.721

Blackmer, J. L., Lee, L. L. and Henneberry, T. J. (2002). Factors Affecting Egg Hatch, Development, and Survival of *Bemisia Argentifolii* (Homoptera: Aleyrodidae) Reared on an Artificial Feeding System. *Environ. Entomol.* 31, 306–312. doi: 10.1603/0046-225X-31.2.306

Camus, T., Rolla, L., Jiang, J. and Zeng, C. (2021). Effects of Microalgal Food Quantity on Several Productivity-Related Parameters of the Calanoid Copepod *Bestiolina Similis* (Calanoida: Paracalanidae). *Front. Mar. Sci.* 8. doi: 10.3389/fmars.2021.812240

Camus, T., & Zeng, C. (2010). Roles of Microalgae on Total Egg Production Over Female Lifespan and Egg Incubation Time, Naupliar and Copepodite Survival, Sex Ratio and Female Life Expectancy of the Copepod Bestiolina similis. *Aquac. Res.* 41, 1717-1726. doi: 10.1111/j.1365-2109.2010.02565.x

Camus, T., Zeng, C. and McKinnon, A. D. (2009). Egg Production, Egg Hatching Success and Population Increase of the Tropical Paracalanid Copepod, *Bestiolina Similis* (Calanoida: Paracalanidae) Fed Different Microalgal Diets. *Aquaculture* 297, 169–175. doi: 10.1016/j.aquaculture.2009.09.018

Castro-Longoria, E. (1998). *Seasonal and Spatial Distribution Patterns of the Congeneric Group Acartia in the Solent–Southampton Water Estuarine System, With Special Reference to Aspects of Their Fecundity* (Southampton: University of Southampton).

Castro-Longoria, E. (2003). Egg Production and Hatching Success of Four *Acartia* Species Under Different Temperature and Salinity Regimes. *J. Crustac. Biol.* 23, 289–299. doi: 10.1163/20021975-99990339

Chen, L. D. (2014). *Preliminary Study on Ecology of Zooplankton Resting Eggs in Typical Waters of Pearl River Estuary and the Eastern Guangdong Coast* (Guangzhou: Jinan University).

Chinnery, F. E. and Williams, J. A. (2003). Photoperiod and Temperature Regulation of Diapause Egg Production in *Acartia Bifilosa* From Southampton Water. *Mar. Ecol. Prog.* 263, 149–157. doi: 10.3354/meps263149

Chinnery, F. E. and Williams, J. A. (2004). The Influence of Temperature and Salinity on *Acartia* (Copepoda: Calanoida) Nauplii Survival. *Mar. Biol.* 145, 733–738. doi: 10.1007/s00227-004-1354-2

Choi, S. Y., Jeon, S. C. and Soh, H. Y. (2022). Effects of Cold Storage and Salinity on *Acartia Sinjiensis* (Copepoda: Calanoida) Egg Hatching. *Aquac. Res.*, 53, 3568–3574. 1–7. doi: 10.1111/are.15861

Choi, S. Y., Lee, E. H., Soh, H. Y. and Jang, M. C. (2021). Effects of Temperature and Salinity on Egg Production, Hatching, and Mortality Rates in *Acartia Ohtsukai* (Copepoda, Calanoida). *Front. Mar. Sci.* 8. doi: 10.3389/fmars.2021.704479

Conover, R. J. (1967). Reproductive Cycle, Early Development, and Fecundity in Laboratory Populations of the Copepod *Calanus Hyperboreus*. *Crustaceana* 13 (1), 61–72. doi: 10.1163/156854067X00080

Cowey, C. B. and Corner, E. D. S. (1963). Amino Acids and Some Other Nitrogenous Compounds in *Calanus Finmarchicus*. *J. Mar. Biol. Ass. U.K.* 43, 485–493. doi: 10.1017/S0025315400000461

Davis, C. C. (1959). Osmotic Hatching in the Eggs of Some Fresh-Water Copepods. *Biol. Bull.* 116, 15–29. doi: 10.2307/1539152

Devreker, D., Souissi, S., Winkler, G., Forget-Leray, J. and Leboulenger, F. (2009). Effects of Salinity, Temperature and Individual Variability on the Reproduction of *Eurytemora Affinis* (Copepoda; Calanoida) From the Seine Estuary: A Laboratory Study. *J. Exp. Mar. Biol. Ecol.* 368, 113–123. doi: 10.1016/j.jembe.2008.10.015

Drillet, G., Frouël, S., Sichlau, M. H., Jepsen, P. M., Højgaard, J. K., Joarder, A. K., et al. (2011). Status and Recommendations on Marine Copepod Cultivation for Use as Live Feed. *Aquaculture* 315, 155–166. doi: 10.1016/j.aquaculture.2011.02.027

Engel, M. and Hirche, H. J. (2004). Seasonal Variability and Inter-Specific Differences in Hatching of Calanoid Copepod Resting Eggs From Sediments of the German Bight (North Sea). *J. Plankton Res.* 26, 1083–1094. doi: 10.1093/plankt/fbh099

Farmer, L. and Reeve, M. R. (1978). Role of the Free Amino Acid Pool of the Copepod Acartia Tonsa in Adjustment to Salinity Change. *Mar. Biol.* 48, 311–316. doi: 10.1007/BF00391634

Fernández-Ojeda, C., Muniz, M. C., Cardoso, R. P., dos Anjos, R. M., Huaringa, E., Nakazaki, C., et al. (2021). Plastic Debris and Natural Food in Two Commercially Important Fish Species From the Coast of Peru. *Mar. pollut. Bull.* 173, 113039. doi: 10.1016/j.marpolbul.2021.113039

Gao, Q. J. (2014). *Study on Embryonic Development of Centropages Tenuiremis* (Xiamen: Xiamen University).

Gaudy, R., Cervetto, G. and Pagano, M. (2000). Comparison of the Metabolism of Acartia Clausi and A. Tonsa: Influence of Temperature and Salinity. *J. Exp. Mar. Biol. Ecol.* 247, 51–65. doi: 10.1016/S0022-0981(00)00139-8

Gonzalez, C. R. and Bradley, B. P. (1994). "Salinity Stress Proteins in Eurytemora Affinis0," in *Ecology and Morphology of Copepods* (Dordrecht: Springer), 461–468.

Hagemann, A., Øie, G., Evjemo, J. O. and Olsen, Y. (2016). Effects of Light and Short-Term Temperature Elevation on the 48-H Hatching Success of

Cold-Stored *Acartia Tonsa* Dana Eggs. *Aquac. Int.* 24, 57–68. doi: 10.1007/s10499-015-9908-5

Hagiwara, A. and Hino, A. (1989). Effect of Incubation and Preservation on Resting Egg Hatching and Mixis in the Derived Clones of the Rotifer *Brachionus Plicatilis*. *Hydrobiologia* 186 (187), 415–421. doi: 10.1007/BF00048940

Hagiwara, A., Hoshi, N., Kawahara, F., Tominaga, K. and Hirayama, K. (1995). Resting Eggs of the Marine Rotifer *Brachionus Plicatilis* Müller: Development, and Effect of Irradiation on Hatching. *Hydrobiologia* 313, 223–229. doi: 10.1007/BF00025955

Hairston, N. G. and Kearns, C. M. (1995). The Interaction of Photoperiod and Temperature in Diapause Timing: A Copepod Example. *Biol. Bull.* 189, 42–48. doi: 10.2307/1542200

Harding, J. P., Marshall, S. M. and Orr, A. P. (1951). Time of Egg-Laying in the Planktonic Copepod Calanus. *Nature* 167, 953–953. doi: 10.1038/167953a0

Huang, Q. S. and Zheng, Z. (1984). The Relation of Copepods to Salinity in the Estuary of Jiulong River. *J. Xiamen Univ. (Natural Science)* 23, 497–505.

Itoh, M. T. and Sumi, Y. (2000). Circadian Clock Controlling Egg Hatching in the Cricket (Gryllus Bimaculatus). *J. Biol. Rhythms.* 15, 241–245. doi: 10.1177/074873040001500305

Jang, M. C., Shin, K., Hyun, B., Lee, T. and Choi, K. H. (2013). Temperature-Regulated Egg Production Rate, and Seasonal and Interannual Variations in *Paracalanus Parvus*. *J. Plankton Res.* 35 (5), 1035–1045. doi: 10.1093/plankt/fbt050

Karlsson, K., Puiac, S. and Winder, M. (2018). Life-History Responses to Changing Temperature and Salinity of the Baltic Sea Copepod *Eurytemora Affinis*. *Mar. Biol.* 165, 1–11. doi: 10.1007/s00227-017-3279-6

Kimmel, D. G. and Bradley, B. P. (2001). Specific Protein Responses in the Calanoid Copepod *Eurytemora Affinis* (Popp) to Salinity and Temperature Variation. *J. Exp. Mar. Biol. Ecol.* 266, 135–149. doi: 10.1016/S0022-0981(01)00352-5

Kline, M. D. and Laidley, C. W. (2015). Development of Intensive Copepod Culture Technology for *Parvocalanus Crassirostris*: Optimizing Adult Density. *Aquaculture* 435, 128–136. doi: 10.1016/j.aquaculture.2014.09.022

Landry, M. R. (1975). The Relationship Between Temperature and the Development of Life Stages of the Marine Copepod *Acartia Clausi* Giesbr. 1. *Limnol. Oceanogr.* 20, 854–857. doi: 10.4319/lo.1975.20.5.0854

Lee, H. W., Ban, S., Ikeda, T. and Matsuishi, T. (2003). Effect of Temperature on Development, Growth and Reproduction in the Marine Copepod *Pseudocalanus Newmani* at Satiating Food Condition. *J. Plankton Res.* 25, 261–271. doi: 10.1093/plankt/25.3.261

Li, S. J., and Huang, J. Q. (1984). On Two New Species of Planktonic Copepoda From the Estuary of Jiulong River, Fujian, China. *J. Xiamen Univ. Nat. Sci.* 3, 381–390

Li, S. J., Xu, Z. Z., Huang, J. Q., Chao, W. Q., Chen, G., Ke, C. H., et al. (2001). Studies on Biology of Marine Zooplankton in China. *J. xiamen Univ. Natural Sci.* 40, 585–590.

Liang, H. F. and Chen, J. F. (2010)Effects of Four Ecological Factors on Embryonic Development of *Panulirus Ornatus*. Available at: https://xueshu.baidu.com/usercenter/paper/show?paperid=ecac02515a9e7dc7a30541a74a1d062b&site=xueshu_se&hitarticle=1 (Accessed June 3, 2022).

Lian, G. S., Wang, Y. G., Sun, R. X. and Hwang, J. S. (2018). *Species Diversity of Marine Planktonic Copepods in China's Seas* (Beijing: China Ocean Press). doi: 10.3724/SP.J.1003.2011.11130

Loose, G. and Scholtz, G. (2019). The Cleavage Pattern of Calanoid Copepods—a Case Study. *Dev. Genes Evol.* 229, 103–124. doi: 10.1007/s00427-019-00634-8

Marcus, N. (2005). "Calanoid Copepods, Resting Eggs, and Aquaculture," in *Copepods in Aquaculture*. Eds. Cheng-Sheng, L., O'Bryen, P. J. and Marcus, N. H. (Melbourne: Blackwell), 3–9.

Marshall, S. M. and Orr, A. P. (1954). Hatching in *Calanus Finmarchicus* and Some Other Copepods. *J. Mar. Biolog. Assoc. U.K.* 33, 393–401. doi: 10.1017/S0025315400008432

Marshall, S. M. and Orr, A. P. (1955). *The Biology of a Marine Copepod: Calanus Finmarchicus (Gunnerus)* (London: Oliver and Boyd).

McKinnon, A. D., Duggan, S., Nichols, P. D., Rimmer, M. A., Semmens, G. and Robino, B. (2003). The Potential of Tropical Paracalanid Copepods as Live Feeds in Aquaculture. *Aquaculture* 223, 89–106. doi: 10.1016/S0044-8486(03)00161-3

McLaren, I. A., Corkett, C. J. and Zillioux, E. J. (1969). Temperature Adaptations of Copepod Eggs From the Arctic to the Tropics. *Biol. Bull.* 137, 486–493. doi: 10.2307/1540170

Milione, M. and Zeng, C. (2008). The Effects of Temperature and Salinity on Population Growth and Egg Hatching Success of the Tropical Calanoid Copepod, *Acartia Sinjiensis*. *Aquaculture* 275, 116–123. doi: 10.1016/j.aquaculture.2007.12.010

Miller, D. D. and Marcus, N. H. (1994). The Effects of Salinity and Temperature on the Density and Sinking Velocity of Eggs of the Calanoid Copepod *Acartia Tonsa* Dana. *J. Exp. Mar. Biol. Ecol.* 179, 235–252. doi: 10.1016/0022-0981(94)90117-1

Mitchell, S. A. (1990). Factors Affecting the Hatching of *Streptocephalus Macrourus* Daday (Crustacea; Eubranchiopoda) Eggs. *Hidrobiological* 194, 13–22. doi: 10.1007/BF00012108

Moraitou-Apostolopoulou, M. and Verriopoulos, G. (1982). Influence of Light Conditions on the Offspring Production and the Sex Ratio of *Tisbe Holothuriae*, Humes (Copepoda, Harpacticoida). *Arch. Hydrobiol.* 96, 120–127.

Murugan, G. and Dumont, H. J. (1995). Influence of Light, DMSO and Glycerol on the Hatchability of *Thamnocephalus Platyurus* Packard Cysts. *Hidrobiological* 298, 175–178. doi: 10.1007/978-94-011-0291-9_16

Nagaraj, M. (1992). Combined Effects of Temperature and Salinity on the Development of the Copepod *Eurytemora Affinis*. *Aquaculture* 103, 65–71. doi: 10.1016/0044-8486(92)90279-T

Nilsson, B. and Hansen, B. W. (2018). Timing of Embryonic Quiescence Determines Viability of Embryos From the Calanoid Copepod, *Acartia Tonsa* (Dana). *PLos One* 13, e0193727. doi: 10.1371/journal.pone.0193727

Ozaki, K. and Ikeda, T. (1997). The Effect of Temperature on the Development of Eggs and Nauplii of the Mesopelagic Copepod Paraeuchaeta Elongata. *Plankton Biol. Ecol.* 44, 91–95.

Pan, Y. J., Dahms, H. U., Hwang, J. S. and Souissi, S. (2022). Recent Trends in Live Feeds for Marine Larviculture: A Mini Review. *Front. Mar. Sci.* 9. doi: 10.3389/fmars.2022.864165

Peck, M. A., Ewest, B., Holste, L., Kanstinger, P. and Martin, M. (2008). Impacts of Light Regime on Egg Harvests and 48-H Egg Hatching Success of *Acartia Tonsa* (Copepoda: Calanoida) Within Intensive Culture. *Aquaculture* 275, 102–107. doi: 10.1016/j.aquaculture.2007.12.008

Peck, M. A. and Holste, L. (2006). Effects of Salinity, Photoperiod and Adult Stocking Density on Egg Production and Egg Hatching Success in *Acartia Tonsa* (Calanoida: Copepoda): Optimizing Intensive Cultures. *Aquaculture* 255, 341–350. doi: 10.1016/j.aquaculture.2005.11.055

Poulet, S. A., Laabir, M., Ianora, A. and Miralto, A. (1995). Reproductive Response of *Calanus Helgolandicus*. I. Abnormal Embryonic and Naupliar Development. *Mar. Ecol. Prog.* 129, 85–95. doi: 10.3354/meps129085

Radhakrishnan, D. K., AkbarAli, I., Sathrajith, A. T., Schmidt, B. V., Sivanpillai, S. and Vasunambesan, S. T. (2020). Grazing Rates of Freshwater Copepod *Thermocyclops Decipiens* (Kiefe) on Chlorella Vulgaris Under Different Light Intensities. *Aquaculture* 525, 735321. doi: 10.1016/j.aquaculture.2020.735321

Roddie, B. D., Leakey, R. J. G. and Berry, A. J. (1984). Salinity-Temperature Tolerance and Osmoregulation in *Eurytemora Affinis* (Poppe)(Copepoda: Calanoida) in Relation to its Distribution in the Zooplankton of the Upper Reaches of the Forth Estuary. *J. Exp. Mar. Biol. Ecol.* 79, 191–211. doi: 10.1016/0022-0981(84)90219-3

Santhanam, P., Jeyaraj, N., Jothiraj, K., Ananth, S., Kumar, S. D. and Pachiappan, P. (2019). "Assessing the Efficacy of Marine Copepods as an Alternative First Feed for Larval Production of Tiger Shrimp Penaeus Monodon," in *Basic and Applied Zooplankton Biology*. Eds. Santhanam, P., Begum, A. and Pachiappan, P. (Singapore: Springer), 293–303. doi: 10.1007/978-981-10-7953-5_12

Souissi, A., Souissi, S. and Hwang, J. S. (2016). Evaluation of the Copepod *Eurytemora Affinis* Life History Response to Temperature and Salinity Increases. *Zool. Stud.* 55, e4. doi: 10.6620/ZS.2016.55-04

Sun, X. (2008). *Population Dynamics of Small Copepod* (Qingdao: Institute of oceanology, Chinese Academy of Sciences).

Sun, R., Wang, Y., Lian, G. and Lin, M. (2014). Distribution and Community Characteristics of Planktonic Copepods in the Northwest Coastal Waters Off Hainan Island. *Biodiv. Sci.* 22, 320–328. doi: 10.3724/SP.J.1003.2014.13137

Takahashi, F. (1977). Pioneer Life of the Tadpole Shrimps, Triops Spp. (Notostraca: Triopsidae). *Appl. Entomol. Zool.* 12, 104–117.

Valencia, G. A. T., Merino, G. E., Prieto-Guevara, M. J., Portillo, J. E. A., Arboleda, J. E. L. and Chapman, F. A. (2022). Spawning *Parvocalanus Crassirostris* at a High Adult Density: Explaining Low Adult Population Numbers and Means

for Improving Their Intensive Culture. *Aquaculture* 546, 737347. doi: 10.1016/j.aquaculture.2021.737347

VanderLugt, K., Cooney, M. J., Lechner, A. and Lenz, P. H. (2009). Cultivation of the Paracalanid Copepod, *Bestiolina Similis* (Calanoida: Crustacea). *J. World Aquac. Soc* 40, 616–628. doi: 10.1111/J.1749-7345.2009.00282.X

Wang, L., Wang, S., Zeng, C., Wang, Y. and Zeng, C. (2021). Effects of Food Concentration and Photoperiod on Egg Production, Female Life Expectancy and Population Dynamics of the Paracalanid Copepod, *Bestiolina Amoyensis*. *Front. Mar. Sci.* 8. doi: 10.3389/fmars.2021.788744

World Health Organization (2018) *E. Coli*. Available at: https://www.who.int/news-room/fact-sheets/detail/e-coli (Accessed March 15, 2018).

Yang, C. M. (1977). The Egg Development of Paracalanus Crassirostris Dahl 1894 (Copepoda, Calanoida). *Crustaceana* 31, 33–38. doi: 10.1163/156854077X00205

Yang, W. D. (2007). *Studies of Zooplankton Grazing Impacts on Phytoplankton in Xiamen Harbor*. Master's Thesis. Xiamen: Xiamen University.

Zirbel, M. J., Miller, C. B. and Batchelder, H. P. (2007). Staging Egg Development of Marine Copepods With DAPI and PicoGreen®. *Limnol. Oceanogr-Meth.* 5, 106–110. doi: 10.4319/lom.2007.5.106

Conflict of Interest: The authors declare that the research was conducted in the absence of any commercial or financial relationships that could be construed as a potential conflict of interest. The handling editor CZ declared a past co-authorship with the authors SW, LW, and YW.

frontiers | Frontiers in Marine Science

ORIGINAL RESEARCH
published: 20 July 2022
doi: 10.3389/fmars.2022.906730

Full-Length Transcriptome Sequencing and Comparative Transcriptomic Analysis Provide Insights Into the Ovarian Maturation of *Exopalaemon carinicauda*

Jiajia Wang[1,2], *Jitao Li*[1,2], *Qianqian Ge*[2], *Wenyang Li*[1] and *Jian Li*[1,2*]

[1]Key Laboratory for Sustainable Utilization of Marine Fisheries Resources, Ministry of Agriculture and Rural, Yellow Sea Fisheries Research Institute, Chinese Academy of Fishery Sciences, Qingdao, China, [2]Function Laboratory for Marine Fisheries Science and Food Production Processes, Qingdao National Laboratory for Marine Science and Technology, Qingdao, China

OPEN ACCESS

Edited by:
Heinrich Dircksen,
Stockholm University, Sweden

Reviewed by:
Khor Waiho,
University of Malaysia Terengganu, Malaysia
Sirinart Techa,
National Science and Technology Development Agency (NSTDA), Thailand

***Correspondence:**
Jian Li
bigbird@ysfri.ac.cn

Specialty section:
This article was submitted to Aquatic Physiology, a section of the journal Frontiers in Marine Science

Received: 29 March 2022
Accepted: 16 June 2022
Published: 20 July 2022

Citation:
Wang J, Li J, Ge Q, Li W and Li J (2022) Full-Length Transcriptome Sequencing and Comparative Transcriptomic Analysis Provide Insights Into the Ovarian Maturation of Exopalaemon carinicauda. Front. Mar. Sci. 9:906730. doi: 10.3389/fmars.2022.906730

The ridgetail white shrimp *Exopalaemon carinicauda* has the potential to be used as a useful experimental organism in the field of crustacean research due to its transparent body, large egg, and short reproductive cycle. However, little is known about the regulatory mechanisms of ovarian maturation in *E. carinicauda*. In this study, we applied PacBio single-molecule long-read sequencing technology to unveil the whole transcriptome landscape of *Exopalaemon carinicauda* to better understand the molecular mechanisms of ovarian development. A total of 49.05 G polymerase read bases were generated, finally, 15, 151 unigenes were successfully identified with a mean length of 4, 257 bp and an N50 of 4, 884 bp from ovary tissues (five different ovarian developmental stages). A total of 14, 007 unigenes were successfully annotated in at least one public database. In addition, 8, 861 coding sequences, 4, 594 lncRNAs and 895 transcription factors were identified. Furthermore, we performed RNA-Seq analysis combined with Iso-Seq results to investigate ovarian maturation regulation mechanism and validated the results by quantitative real-time PCR. We annotated five vitellogenin isoforms in the full-length transcriptome, meanwhile these five genes and vitellogenin receptor suggested an important role during previtellogenesis of *E. carinicauda*. Genes were involved in PI3K-Akt signaling pathway, retinol metabolism, cell cycle and hedgehog signaling pathway, which showed obvious associations with ovarian maturation of E. carinicauda. We identified 40 DEGs, such as forkhead box protein L2, which may be related to ovarian development in the comparisons. The expression profiles of genes such as ecdysone receptor, ecdysone-induced protein 74EF, ecdysone inducible gene E75 and post-molt protein suggest that they were significantly associated with reproductive molting in the ovarian mature stage. In conclusion, the present study identified important genes and pathways involved in ovarian maturation, which might be useful for studying the reproductive regulation and mechanisms of ovarian maturation in *E. carinicauda*.

Keywords: iso-seq, full-length transcripts, shrimp, vitellogenin, ovarian maturation, vitellogenesis

INTRODUCTION

The ridgetail white shrimp *Exopalaemon carinicauda*, belonging to the Palaemonidae family of crustaceans, is a major commercial mariculture species that is naturally distributed on the coasts of the Yellow Sea and Bohai Sea (Xu et al., 2010). Owing to its rapid growth and high tolerance to environmental stress, the scale at which *E. carinicauda* is cultured has expanded in recent years (Zhang et al., 2015a). However, aquaculture production and large-scale cultivation are still restricted by the supply of high-quality broodstock. In addition to its economic value, *E. carinicauda* is a useful experimental organism in the field of crustacean developmental biology due to its transparent body, large egg, and high reproductive capacity, and short reproductive cycle of only 2–3 months (Yuan et al., 2017; Liang et al., 2020; Wang et al., 2020). The female shrimps generate at least three consecutive ovarian development during reproductive stage, but the ovaries of some shrimps gradually atrophy into cystic tubes after first ovarian mature. It is important to provide valuable information for understanding the vitellogenesis and ovarian development and clarify the regulatory mechanism of ovarian development of *E. carinicauda*.

Previous studies have reported the different ovarian maturation stages of *E. carinicauda* (Wang, 1987); the ovary size and color undergo visible changes during ovarian maturation. Researchers have cloned, expressed, and studied the functions of ovarian maturation-related genes in *E. carinicauda*, including those that encode farnesoic acid O-methyltransferase (FAMeT), vitellogenin (Vtg) and heat shock protein 90 (Duan et al., 2014; Li et al., 2016; Liang et al., 2020). These genes have also been studied in the Palaemonidae family, including *Macrobrachium nipponense* (Bai et al., 2016) and *Macrobrachium rosenbergii* (Guo et al., 2019a; Qian and Liu, 2019). However, the regulatory genes identified using these methods are incomplete, and the regulation of ovarian maturation remains unclear. It is, therefore, essential to investigate the molecular mechanisms that regulate ovarian maturation. Next-generation RNA-seq is one method in which to do this.

Illumina RNA-Seq is a powerful tool for the identification of differentially expressed genes (DEGs) (Santos et al., 2021). However, low-quality transcripts obtained through Illumina RNA sequencing result in incorrect annotation information and limit the scope of analysis of alternative splicing variants (Zhang et al., 2020). It is difficult to identify full-length transcript in the absence of a reference sequence in most crustaceans (Bankar et al., 2015). Additionally, genome resources have been identified in only a few crustaceans because of their large genome size and complexity (Rotllant et al., 2018). Fortunately, full-length transcriptome sequencing has been employed as an effective approach to obtain high-quality transcript sequences in the absence of reference genomes. Single-molecule real-time (SMRT) sequencing developed by Pacific Biosciences (PacBio) can obtain full-length sequences without post-sequencing assembly (Holmes et al., 2021), which has been used for whole-transcriptome profiling in many crustaceans (Cao et al., 2020; Ren et al., 2020; Zheng et al., 2020).

In the present study, a high-quality full-length transcriptome of the ovaries of *E. carinicauda* was generated by a combination of PacBio SMRT sequencing and Illumina RNA-Seq, and was further used for comparative transcriptomic analysis of the different ovarian developmental stages. Transcript functional annotation, long noncoding RNA (lncRNA) prediction, transcription factor and coding sequence were performed based on the data. Putative genes involved in ovarian development and vitellogenesis were identified according to the characteristics of the different ovarian developmental stages. This study provides a better understanding of the molecular mechanism of ovarian development and may be a valuable resource for further investigation of *E. carinicauda*.

MATERIALS AND METHODS

Animals and Sample Preparation

Female *E. carinicauda* adults (body length 52.29 ± 2.09 mm, body weight 2.37 ± 0.18 g) were collected from Haichen Aquatic Products Co. LTD in Rizhao, China. The shrimps were cultured in filtered aerated seawater at 25.0–26.0°C with an initial salinity of 31 ± 0.5, for one week. Aeration was used to maintain an adequate dissolved oxygen level. During the experimental periods, the shrimps were fed with commercial shrimp feed (~1.0 mm in diameter) twice daily (8:00 and 18:00), with food quantities equaling 10% of their body mass.

The females were assigned to one of five ovarian developmental stages using the criteria of Wang (1987) defined as: proliferative phase (stage I), the ovary is small and completely transparent when anatomically observed and its morphology and color cannot be distinguished by *in vitro* observation; minor growth phase (stage II), the ovary is enlarged, translucent with small black spots over its outer membrane, and positioned above the heart; major growth phase (stage III), ovarian volume continues to increase and its length has reached the 1/2 cephalothorax length, and the ovary is faintly yellow with small black dots over its ovarian membrane; mature phase (stage IV), the ovary covers almost the entire stomach, hepatopancreas, and heart, is bright yellow with dark green or tan spots, and the lateral shell of the first to fourth ventral segments is bluish; postpartum recovery (stage V), the ovary is very small and not obvious *in vitro*, and anatomical observation shows that it is transparent or translucent (Wang, 1987).

According to the criteria, ovarian development was assessed daily by observing the size and color of gonads, and the five different ovarian developmental females were obtained in three weeks. A total of one hundred and five shrimps were collected, ten shrimps (2 individuals×5 stages) were used for histological examination, other for transcriptomic analysis. Among them, five shrimps (different ovarian development stage) were used for single-molecule full-length transcriptome sequencing, and ninety shrimps (6 individuals×5 stages×3 three replicates) were used for Illumina RNA-seq, they were separately flash-frozen in liquid nitrogen and then preserved at -80°C.

Histological Procedure

Ten samples of *E. carinicauda* from each developmental stage were used for histological examination. Ovarian tissue slices, taken from the middle of each ovary, were fixed in 4% paraformaldehyde for 24 h. After dehydration in a gradient of ethanol solutions, the fixed tissues were embedded in paraffin wax. Paraffin-embedded tissues were sectioned to 4 μm and stained with Mayer's hematoxylin and eosin. Tissue sections were observed microscopically to assess the stage of ovarian development.

RNA Extraction and Quality Evaluation

Total RNA was isolated using TransZol Up Plus RNA Kit (Trans, China) according to the manufacturer's instructions, respectively. The integrity of RNA was assessed with the Agilent 2100 Bioanalyzer (Agilent Technologies, USA) and agarose gel electrophoresis. The purity and concentration of RNA were determined using a Nanodrop 2000 microspectrophotometer (Thermo Scientific).

Library Construction and Sequencing

To construct the full-length transcriptome sequencing library for PacBio sequencing, qualified RNA from five ovaries of the different ovarian development stage, were pooled in equal amounts. RNA sequencing and analysis were performed using Novogene (Beijing, China). The full-length cDNA library was sequenced on a SMRT Cell of PacBio platform, and the Blue Pippin Size Selection System protocol was used as described by PacBio (PN 100-092-800-03). Briefly, mRNA was enriched using Oligo (dT) magnetic beads, and subsequently reverse transcribed into full length 1st strand cDNA. Full-length cDNAs were subjected to restoration of DNA damage, end repair, ligation to sequencing adapters, and digestion with exonuclease. Qualified libraries were sequenced on the PacBio Sequel platform according to their effective concentration and data output requirements.

PacBio Long-Read Processing

According to the PacBio protocol, the sequence data were first processed using the SMRTlink 7.0 software to remove the SMRTbell™ adapter and low-quality data. The circular consensus sequences, also known as the reads of insert, were generated from subreads with BAM files. All the reads of inserts were further classified into full-length and non full-length transcript sequences based on whether the polyA tail signal and 5′ and 3′ cDNA primers could be simultaneously observed. The full-length consensus isoforms were obtained using the ICE Quiver algorithm and subsequently polished. These polished consensus sequences were further subjected to correction using the Illumina short reads. The final transcriptome sequences were filtered by removing redundancy using the CD-HIT program with a threshold identity of 0.99.

Functional Annotation

Gene function was annotated using BLAST software (version 2.2.26) (Altschul et al., 1997) based on the following seven databases: NR (NCBI non-redundant protein sequences), NT (NCBI non-redundant nucleotide sequences), Pfam (Protein family) (Finn et al., 2013), KOG/COG (Clusters of Orthologous Groups of proteins) (Tatusov et al., 2000), Swiss-Prot (A manually annotated and reviewed protein sequence database) (Apweiler et al., 2004), KO (KEGG Ortholog database) (Kanehisa et al., 2004) and GO (Gene Ontology) (Ashburner et al., 2000).

Structure Analysis of the Transcriptome

Candidate coding regions within the transcript sequences were identified by ANGEL software (Shimizu et al., 2006). We used *E. carinicauda* or closely related species confident protein sequences for ANGEL training and then run the ANGEL prediction for given sequences. Transcripts with a length of more than 200 nucleotides and having more than two exons were selected as lncRNA candidates. Four computational approaches, coding-noncoding-Index (CNCI) (Sun et al., 2013), coding potential calculator (CPC) (Kang et al., 2017), PLEK (Li et al., 2014) and Pfam-scan (Bateman et al., 2000), were employed to further screen the protein-coding unigenes from the non-coding unigenes. Transcripts predicted with coding potential were filtered out, and those without coding potential formed our candidate set of lncRNAs. Transcription factor related unigenes were predicted using the AnimalTFDB 2.0 database.

RNA-Seq Library Construction and Sequencing

Total RNA was extracted using same method mentioned above. A total of 15 libraries (three replicates from five groups) were generated using the NEBNext® Ultra™ RNA Library Prep Kit (Illumina, CA, USA). The libraries were sequenced on an Illumina HiSeq 4000 platform and 150 bp paired-end raw reads were generated. Clean data were obtained by removing low-quality reads and reads containing adapters and ploy-N, and used for subsequent analysis.

Differentially Expressed Transcript Analysis

The clean reads of each RNA-seq library were aligned to the full-length reference transcriptome to obtain unique mapped reads using STAR (Dobin et al., 2013) with default parameters. The mapped reads were counted, and the expression value was normalized to fragments per kilobase of transcript per million fragments mapped. Differential expression analysis of the two groups was performed using the DEseq R package. *P*-values were adjusted using Benjamini and Hochberg's approach for controlling the false discovery rate. We set the conditions of the false discovery rate <0.05 and $|\log2(\text{foldchange})| \geq 1$ as the thresholds for significantly differentially expressed transcripts.

Validation Experiments

Differentially expressed transcripts were verified using quantitative real-time PCR (qPCR) analysis. cDNA was synthesized using the PrimeScript™ Real-time PCR Kit (TaKaRa) for qPCR analysis. The specific primers of transcripts for qPCR were designed using Primer 5.0 software and listed in **Supplementary Table 1**. The qPCR assay was performed using the ChamQ SYBR Color qPCR Master Mix (Vazyme, China). Each qPCR reaction consisted of 10 μl 2×ChamQTM SYBR Color qPCR Master Mix, 50-100 ng of cDNA, 0.8 μl each of forward and reverse primer, 0.4 μl 50×ROX Reference Dye 2, and added sterile ddH_2O to total volume of 20 μl. The PCR was performed on the ABI PRISM 7500 Sequence Detection System (Applied Biosystems, USA) under the following conditions: one cycle at 95°C for 30 s, then 40 cycles of 95°C for 10 s, 60°C for 30 s followed by 1 cycle of 95°C 15 s, 60°C for 1 min and 95°C for 15 s. The β-actin of *E. carinicauda* (GenBank accession number: JQ045354.1) was used as an internal control for expression analysis of *E. carinicauda*, which was abundant and stable in cells, and hardly affected by the external regulation (Liang et al., 2017). The primers of all assays for the real-time PCR perform were conducted in triplicate. All analyzed were based on the C_T values of the PCR products. The expression was calculated with $2^{-\Delta\Delta CT}$ methods. Differences in gene expression were considered statistically significant at $P<0.05$ using one-way ANOVA and Tukey's multiple comparison test.

RESULTS

Histological Analysis of Different Ovarian Developmental Stages in *E. carinicauda*

According to Wang's study, the of *E. carinicauda* ovarian development can be divided into five stages. Histological examination of stage I showed that basophilic oogonia (OG) were located in the ovarian middle zone, and their mean long and short diameters were 9.45 ± 2.06 μm and 7.74 ± 1.64 μm, respectively. Basophilic previtellogenic oocytes (PR) were found on the periphery of OG, and their mean long and short diameters were 33.8 ± 5.41 μm and 26.65 ± 5.23 μm, respectively (**Figure 1A**).

In stage II, the PR were located in the ovarian middle zone, and were surrounded by endogenous vitellogenic oocytes (EN). The mean long and short diameters of EN were 153.88 ± 18.59 μm and 120.45 ± 20.59 μm, respectively (**Figure 1B**).

In stage III, the main cell type was exogenous vitellogenic oocytes (EX) with mean long and short diameters of 313.12 ± 35.14 μm and 254.64 ± 16.13 μm, respectively. The yolk granules (YG) appeared in the EX, and the follicular cells (FC) migrated to the periphery of EX (**Figure 1C**).

Mature oocytes (MO) were the main cell type in stage IV, with mean long and short diameters of 562.75 ± 34.51 μm and 446.8 ± 24.26 μm, respectively. The oocytes were squeezed into each other in a polygonal shape, and most cells in the nucellus were invisible (**Figure 1D**).

A Global Description of Full-Length Transcriptome

The full-length transcriptome of *E. carinicauda* was generated from pooled ovarian RNA using the PacBio Sequel platform (**Figure 2**). A total of 49.05 G polymerase read bases were generated. After filtering out adaptors and low-quality reads (less than 50 bp), 48.05 G subreads with a mean length of 3, 472 bp were obtained. Using SMRT Link 4.0 software, 486, 196 circular consensus sequences were generated, and approximately 77.80% of them were full-length non-chimeric reads, containing 5′ and 3′ primers, and the poly (A) tail. After clustering and polishing, a total of 24, 112 consensus reads were obtained with a mean length of 4, 076 bp. These consensus reads were subsequently corrected using LoRDEC and CD-HIT to eliminate up to 99.99% sequencing errors. Finally, 15, 151 unigenes with an average length of 4, 257 bp and an N50 of 4, 884 bp were successfully identified. Of these, 10, 510 were longer than 3, 000 bp.

Functional Annotation of Transcript

All 15, 151 unigenes were aligned with seven different databases, including NR, GO, KEGG, KOG, NT, Pfam, and SwissProt. A total of 14, 007 (92.45%) transcripts were successfully annotated in at least one public database, and 3, 578 transcripts annotated in all the databases (**Figure 3**). The remaining unannotated unigenes (1, 144 unigenes) may represent novel *E. carinicauda* species-specific genes.

GO analysis revealed that 10, 899 transcripts were assigned to 58 level-2 GO terms. Metabolic processes (4, 256), binding (7, 106) and cell parts (2, 531) were the most enriched subcategories within the biological process, molecular function, and cellular component level-2 categories, respectively (**Supplementary Figure 1A**).

A total of 13, 208 transcripts were mapped to KEGG Ortholog categories and grouped into 353 signaling pathways. The annotated pathways were grouped into six level-1 KEGG Ortholog terms, and signal transduction, transport and catabolism, and cancers were the top three most annotated level-2 KEGG Ortholog terms (**Supplementary Figure 1B**).

A total of 12, 140 transcripts were classified into 26 KOG classifications. The largest classification was general function prediction (2, 108 unigenes), followed by signal transduction mechanisms (1, 891 unigenes) then posttranslational modification, protein turnover and chaperones (1, 060 unigenes). (**Supplementary Figure 1C**)

Transcription Factor, Coding Sequence, and lncRNA Predictions

Using AnimalTFDB 2.0, a total of 895 transcripts were predicted to be transcription factors, whereby zf-C2H2 and ZBTB were the main ones identified (**Supplementary Figure 2A**). There were 8, 861 coding sequences identified by ANGEL, the distribution of the coding sequence lengths of complete open reading frames is shown in **Supplementary Figure 2B**. A total of 4, 594 lncRNAs were identified using the CNCI, CPC, PLEK, and Pfam approaches (**Supplementary Figure 2C**).

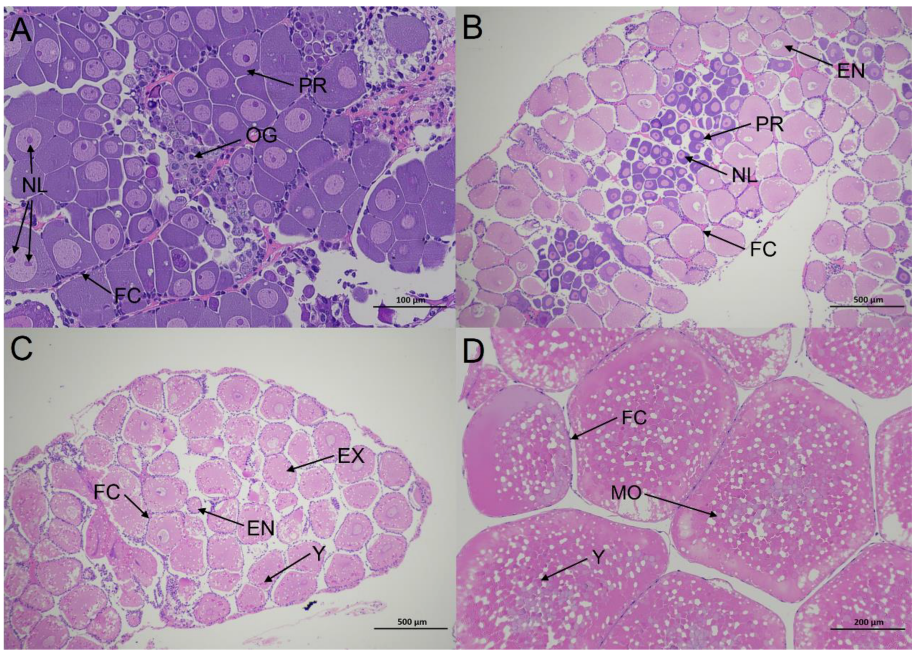

FIGURE 1 | Histological sections illustrating the ovarian status at different stages in *E. carinicauda* **(A)** proliferative phase (Stage I), ×200. **(B)** minor growth phase (Stage II), ×40. **(C)** major growth phase (Stage III), ×40. **(D)** mature phase (Stage IV), ×100. EN, endogenous vitellogenic oocytes. EX, exogenous vitellogenic oocytes. FC, follicle cell; MO, mature oocytes; NL, nucleolus; OG, oogonium; PR, previtellogenic oocytes; Y, yolk granule.

Differentially Expressed Transcript Analysis

We calculated and compared the expression levels of DEGs among the five groups (Stage I, Stage II, Stage III, Stage IV and Stage V) to identify reproduction-related genes. A total of 867 DEGs (204 up-regulated, 663 down-regulated) were detected between the Stage II and Stage I. For the Stage III and Stage II, 80 DEGs (41 up-regulated, 39 down-regulated) were detected, and for the Stage IV and Stage III, 333 DEGs (132 up-regulated, 201 down-regulated) were detected, and for the Stage IV and Stage IV, the number were 734 (389 up-regulated, 345 down-regulated) (**Figure 4**).

We recorded the most important pathways associated to ovarian development by comparing the DEGs with the KEGG pathway. Six pathways were involved in the regulation of ovarian development of *E. carinicauda*. There were three pathways (folate biosynthesis, PI3K-Akt signaling pathway and retinol metabolism) related to ovarian development in the comparison of Stage II and Stage I. Only folate biosynthesis pathway was significantly different between the Stage III and Stage II. There were three pathways (cell cycle, hedgehog signaling pathway and PI3K-Akt signaling pathway) were significantly different between the Stage IV and Stage III. The folate biosynthesis, phototransduction-fly and Hedgehog signaling pathway were significantly different between the Stage V and Stage IV. (**Table 1**)

Screening and Expression of Genes Related to Ovarian Development

Based on the analysis of DEGs, we manually screened 40 genes related to ovarian development by combining the q-value of the DEG enrichment pathways in the comparison groups Stage I vs Stage II, Stage II vs Stage III, Stage III vs Stage IV and Stage IV vs Stage V (**Figure 5**). The expressions of six genes were higher in the Stage II than the Stage I indicated that these genes participated in the regulation of the initiation of vitellogenesis. Seven genes and nineteen genes were highest expressed in the Stage III and Stage IV, respectively. Among them, ecdysone receptor, ecdysone-induced protein, 74EF, ecdysone inducible gene E75 and post-molt protein 1 expressed higher in the Stage IV for reproductive molting. The RYamide receptor like and dopamine receptor 2 were expressed higher in the Stage I than in the Stage II indicated that they are related to the inhibition of vitellogenesis.

Validation of DEGs by qRT-PCR

Expression levels of upregulated and downregulated unigenes were determined using quantitative real-time PCR (qRT-PCR). Between Stage II and Stage I, the expression levels were determined for five upregulated unigenes coding for CYP307, adenylyl cyclase-associated protein, checkpoint kinase 1, glutathione S-transferase and adiponectin receptor; and five downregulated unigenes coding for serine/threonine-protein kinase Doa, cyclophilin A, lipoprotein receptor 2A, guanylate cyclase PcGC-M2 precursor and ficolin-like protein 2. Similarly, between Stage IV and Stage III, the expression levels were measured for five upregulated unigenes coding for aurora kinase B, calcified cuticle protein, cyclin-dependent kinases 2, fork-head box L2, and serine/threonine-protein kinase D3, and five downregulated unigenes encoding alkaline phosphatase, growth/differentiation factor 8, cathepsin L, cyclin-dependent kinase

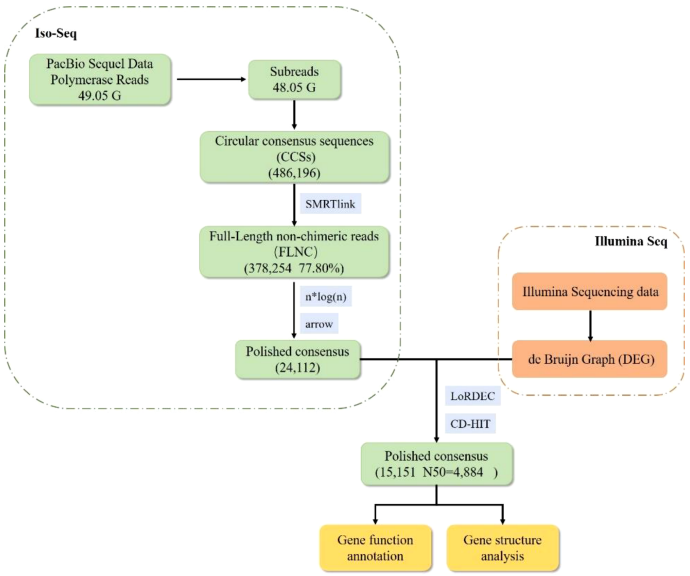

FIGURE 2 | The process and characteristics of Iso-Sequencing

inhibitor, and fatty acid synthase. The fold-changes determined by qRT-PCR and RNA-seq were compared for each DEG (**Figure 6**).

Analysis of Vitellogenin in *E. carinicauda*

Vitellogenin (Vtg) is an important source of nutrients for the development of ovaries and embryos in almost all oviparous organisms. We annotated five members of vitellogenin in the full-length transcriptome, including t_9427, t_7810, t_7815, t_7987 and t_8253, which were subsequently named EcVtg1 to EcVtg5, respectively. EcVtg1 and EcVtg2 had four functional domains: Lipoprotein N-terminal domain, DUF1943, DUF 1081 and VWD structure. EcVtg3, EcVtg4 and EcVtg5 have the same functional domains, except for DUF 1081. All the EcVgs contained signal peptide that start at position 1 and ended at positions 18–22. The expression patterns of EcVtg1, EcVtg2, EcVtg3 and EcVtg5 were similar, and their expression was highest in the Stage III stage, whereas EcVtg4 was highest in the Stage II stage ($P < 0.05$) (**Figure 7**).

DISCUSSION

Ovarian development is a very important physiological process for crustacean reproduction and is closely related to the reproductive capacity of the female broodstock. However, there is limited knowledge of the regulatory genes and pathways involved in crustacean ovarian development because of the limited transcriptomic information on target organs. We identified several key genes and pathways are potentially involved in the regulation of ovarian maturation within the ovary using PacBio

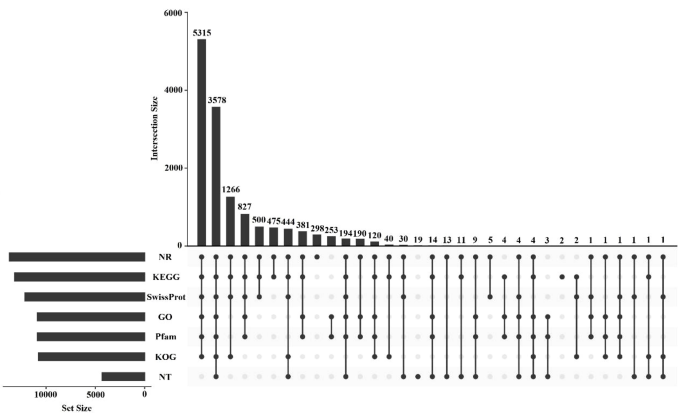

FIGURE 3 | UpSet plot showing the results of the annotated transcripts and the number of unique annotated transcripts for each database

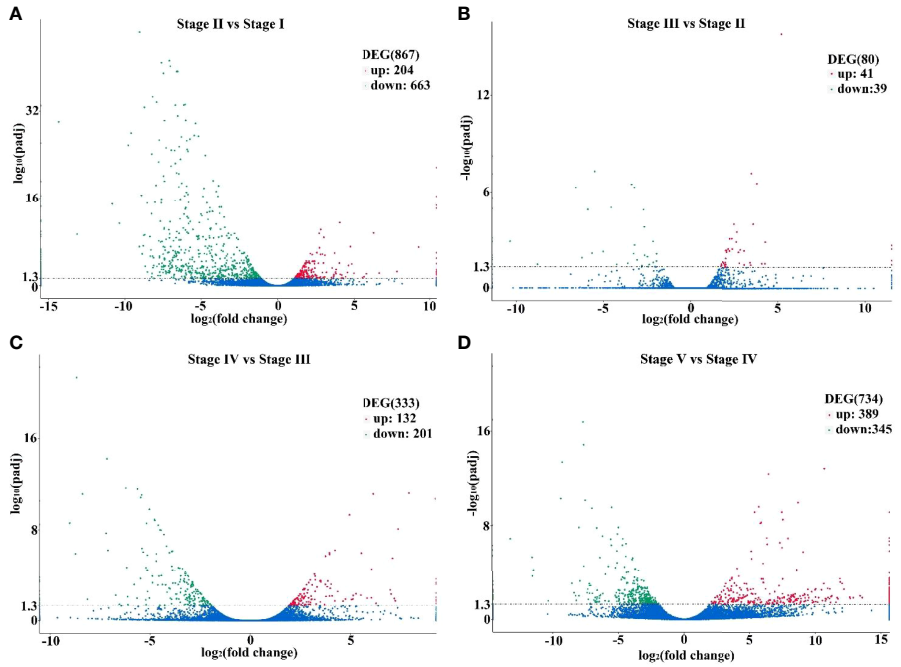

FIGURE 4 | Volcano plots displaying differentially expressed genes in Stage II vs Stage I **(A)**, Stage III vs Stage II **(B)**, Stage IV vs Stage III **(C)** and Stage V vs Stage IV **(D)**. Those that are significantly upregulated and downregulated are indicated in red and green, respectively, and those are not significantly different are in blue.

and RNA-seq technology. The PacBio platform can achieve the full-length sequence of transcripts and identify full coding sequences and multiple encoded isoforms (Weirather et al., 2017), which is necessary for gene discovery of some species without a published genome. In this study, we first produced high confidence and full-length transcriptome data from ovary tissue (five different ovarian developmental stages) using the PacBio Sequel sequencing approach. A large amount of transcriptome data was generated, including 15, 151 high-quality full-length transcripts with a mean length of 4, 257 bp, and N50 length were higher than those in a previous study that did not use full-length transcript information of the ovary (Shi et al., 2020). This dataset may provide new information for (i) studying the molecular regulatory mechanisms involved in female reproduction, (ii) developing new technology for genetic control within the aquaculture industry, and (iii) helping industry proactively solve various production problems caused by ovary maturation in *E. carinicauda*.

TABLE 1 | The enriched KEGG pathways related to ovarian development of *E. carinicauda.*

Groups	KEGG pathways	Total	Up	Down
Stage II vs Stage I	Folate biosynthesis	4	4	0
	PI3K-Akt signaling pathway	9	8	1
	Retinol metabolism	6	5	1
Stage III vs Stage II	Folate biosynthesis	2	2	0
Stage IV vs Stage III	Cell cycle	5	4	1
	Hedgehog signaling pathway	4	4	0
	PI3K-Akt signaling pathway	15	1	14
Stage V vs Stage IV	Folate biosynthesis	2	2	0
	Phototransduction - fly	5	5	0
	Hedgehog signaling pathway	8	0	8

Ovarian development is a complex physiological process, which involves activation or inhibition of many genes. The cell cycle and oocyte meiosis pathways play important roles during the ovarian developmental stage in *E. carinicauda*. The cyclin B and cyclin-dependent kinase play an important role in the development and maturation of oocytes/ovaries in crustacean (Visudtiphole et al., 2009; Han et al., 2012; Phinyo et al., 2013; Phinyo et al., 2014). Serotonin promotes vitellogenesis of *Penaeus indicus*, and shrimps treated with serotonin exhibited higher transcript levels of vitellogenin and cyclin B (Tomy et al., 2016). The mRNA level of Cyclin B in mature stage was greater than that of oogonia stage in *Penaeus monodon* (Visudtiphole et al., 2009), *Scylla paramamosain* (Han et al., 2012) and *Tachypleus tridentatus* (Li et al., 2015c). In our study, cyclin-dependent kinases 8 was highest expressed in the major growth phase, and the cyclin B and cyclin-dependent kinases 2 were highest expressed in the mature growth phase. Techa et al. suggested that genes related to growth and molt play a critical role in the early embryogenesis of arthropods (Techa et al., 2015). The expression of cell division cycle 2 mRNA is relatively stable between oogenesis and early embryogenesis with the exception of a drop in early vitellogenesis ovary in *Oncorhynchus mykiss* (Qiu et al., 2008). These data indicated that four genes for cell cycle pathways not only possibly related to ovarian development of *E. carinicauda*, but also are maternal-mRNAs stored for newly fertilized embryos to presume translation.

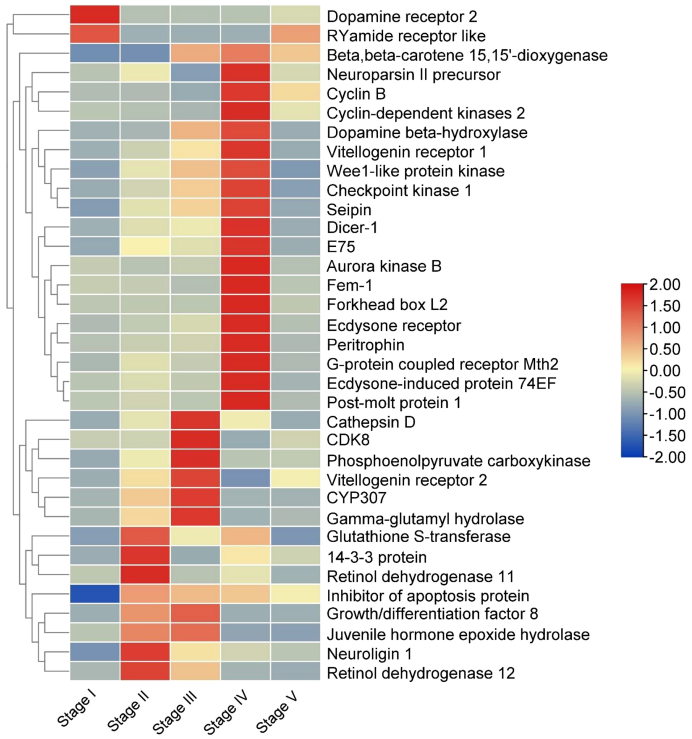

FIGURE 5 | Heat map of genes related to ovarian development. The columns and rows indicate individuals and genes, respectively. The color scale represents FPKM after standard normalization.

Vitellogenin is an important precursor of egg yolk in nearly all oviparous animals (Harwood and Amdam, 2021). The accumulation of vitellogenin acts as a pivotal regulator of nutritional accumulation within oocytes, which drives gonadal maturation in females. Vitellogenesis originates in both the hepatopancreas and ovary in most crustacean (Zmora et al., 2007). Liang et al., found that vitellogenin of *E. carinicauda* is synthesized both in the ovary and hepatopancreas (Liang et al., 2020). In this study, the mRNA expression level of Vtgs and vitellogenin receptor (Vtgr) in the stage II were significantly higher than that in the stage I. The vitellogenin mRNAs are translated and stored in the stage II and stage III for the highly expressed level of five Vtgs at stage II and stage III. Most studies on the function of the vitellogenin gene in crustaceans mainly involve one vitellogenin gene, but many oviparous animals, such as fish (Williams et al., 2014) and insects (Boldbaatar et al.,

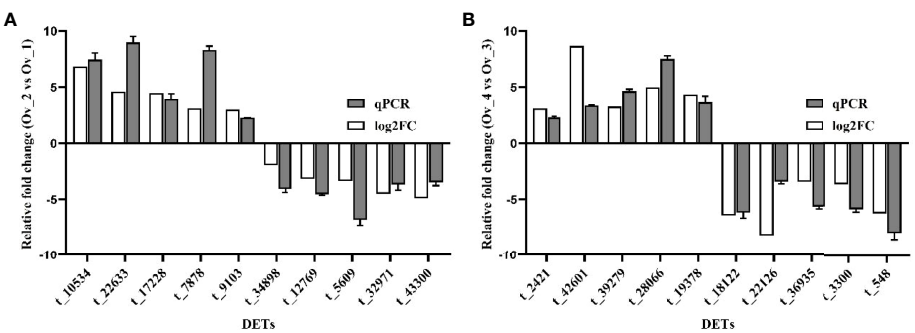

FIGURE 6 | Validation of the expression levels of five upregulated and five downregulated DEGs in Stage II vs Stage I **(A)** and Stage IV vs Stage III **(B)** RNA-Seq and qRT-PCR data are indicated in grey and white, respectively t_10534, CYP307; t_22633, Adenylyl cyclase-associated protein; t_17228, checkpoint kinase 1; t_7878, glutathione S-transferase; t_9103, adiponectin receptor; t_34898, serine/threonine-protein kinase Doa; t_12769, cyclophilin A; t_5609, lipoprotein receptor 2A; t_32971, guanylate cyclase PcGC-M2 precursor; t_43300, ficolin-like protein 2; t_2421, aurora kinase B; t_42601, calcified cuticle protein; t_39279, cyclin-dependent kinases 2; t_28066, forkhead box L2; t_19378, Serine/threonine-protein kinase D3; t_18122, alkaline phosphatase; t_22126, growth/differentiation factor 8; t_36935, cathepsin L; t_3300, cyclin-dependent kinase inhibitor; t_548, fatty acid synthase.

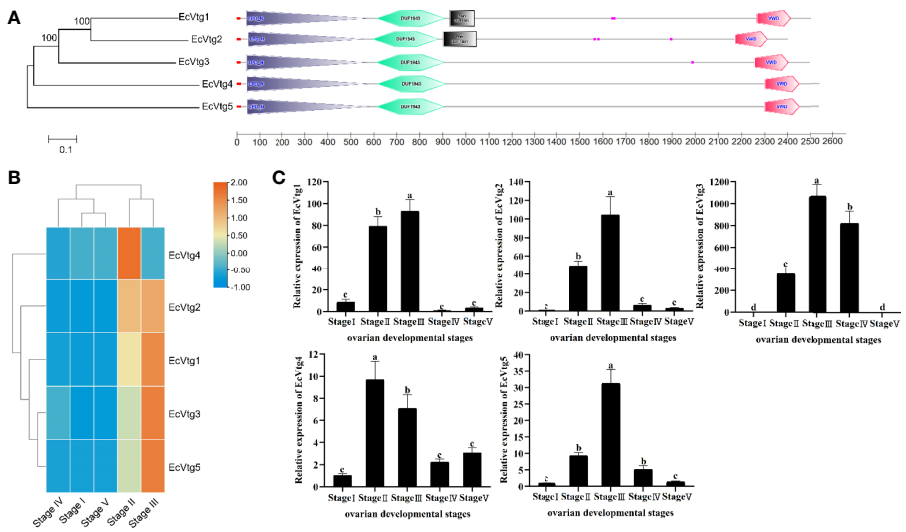

FIGURE 7 | The five types of vitellogenin genes in *E. carinicauda* **(A)** Schematic representation of gene structures of Vtg genes in *E. carinicauda*. The phylogenetic relationship was shown on the left. The functional domains were marked with different colors. The signal peptide is red line, the LPD_N domain is gray boxed, the DUF1943 is green boxed, the DUF 1081 is black boxed and the VWD is red boxed. **(B)** Visualizing the genes using a heatmap plot. The columns and rows indicate individuals and genes, respectively. The color scale represents FPKM after standard normalization. **(C)** The mRNA expression of EcVtgs in five ovarian developmental stages. Data with different letters significantly differ ($P < 0.05$) among stages. Each bar represents the mean ± SE (n = 3). The β-*actin* serves as internal reference gene.

2010), have multiple vitellogenin genes. Previous studies on *Metapenaeus ensis* (Kung et al., 2004) and *Pandalopsis japonica* (Jeon et al., 2011) have indicated the presence of multiple Vtg genes. In this study, five EcVtgs were identified in the full-length transcripts, which were expressed in the ovaries at different ovarian developmental stages. It is the first time that five vitellogenin isoforms has been identified in crustaceans. The relative abundance of the EcVtgs mRNA transcripts changed with ovarian development, and EcVtg1, EcVtg2, EcVtg3 and EcVtg5 were expressed similarly during the ovarian developmental stage. These results indicated that these five vitellogenin isoforms play important roles in ovarian developmental stages.

Retinol and its derivatives play key roles in the initiating meiosis in germ cells of mammalian fetal ovaries (Jiang et al., 2017), follicular development (Kawai et al., 2016), ovarian steroidogenesis (Damdimopoulou et al., 2019), and oocyte maturation (Tahaei et al., 2011). Full-length transcriptomic analysis was performed to identify 22 transcripts in retinol metabolism, and five of them were confirmed to be upregulated from the stage I to the growth phase, with four genes coding for retinol dehydrogenase (RDH) and β, β-carotene 15,15'-dioxygenase. Three RDHs, RDH11, RDH12 and RDH13, were detected in the transcriptome sequences. RDH12 is involved in steroid metabolism (Keller and Adamski, 2007), and RDH13 in zebrafish shows significantly higher expression levels in vitellogenic ovaries than in non-vitellogenic ovaries (Levi et al., 2011). Knockdown of RDH11 resulted in decreased transcription of vitellogenin and vitellogenin receptor in *Procambarus clarkii* (Kang et al., 2019). Our results revealed that retinol metabolism is critical for ovarian development in *E. carinicauda*. An appropriate feed proportion with adequate vitamin A levels in the stage I may be beneficial for the reproduction of *E. carinicauda*.

Juvenile hormones (JH) play important roles in the regulation of molting, development, metamorphosis and reproductive maturation in arthropods (Li et al., 2019; Santos et al., 2019). An increase in JH initiates vitellogenesis and egg development in adult insects. JH degradation in insects occurs by JH esterase and JH epoxide hydrolase (JHEH) (Lü et al., 2015). Knocking down JHEH in *Colaphellus bowringi* elevated JH signaling and increased expressions of vitellogenin genes (Guo et al., 2019b). In crustaceans, the JHEH-like genes have been identified in *Daphnia magna* (Toyota et al., 2014), *M. rosenbergii* (Chen et al., 2021) and *Penaeus vannamei* (Liu et al., 2022). JHEH-like is indispensable for the regulation of larval development and ecdysteroidogenesis in *M. rosenbergii* (Chen et al., 2021) and plays an essential role in shrimp survival during bacterial infection in *P. vannamei* (Liu et al., 2022). In this study, the expression of JHEH-like was significantly highest in the major growth stage among the five ovarian developmental stages in *E. carinicauda*. However, there was no evidence that JHEH plays an important role in the regulation of ovarian development in other crustacean. The JHEH-like proteins may exist in crustaceans, but compared to insects with probably different functions. We will properly investigate the function of JHEH-like gene in *E. carinicauda*.

Reproductive development in crustaceans requires neuropeptides, ecdysone and methyl farnesoate (Nagaraju, 2011). Methyl farnesoate is the crustacean analogue of JH III. Similar to the pleiotropic functions of JH in insects, methyl farnesoate participates in numerous physiological processes in crustaceans, including molting (Nagaraju et al., 2006), sex determination (Suppa et al., 2021) and vitellogenesis (Li et al.,

2021). The FAMeT catalyzes the conversion of farnesoic acid to methyl farnesoate, which is a rate-limiting step in the synthesis of methyl farnesoate. In our previous study, we have identified the expression profile of FAMeT in *E. carinicauda* (Li et al., 2016), which indicated that FAMeT was widely distributed but with higher expression levels in the mandibular organ. During the first ovarian development of *E. carinicauda*, the expression trend of FAMeT in the mandibular organ was similar to that in the hepatopancreas, which showed that the expression of FAMeT decreased gradually from stage I to stage IV, and decreased to the lowest in the stage IV, then rapidly recovered to a higher state in the stage V. Different from the expression of FAMeT in the mandibular organ and hepatopancreas, the expression of FAMeT in the stage IV of ovary was lowest among five stages, but there were no significant differences among the stage I, stage II, stage III and stage V. In this study, a full-length transcript of FAMeT was identified, but there was no significant difference between any two different stages of ovarian development in ovary. According to these results and the previous study, we supposed that the mandibular organ is the main tissue for FAMeT synthesis, which plays an important role in the regulation of ovarian development.

Neuropeptides play a critical role in regulating animal reproduction (Webster et al., 2012; Bao et al., 2015). A number of neuropeptide families were identified in crustaceans. The crustacean hyperglycemic hormone family including crustacean hyperglycemic hormone, molt inhibiting hormone, vitellogenesis inhibiting hormone and mandibular organ-inhibiting hormone, are known to regulate several important functions in decapod crustaceans such as energetic metabolism, molting and reproduction (Montagné et al., 2010; Webster et al., 2012). Crustacean hyperglycemic hormone has been shown to inhibit protein and mRNA synthesis *in vitro* in ovarian fragments of crustacean (Khayat et al., 1998), and might inhibit the synthesis of ecdysteroids by Y-organs and be involved in promoting vitellogenesis in *Scylla paramamosain* (Fu et al., 2016). Molt inhibiting hormone is a key endocrine regulator in the coordination of molting and likely reproduction in crustaceans, which simultaneously inhibits molt and induces ovarian maturation (Huang et al., 2015). The vitellogenesis-inhibiting hormone plays a major regulatory role in vitellogenesis and the reproductive cycle (Cohen et al., 2021). In our study, only crustacean hyperglycemic hormone was identified in ovary by Illumina RNA-Seq. The crustacean hyperglycemic hormone family members are best known for being secreted from the X-organ sinus gland complex of the eyestalk. In this study, crustacean hyperglycemic hormone gene was identified in ovary tissue by Illumina RNA-Seq, which is identical in amino acid sequence to that of eyestalk in our previous study (Li et al., 2015a). A total of 22 neuropeptides and related transcripts were predicted from the transcriptome data of female *E. carinicauda* (**Table 2** and **Supplementary Table 2**). Of these transcripts, the neuroparsin II precursor, RYamide receptor like, dopamine receptor 2, and dopamine beta-hydroxylase were identified as DEGs in the four comparisons.

It is well-known that neuroparsin displays multiple biological activities, including antidiuretic and inhibition of

TABLE 2 Putative neuropeptides and related transcripts in the full-length transcriptome of *E. carinicauda*.

Gene_ID	Families	BLAST hit genes	NCBI	Size	Blastx			
			number	(aa)	Species name	E-value	Ident	NCBI number
	RFamide peptides							
t_22871		Neuropeptide F2	ON681732	104	Cherax quadricarinatus	3.00E-27	72.97%	AWK57534.1
t_25328		Short neuropeptide F	ON681739	163	*Cherax quadricarinatus*	2.00E-37	59.52%	AWK57543.1
t_33679		Myosuppressin-like precursor	ON681741	101	*Penaeus monodon*	3.00E-44	89.47%	XP_037788333.1
t_42661		Sulfakinin	ON681742	136	*Nephrops norvegicus*	1.00E-31	57.69%	QBX89077.1
t_32785		FMRFamide receptor like	ON681751	442	*Penaeus monodon*	2.00E-149	67.76%	XP_037787263.1
t_27766		Neuropeptide F receptor like	ON681743	398	*Penaeus japonicus*	0	77.06%	XP_042857044.1
	Neuroparsins							
t_22799		Neuroparsin I precursor	ON681744	99	*Macrobrachium nipponense*	8.00E-40	93.94%	QBG05396.1
t_24196		Neuroparsin II precursor	ON681745	101	*Macrobrachium nipponense*	2.00E-28	89.00%	QBG05397.1
	Others							
t_90926		Crustacean cardioactive peptide precursor	ON681733	141	Macrobrachium nipponense	3.00E-65	90.62%	ASH96804.1
t_2144		Crustacean hyperglycemic hormone	ON681734	135	Macrobrachium rosenbergii	6.00E-58	80.74%	AAL40916.1
t_30965		Diuretic hormone class 2 like	ON681746	142	*Penaeus japonicus*	2.00E-62	95.15%	XP_042873779.1
t_33554		Eclosion hormone like	ON681747	82	*Procambarus clarkii*	1.00E-37	85.37%	XP_045581480.1
t_7809		Pigment dispersing hormone 1	ON681735	78	Cherax quadricarinatus	2.00E-12	64.71%	AWK57537.1
t_31903		Pigment dispersing hormone 2	ON681736	80	Nephrops norvegicus	1.00E-27	67.50%	QBX89065.1
t_23096		Preprotachykinin A	ON681748	209	*Panulirus interruptus*	5.00E-81	69.57%	BAD06362.1
t_24706		Preprotachykinin B	ON681749	209	*Panulirus interruptus*	6.00E-81	69.57%	BAD06363.1
t_37648		Prohormone-1 like	ON681737	105	*Penaeus chinensis*	1.00E-45	72.38%	XP_047484509.1
t_29602		Prohormone-3 like	ON681738	196	*Penaeus chinensis*	9.00E-104	74.37%	XP_047492252.1
t_12300		Orexin receptor type 1 like	ON681752	497	*Homarus americanus*	4.00E-177	74.05%	XP_042236317.1
t_30771		RYamide receptor like	ON681753	493	*Procambarus clarkii*	0	60.48%	XP_045591516.1
t_26194		Dopamine receptor 2	ON681750	618	*Panulirus interruptus*	0	68.70%	ABI64137.1
t_16973		Dopamine beta-hydroxylase	ON681754	680	*Penaeus vannamei*	0	59.50%	ROT77268.1

vitellogenesis in insects. Also, in the crab *Scylla paramamosain*, the neuroparsin possibly can inhibit the production of vitellogenin in the hepatopancreas (Liu et al., 2020). In this study, the expression levels of Neuroparsin II precursor in the major growth phase was lowest in five ovarian development stages, which also indicated that the neuroparsin possibly inhibit vitellogenesis in *E. carinicauda*. The RYamide was thought to be another counterpart of neuropeptide Y, and may play a role in the regulation of feeding and digestion in insects (Roller et al., 2016). The RYamides exhibited changes in its relative abundance for salinity stress in *Carcinus maenas* (Zhang et al., 2015b). However, the function of RYamide to reproduction have not been determined in crustaceans. In this study, the expression of RYamide receptor like in stage I was higher than the growth and mature stages, which indicated that the RYamide receptor was possibly related inhibition of vitellogenesis.

The synthesis and release of neurohormones in crustaceans are believed to be regulated by biogenic amines (Richardson et al., 1991). The dopamine was shown to inhibit ovarian maturation in *Procambarus clarkii* (Sarojini et al., 1995). Furthermore, dopamine depressed vitellogenin synthesis through inhibition of vitellogenesis-stimulating hormone release at the thoracic ganglia in *M. rosenbergii* (Chen et al., 2003). In this study, the expression of dopamine receptor 2 was higher in the Stage I than the growth and mature stages, which indicated that the dopamine receptor 2 may inhibit ovarian development in *E. carinicauda.* Dopamine beta-hydroxylase converts dopamine to noradrenaline and plays an crucial role in catecholamine synthesis of the neuroendocrine regulatory network (Cheng et al., 2016). Cheng et al., suggested that it played a crucial role in the neuroendocrine-immune regulation of *L. vannamei* (Cheng et al., 2017). Due to the lack of related research, it is not clear whether dopamine beta-hydroxylase has a function in crustacean ovarian development, but our results indicated that dopamine beta-hydroxylase possibly related to vitellogenesis in *E. carinicauda*.

The forkhead box protein L2 (foxl2) is a critical transcriptional regulator factor and has been extensively studied in crustacean and confirmed its critical roles in gonad differentiation and development (Farhadi et al., 2021; Wan et al., 2022). The knockdown of foxl2 mediated by RNAi technology repressed the expression of vtg in *Eriocheir sinensis* (Li et al., 2015b) and *Scylla paramamosain* (Wan et al., 2021). In our study, a total of a total of 895 transcripts were predicted to be transcription factors, and only 22 transcripts were the DEGs (**Supplementary Table 3**). Furthermore, foxl2, as transcriptional regulator factor, were highest expressed in the mature stage than that in other four stages. We speculated that foxl2 closely related to ovarian maturation in *E. carinicauda*.

After the ovaries mature, females must molt to mate and lay eggs. Copulation occurs immediately after molting of the female, while the exoskeleton is still soft. The pre-mating molt, also known as reproductive molting, is a significant indicator of the complete maturation of the ovary (Asmat-Ullah et al., 2021). Ecdysteroids play major roles in regulating vitellogenesis, ovarian maturation and protein synthesis in decapods (Nagaraju, 2011). Crustacean ecdysteroids trigger the specific regulation of several genes in different tissues and developmental stages through interaction with the ecdysteroid receptor (EcR) (Hopkins, 2009). Low EcR expression levels have been shown to cause defective ovarian differentiation in Drosophila, egg degeneration and increased resistance to starvation (Schwedes and Carney, 2012). Higher EcR expression level was observed in the ovaries of breeding *Metopograpsus messor* than in the ovaries of non-breeding crabs (Shyamal et al., 2015). Additionally, EcR is necessary for ovarian development during the mid-late vitellogenesis stage in *Eriocheir sinensis* (Su et al., 2020). In this study, the expression of four genes (ecdysone receptor, ecdysone-induced protein 74EF, ecdysone inducible gene E75 and post-molt protein 1) which associated to molting in crustacean in the stage IV was higher than that in the other ovarian developmental stages. Techa et al., suggested that the ecdysteroid-responsive factors *Callinectes sapidus*, including ecdysone receptor, retinoid X receptor and molt-inhibiting hormone may be utilized at the initiation of early embryogenesis (Techa et al., 2015). Therefore, we speculate the four genes regulate the reproductive molting of *E. carinicauda* and plays an important role in the late vitellogenesis stage and early embryogenesis.

CONCLUSION

To conclude, a comprehensive full-length transcriptome ovarian tissue from five different ovarian developmental stages was obtained for the first time through SMRT sequencing in *E. carinicauda*. By using the full-length transcriptome as reference, we performed Illumina sequencing to analyze the gene expression difference among different ovarian developmental stages of the ovary and validated the results by quantitative real time-PCR. The PI3K-Akt signaling pathway, retinol metabolism, cell cycle and ovarian steroidogenesis pathways play important roles in ovarian development. We identified 37 DEGs that may be related to ovary maturation in significant pathways identified in the comparisons. Five vitellogenin isoforms and vitellogenin receptor suggested an important role during previtellogenesis of *E. carinicauda*. We can suggest that supplementation of Vitamin A to *E. carinicauda* feed could enhance female reproductive success. This study provides valuable information about the regulation of ovarian development in *E. carinicauda* and enhances the understanding of reproductive regulatory mechanisms in shrimp. The relationship between regulatory genes and ovarian development requires further study.

DATA AVAILABILITY STATEMENT

The datasets presented in this study can be found in online repositories. The names of the repository/repositories and accession number(s) can be found below: NCBI accession, PRJNA746617, https://www.ncbi.nlm.nih.gov/bioproject/?term=PRJNA746617.

ETHICS STATEMENT

All animal experiments were performed according to the protocols approved by The Animal Research and Ethics Committees of Yellow Sea Fisheries Research Institute, Chinese Academy of Fishery Sciences.

AUTHOR CONTRIBUTIONS

JW and JL conceived the study. WL collected samples and extracted RNA samples. JW and JTL participated in analyzing the sequencing data. QG verified the sequencing results. All authors contributed to the article and approved the submitted version.

FUNDING

This project was financially supported by National Key R & D Program of China (No. 2019YFD0900403), National Natural Science Foundation of China (No. 31902368), China Agriculture Research System of MOF and MARA (No. CARS-48), Central Public-interest Scientific Institution Basal Research Fund, CAFS (No. 2020TD46).

SUPPLEMENTARY MATERIAL

The Supplementary Material for this article can be found online at: https://www.frontiersin.org/articles/10.3389/fmars.2022.906730/full#supplementary-material

REFERENCES

Altschul, S. F., Madden, T. L., Schäffer, A. A., Zhang, J., Zhang, Z., Miller, W., et al. (1997). Gapped BLAST and PSI-BLAST: A New Generation of Protein Database Search Programs. *Nucleic Acids Res.* 25 (17), 3389–3402. doi: 10.1093/nar/25.17.3389

Apweiler, R., Bairoch, A., Wu, C. H., Barker, W. C., Boeckmann, B., Ferro, S., et al. (2004). UniProt: The Universal Protein Knowledgebase. *Nucleic Acids Res.* 32, 115–119. doi: 10.1093/nar/gkh131

Ashburner, M., Ball, C. A., Blake, J. A., Botstein, D., Butler, H., Cherry, J. M., et al. (2000). Gene Ontology: Tool for the Unification of Biology. *Nat. Genet.* 25 (1), 25–29. doi: 10.1038/75556

Asmat-Ullah, M., Waiho, K., Azra, M. N., Norainy, M. H., Syafaat, M. N., Nahid, S. A. A., et al. (2021). Induced Mating of Newly Molted Females of Orange Mud Crab, *Scylla Olivacea* (Herbst 1796), in Captivity. *Aquaculture* 533, 736159. doi: 10.1016/j.aquaculture.2020.736159

Bai, H., Qiao, H., Li, F., Fu, H., Jiang, S., Zhang, W., et al. (2016). Molecular and Functional Characterization of the Vitellogenin Receptor in Oriental River Prawn, *Macrobrachium Nipponense*. *Comp. Biochem. Physiol. Part A: Mol. Integr. Physiol.* 194, 45–55. doi: 10.1016/j.cbpa.2015.12.008

Bankar, K. G., Todur, V. N., Shukla, R. N. and Vasudevan, M. (2015). Ameliorated *De Novo* Transcriptome Assembly Using Illumina Paired End Sequence Data With Trinity Assembler. *Genomics Data* 5, 352–359. doi: 10.1016/j.gdata.2015.07.012

Bao, C., Yang, Y., Huang, H. and Ye, H. (2015). Neuropeptides in the Cerebral Ganglia of the Mud Crab, Scylla Paramamosain: Transcriptomic Analysis and Expression Profiles During Vitellogenesis. *Sci. Rep.* 5 (1), 17055. doi: 10.1038/srep17055

Bateman, A., Birney, E., Durbin, R., Eddy, S. R., Howe, K. L. and Sonnhammer, E. L. L. (2000). The Pfam Protein Families Database. *Nucleic Acids Res.* 28 (1), 263–266. doi: 10.1093/nar/28.1.263

Boldbaatar, D., Umemiya-Shirafuji, R., Liao, M., Tanaka, T., Xuan, X. and Fujisaki, K. (2010). Multiple Vitellogenins From the *Haemaphysalis Longicornis* Tick are Crucial for Ovarian Development. *J. Insect Physiol.* 56 (11), 1587–1598. doi: 10.1016/j.jinsphys.2010.05.019

Cao, M., Zhang, M., Yang, N., Fu, Q., Su, B., Zhang, X., et al. (2020). Full Length Transcriptome Profiling Reveals Novel Immune-Related Genes in Black Rockfish (*Sebastes Schlegelii*). *Fish. Shellfish. Immunol.* 106, 1078–1086. doi: 10.1016/j.fsi.2020.09.015

Chen, Y. N., Fan, H. F., Hsieh, S. L. and Kuo, C. M. (2003). Physiological Involvement of DA in Ovarian Development of the Freshwater Giant Prawn, *Macrobrachium Rosenbergii*. *Aquaculture* 228 (1), 383–395. doi: 10.1016/S0044-8486(03)00324-7

Chen, X., Gao, Q., Cheng, H., Peng, F., Wang, C. and Xu, B. (2021). Molecular Cloning and Expression Pattern of the Juvenile Hormone Epoxide Hydrolase Gene From the Giant Freshwater Prawn *Macrobrachium Rosenbergii* During Larval Development and the Moult Cycle. *Aquacult. Res.* 52 (8), 3890–3899. doi: 10.1111/are.15233

Cheng, W., Ka, Y.-W. and Chang, C.-C. (2016). Dopamine Beta-Hydroxylase Participate in the Immunoendocrine Responses of Hypothermal Stressed White Shrimp, *Litopenaeus Vannamei*. *Fish. Shellfish. Immunol.* 59, 166–178. doi: 10.1016/j.fsi.2016.10.036

Cheng, W., Ka, Y.-W. and Chang, C.-C. (2017). Involvement of Dopamine Beta-Hydroxylase in the Neuroendocrine-Immune Regulatory Network of White Shrimp, *Litopenaeus Vannamei*. *Fish. Shellfish. Immunol.* 68, 92–101. doi: 10.1016/j.fsi.2017.07.028

Cohen, S., Ilouz, O., Manor, R., Sagi, A. and Khalaila, I. (2021). Transcriptional Silencing of Vitellogenesis-Inhibiting and Molt-Inhibiting Hormones in the Giant Freshwater Prawn, *Macrobrachium Rosenbergii*, and Evaluation of the Associated Effects on Ovarian Development. *Aquaculture* 538, 736540. doi: 10.1016/j.aquaculture.2021.736540

Damdimopoulou, P., Chiang, C. and Flaws, J. A. (2019). Retinoic Acid Signaling in Ovarian Folliculogenesis and Steroidogenesis. *Reprod. Toxicol.* 87, 32–41. doi: 10.1016/j.reprotox.2019.04.007

Dobin, A., Davis, C. A., Schlesinger, F., Drenkow, J., Zaleski, C., Jha, S., et al. (2013). STAR: Ultrafast Universal RNA-Seq Aligner. *Bioinformatics* 29 (1), 15–21. doi: 10.1093/bioinformatics/bts635

Duan, Y., Liu, P., Li, J., Wang, Y., Li, J. and Chen, P. (2014). A Farnesoic Acid O-Methyltransferase (FAMeT) From *Exopalaemon Carinicauda* is Responsive to Vibrio Anguillarum and WSSV Challenge. *Cell Stress Chaperones* 19 (3), 367–377. doi: 10.1007/s12192-013-0464-5

Farhadi, A., Cui, W., Zheng, H., Li, S., Zhang, Y., Ikhwanuddin, M., et al. (2021). The Regulatory Mechanism of Sexual Development in Decapod Crustaceans. *Front. Mar. Sci.* 8. doi: 10.3389/fmars.2021.679687

Finn, R. D., Bateman, A., Clements, J., Coggill, P., Eberhardt, R. Y., Eddy, S. R., et al. (2013). Pfam: The Protein Families Database. *Nucleic Acids Res.* 42 (1), 222–230. doi: 10.1093/nar/gkt1223

Fu, C., Huang, X., Gong, J., Chen, X., Huang, H. and Ye, H. (2016). Crustacean Hyperglycaemic Hormone Gene From the Mud Crab, *Scylla Paramamosain*: Cloning, Distribution and Expression Profiles During the Moulting Cycle and Ovarian Development. *Aquacult. Res.* 47 (7), 2183–2194. doi: 10.1111/are.12671

Guo, H., Chen, L.-L., Li, G.-L., Deng, S.-P. and Zhu, C.-H. (2019a). Accumulation and Depuration of Nonylphenol and Its Effect on the Expressions of Vitellogenin and Vitellogenin Receptor in Freshwater Prawn Macrobrachium Rosenbergii. *Bull. Environ. Contamination Toxicol.* 103 (5), 729–733. doi: 10.1007/s00128-019-02714-x

Guo, S., Sun, D., Tian, Z., Liu, W., Zhu, F. and Wang, X.-P. (2019b). The Limited Regulatory Roles of Juvenile Hormone Degradation Pathways in Reproductive Diapause Preparation of the Cabbage Beetle, *Colaphellus Bowringi*. *J. Insect Physiol.* 119, 103967. doi: 10.1016/j.jinsphys.2019.103967

Han, K., Dai, Y., Zou, Z., Fu, M., Wang, Y. and Zhang, Z. (2012). Molecular Characterization and Expression Profiles of Cdc2 and Cyclin B During Oogenesis and Spermatogenesis in Green Mud Crab (*Scylla Paramamosain*). *Comp. Biochem. Physiol. Part B: Biochem. Mol. Biol.* 163 (3), 292–302. doi: 10.1016/j.cbpb.2012.07.001

Harwood, G. and Amdam, G. (2021). Vitellogenin in the Honey Bee Midgut. *Apidologie* 52 (4), 837–847. doi: 10.1007/s13592-021-00869-3

Holmes, J. C., Scholl, E. H., Dickey, A. N. and Hess, P. R. (2021). High-Resolution Characterization of the Structural Features and Genetic Variation of Six Feline Leukocyte Antigen Class I Loci *via* Single Molecule, Real-Time (SMRT) Sequencing. *Immunogenetics* 73 (5), 381–393. doi: 10.1007/s00251-021-01221-w

Hopkins, P. M. (2009). "Crustacean Ecdysteroids and Their Receptors," in *Ecdysone: Structures and Functions,* ed. G. Smagghe. (Springer Verlag, Netherlands Press), 73-97. doi: 10.1007/978-1-4020-9112-4_3

Huang, H., Fu, C., Chen, X., Gong, J., Huang, X. and Ye, H. (2015). Molt-Inhibiting Hormone (MIH) Gene From the Green Mud Crab *Scylla Paramamosain* and its Expression During the Molting and Ovarian Cycle. *Aquacult. Res.* 46 (11), 2665–2675. doi: 10.1111/are.12421

Jeon, J. M., Kim, B. K., Kim, Y. J. and Kim, H. W. (2011). Structural Similarity and Expression Differences of Two Pj-Vg Genes From the Pandalus Shrimp *Pandalopsis Japonica*. *Fisher. Aquat. Sci.* 14 (1), 22–30. doi: 10.5657/fas.2011.14.1.022

Jiang, Y., Li, C., Chen, L., Wang, F. and Zhou, X. (2017). Potential Role of Retinoids in Ovarian Physiology and Pathogenesis of Polycystic Ovary Syndrome. *Clinica. Chimica. Acta* 469, 87–93. doi: 10.1016/j.cca.2017.03.025

Kanehisa, M., Goto, S., Kawashima, S., Okuno, Y. and Hattori, M. (2004). The KEGG Resource for Deciphering the Genome. *Nucleic Acids Res.* 32, 277–280. doi: 10.1093/nar/gkh063

Kang, P.-F., Mao, B., Fan, C. and Wang, Y.-F. (2019). Transcriptomic Information From the Ovaries of Red Swamp Crayfish (*Procambarus Clarkii*) Provides New Insights Into Development of Ovaries and Embryos. *Aquaculture* 505, 333–343. doi: 10.1016/j.aquaculture.2019.02.074

Kang, Y., Yang, D., Kong, L., Hou, M., Meng, Y., Wei, L., et al. (2017). CPC2: A Fast and Accurate Coding Potential Calculator Based on Sequence Intrinsic Features. *Nucleic Acids Res.* 45 (1), 12–16. doi: 10.1093/nar/gkx428

Kawai, T., Yanaka, N., Richards, J. S. and Shimada, M. (2016). *De Novo*-Synthesized Retinoic Acid in Ovarian Antral Follicles Enhances FSH-Mediated Ovarian Follicular Cell Differentiation and Female Fertility. *Endocrinology* 157 (5), 2160–2172. doi: 10.1210/en.2015-2064

Keller, B. and Adamski, J. (2007). RDH12, a Retinol Dehydrogenase Causing Leber's Congenital Amaurosis, is Also Involved in Steroid Metabolism. *J. Steroid Biochem. Mol. Biol.* 104 (3), 190–194. doi: 10.1016/j.jsbmb.2007.03.015

Khayat, M., Yang, W. J., Aida, K., Nagasawa, H., Tietz, A., Funkenstein, B., et al. (1998). Hyperglycaemic Hormones Inhibit Protein and mRNA Synthesis Inin Vitro-Incubated Ovarian Fragments of the Marine Shrimp *Penaeus Semisulcatus*. *Gen. Comp. Endocrinol.* 110 (3), 307–318. doi: 10.1006/gcen.1998.7078

Kung, S. Y., Chan, S.-M., Hui, J. H. L., Tsang, W. S., Mak, A. and He, J. G. (2004). Vitellogenesis in the Sand Shrimp, *Metapenaeus Ensis*: The Contribution From the Hepatopancreas-Specific Vitellogenin Gene (Mevg2)1. *Biol. Reprod.* 71 (3), 863–870. doi: 10.1095/biolreprod.103.022905

Levi, L., Ziv, T., Admon, A., Levavi-Sivan, B. and Lubzens, E. (2011). Insight Into Molecular Pathways of Retinal Metabolism, Associated With Vitellogenesis in Zebrafish. *Am. J. Physiol.-Endocrinol. Metab.* 302 (6), E626–E644. doi: 10.1152/ajpendo.00310.2011

Liang, J., Zhang, W., Li, H., Li, J.-T. and Li, J. (2020). Abundances of Vitellogenin and Heat Shock Protein 90 During Ovarian and Embryonic Development of Exopalaemon Carinicauda. *Anim. Reprod. Sci.* 223, 106633. doi: 10.1016/j.anireprosci.2020.106633

Liang, B., Zhang, P., Li, Z., Zhao, L., Lai, X., Gao, H., et al. (2017). Cloning, Expression and Stability Analysis of the Reference Gene Glyceraldehyde-3-Phosphate Dehydrogenase (GAPDH) in *Exopalaemon Carinicauda*. *J. Fish. Sci. China* 24 (5), 1003–1012. doi: 10.3724/SP.J.1118.2017.17018

Li, X., Chen, T., Jiang, H., Huang, J., Huang, M., Xu, R., et al. (2021). Effects of Methyl Farnesoate on Krüppel Homolog 1 (Kr-H1) During Vitellogenesis in the Chinese Mitten Crab (*Eriocheir Sinensis*). *Anim. Reprod. Sci.* 224, 106653. doi: 10.1016/j.anireprosci.2020.106653

Li, W., Huang, H., Huang, J. and Ye, H. (2015c). Evidence for Cyclin A and Cyclin B Genes in the Ovary of the Horseshoe Crab, *Tachypleus Tridentatus*: Molecular Cloning and Expression Profiles. *Mar. Freshw. Behav. Physiol.* 48 (3), 163–176. doi: 10.1080/10236244.2015.1027540

Li, J., Li, J., Chen, P., Liu, P. and He, Y. (2015a). Transcriptome Analysis of Eyestalk and Hemocytes in the Ridgetail White Prawn *Exopalaemon Carinicauda*: Assembly, Annotation and Marker Discovery. *Mol. Biol. Rep.* 42 (1), 135–147. doi: 10.1007/s11033-014-3749-6

Li, Z., Li, J., Li, J., He, Y., Ge, Q. and Suo, S. (2016). The Expression Analysis of Farnesoic Acid O-Methyl Transferase (FAMeT) Gene During the Ovarian Development Cycles of *Exopalaemon Carinicauda*. *Prog. Fish. Sci.* 37 (1), 46–51. doi: 10.11758/yykxjz.20141217001

Li, G., Sun, Q.-Z., Liu, X.-Y., Zhang, J., Dou, W., Niu, J.-Z., et al. (2019). Expression Dynamics of Key Ecdysteroid and Juvenile Hormone Biosynthesis Genes Imply a Coordinated Regulation Pattern in the Molting Process of a Spider Mite, Tetranychus Urticae. *Exp. Appl. Acarol.* 78 (3), 361–372. doi: 10.1007/s10493-019-00396-y

Liu, Z., Huang, Z., Zheng, X., Zheng, Z., Yao, D., Zhang, Y., et al. (2022). The Juvenile Hormone Epoxide Hydrolase Homolog in *Penaeus Vannamei* Plays Immune-Related Functions. *Dev. Comp. Immunol.* 132, 104410. doi: 10.1016/j.dci.2022.104410

Liu, J., Liu, A., Liu, F., Huang, H. and Ye, H. (2020). Role of Neuroparsin 1 in Vitellogenesis in the Mud Crab, *Scylla Paramamosain*. *Gen. Comp. Endocrinol.* 285, 113248. doi: 10.1016/j.ygcen.2019.113248

Li, Q., Xie, J., He, L., Wang, Y., Yang, H., Duan, Z., et al. (2015b). FOXL2 Down-Regulates Vitellogenin Expression at Mature Stage in Eriocheir Sinensis. *Biosci. Rep.* 35 (6), e00278. doi: 10.1042/bsr20150151

Li, A., Zhang, J. and Zhou, Z. (2014). PLEK: A Tool for Predicting Long Non-Coding RNAs and Messenger RNAs Based on an Improved K-Mer Scheme. *BMC Bioinf.* 15 (1), 311. doi: 10.1186/1471-2105-15-311

Lü, F.-G., Fu, K.-Y., Guo, W.-C. and Li, G.-Q. (2015). Characterization of Two Juvenile Hormone Epoxide Hydrolases by RNA Interference in the Colorado Potato Beetle. *Gene* 570 (2), 264–271. doi: 10.1016/j.gene.2015.06.032

Montagné, N., Desdevises, Y., Soyez, D. and Toullec, J.-Y. (2010). Molecular Evolution of the Crustacean Hyperglycemic Hormone Family in Ecdysozoans. *BMC Evolution. Biol.* 10 (1), 62. doi: 10.1186/1471-2148-10-62

Nagaraju, G. P. C. (2011). Reproductive Regulators in Decapod Crustaceans: An Overview. *J. Exp. Biol.* 214 (1), 3–16. doi: 10.1242/jeb.047183

Nagaraju, G. P. C., Reddy, P. R. and Reddy, P. S. (2006). *In Vitro* Methyl Farnesoate Secretion by Mandibular Organs Isolated From Different Molt and Reproductive Stages of the Crab *Oziotelphusa Senex Senex*. *Fisher. Sci.* 72 (2), 410–414. doi: 10.1111/j.1444-2906.2006.01164.x

Phinyo, M., Nounurai, P., Hiransuchalert, R., Jarayabhand, P. and Klinbunga, S. (2014). Characterization and Expression Analysis of Cyclin-Dependent Kinase 7 Gene and Protein in Ovaries of the Giant Tiger Shrimp *Penaeus Monodon*. *Aquaculture* 432, 286–294. doi: 10.1016/j.aquaculture.2014.05.022

Phinyo, M., Visudtiphole, V., Roytrakul, S., Phaonakrop, N., Jarayabhand, P. and Klinbunga, S. (2013). Characterization and Expression of Cell Division Cycle 2 (Cdc2) mRNA and Protein During Ovarian Development of the Giant Tiger Shrimp *Penaeus Monodon*. *Gen. Comp. Endocrinol.* 193, 103–111. doi: 10.1016/j.ygcen.2013.07.012

Qian, Z. and Liu, X. (2019). Elucidation of the Role of Farnesoic Acid O-Methyltransferase (FAMeT) in the Giant Freshwater Prawn, *Macrobrachium Rosenbergii*: Possible Functional Correlation With Ecdysteroid Signaling. *Comp. Biochem. Physiol. Part A: Mol. Integr. Physiol.* 232, 1–12. doi: 10.1016/j.cbpa.2019.03.003

Qiu, G.-F., Ramachandra, R. K., Rexroad, C. E. and Yao, J. (2008). Molecular Characterization and Expression Profiles of Cyclin B1, B2 and Cdc2 Kinase During Oogenesis and Spermatogenesis in Rainbow Trout (*Oncorhynchus Mykiss*). *Anim. Reprod. Sci.* 105 (3), 209–225. doi: 10.1016/j.anireprosci.2007.03.005

Ren, Y., Li, J., Guo, L., Liu, J. N., Wan, H., Meng, Q., et al. (2020). Full-Length Transcriptome and Long non-Coding RNA Profiling of Whiteleg Shrimp *Penaeus Vannamei* Hemocytes in Response to *Spiroplasma Eriocheiris* Infection. *Fish. Shellfish. Immunol.* 106, 876–886. doi: 10.1016/j.fsi.2020.06.057

Richardson, H. G., Deecaraman, M. and Fingerman, M. (1991). The Effect of Biogenic Amines on Ovarian Development in the Fiddler Crab, *Uca Pugilator*. *Comp. Biochem. Physiol. Part C: Comp. Pharmacol.* 99 (1), 53–56. doi: 10.1016/0742-8413(91)90074-4

Roller, L., Čižmár, D., Bednár, B. and Žitňan, D. (2016). Expression of RYamide in the Nervous and Endocrine System of Bombyx Mori. *Peptides* 80, 72–79. doi: 10.1016/j.peptides.2016.02.003

Rotllant, G., Palero, F., Mather, P. B., Bracken-Grissom, H. D. and Santos, M. B. (2018). Preface: Recent Advances in Crustacean Genomics. *Hydrobiologia* 825 (1), 1–4. doi: 10.1007/s10750-018-3773-y

Santos, C. A., Andrade, S. C. S., Teixeira, A. K., Farias, F., Guerrelhas, A. C., Rocha, J. L., et al. (2021). Transcriptome Differential Expression Analysis Reveals the Activated Genes in *Litopenaeus Vannamei* Shrimp Families of Superior Growth Performance. *Aquaculture* 531, 735871. doi: 10.1016/j.aquaculture.2020.735871

Santos, C. G., Humann, F. C. and Hartfelder, K. (2019). Juvenile Hormone Signaling in Insect Oogenesis. *Curr. Opin. Insect Sci.* 31, 43–48. doi: 10.1016/j.cois.2018.07.010

Sarojini, R., Nagabhushanam, R. and Fingerman, M. (1995). *In Vivo* Effects of Dopamine and Dopaminergic Antagonists on Testicular Maturation in the Red Swamp Crayfish, *Procambarus Clarkii*. *Biol. Bull.* 189 (3), 340–346. doi: 10.2307/1542151

Schwedes, C. C. and Carney, G. E. (2012). Ecdysone Signaling in Adult *Drosophila Melanogaster*. *J. Insect Physiol.* 58 (3), 293–302. doi: 10.1016/j.jinsphys.2012.01.013

Shi, K., Li, J., Lv, J., Liu, P., Li, J. and Li, S. (2020). Full-Length Transcriptome Sequences of Ridgetail White Prawn *Exopalaemon Carinicauda* Provide Insight Into Gene Expression Dynamics During Thermal Stress. *Sci. Total Environ.* 747, 141238. doi: 10.1016/j.scitotenv.2020.141238

Shimizu, K., Adachi, J. and Muraoka, Y. (2006). ANGLE: A Sequencing Errors Resistant Program for Predicting Protein Coding Regions in Unfinished cDNA. *J. Bioinf. Comput. Biol.* 4 (3), 649–664. doi: 10.1142/s0219720006002260

Shyamal, S., Anilkumar, G., Bhaskaran, R., Doss, G. P. and Durica, D. S. (2015). Significant Fluctuations in Ecdysteroid Receptor Gene (EcR) Expression in Relation to Seasons of Molt and Reproduction in the Grapsid Crab, *Metopograpsus Messor* (Brachyura: Decapoda). *Gen. Comp. Endocrinol.* 211, 39–51. doi: 10.1016/j.ygcen.2014.11.006

Su, Y., Guo, Q., Gong, J., Cheng, Y. and Wu, X. (2020). Functional Expression Patterns of Four Ecdysteroid Receptor Isoforms Indicate Their Different Functions During Vitellogenesis of Chinese Mitten Crab, *Eriocheir Sinensis*. *Comp. Biochem. Physiol. Part A: Mol. Integr. Physiol.* 248, 110754. doi: 10.1016/j.cbpa.2020.110754

Sun, L., Luo, H., Bu, D., Zhao, G., Yu, K., Zhang, C., et al. (2013). Utilizing Sequence Intrinsic Composition to Classify Protein-Coding and Long Non-Coding Transcripts. *Nucleic Acids Res.* 41 (17), 166. doi: 10.1093/nar/gkt646

Suppa, A., Gorbi, G., Marková, S., Buschini, A. and Rossi, V. (2021). Transgenerational Effects of Methyl Farnesoate on *Daphnia Pulex* Clones: Male and Ephippia Production and Expression of Genes Involved in Sex Determination. *Freshw. Biol.* 66 (2), 374–390. doi: 10.1111/fwb.13644

Tahaei, L. S., Eimani, H., Yazdi, P. E., Ebrahimi, B. and Fathi, R. (2011). Effects of Retinoic Acid on Maturation of Immature Mouse Oocytes in the Presence and Absence of a Granulosa Cell Co-Culture System. *J. Assisted Reprod. Genet.* 28 (6), 553–558. doi: 10.1007/s10815-011-9579-8

Tatusov, R. L., Galperin, M. Y., Natale, D. A. and Koonin, E. V. (2000). The COG Database: A Tool for Genome-Scale Analysis of Protein Functions and Evolution. *Nucleic Acids Res.* 28 (1), 33–36. doi: 10.1093/nar/28.1.33

Techa, S., Alvarez, J. V. and Sook Chung, J. (2015). Changes in Ecdysteroid Levels and Expression Patterns of Ecdysteroid-Responsive Factors and Neuropeptide Hormones During the Embryogenesis of the Blue Crab, *Callinectes Sapidus*. *Gen. Comp. Endocrinol.* 214, 157–166. doi: 10.1016/j.ygcen.2014.07.017

Tomy, S., Saikrithi, P., James, N., Balasubramanian, C. P., Panigrahi, A., Otta, S. K., et al. (2016). Serotonin Induced Changes in the Expression of Ovarian Gene Network in the Indian White Shrimp, *Penaeus Indicus*. *Aquaculture* 452, 239–246. doi: 10.1016/j.aquaculture.2015.11.003

Toyota, K., Kato, Y., Miyakawa, H., Yatsu, R., Mizutani, T., Ogino, Y., et al. (2014). Molecular Impact of Juvenile Hormone Agonists on Neonatal *Daphnia Magna*. *J. Appl. Toxicol.* 34 (5), 537–544. doi: 10.1002/jat.2922

Visudtiphole, V., Klinbunga, S. and Kirtikara, K. (2009). Molecular Characterization and Expression Profiles of Cyclin A and Cyclin B During Ovarian Development of the Giant Tiger Shrimp *Penaeus Monodon*. *Comp. Biochem. Physiol. Part A: Mol. Integr. Physiol.* 152 (4), 535–543. doi: 10.1016/j.cbpa.2008.12.011

Wang, X. E. (1987). A Preliminary Observation on the Reproductive Biology of *Exopalaemon Carinicauda*. *J. Zool.* 22 (1), 6–10. doi: 10.13859/j.cjz.1987.01.003

Wang, J., Ge, Q., Li, J. and Li, J. (2020). Effects of Inbreeding on Growth and Survival Rates, and Immune Responses of Ridgetail White Prawn *Exopalaemon Carinicauda* Against the Infection of *Vibrio Parahaemolyticus*. *Aquaculture* 519, 734755. doi: 10.1016/j.aquaculture.2019.734755

Wan, H., Zhong, J., Zhang, Z., Xie, Y. and Wang, Y. (2021). Characterization of the Foxl2 Gene Involved in the Vtg Expression in Mud Crab (*Scylla Paramamosain*). *Gene* 798, 145807. doi: 10.1016/j.gene.2021.145807

Wan, H., Zhong, J., Zhang, Z., Zou, P. and Wang, Y. (2022). Comparative Transcriptome Reveals the Potential Modulation Mechanisms of Spfoxl-2 Affecting Ovarian Development of *Scylla Paramamosain*. *Mar. Biotechnol.* 24 (1), 125–135. doi: 10.1007/s10126-022-10091-6

Webster, S. G., Keller, R. and Dircksen, H. (2012). The CHH-Superfamily of Multifunctional Peptide Hormones Controlling Crustacean Metabolism, Osmoregulation, Moulting, and Reproduction. *Gen. Comp. Endocrinol.* 175 (2), 217–233. doi: 10.1016/j.ygcen.2011.11.035

Weirather, J., de Cesare, M., Wang, Y., Piazza, P., Sebastiano, V., Wang, X., et al. (2017). Comprehensive Comparison of Pacific Biosciences and Oxford Nanopore Technologies and Their Applications to Transcriptome Analysis. *F1000Research* 6 (100), 1–32. doi: 10.12688/f1000research.10571.1

Williams, V. N., Reading, B. J., Hiramatsu, N., Amano, H., Glassbrook, N., Hara, A., et al. (2014). Multiple Vitellogenins and Product Yolk Proteins in Striped Bass, *Morone Saxatilis*: Molecular Characterization and Processing During Oocyte Growth and Maturation. *Fish. Physiol. Biochem.* 40 (2), 395–415. doi: 10.1007/s10695-013-9852-0

Xu, W., Xie, J., Shi, H. and Li, C. (2010). Hematodinium Infections in Cultured Ridgetail White Prawns, *Exopalaemon Carinicauda*, in Eastern China. *Aquaculture* 300 (1), 25–31. doi: 10.1016/j.aquaculture.2009.12.024

Yuan, J., Gao, Y., Zhang, X., Wei, J., Liu, C., Li, F., et al. (2017). Genome Sequences of Marine Shrimp *Exopalaemon Carinicauda* Holthuis Provide Insights Into Genome Size Evolution of Caridea. *Mar. Drugs* 15 (7), 213. doi: 10.3390/md15070213

Zhang, Y., Buchberger, A., Muthuvel, G. and Li, L. (2015b). Expression and Distribution of Neuropeptides in the Nervous System of the Crab *Carcinus Maenas* and Their Roles in Environmental Stress. *Proteomics* 15 (23-24), 3969–3979. doi: 10.1002/pmic.201500256

Zhang, J., Gao, S., Shi, Y., Yan, Y. and Liu, Q. (2020). Full-Length Transcriptome of Anadromous *Coilia Nasus* Using Single Molecule Real-Time (SMRT) Sequencing. *Aquacult. Fisher.* 7 (6), 420–426. doi: 10.1016/j.aaf.2020.08.006

Zhang, C., Li, Z., Li, F. and Xiang, J. (2015a). Effects of Starvation on Survival, Growth and Development of *Exopalaemon Carinicauda* Larvae. *Aquacult. Res.* 46 (9), 2289–2299. doi: 10.1111/are.12386

Zheng, J., Wang, P., Mao, Y., Su, Y. and Wang, J. (2020). Full-Length Transcriptome Analysis Provides New Insights Into the Innate Immune System of *Marsupenaeus Japonicus*. *Fish. Shellfish. Immunol.* 106, 283–295. doi: 10.1016/j.fsi.2020.07.018

Zmora, N., Trant, J., Chan, S.-M. and Chung, J. S. (2007). Vitellogenin and Its Messenger RNA During Ovarian Development in the Female Blue Crab, *Callinectes Sapidus*: Gene Expression, Synthesis, Transport, and Cleavage. *Biol. Reprod.* 77 (1), 138–146. doi: 10.1095/biolreprod.106.055483

Conflict of Interest: The authors declare that the research was conducted in the absence of any commercial or financial relationships that could be construed as a potential conflict of interest.

Publisher's Note: All claims expressed in this article are solely those of the authors and do not necessarily represent those of their affiliated organizations, or those of the publisher, the editors and the reviewers. Any product that may be evaluated in this article, or claim that may be made by its manufacturer, is not guaranteed or endorsed by the publisher.

frontiers | Frontiers in Marine Science

ORIGINAL RESEARCH
published: 20 July 2022
doi: 10.3389/fmars.2022.917274

Neuroparsin 1 (MrNP1) and Neuroparsin 2 (MrNP2) Are Involved in the Regulation of Vitellogenesis in the Shrimp *Macrobrachium rosenbergii*

Chun Mei Ao, Li Li Shi, Wei Wang, Cheng Gui Wang and Siuming F. Chan**

Fisheries College, Guangdong Ocean University, Zhanjiang, China

Neuroparsins (NP) are small-size cysteine-rich neuropeptides first discovered in insects. They are known to be involved in insect reproduction. In this study, we have cloned two neuroparsin cDNAs (i.e., MrNP1 and MrNP2) from the freshwater shrimp *Macrobrachium rosenbergii*. The two neuroparsins consist of 12 cysteines, which is characteristic of the neuroparsin family. These cysteines are arranged in identical relative positions that form 6-disulfide bonds. MrNP1 and MrNP2 are most similar to the corresponding neuroparsin counterparts of the shrimp *Macrobrachium nipponense*. Phylogenetic study results suggested that MrNP1 and MrNP2 are closely related to MnNP1 and MnNP3, respectively. Also, an additional MrNP gene similar to MnNP2 is expected to exist in *M. rosenbergii.* The MrNP1 expression level is the highest in the ovary, and MrNP2 expression is higher in the brain and heart of the females. In addition, during the ovary maturation cycle, MrNP1 expression in the hepatopancreas is highest in stage V; in the ovary it is variable. MrNP2 expression in the hepatopancreas and ovary is the highest in stage II and stage I, respectively. *In vivo* and *in vitro* bioassay experiment results indicate that MrNP1 and MrNP2 recombinant proteins can stimulate the expression of the MrVg gene. In contrast, silencing of MrNP1 and MrNP2 genes would suppress MrVg, VgR, and CyclinB gene expressions. The results indicate that the products of both genes can stimulate vitellogenesis by up-regulating the MrVg gene expression. Results from their difference in expression patterns indicate that they might have different regulatory roles in vitellogenin synthesis. Since gene silencing of either MrNP1 or MrNP2 affected the expression of the other NP, we have hypothesized that coordinated regulatory action between MrNP1 and MrNP2 may be necessary for the normal vitellogenesis in *M. rosenbergii.*

Keywords: neuroparsin, vitellogenin, *Macrobrachium rosenbergii*, reproduction, cysteine-rich protein

OPEN ACCESS

Edited by:
Heinrich Dircksen, Stockholm University, Sweden

Reviewed by:
Isam Khalaila, Ben-Gurion University of the Negev, Israel
Wenying Shen, Shaoxing University, China

****Correspondence:***
Siuming F. Chan
siuming573@sina.com
Cheng Gui Wang
longshore@163.com

Specialty section:
This article was submitted to Aquatic Physiology, a section of the journal Frontiers in Marine Science

Received: *11 April 2022*
Accepted: *30 May 2022*
Published: *20 July 2022*

Citation:
Ao CM, Shi LL, Wang W, Wang CG and Chan SF (2022) Neuroparsin 1 (MrNP1) and Neuroparsin 2 (MrNP2) Are Involved in the Regulation of Vitellogenesis in the Shrimp Macrobrachium rosenbergii. Front. Mar. Sci. 9:917274. doi: 10.3389/fmars.2022.917274

INTRODUCTION

Insects and crustaceans belong to the subphylum of Arthropoda. They share many similar structural/anatomical features. For example, they share many similar/identical hormones that regulate similar or different biological processes (Veenstra, 2016). These hormones include ecdysteroids, juvenoids, CHH-family neuropeptides, and neuroparsins (Chung et al., 2010). The first neuroparsin (NP) was

isolated from the pars intercerebralis-corpora cardiaca complex of the locust *Locusta migratoria* (Girardie et al., 1987; Moreau et al., 1988; Girardie et al., 1989). Neuroparsin is involved in the regulation of mineral, water, and reproduction. In addition to their roles in reproduction, they are involved in promoting nerve growth, green coloration of insect larvae, anti-diuretic, adipokinetic hormone (AKH) regulation of carbohydrates and lipids, and behavioral regulation of locust phase migration. Therefore, they are also known as multi-effect neuropeptides (Fournier et al., 1987; Girardie et al., 1987; Nogaro et al., 1995; Claeys et al., 2010; Claeys et al., 2006).

In recent years, with the rapid development of RNA and genomic DNA sequencing technology, many neuroparsin-like cDNAs have been identified from different crustaceans including *Litopenaeus vannamei*, *Scylla paramamosain*, lobster *Homarus americanus*, *M. rosenbergii*, *Carcinus maenas*, and *Panulirus argus* (Badisco et al., 2007; Ma et al., 2010; Marco et al., 2014; Bao et al., 2015; Christie et al., 2015; Andrew, 2020; Kyei et al., 2020; Liu et al., 2020). Biochemically, crustacean neuroparsins are poly-cysteine-rich compounds. They consist of 12 cysteine residues that form six disulfide bonds for tertiary structure formation. They share some similarities with the neuroparsin of the locust and the ovary ecdysteroidogenic hormone (OEH) of mosquitoes (Brown et al., 1998), the N-terminal end of the growth factor-binding protein region of the vertebrate and molluscan insulin-like growth factor-binding protein and single insulin-binding domain protein (Kyei et al., 2020). The major characteristic of neuroparsin is that the spacing of Cys residues is conserved for different groups of cysteine-rich neuropeptides (Badisco et al., 2007; Tanaka, 2021). Different neuroparsins were initially identified as anti-gonadotropic peptides from the pars intercerebralis-corpora cardiaca complex of the migratory locust, *Locusta migratoria*, and further studies revealed the pleiotropic activities of these peptides. Discovered in crustaceans quite late as compared to insects, neuroparsins have also been found in many Decapoda in recent years. Similar to insects, the crustacean neuroparsins are reported to have gonad regulatory function. For example, in the shrimp *M. ensis*, *in vivo* gene silencing of neuroparsins could cause a significant decrease in vitellogenin transcript level in the hepatopancreas and ovary (Yang et al., 2014). In *Marsupenaeus japonicus*, *in vivo* injection of recombinant neuroparsin could increase the expression of MjVg (Tsutsui et al., 2020).

The freshwater shrimp *M. rosenbergii* is one of the most important freshwater crustaceans cultured in China. There is a rapid increase in demand for high-quality shrimp fry for aquaculture. In this study, we have reported the characterization of two neuroparsins and investigated the role of the two neuroparsins in the regulation of vitellogenesis. Because the amount of culture has increased, the need for shrimp seedling has also increased greatly in recent years. The production of high-quality healthy seedings has become the bottleneck for the further increase in *M. rosenbergii* culture. Therefore, the study on the reproductive physiology mechanism of *M. rosenbergii* is of great significance for understanding their reproduction and for better development of contemporary farming techniques. Recently, we have identified two neuroparsin cDNA sequences from the transcriptome of *M. rosenbergii*. We have used gene cloning techniques to obtain two neuroparsin open reading frame (ORF) sequences and have studied their gene expression patterns in the early stages of female shrimp gonad development and the level of mRNA expression in the hepatopancreas (Hp) and ovary (Ov) during different developmental cycles. Using RNAi interference technology, the regulatory role of neuroparsin in the expression of the major egg yolk protein of *M. rosenbergii* (vitellogenin, Vg) is explored. It is hoped that these data can provide background information for the role of the neuroparsins in shrimp.

MATERIAL AND METHODS

Animals

Female *M. rosenbergii* used in the study were obtained from the shrimp-breeding research facility of Guangdong Ocean University, Zhanjiang, Guangdong, China. They were temporarily cultured in a small container (i.e., 1 M^3) for 2–3 days. About 50% of water was changed daily, and shrimps were fed thrice daily with pellet diets. The reproduction status of the animal was determined before the experiment following the reported methods (Chang and Shih, 1995; Yang et al., 2000); shrimps at different ovarian development stages (stage I–V) in this study are listed in **Table 1**.

RNA Preparation, cDNA Synthesis, and Gene Cloning

Based on the anatomical structure and external appearance of the ovary, the developmental conditions of the shrimps were determined (Chang and Shih, 1995). Various tissues including the hepatopancreas (Hp), eyestalk (Es), brain (Br), stomach (St), thoracic ganglion (Tg), intestine (Int), heart (He), and ovary (Ov) were dissected and extracted for total RNA using a spin-column-based TransZol Up Plus RNA preparation kit (TransGen Biotech, Peking, China). After elution of the total RNA from the column, the quality of total RNA was analyzed by 1.5% agarose gel electrophoresis and the concentration was determined by a NanoDrop 2000 spectrophotometer (Thermo Fisher Scientific, Inc., Waltham, MA, USA). High-quality total RNAs were used for first-stranded cDNA synthesis using the 5× All-In-One RT MasterMix cDNA synthesis kit (ABM, Vancouver, Canada). The cDNA synthesis condition followed the program as follows: 25°C for 10 min, 42°C for 15 min, 85°C for 5 min. At the end of the synthesis, the cDNA was diluted 20× for real-time quantitative PCR (qRT-PCR) analysis or for use (1 μl) directly in semiquantitative RT-PCR. The PCR reaction in general consists of 20 μl: 10 μl 2× PCR mix, 0.5 μl cDNA, 1 μl primer (forward and reverse 1 μl, respectively), and 7 μl free water, and the PCR condition was 95°C for 3 min, 95°C for 30 s, 58°C for 30 s (MrNP1 and MrNP2 have the same temperature), 72°C for 30 s for 34 cycles, and 72°C for 10 min. At the end of the PCR, the PCR products were analyzed by 1.5% agarose gel.

TABLE 1 | GIS of *M. rosenbergii* at different ovarian development stages (stages I–V).

Ovarian stage	Ovarian color	Ovarian features	GSI[a] (%) in this study
Stage I	White/creamy	Mainly comprised of oogonia and previtellogenic oocytes	0.49 ± 0.03
Stage II	Yellow	Majorly compose previtellogenic oocytes and endogenous vitellogenetic oocytes	1.48 ± 0.38
Stage III	Orange	A large number of oocytes developing from endogenous vitellogenetic oocytes to exogenous vitellogenetic oocytes	2.7 ± 0.51
Stage IV	Orange	Exogenous vitellogenetic oocytes and mature oocytes predominate in the ovaries	5.6 ± 0.64
Stage V	Reddish	Ready to spawn	7.03 ± 0.48

GSI (%), gonadosomatic index.

The amplified target cDNA in the gel was cut and purified by a spin-column based purification kit, subcloned and the DNA sequence was determined. Obtaining the cDNA of containing tagetart band by a spin column-based gel purification kit, for gene cloning.

Bioinformatic Characterization of MrNPs

The program SingnalP5.0 (http://www.cbs.dtu.dk/services/SignalP/) was used to identify the signal peptide region. The pI and pMW of NPs were estimated using the pI/pMW program from Expasy (http://web.expasy.org/protparam/). For alignment analysis, several invertebrate neuroparsin molecules were obtained through the BLAST program in the NCBI database (https://blast.ncbi.nlm.nih.gov/Blast.cgi) similarity search and analyzed using the program ClustalX (http://www.ebi.ac.uk/Tools/msa/clustalo/). All primers were designed using the Primer 5.0 program, and EF-1α was used as internal reference gene (**Table 2**). MEGA6.0 (megasoftware.net) was used to build the phylogenetic tree with the neighbor-joining method (NJ) with confidence intervals set at 1,000 bootstrap replications.

Expression Study of MrNP1 and MrNP2

Gene-specific primers for neuroparsin (MrNPI, MrNP2), vitellogenin (Vg, GenBank: ADK55596.1), vitellogenin receptor (VgR, GenBank: ADK55596.1), cyclin B (GenBank: ADP95148.1), elongation factor (EF-1α), and β-actin are listed in **Table 2** (i.e., qNP1F, qNP1R, qNP2F, qNP2R, qVgF, qVgR, qVgRF, qVgRR, qCBF, qCBR). qRT-PCR was performed using the SYBR qPCR kit (Vazyme, Nanjing, China). For the 20-μl reaction, it consisted of 10 μl SYBR Premix Ex Taq, 1 μl cDNA, and 1 μl of each forward and reverse primer (10 μM). PCR was performed in a real-time PCR machine (Bio-Rad CFX® 96 system, Bio-Rad, USA), and the conditions were 95°C denature and 35 cycles of 95°C 30 s, annealing at 55°C for 30 s and denature at 72°C for 30 s. A further 10 min at 72°C was included for complete product extension. The results were determined using $2^{-\Delta\Delta Ct}$ and further analyzed by statistical methods. The sample size N = 5 and the experiment were triplicated.

TABLE 2 | Primers used in this paper.

Primer name	Sequence 5′→3′	Length (dp)
CNP1F	TGTTAAATTCGTTCTCAAGAGCACC	328
CNP1R	TTAGCAAAAAGTGCCGGACCAGCATTCC	
CNP2F	TGAAGTCGTTTGCTGCTTGC	297
CNP2R	AGCAGACCAGGGACGAGCGGAAG	
qNP1F	TTCGTTCTCAAGAGCACCAT	144
qNP1R	GCATGTCTCGACGTTCACC	
qNP2F	CTTACAGCCACCACCATC	164
qNP2R	TTGAGTACAACGAGGAGCA	
qVgF	GTCAGCGAGGAAATGAAAAG	168
qVgR	GCCATTCAGCTCCAATTTTACT	
qVgRF	GATGAGAATGACTGCCACGG	203
qVgRR	CTCATCTGACCTGTCCGTGC	
qCBF	AAGGAAAATGAGAATGTCAGGGA	167
qCBR	CATTCACATACTCAAAGACCAACTG	
T7NP1F	TAATACGACTCACTATAGGGGTTAAATTCGTTCTCAAGAGC	324
T7NP1R	TAATACGACTCACTATAGGGTAGCAAAAAGTGCCGGAC	
T7NP2F	TAATACGACTCACTATAGGGGAAGTCGTTTGCTGCTTGC	295
T7NP2R	TAATACGACTCACTATAGGGTAGCAGACCAGGGACGAGCGGAAG	
EFF	GAGGAAGATTGAACGCAAGA	
EFR	TTAAGGATGCCAGTCTCCAC	
M13F(-47)	CGCCAGGGTTTTCCCAGTCACGAC	
M13R(-48)	AGCGGATAACAATTTCACACAGGA	

Functional Study by Recombinant Protein Technology and RNA Interference

Production of His-tagged recombinant protein: For rMrNP1, a pair of restriction enzyme sequence-linked primers (**Table 2**) were used to amplify the mature peptide sequence of MrNP1 from the full-length cDNA. After PCR, the product was digested with the restriction Kpn I and BamH I, respectively, and the digested fragments were ligated into Kpn I and BamH I cut sites of the linearized pET-32a protein expression vector. The ligated product was transformed into DH5a *E. coli* bacterial cells. For protein expression, the positive clone (i.e., rMrNP1 plasmid) was transformed into a BL21 cell. Positive clones were induced by isopropyl β-d-1-thiogalactopyranoside (IPTG) for fusion protein generation. After optimization for incubation time, IPTG, and temperature, mass production was performed in 500 ml of LB medium buffer using the determined parameters. Mass production and subsequent purification of the his-tagged recombinant protein followed the procedure as described before. Similar procedures were used for the production of recombinant protein MrNP2. Primer sequences are found in **Table 2**.

For double-strand RNA (dsRNA) production, forward and reverse primers (i.e., T7MrNP1F (**Table 2**), T7MrNP1R, T7MrNP1F, and T7MrNP2R containing T7 adapters) were designed using the program Primer 5.0 to synthesize dsNP1 and dsNP2 with MrNP1 and MrNP2 clones as templates. The PCR reaction in general consists of 20 μl: 10 μl 2× PCR mix and 0.5 μl cDNA, and the PCR reaction used the following procedure: 95°C for 3 min; 34 cycles of 95°C for 30 s, 63°C (T7NP1) or 60°C (T7NP2) for 30 s, 72°C for 30 s, and 72°C for 10 min. The purified product was the template for dsRNA production using the OneScribe T7 Synthesis Kit (ABM, Vancouver, Canada). The control double-strand RNA included the dsRNA for the Tiger Frog virus (dsTFV), as described previously (Tiu and Chan, 2007), and it has no effect on *M. rosenbergii* in this study.

Adult females at the early stage of gonadal development were selected for *in vivo* injection study. The experimental group was injected with 50 μl injection volume containing 2 μg/g of double-stranded RNA (i.e., dsMrNP1 and dsMrNP2), and the control group was injected with the same volume of dsTFV (Tiu and Chan, 2007). All animals were placed in the same culture environment for 48 h until sampling. Shrimps were dissected for collecting the hepatopancreas and ovary for total RNA preparation. The interference efficiency of dsRNA and gonad maturation conditions were determined for monitoring the expression of related genes (i.e., MrNP1, MrNP2, vitellogenin, VgR, and CyclinB). For *in vitro* RNAi and recombinant protein study, a the nutrient medium M199 (Sigma, USA) was sterile filtered with a 0.45-μM filter unit. Culture medium (1.5 ml) was added to each well of the 12-well culture plate. The hepatopancreas and ovary were dissected and cut to small fragments of similar size (i.e., 8 cm^3). They were first rinsed separately in 1× cold PBS and placed in a well containing the recombinant proteins or dsRNA and control 1× cold PBS or control dsTFV. The culture plate was placed on an orbital shaker and incubated at 25°C. After 3 h, for the *in vitro* recombinant protein experiment, the tissue pieces were extracted for crude protein for SDS-PAGE analysis (Okuno et al, 2002). In the experiment of adding dsRNA *in vitro*, the tissue pieces were extracted for total RNA using the TRIzol RNA preparation kit, and total RNA was extracted to determine the RNA interference efficiency and changes in the expression of related genes. Both experiments were repeated five times (i.e., N = 5).

RESULTS

Characterization of the Shrimp Neuroparsins

Two different neuroparsin-like cDNAs (i.e., MrNP1 and MrNP2) were cloned from the eyestalk of the freshwater shrimp *M. rosenbergii.* The open reading frame of MrNP1 was 303 bp encoding for a peptide of 100 amino acid residues. The signal peptide was from AA1 to AA26, and the mature peptide contains 74 aas in size (**Figure 1**). For pI and pMW, MrNP1 is predicted to have theoretical pI and pMW values of 7.34/10,862.6 and 6.28/8014.9, respectively. The open reading frame of MrNP2 was 300 bp encoding for a peptide of 99 amino acid residues. The signal peptide was from AA1 to AA24, and the mature peptide contains 75 AAs (**Figure 1**). The pro-peptide and mature peptide of MrNP2 are predicted to have a theoretical pI/pMW of 7.96/10,808.56 and pI/MW of 8.06/8150.3, respectively. Although MrNP1 and MrNP2 share low sequence homology in the signal peptide region, they both consist of 12 cysteine residues forming six disulfide bridges and the spacing of these cysteines is identical, which suggests that they share a similar tertiary structure (**Figure 2A**).

Multiple-sequence alignment results (**Figure 2B**) indicate that MrNP1 shared the highest amino acid sequence identity with the neuroparsin 3 precursor of *M. nipponense* (MnNP3, 84.2%), followed by that of the shrimp *M. ensis* neuroparsin (MeNP, 55%), *Penaeus monodon* neuroparsin (PmNP, 55%), the crayfish *Procambarus clarkii* neuroparsin A-like (PcNPA, 50.5%), the neuroparsin A-like of the lobster *Homarus americanus* (HaNPA, 44%), the neuroparsin A of the crab *Portunus trituberculatus* (PtNPA, 44%), and *M. nipponense* neuroparsin 1 (MnNP1, 42.4%), and the lowest homology (39%) with *Cherax quadricarinatus* neuroparsin 2 (CqNP2), while MrNP2 shared the highest amino acid sequence identity with MnNP1 (97%), followed by CqNP2 (64%), HaNPA (64.7%), PtNPA (63.8%) and PcNPA (46.5%), MnNP3 (42.4%), MeNP (41.4%), and the lowest homology (38.4%) with PmNP.

Based on the amino acid sequence of the neuroparsin-like and other cysteine-rich peptides from vertebrates and invertebrates, the phylogenetic tree result indicates that neuroparsins and other cysteine-rich peptides were clustered into three major groups: i.e., the crustacean NPs, insect NPs, and other cysteine-rich peptides. The first group consisted of crustacean neuroparsins containing MrNP1 and MrNP2 which are evolutionarily related. Group 2, the neuroparsins of insects, includes NP1, NP2, NP3, and NP4 of *S. paramamosain* and *L. migratoria* NPA and OEH protein of *Acedes aegypti* and *Culex*

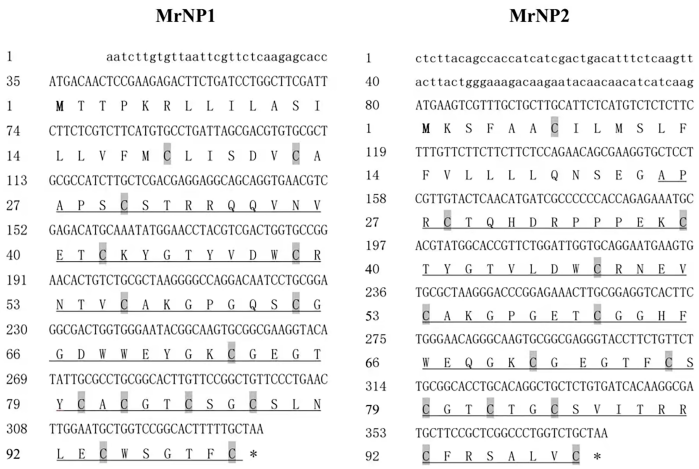

FIGURE 1 | Deduced amino acid of the partial cDNAs of MrNP1 (left) and MrNP2 (right). One letter amino acid code is shown. The two partial cDNAs consist of all the coding/translation information. Underlined parts represent mature peptide.

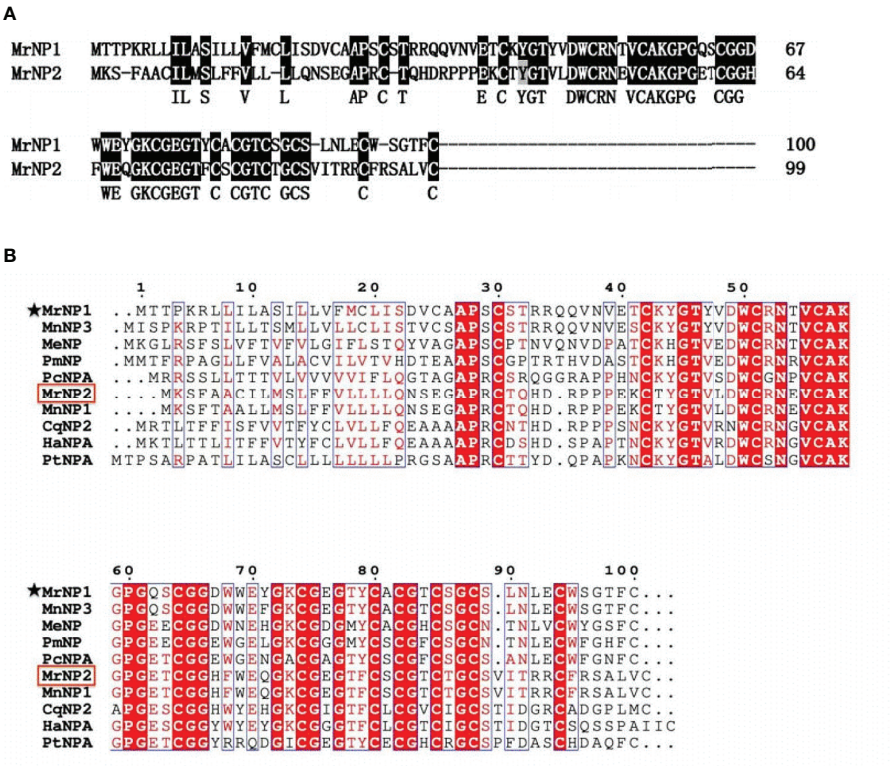

FIGURE 2 | (A) Alignment of MrNP1 and MrNP2. **(B)** Multiple-sequence alignment of selected neuroparsins from different arthropods including the insects and crustaceans. These sequences are as follows: *M. nipponense* NP3 (GenBank# QBG05398.1); *Metapenaeus ensis* NP (GenBank# AHX39208.1); *Penaeus monodon* NP (GenBank# ALO17555.1); *Procambarus clarkii* NPA (GenBank# XP_045591875.1); *Macrobrachium nipponense* NP1 (GenBank# QBG05396.1); *Culex quinquefasciatus* NP2 (GenBank# AWK57531); *Homarus americanus* NPA (GenBank# XP042239197.1); *Portunus trituberculatus* NPA (GenBank# XP045122305.1). *M. rosenbergii* neuroparsin 1 and neuroparsin 2 (MrNP1, MrNP2) were marked with an asterisk and a box, respectively.

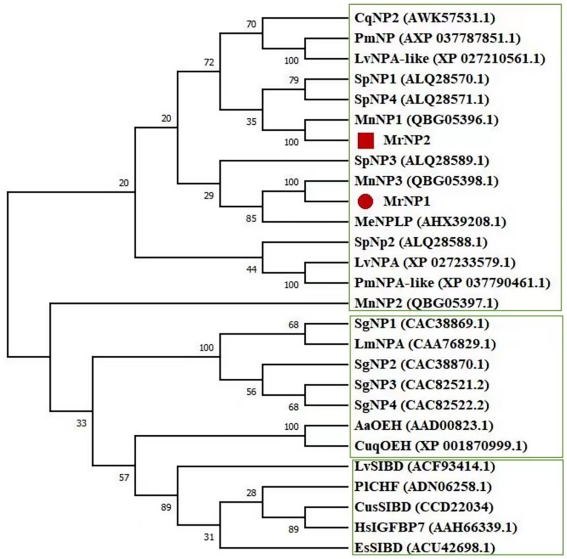

FIGURE 3 | Phylogenetic tree analysis of the *M. rosenbergii* neuroparsins (MrNP1, MrNP2) with other cysteine-rich related peptides from the crustaceans, insects, and other species. The sequences include *Penaeus monodon* NPA-like (GenBank# XP037790461.1); *Litopenaeus vannamei* NPA (GenBank# XP027233579.1); the locust *Schistocerca gregaria* NP1 (GenBank# CAC38869.1); *S. gregaria* NP2 (GenBank# CAC38870.1); *S. gregaria* NP3 (GenBank# CAC82521.2); *S. gregaria* NP4 (GenBank# CAC82522.2); *L. migratoria* LmNPA (GenBank# CAA76829.1); *Acedes aegypti* AeOEH (GenBank# AAD00823.1); *Culex quinquefasciatus* CuqOEH (GenBank# XP_001870999.1); the crab *S. paramamosain* SpNP1 (GenBank# ALQ28588.1); *S. paramamosain* SpNP2 (GenBank# ALQ28570.1); *S. paramamosain* SpNP3 (GenBank# ALQ28589.1); *S. paramamosain* SpNP4 (GenBank# ALQ28571.1); *M. nipponense* MnNP1 (GenBank# QBG05396.1); *M. nipponense* MnNP2 (GenBank# QBG05397.1); *M. nipponense* MnNP3 (GenBank# QBG05398.1); *M. ensis* MeNP (GenBank# AHX39208.1); *L. vannamei* single IB domain protein (LvSIBD, GenBank# ACF93414.1); *Pacifastacus leniusculus* crustacean hematopoietic factor (PlCHF, GenBank# ADN06258.1); crab *Eriocheir sinensis* single insulin binding domain protein (EsSIBD, GenBank# ACU42698.1); spider *Cupiennius salei* SIBD (CusSIBD, GenBank# CCD22034); *Homo sapiens* insulin-like growth factor-binding protein 7 (HsIGFBP7,GenBank# AAH66339.1).

quinquefasciatus. The single insulin-binding domain (SIBD) protein of invertebrates and insulin-like growth factor-binding protein (IGFBP) of the cysteine-rich peptides were clustered into group 3 (**Figure 3**).

Expression of MrNP1 and MrNP2 in Female *M. rosenbergii*

QRT-PCR results showed that the MrNP1 expression level was the highest in the ovary (Ov), followed by the hepatopancreas (Hp), and it is only moderately expressed in the eyestalk (**Figure 4A**). In contrast, MrNP2 transcript levels were higher in the heart and brain. It is moderately expressed in the thoracic ganglion and intestine, and only traces of transcripts were detected in the gill, eyestalk, and hepatopancreas (**Figure 4B**). Since the ovary (Ov) and hepatopancreas (Hp) are major sites for vitellogenesis, we also studied the expression of these two genes during the gonad maturation cycle of *M. rosenbergii*. In the Hp, MrNP1 expression was high in stage V (GSI^a = 7.03 ± 0.48) and the MrNP2 expression level is the highest in stage II (GSI^a = 1.48 ± 0.38) (**Figures 5A, B**); in the Ov, the MrNP1 transcript level is variable but the expression level of MrNP2 is the highest in stage I (GSI^a = 0.49 ± 0.03) (**Figures 5C, D**).

RNAi and Recombinant Protein Assay to Study the Function of MrNP1 and MrNP2 in Vitellogenesis

Females at the early (stage II) to early-middle (stages II–III) stages of the ovary maturation were used for *in vivo* and *in vitro* recombinant protein and RNAi bioassay experiments. Shrimp were selected at the early (stage II) for *in vivo* dsRNA injection studies, and they were sacrificed for 48 h after dsRNA injections. The injection of dsMrNP1 and dsMrNP2 had no observable harmful effects as there was no mortality in any of the groups. For dsMrNP1-injected shrimps, MrNP1 transcript levels in the hepatopancreas and ovary had decreased significantly. Also, there was a significant reduction in MrNP2 transcript level in the hepatopancreas ($P < 0.05$) but not in the ovary. The injection of dsMrNP2 had little effect on MrNP1 transcript level in the ovary,

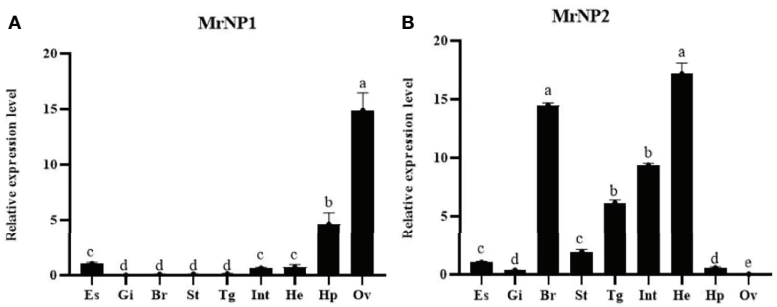

FIGURE 4 | QRT-PCR expression study of **(A)** MrNP1 and **(B)** MrNP2 in various tissues of female *M. rosenbergii*. Tissues used in the study are eyestalk (Es), gill (Gi), brain (Br), stomach (St), thoracic ganglion (Tg), intestine (Int), heart (Ht), hepatopancreas (Hp), and ovary (Ov). Values are relative expression level ± standard deviation (SD) (N = 5). Different letters indicate significant differences at $P < 0.05$ computed with ANOVA and the Tukey–Kramer test.

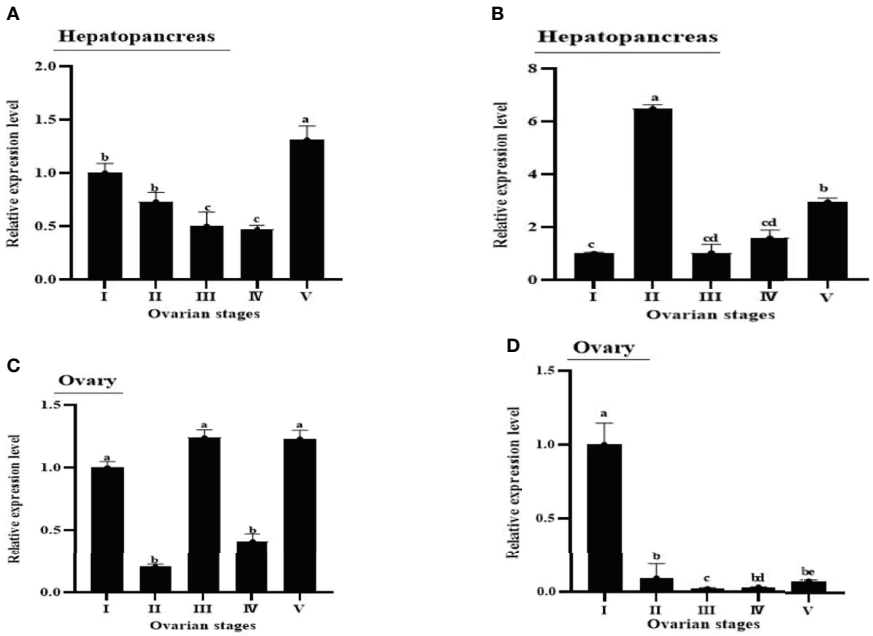

FIGURE 5 | Expression patterns of MrNP1 and MrNP2 in **(A, B)** hepatopancreas and **(C, D)** ovary in female *M. rosenbergii* in different reproductive stages (i.e., I, II, III, IV, V). Data shown are means of relative expression levels ± SD. Different letters indicate significant differences at $P < 0.05$ computed with ANOVA and the Tukey–Kramer test.

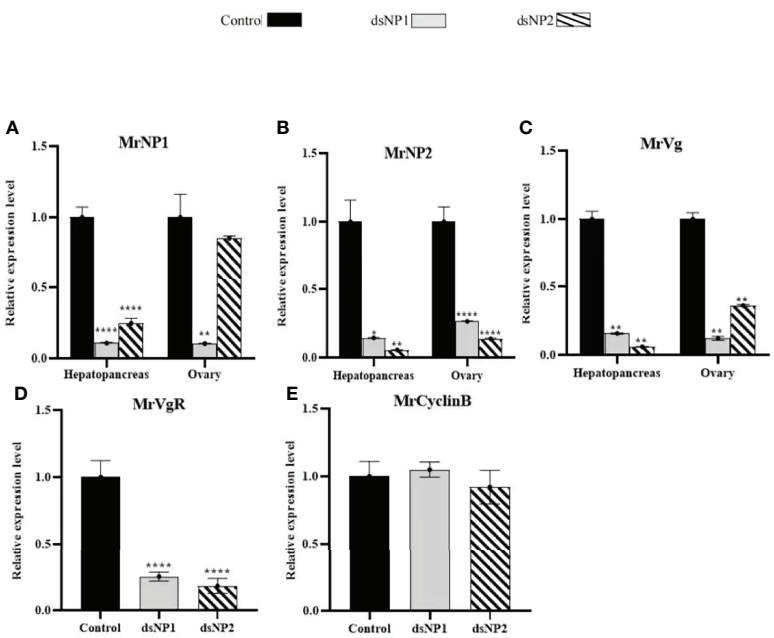

FIGURE 6 | *In vivo* RNA interference of dsMrNP1 and dsMrNP2. Expression of **(A)** MrNP1, **(B)** MrNP2, and **(C)** MrVg after shrimps were injected with dsTFV (black bar), dsMrNP1 (gray bar) and dsMrNP2 (diagonally stripe bar). Expression of VgR **(D)** and CyclinB **(E)** in the ovary (data shown are means of relative expression levels ± SD. One-way ANOVA method was used in the statistical analysis . The significance levels are: * , ($P < 0.05$); **,($P < 0.01$); ***, ($P < 0.005$) ; and ****,($P<0.001$).

but the level has reduced to only 30% in the hepatopancreas as compared to the control. Interestingly, the hepatopancreas and ovary expression of the MrNP1 transcript and MrNP2 was reduced significantly (**Figures 6A, B**). The gene knockdown of MrNP1 and MrNP2 has caused a significant reduction in MrVg transcript levels in the hepatopancreas and ovary (**Figure 6C**). Also, the ovary vitellogenin receptor transcript level was reduced significantly. However, the injection of dsMrNP1 and dsMrNP2 had little effect on the transcript levels of CyclinB (**Figures 6D, E**).

The *in vitro* RNAi results were similar to those of the *in vivo* RNAi experiment with minor differences (**Figures 7A, B, D, E**). The change in transcript levels of MrNP1, MrNP2, MrVg, and MrVgR in dsMrNP1- and dsMrNP2-treated tissues was similar in the *in vitro* and *in vivo* experiments. However, in the hepatopancreas the expression level of MrVg was unaffected after dsRNA treatments (**Figure 7C**).

Since the expressions of MrNP1 and MrNP2 are important for the expression of MrVg, we extend the *in vitro* functional study by treating the hepatopancreas and ovary fragments with recombinant proteins for MrNP1 and MrNP2. Compared to the control, hepatopancreas and ovary fragments treated with recombinant proteins for MrNP1 and MrNP2 express a higher level of MrVg (the densitometry results in **Supplement 1**). The effect existed in the ovary of early stage (stage II) and also in ovaries of further matured stages II to III (stages II–III) (**Figure 8**).

DISCUSSION

Compared with other neuropeptide hormones, neuroparsins are more recently discovered cysteine-rich signaling biomolecules in Arthropoda. Sequence comparison and multiple alignments of neuroparsins with other selected cysteine-rich peptides revealed that there are significant sequence similarities among arthropod neuroparsins, crustacean hematopoietic factor, single insulin-binding domain protein of vertebrate, and mollusk insulin-like growth factor-binding proteins (IGFBP) (Kleijn and Herp, 1998). Therefore, we agreed with that neuroparsins might interact with endogenous insulin-related peptides (Badisco et al., 2007). Lm-NPA was initially identified from corpora cardiaca of the locust based on its inhibiting role in vitellogenesis. Later in Aedes aegypti, a neuroparsin ortholog was identified and named ovary ecdysis hormone (i.e., OEH) (Brown et al., 1998; Matsumoto et al., 1989). Although the OEH shared only 29% amino acid sequence similarity to Lm-NP, it has eight cysteine residues spaced in a conserved identical position similar to that of Lm-NP, which is considered to be a major characteristic of the NP family (Tanaka, 2021). Also, most of these cysteine sites are concentrated in the mature peptide region, and there are 12 cysteines in them.

Three different NPs were identified in M. nipponense (Qiao et al., 2020). Despite that M. rosenbergii MrNP1 and

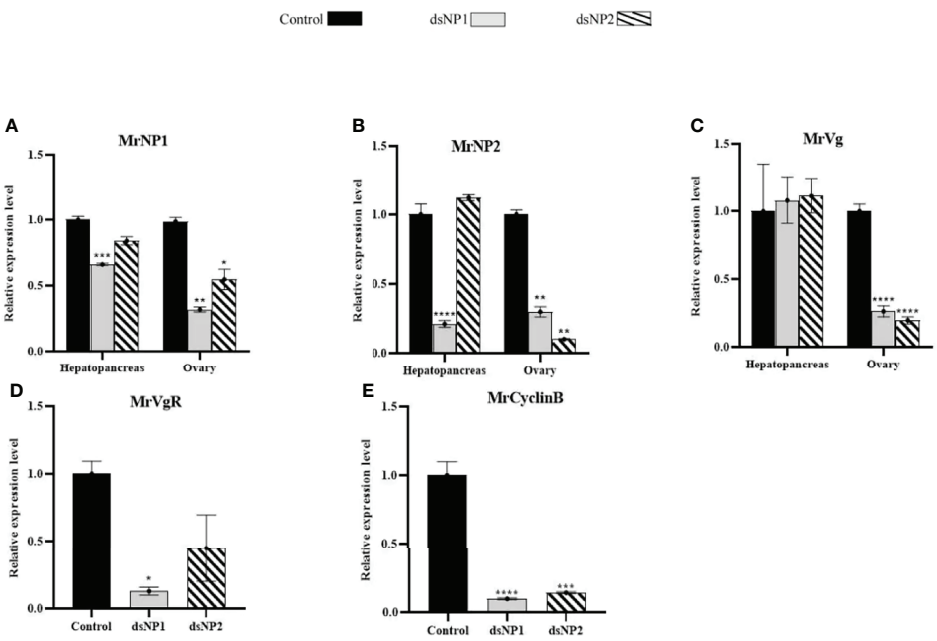

FIGURE 7 | *In vitro* RNA interference of dsMrNP1 and dsMrNP2. Expression of **(A)** MrNP1, **(B)** MrNP2, and **(C)** MrVg after shrimp hepatopancreas and ovary fragments were treated with dsTFV (black bar), dsMrNP1 (gray bar), and dsMrNP2 (diagonally stripe bar); expression of VgR **(D)** and CyclinB **(E)** after RNAi. Data were mean relative expression levels ± SD. One-way ANOVA method was used in the statistical analysis. The significance levels are: * , ($P < 0.05$); **, ($P < 0.01$); ***, ($P < 0.005$); and ****, ($P<0.001$).

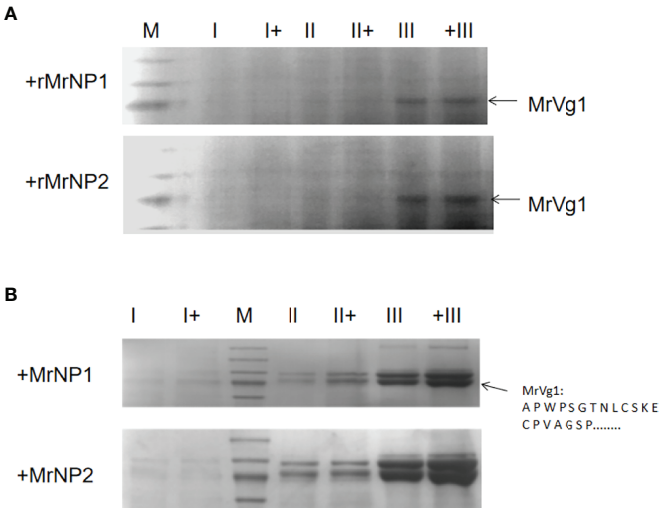

FIGURE 8 | Analysis of hepatopancreas **(A)** and ovary **(B)** tissue protein by 7% SDS-PAGE after *in vitro* treatment with recombinant protein for MrNP1 and MrNP2 (N = 3). Representative Coomassie Blue-stained gel after SDS-PAGE. Each lane represents protein extracted from the from medium. Protein in gel (78 kDa, arrow) was excised, and the amino acid sequence was determined by amino acid sequencing and confirmed to be MrVg as previously (Okuno et al., 2002). Hepatopancreas from the early (stage I), middle (stage II), and late (stage III) stages of ovary maturation were either incubated with (+) or without the recombinant proteins (i.e., rMrNP1 and rMrNP2).

MrNP2 share only 56% amino acid identity, the comparison between M. rosenbergii MrNP1 and M. nipponense MnNP3 and the comparison between M. rosenbergii MrNP2 and M. nipponense MnNP1 show high degrees of amino acid sequence identity (97%), which suggests that they should have a strong structure–function relationship. From an evolutionary standpoint, the presence of a third NP in *M. nipponense* suggested that a third MrNP3 that shared a high sequence identity with NP2 of *M. nipponense* may exist in *M. rosenbergii*. Further experiments are needed to confirm or identify this NP. The locust neuroparsin gene produces five different transcripts, of which only one coding for the neurohormone was identified from the corpora cardiaca. The existences of multiple-neuroparsin genes have been reported in some insects including the beg bug *Cimex lectularius* (GenBank# Q034340.1) (Predel et al., 2018). In locust, the organically reported LmNPB was actually derived from the alternative splicing of the LmNP giving rise only to the Lm-NPA transcript. Considering high sequence similarity with the crab NP (Sp-NP1), the two NPs found in *M. rosenbergii* may also have a similar function of promoting the development of gonads (Liu et al., 2020).

The development of ovary in M. rosenbergii is artificially divided into five stages based on the amount of the major yolk protein vitellin present in the oocytes (Chang and Shih, 1995; Ching and Tung, 2011). During the early phase of ovary maturation, vitellogenin, the precursor of vitellin, was produced in large quantity (Meusy, 1980). The understanding of how vitellogenin synthesis is regulated in the early stage of maturation is valuable as its knowledge may contribute to the development of a technique to stimulate ovary maturation in hatchery production. Therefore, *M. rosenbergii* at the early stage of development was used in this study. The hepatopancreas and the ovary are the major non-neuronal tissues that express NP in female *M. rosenbergii*. However, the expression patterns of *M. rosenbergii* MrNP1 and MrNP2 are different. In the ovary, MrNP1 expression is the highest in stage III, while the MrNP2 expression level is the highest in stage I. Because of the difference in the expression patterns of MrNP1 and MrNP2, it is likely that the main regulation of Vg by the two MrNPs occurred in different developmental stages.

After vitellogenin is synthesized in the Hp, Vg produced in the hepatopancreas is secreted into the hemolymph and transported to the oocytes (Chen and Raikhel, 1996). In the oocytes, Vg interacts with VgR to form a complex and then enters the cytoplasm through endocytosis. Therefore, an up-regulated Vg production, in general, is accompanied by an increase in expression of VgR in the ovary (Tiu et al., 2008). CyclinB is an important maturation factor (i.e., MPF) involved in cell division and is highly expressed in the ovary in oocyte formation. In rainbow trout (*Oncorhynchus mykiss*) (Feng et al., 2020), Cyclin B1 was absent in vitellogenic oocytes but present in young previtellogenic and mature oocytes and showed a strong relationship with vitellogenesis (Draetta et al.,1989; Qiu et al., 2008). In the crab, *Eriocheir sinensis*, it was reported that CyclinB is involved in the oogenesis during ovary maturation (Fang and Qiu, 2009). To further understand and explore the function of two NP genes in *M. rosenbergii*, the expressions of the Vg, VgR, and CyclinB genes were analyzed as indicators. The results of the RNAi *in vivo* and *in vitro* experiments were monitored by the gene knockdown of MrNP1 and MrNP2 genes and also the expression of the reproduction-related marker gene. The *in vivo* and *in vitro* knockdown of MrNP1 and MrNP2 genes was highly effective as the gene expression levels of the MrNP1

and MrNP2 were reduced significantly. As in other decapods, vitellogenin in *M. rosenbergii* is produced in the hepatopancreas during vitellogenesis. After synthesis, Vg is transported through the hemolymph to the ovarian tissue for further processing and storage. Our experimental results show that it is very likely that neuroparsin can directly affect the synthesis and storage of Vg in *M. rosenbergii*. Therefore, contrasting vitellogenin stimulation and inhibition results have been reported in crustaceans, which is consistent with our experimental results; the expression of the VgR gene in the ovary decreases significantly. Knockdown of MrNP1 and MrNP2 genes can significantly reduce the expression of VgR genes, indicating that MrNP1 and MrNP2 genes may participate in the processing of Vg. There is a significant difference between the amount and the control group. The CyclinB gene mainly plays a role in the process of oocyte mitosis. During the entire vitellogenesis period, the CyclinB gene expression is the highest during the prophase of vitellogenesis; therefore, knockdown of the NP1 and NP2 genes have no effect in CyclinB expression.

In locusts, the deposition of NP can inhibit the growth of oocytes and production of Vg (Girardie et al., 1998; Badisco et al., 2011). In mosquitoes, OEH can increase the expression of the Vg gene (Riehle et al., 2002; Gulia-Nuss et al., 2012). In *Scylla paramamosain*, NP could down-regulate the expression of the Vg gene (Liu et al., 2020), while the expression of the Vg gene decreased significantly after injection of dsNP in female *M. ensis* (Yang et al., 2014). These results show that the function of the NP gene may be species-specific. In this study, we found that knockdown of MrNP1 and MrNP2 could decrease the expression of the Vg gene in both hepatopancreas and ovary, and addition of recombinant protein could increase the expression of Vg. At this stage, the reason for the lack of change in MrVg expression after RNAi by dsMrNP1 and dsMrNP2 is unknown. However, since there was no significant change in Vg expression in these animals, the results reaffirmed that NP2 was involved in Vg regulation.

During the early stage of ovary maturation, it was estimated that 90% of Vg was synthesized in the hepatopancreas in *M. rosenbergii* (Li, 2012). Unlike the *in vivo* injection study, *in vitro* treatment of the hepatopancreas with dsMrNP1 did not affect the expression of MrVg. The results suggest that MrNP1 may not directly be involved in the synthesis of Vg. After the synthesis of Vg by the hepatopancreas, it is transported from the hemolymph to the ovary and binds to VgR to form a Vg/VgR complex. The Vg/VgR complex enters the oocytes cytoplasm *via* endocytosis (Meusy, 1980).

The presence of SpNP1 in the hemolymph has been reported in the crab *S. paramamosain* through Western blot, which indicates that SpNP1 serves as an endocrine factor in the regulation of physiological activities. *In vitro* experiments have further shown that the mRNA level of vitellogenin in the hepatopancreas notably decreases following administration of recombinant SpNP1, while the mRNA levels of the vitellogenin receptor and cyclin B in the ovary showed no significant differences. In *S. paramamosain*, *in vitro* experiments confirmed that recombinant SpNP1 inhibited the expression of Vg, but it had no effect on the expression of the VgR gene in the ovary (Liu et al., 2020). However, in *M. rosenberg* in an *in vivo* study showed that knockdown of MrNP1/2 could significantly decrease the expression of the VgR gene. Therefore, MrNP1 and MrNP2 play important roles in the transportation of Vg from hepatopancreas to ovary.

The oocytes' meiotic competence and maturation occur at the termination of vitellogenesis. In this physiological process, cyclin B acts as a regulatory subunit of the maturation-promoting factor and plays a key role in the regulation of meiotic resumption (Okano-Uchida et al., 1998); the maturation-promoting factor controls the G2/M checkpoint in eukaryotic cell division cycles and induces oocytes to enter the M phase and develop into meiosis maturation (Basu et al., 2004; Tomy et al., 2016). Thus, a high level of cyclin B in the ovary is necessary for the maturation of oocytes (Phinyo et al., 2013). Moreover, researchers found that cyclin B has high expression at both the previtellogenesis and late vitellogenesis stages (Phinyo et al., 2013; Tomy et al., 2016; Xie et al., 2001). The result of the *in vivo* injection experiment showed that the expression of the cyclin B gene had no obvious change, while significant decreases were seen after the addition of dsMrNP1/2 *in vitro* incubating experiments. These results indicated that cyclin B could be regulated by MrNP1 and MrNP2 in the individual ovary, while in *M. rosenbergii* at the early vitellogenesis stage, the expression of cyclin B may be influenced by some unknown factors so as not to be decreased with the knockdown of MrNP1/2. According to this result, and combining with the results of the characteristics of sequences, patterns of expression, and experiments of injection and incubation, we concluded that both MrNP1 and MrNP2 can promote the synthesis of vitellogenin in *M. rosenbergii*, which might have different regulatory roles in the regulatory mechanism. However, the relationship between MrNPs and CyclinB gene is still unclear and needs further study.

CONCLUSION

In brief, the complete ORF sequences of MrNP1 and MrNP2 in *M. rosenbergii* have been cloned and confirmed as members of the neuroparsin family. The expression patterns of MrNP1 and MrNP2 were different, which indicate different regulatory roles. RNAi and overexpression experiments were carried out to identify the roles of MrNP1 and MrNP2 in the development of vitellogenin within *M. rosenbergii* in the early stage of the ovary. MrNP1 and MrNP2 may act as stimulators of early ovarian development *via* promoting the expression of the MrVg gene, MrVgR gene, and MrCyclinB gene. The current study expands our understanding of the regulatory mechanism of ovary in *M. rosenbergii* and provides valuable information for regulating ovarian maturation in the aquaculture of *M. rosenbergii*. However, the differences with regard to regulatory mechanisms observed for MrNP1 and MrNP2 in *M. rosenbergii* need further exploration and will help to better understand the developmental mechanism of the ovary in crustaceans.

DATA AVAILABILITY

The datasets presented in this study can be found in online repositories. The names of the repository/repositories and accession number(s) can be found in the article/**Supplementary Material**.

AUTHOR CONTRIBUTIONS

Conceptualization, SC; methodology, SC; software, CW; validation, LS and WW; formal analysis, CA, SC, and WW; investigation, CA; resources, CW; writing—original draft preparation, CA, CW; writing—review and editing, CW and SC; visualization, LS; supervision, WW, LS; project administration, SC; funding acquisition, SC. All authors contributed to the article and approved the submitted version.

FUNDING

This research was funded by the Guangdong Provisional Research Grant (#2014B020202014).

SUPPLEMENTARY MATERIAL

The Supplementary Material for this article can be found online at: https://www.frontiersin.org/articles/10.3389/fmars.2022.917274/full#supplementary-material

REFERENCES

Andrew, E. C. (2020). Identification of Putative Neuropeptidergic Signaling Systems in the Spiny Lobster, *Panulirus Argus*. *Invertebrate Neurosci.* 20 (1), 1–12. doi: 10.1007/s10158-020-0235-9

Badisco, L., Claeys, I., Loy, T. V., Hiel, M. V., Franssens, V., Simonet, G., et al. (2007). Neuroparsins, a Family of Conserved Arthropod Neuropeptides. *Gen. Comp. Endocrinol.* 153, 64–71.

Badisco, L., Marchal, E., Wielendaele, P. V., Verlinden, H., Vleugels, R. and Broeck, J. V. (2011). RNA Interference of Insulin-Related Peptide and Neuroparsins Affects Vitellogenesis in the Desert Locust *Schistocerca Gregaria*. *Peptides* 32, 573–580. doi: 10.1016/j.peptides.2010.11.008

Bao, C., Yang, Y., Huang, H. and Ye, H. (2015). Neuropeptides in the Cerebral Ganglia of the Mud Crab, *S. Paramamosain*: Transcriptomic Analysis and Expression Profiles During Vitellogenesis. *Sci. Rep.* 5, 17055. doi: 10.1038/srep17055

Basu, D., Navneet, A. K., Dasgupta, S. and Bhattacharya, S. (2004). Cdc2-Cyclin B-Induced G2 to M Transition in Perch Oocytes is Dependent on Cdc25. *Biol. Reprod.* 71, 894–900. doi: 10.1095/biolreprod.104.029611

Brown, M. ,. R., Graf, R., Swiderk, K. M., Fendley, D., Stracker, T. H., Champagne, D. E., et al. (1998). Identification of a Steroidogenic Neurohormone in Female Mosquitoes. *J. Bio. Chem.* 273, 3967–3971. doi: 10.1074/jbc.273.7.3967

Chang, C. F. and Shih, T. W. (1995). Reproductive Cycle of Ovarian Development and Vitellogenin Profies in the Freshwater Prawns, *Macrobrachium Rosenbergii*. *Invertebr. Reprod. Dev.* 27, 11–20. doi: 10.1080/07924259.1995.9672429

Chen, J. S. and Raikhel, A. S. (1996). Subunit Cleavage of Mosquito Pro-Vitellogenin by a Subtilisin-Like Convertase. *Proc. Natl. Acad. Sci. U.S.A.* 93, 6186–6190.

Ching, F. C. and Tung, W. S. (2011). Reproductive Cycle of Ovarian Development and Vitellogenin Profiles in the Freshwater Prawns, *Macrobrachium Rosenbergii*. *Invertebr. Reprod. Dev.* 27, 11–20. doi: 10.1080/07924259.1995.9672429

Christie, A. E., Chi, M., Lameyer, T. J., Pascual, M. G., Shea, D. N., Stanhope, M. E., et al. (2015). Neuropeptidergic Signaling in the American Lobster *Homarus Americanus*: New Insights From High-Throughput Nucleotide Sequencing. *PLos One* 10, e0145964. doi: 10.1371/journal.pone.0145964

Chung, J. S., Zmora, N., Katayama, H. and Tsutsui, N. (2010). Crustacean Hyperglycemic Hormone (CHH) Neuropeptides Family: Functions, Titer, and Binding to Target Tissues. *Gen. Comp. Endocrinol.* 166, 447–454. doi: 10.1016/j.ygcen.2009.12.011

Claeys, I., Breugelmans, B., Simonet, G., Franssens, V. and Broeck, J. V. (2006). Regulation of *Schistocerca Gregaria* Neuroparsin Transcript Levels by Juvenile Hormone and 20-Hydroxyecdysone. *Arch. Insect Biochem. Physiol.* 62, 107–115. doi: 10.1002/arch.20127

Claeys, G., Simonet, B., Breugelmans, S., Van, S. V., Franssens, F., Sas, A., et al. (2010). Quantitative Real-Time RT-PCR Analysis in Desert Locusts Reveals Phase Dependent Differences in Neuroparsin Transcript Levels. *Insect Mol. Biol.* 14, 415–422. doi: 10.1111/j.1365-2583.2005.00572.x

Draetta, G., Luca, F., Westendorf, J., Brizuela, L., Ruderman, J. and Beach, D. (1989). Cdc2 Protein Kinase I Complexed With Both Cyclin A and B: Evidence for Proteolytic Inactivation of MPF. *Cell* 56, 829–838. doi: 10.1016/0092-8674(89)90687-9

Fang, J. J. and Qiu, G. F. (2009). Molecular Cloning of Cyclin B Transcript With an Unusually Long 3' Untranslation Region and its Expression Analysis During Oogenesis in the Chinese Mitten Crab, *Eriocheir Sinensis*. *Mol. Bio. Rep.* 36, 1521–1529. doi: 10.1007/s11033-008-9346-9

Feng, H., Dong, Y. T., Liu, X. and Qiu, G. F. (2020). Cyclin B Protein Undergoes Increased Expression and Nuclear Relocation During Oocytes Meiotic Maturation of the Freshwater Prawn *Macrobrachium Rosenberg*ii and the Chinese Mitten Crab *Eriocheir Sinensis*. *Gene* 758, 144955. doi: 10.1016/j.gene.2020.144955

Fournier, B., Herault, J. P. and Proux, J. (1987). Antidiuretic Factor From the Nervous Corpora Cardiaca of the Migratory Locust: Improvement of an Existing *In Vitro* Bioassay. *Gen. Com. Endocrinol.* 68, 49–56. doi: 10.1016/0016-6480(87)90059-1

Girardie, J., Boureme, D., Couillaud, F., Tamarelle, M. and Girardie, A. (1987). Anti-Juvenile Effect of Neuroparsin a, a Neuroprotein Isolated From Locust Corpora Cardiaca. *Insect Biochem.* 17, 977–983. doi: 10.1016/0020-1790(87)90106-5

Girardie, J., Girardie, A., Huet, J. C. and Pernollet, J. C. (1989). Amino Acid Sequence of Locust Neuroparsins. *FEBS Lett.* 245, 4–8. doi: 10.1016/0014-5793(89)80179-6

Girardie, J., Huet, J. C., Atay-Kadiri, Z., Ettaouil, S., Delbecque, J. P., Fournier, B., et al. (1998). Isolation, Sequence Determination, Physical and Physiological Characterization of the Neuroparsins and Ovary Maturing Parsins of *Schistocerca Gregaria*. *Insect Biochem. Mol. Biol.* 28, 641–650. doi: 10.1016/s0965-1748(98)00053-8

Gulia-Nuss, M., Eum, J. H., Strand, M. R. and Brown, M. R. (2012). Ovary Ecdysteroidogenic Hormone Activates Egg Maturation in the Mosquito *Georgecraigius Atropalpus* After Adult Eclosion or a Blood Meal. *J. Exp. Biol.* 215, 3758–3767. doi: 10.1242/jeb.074617

Kleijn, D. and Herp, F. V. (1998). Involvement of the Hyperglycemic Neurohormone Family in the Control of Reproduction in Decapod Crustaceans. *Inverterb. Reprod. Dev.* 33, 263–272. doi: 10.1080/07924259.1998.9652637

Kyei, A. B., Wang, C. G., Sun, C. B., Wang, W. and Chan, S. (2020). Crustacean Neuroparsins-a Mini-Review. *Gene* 732, 144361. doi: 10.1016/j.gene.2020.144361

Li, Y. Y. (2012). Study on Site of Vitellogenin Synthesis in the Shrimp *Litopenaeus Vannamei* and *Macrobrachium Rosenbergii*. *J. Fisheries China*. 36, 1025-1027. doi: 10.3724/SP.J.1231.2012.27893

Liu, J., Liu, A., Liu, F., Huang, H. and Ye, H. (2020). Role of Neuroparsin 1 in Vitellogenesis in the Mud Crab, *S Paramamosain*. *Gen. Com. Endocrinol.* 285, 113248.

Ma, M., Gard, A. L., Xiang, F., Wang, J., Davoodian, N., Lenz, P. H., et al. (2010). Combining in Silico Transcriptome Mining and Biological Mass Spectrometry for Neuropeptide Discovery in the Pacific White Shrimp *Litopenaeus Vannamei*. *Peptides* 31, 27–43. doi: 10.1016/j.peptides.2009.10.007

Marco, H. G., Anders, L. and Gerad, G. (2014). cDNA Cloning and Transcript Distribution of Two Novel Members of the Neuroparsin Peptide Family in a Hemipteran Insect (*Nezara Viridula*) and a Decapod Crustacean (*Jasus Lalandii*). *Peptides* 53, 97–105. doi: 10.1016/j.peptides.2013.10.013

Matsumoto, S., Brown, M. R., Suzuki, A. and Lea, A. O. (1989). Isolation and Characterization of Ovarian Ecdysteroidogenic Hormones From the Mosquito, *Aedes Aegypti*. *Insect Biochem.* 19, 651–656. doi: 10.1016/0020-1790(89)90100-5

Meusy, J. J. (1980). Vitellogenin, the Extraovarian Precursor of the Protein Yolk in Crustacea: A Review. *Reprod. Nutr. Dev.* 20, 1–21. doi: 10.1051/rnd:19800101

Moreau, R., Gourdoux, L. and Girardie, J. (1988). Neuroparsin: A New Energetic Neurohormone in the African Locust. *Arch. Insect. Biochem. Physiol.* 8, 135–145. doi: 10.1002/arch.940080207

Nogaro, M., Radallah, D., Guillon, G. and Fournier, B. (1995). Hplc Analysis of Inositol Phosphate Isomers Induced by Neuroparsin in Rectal Epithelial Cells of the African Locust: Role of External Calcium. *Insect Biochem. Mol. Biol.* 25, 559–567. doi: 10.1016/0965-1748(94)00094-X

Okano-Uchida, T., Sekiai, T., Lee, K. S., Okumura, E., Tachibana, K. and Kishimoto, T. (1998). *In Vivo* Regulation of Cyclin A/Cdc2 and Cyclin B/Cdc2 Through Meiotic and Early Cleavage Cycles in Starfish. *Dev. Biol.* 197, 39–53. doi: 10.1006/dbio.1998.8881

Okuno, A., Yang, W. J., Jayasankar, V., Saido-Sakanaka, H., Huong, D. T., Jasmani, S., et al. (2002). Deduced Primary Structure of Vitellogenin in the Giant Freshwater Prawn, *Macrobrachium Rosenbergii*, and Yolk Processing During Ovarian Maturation. *J. Exp. Zool.* 292, 417–429. doi: 10.1002/jez.10083

Phinyo, M., Visudtiphole, V., Roytrakul, S., Phaonakrop, N., Jarayabhand, P. and Klinbunga, S. (2013). Characterization and Expression of Cell Division Cycle 2 (Cdc2) mRNA and Protein During Ovarian Development of the Giant Tiger Shrimp *Penaeus Monodon*. *Gen. Comp. Endocrinol.* 193, 103–111. doi: 10.1016/j.ygcen.2013.07.012

Predel, R., Neupert, S., Derst, C., Reinhardt, K. and Wegener, C. (2018). Neuropeptidomics of the Bed Bug *Cimex Lectularius*. *J. Proteome. Res.* 17, 440–454. doi: 10.1021/acs.jproteome.7b00630

Qiao, H., Xiong, Y., Jiang, S., Zhang, W. and Fu, H. (2020). Three Neuroparsin Genes From Oriental River Prawn, *Macrobrachium Nipponense*, Involved in Ovary Maturation. *Biotech* 10, 537. doi: 10.1007/s13205-020-02531-8

Qiu, G.-F., Ramachandra, R. and Yao, J. B. (2008). Molecular Characterization and Expression Profiles of Cyclin B1, B2 and Cdc2 Kinase During Oogenesis and Spermatogenesis in Rainbow Trout (*Oncorhynchus Mykiss*). *Anim. Reprod. science.* 105, 209–225. doi: 10.1016/j.anireprosci.2007.03.005

Riehle, M. A., Garczynski, S. F., Crim, J. W., Hill, C. A. and Brown, M. R. (2002). Neuropeptides and Peptide Hormones in *Anopheles Gambiae*. *Science* 298, 172–175. doi: 10.1126/science.1076827

Tanaka, Y. (2021). "Neuroparsin-ScienceDirect," in *Handbook of Hormones*, (Amsterdam, Netherlands: Elsevier) 2nd ed., vol. 2. , 761–763. doi: 10.1016/B978-0-12-820649-2.00204-7

Tiu, S. H., Benzie, J. and Chan, S. M. (2008). From Hepatopancreas to Ovary: Molecular Characterization of a Shrimp Vitellogenin Receptor Involved in the Processing of Vitellogenin. *Biol. Reprod.* 79, 66–74. doi: 10.1095/biolreprod.107.066258

Tiu, S. H. K. and Chan, S. M. (2007). The Use of Recombinant Protein and RNA Interference Approaches to Study the Reproductive Functions of a Gonad-Stimulating Hormone From the Shrimp *Metapenaeus Ensis*. *FEBS J.* 274, 4385–4395. doi: 10.1111/j.1742-4658.2007.05968.x

Tomy, S., Saikrithi, P., James, N., Balasubramanian, C. P., Panigrahi, A., Otta, S. K., et al. (2016). Serotonin Induced Changes in the Expression of Ovarian Gene Network in the Indian White Shrimp, *Penaeus Indicus*. *Aquaculture* 452, 239–246. doi: 10.1016/j.aquaculture.2015.11.003

Tsutsui, N., Kobayashi, Y., Izumikawa, K., et al. (2020). Transcriptomic Analysis of the Kuruma Prawn *Marsupenaeus Japonicus* Reveals Possible Peripheral Regulation of the Ovary. *Front. Endocrinol.* 11. doi: 10.3389/fendo.2020.0054

Veenstra, J. A. (2016). Similarities Between Decapod and Insect Neuropeptidomes. *PeerJ* 4, e2043. doi: 10.7717/peerj.2043

Xie, J., Wen, J. J., Chen, B. and Gui, J. F. (2001). Differential Gene Expression in Fully-Grown Oocytess Between Gynogenetic and Gonochoristic Crucian Carps. *Gene* 271, 109–116. doi: 10.1016/S0378-1119(01)00491-7

Yang, S. P., He, J. G., Sun, C. B. and Chan, S. F. (2014). Characterization of the Shrimp Neuroparsin (MeNPLP): RNAi Silencing Resulted in Inhibition of Vitellogenesis. *FEBS Open Bio.* 4, 976–986. doi: 10.1016/j.fob.2014.09.005

Yang, W. J., Ohira, T., Tsutsui, N., Subramoniam, T. and Wilder, M. N. (2000). Determination of Amino Acid Sequence and Site of mRNA Expression of Four Vitellins in the Giant Freshwater Prawn, *Macrobrachium Rosenbergii*. *J. Exp. Zool.* 287, 413–422.

Conflict of Interest: The authors declare that the research was conducted in the absence of any commercial or financial relationships that could be construed as a potential conflict of interest.

Publisher's Note: All claims expressed in this article are solely those of the authors and do not necessarily represent those of their affiliated organizations, or those of the publisher, the editors and the reviewers. Any product that may be evaluated in this article, or claim that may be made by its manufacturer, is not guaranteed or endorsed by the publisher.

frontiers | Frontiers in Marine Science

TYPE Original Research
PUBLISHED 02 August 2022
DOI 10.3389/fmars.2022.948105

OPEN ACCESS

EDITED BY
Naoaki Tsutsui,
Mie University, Japan

REVIEWED BY
Jude Juventus Aweya,
Jimei University, China
Haibo Yu,
Northwest A&F University, China

*CORRESPONDENCE
Ting Chen
chan1010@scsio.ac.cn
Xugan Wu
xgwu@shou.edu.cn

†These authors have contributed equally to this work

SPECIALTY SECTION
This article was submitted to Aquatic Physiology, a section of the journal Frontiers in Marine Science

RECEIVED 19 May 2022
ACCEPTED 11 July 2022
PUBLISHED 02 August 2022

CITATION
Li Z, Zhou M, Ruan Y, Chen X, Ren C, Yang H, Zhang X, Liu J, Li H, Zhang L, Hu C, Chen T and Wu X (2022) Transcriptomic Analysis Reveals Yolk Accumulation Mechanism From the Hepatopancreas to Ovary in the Pacific White Shrimp *Litopenaeus vannamei*. *Front. Mar. Sci.* 9:948105. doi: 10.3389/fmars.2022.948105

Transcriptomic analysis reveals yolk accumulation mechanism from the hepatopancreas to ovary in the pacific white shrimp *Litopenaeus vannamei*

Zhi Li[1†], Minyu Zhou[1†], Yao Ruan[2], Xiaoli Chen[3], Chunhua Ren[2], Hao Yang[4], Xin Zhang[2], Jinshang Liu[5], Huo Li[5], Lvping Zhang[2], Chaoqun Hu[2], Ting Chen[2*] and Xugan Wu[1*]

[1]Key Laboratory of Exploration and Utilization of Aquatic Genetic Resources, College of Fisheries and Life Science, Shanghai Ocean University, Shanghai, China, [2]Chinese Academy of Sciences Key Laboratory of Tropical Marine Bio-resources and Ecology (LMB), South China Sea Institute of Oceanology, Chinese Academy of Sciences, Guangzhou, China, [3]Guangdong Research Center on Reproductive Control and Breeding Technology of Indigenous Valuable Fish Species, Fisheries College, Guangdong Ocean University, Zhanjiang, China, [4]Laboratory of Zoological Systematics and Application of Hebei Province, College of Life Sciences, Hebei University, Baoding, China, [5]Jinyang Biotechnology Co. Ltd., Maoming, China

The Pacific white shrimp *Litopenaeus vannamei* is an economically important penaeid species worldwide. Under farming conditions, the full ovarian maturation of *L. vannamei* generally depends on the combination of artificial ablation of unilateral eyestalk and feeding high-quality natural diets, suggesting that nutrient accumulation is important to ovarian maturation. In this study, we aimed to investigate the gene expression related to nutritional accumulation in *L. vannamei* during ovarian development by transcriptomic analysis. A total of 52.45 Gb of high-quality transcriptome data were obtained from 8 samples from the hepatopancreas and ovaries from shrimp in gonadal developmental stages I-IV. A total of 23,149 expressed genes were detected, of which 19,852 were known genes and 3,297 were novel genes. Our study found that genes related to amino acid, carbohydrate and lipid metabolism were expressed at higher levels in the hepatopancreas than in the ovary. The genes for most lipoproteins and their receptors were predominantly expressed in the hepatopancreas, while vitellogenin receptor (*VgR*) was specifically expressed in the ovary. Moreover, two vitellogenin (*Vg*) genes were identified, in which one was specifically expressed in the hepatopancreas and defined as *Hp-Vg*, and the other was specifically expressed in the ovary and defined as *Ov-Vg*. In addition, genes related to carotenoid metabolism were enriched in the hepatopancreas. This study provides solid evidence that the hepatopancreas is the major exogenous vitellogenesis site for ovarian maturation of *L. vannamei*. Two distinct *Vg* genes perform exogenous and endogenous vitellogenesis in the hepatopancreas and ovary in *L. vannamei*, respectively.

The results of this study also presented some new insights for understanding the nutritional dynamics from the hepatopancreas to ovary during ovarian maturation in penaeids.

KEYWORDS

transcriptome, *Litopenaeus vannamei*, hepatopancreas, ovarian maturation, vitellogenesis, carotenoid

Introduction

The Pacific white shrimp Litopenaeus vannamei (Crustacea: Decapoda) is the most economically important shrimp worldwide. Under artificial conditions, however, domesticated L. vannamei generally cannot undergo full maturation without eyestalk ablation (Ceballos-Vázquez et al., 2010). After artificial ablation of unilateral eyestalk combined with feeding high-quality natural diets, female L. vannamei can undergo ovarian maturation quickly and spawn within 3-5 days post-eyestalk ablation (Nagaraju, 2011; Chen et al., 2018). Similar to other oviparous animals, the ovarian development of crustaceans is delicately divided into two processes, namely, oogenesis and vitellogenesis (Tsukimura, 2001). During vitellogenesis, the nutrients that mainly comprise proteins and lipids accumulate rapidly in oocytes (Wouters et al., 2001; Zmora et al., 2007) for the subsequent energy consumption of embryonic development (Heras et al., 2000). In shrimp, vitellin (Vn) is the major yolk protein component in mature oocytes, accounting for 60-90% of the total ovarian protein (Quackenbush, 2001). Structurally, Vn is a kind of apolipoprotein that binds to lipids to form lipoproteins (Avarre et al., 2007). Vn is encoded by its precursor gene vitellogenin (Vg) and is processed into mature protein by posttranslation proteolytic cleavage. In some shrimp species, the concentration of Vg could predict gonadal maturity status in adult females (Arcos et al., 2011).

Vitellogenesis is generally considered to be conducted in two ways, namely, endogenous and exogenous. The original sites for Vg production are distant in different oviparous animals: In birds (Tian et al., 2010) and fishes (Hiramatsu et al., 2015), Vg is synthesized in the liver; in insects, Vg is generated in the fat body (Tufail and Takeda, 2008); and in mollusks, Vg is consistently produced in the ovary (Ni et al., 2014). In crustaceans, the major sites for Vg production vary in different species, which have been reported from the hepatopancreas and ovaries (Mak et al., 2005; Jia et al., 2013). In some species of decapods, such as the mud crab Scylla paramamosain (Gong et al., 2015) and giant river prawn Macrobrachium rosenbergii, the ovary is only known as a site for Vg uptake and accumulation during ovarian development, synthesizing only small amounts of Vg (Tiu et al., 2006). In the ridgeback prawn Sicyonia ingentis, kuruma shrimp P. japonicus and swimming crab Callinectes sapidus (Zmora et al., 2009; Thongda et al., 2015), Vg synthesis occurs in both the hepatopancreas and ovaries. In L. vannamei, the expression of Vg mRNA was first detected in either the hepatopancreas or ovary (Tseng et al., 2002). The first L. vannamei Vg cDNA was identified from the ovary (Raviv et al., 2006), and a further study demonstrated that three Vg isoforms were differentially expressed in the hepatopancreas and ovary (Hoeger and Schenk, 2020). Thus, the regulation of Vg transcripts has also been investigated in the ovary (Tsutsui et al., 2013; Kang et al., 2014; Bae et al., 2017) and hepatopancreas (Chen et al., 2014; Luo et al., 2015).

In addition to yolk proteins, other nutrients, such as lipids and carotenoids, also accumulate in the ovaries during the gonadal development of shrimp (Chen et al., 2014; Luo et al., 2015). Carotenoids are considered to be essential nutrients for optimal nutritional requirements in shrimp feed (Lin et al., 2015). Naturally, carotenoids are produced by photosynthetic plants and bacteria, and like most animals, crustaceans do not have a capability to produce carotenoids de novo and have to acquire carotenoids by diet (Chen et al., 2014; Luo et al., 2015). The presence of various free and esterified forms of carotenoids, mainly astaxanthin (Axn) (Lee et al., 2010), was reported in all wild and cultured crustacean species. The esterification of Axn with specific fatty acids and the presence of carotenoid isoforms can greatly increase the complexity of their interactions with other biomolecules (Britton, 1995). Previous studies have shown that some crustaceans have a certain ability to convert β-carotene to Axn in some organs (Teruhisa et al., 1973; Wade et al., 2017). However, the conversion mechanism and tissue deposition of carotenoids remain unclear during the ovarian development cycle of L. vannamei.

To illustrate the nutritional dynamics from the hepatoscreas to ovaries and the nutrient deposition of the ovaries and hepatoscreas in the ovarian development cycle of crustaceans, we will use transcriptomes to analyze the expression of relevant genes, which will facilitate the improvement of artificial breeding and sustainable aquaculture of this economically valuable species.

Materials and methods

Animals and artificial induction of ovarian maturation

Female Pacific white shrimp (L. vannamei) were cultured at Jinyang Biotechnology Co. Ltd., Maoming, Guangdong, China. The shrimp were maintained in artificial seawater [pH 8.2 and 30 parts per thousand (ppt)] at 28°C and fed every morning with a normal shrimp diet. Female shrimp grown until body weights of 47.2±1.5 g and body lengths of 18.1±0.3 cm were used for analysis of ovarian development. At 7 days prior to artificially induced maturation, the shrimp were fed fresh clam worms, squid and oysters for nutritional reinforcement (Figure 1A). The animal experiments were conducted in accordance with the guidelines and approval of the Ethics Committees of South China Sea Institute of Oceanology, Chinese Academy of Sciences.

Sample collection and RNA extraction

Ovaries and hepatopancreas samples from female shrimp were collected from 1 to 6 days after unilateral eyestalk ablation for stages I, II, III and IV, respectively (Figure 1B). Ovarian maturation stages (stage I–IV) were assigned after histological processing of the anterior end of ovarian explants with the number 2–9 lobes (Liaaen-Jensen, 1997; Bae et al., 2017). Stage I ovaries are mainly comprised of oogonia and previtellogenic oocytes; stage II ovaries primarily comprise previtellogenic oocytes and endogenous vitellogenic oocytes; stage III ovaries process a large number of oocytes developing from endogenous vitellogenetic oocytes to exogenous vitellogenetic oocytes; and exogenous vitellogenic oocytes and mature oocytes predominate in stage IV ovaries (Figure 1D). The gonadosomatic index (GSI) of each shrimp was calculated as a percentage of ovary weight to body weight, and the GSIs for shrimp in stages I, II, III and IV were 0.5–1.0%, 1.0–2.5%, 2.5–5.0% and >5.0%, respectively

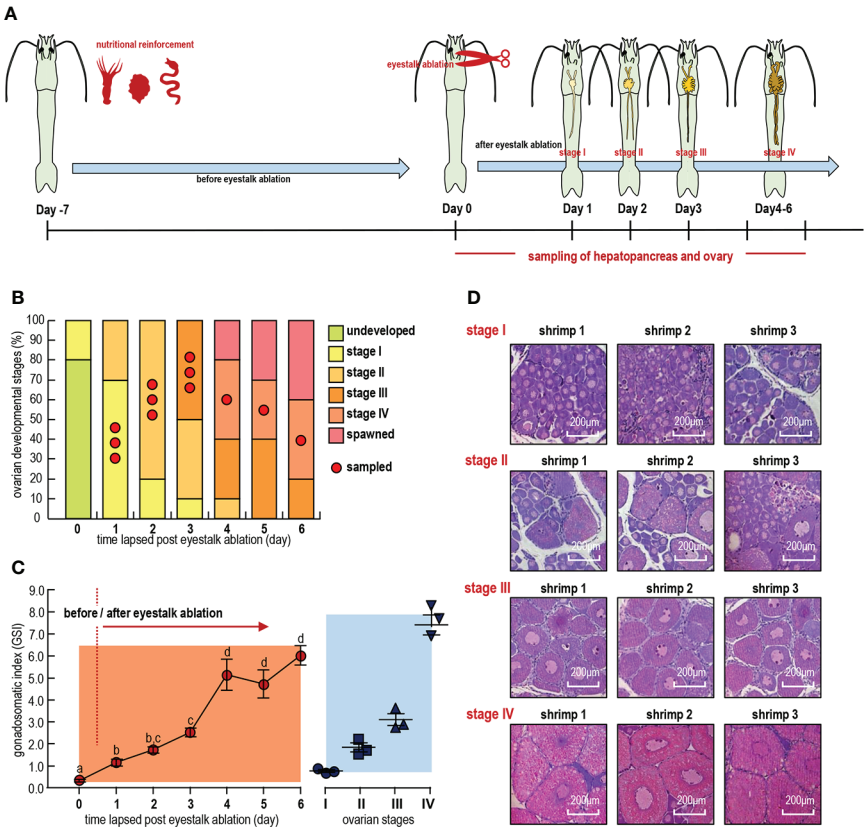

FIGURE 1
(A) Representative ovaries at different time points. **(B)** Distribution of samples over ovarian developmental stages. **(C)** Changes in gonadosomatic index (GSI) with days and ovarian developmental stages after eyestalk removal. Error bars represent standard derivations. Different letters indicate significant differences between time points of the same feed group (n = 3, mean ± sem, $P < 0.05$, ANOVA Duncan test). **(D)** HE staining of the ovaries and liver and pancreas. Stage: Four periods of ovarian development.

(Figure 1C). All samples were frozen immediately in liquid nitrogen after dissection, and total RNA was extracted by using TRIzol Reagent (Invitrogen, Carlsbad, CA, USA).

Library construction and sequencing

The RNA integrity value (RIN) was checked by an Agilent 2100 Bianalyzer (Agilent, USA), and RNA-seq libraries were prepared following the standard Illumina protocols by the Beijing Genomics Institute (Beijing Genomics Institute, Beijing, China). In brief, mRNA equally contributed from 3 individuals was enriched by oligo-dT selection. Double-stranded cDNAs were synthesized using the fragmented mRNA as templates with random hexamer primers. The short fragments were connected with adapters, and suitable fragments were selected for PCR amplification. Then, the library was sequenced using an Illumina HiSeq 6000 (Illumina Inc., San Diego, CA, USA) in BGI.

Transcriptome assembly and annotation

The raw sequencing data were first filtered to remove the noise reads that contained additional low-quality, adaptor-polluted and high content of unknown base (N) reads by fastp software. Transcriptome assembly was performed based on the sequence of the L. vannamei genome (GenBank GCA_003789085.1) as a reference (Zhang et al., 2019). Clean data (reads) were compared with the reference genome using TopHat2 (http://tophat.cbcb.umd.edu/) to obtain the mapped data (reads) for subsequent analysis.

Functional annotation of the transcriptome was performed with 6 functional databases, including the nonredundant protein sequence database (NR), Swiss-Prot, Pfam, EggNOG (Clusters of Orthologous Groups of proteins), Gene Ontology (GO) and Kyoto Encyclopedia of Genes and Genomes (KEGG), as described previously (Jinxia et al., 2015).

Identification and validation of differentially expressed genes

Using RNA-Seq by Expectation-Maximization (RSEM), the read counts of each sample gene/transcript were obtained using the results of comparison to the genome as well as the genome annotation file. They were then converted to Fragments Per Kilobase of exon model per Million mapped fragments (FPKM), which in turn yielded normalized gene/transcript expression levels. After obtaining the number of read counts of genes/transcripts, differential expression analysis was performed on multiple samples (≥2) to identify differentially expressed genes/transcripts between samples and to investigate the function of differentially expressed genes/transcripts. Differentially expressed genes (DEGs) were detected with PossionDis based on the Poisson distribution, and genes with a fold change≥2.00 and a false discovery rate (FDR) ≤0.001 were considered significant DEGs. For pathway enrichment analysis, all DEGs were annotated using GO and KEGG databases.

Measurement of mRNA levels for lipoprotein transportation and carotenoid synthesis-related genes

Eight candidate genes from the apolipoprotein and carotenoid metabolic pathways were selected for fluorescent quantitative PCR validation. Total RNA was extracted from the ovaries and hepatopancreas of shrimp at four stages of ovarian development using TRIzol™ reagent (Invitrogen, Carlsbad, CA, USA), and RNA samples were reverse transcribed using Evo M-MLV RT Premix for RT–qPCR AG11706 (ACCURATE BIOTECHNOLOGY, Hunan, China), which allows for the amplification of cDNA from total RNA to amplify cDNA without isolating mRNA. Oligonucleotide primers (Table 1) specific to eight genes and the housekeeping gene (β-actin) were designed with Primer Premier 5.0 software and synthesized by Sangon Biotech (Shanghai) Co., Ltd. Each pair of primers was examined by PCR, which was conducted using SYBR Premix Ex Taq II (Takara, Kyoto, Japan) to ensure their availability for RT–qPCR. The PCR program for every target gene and β-actin was 95°C for 30 s, followed by 40 cycles of 95°C for 10 s and 60°C for 30 s. RT-qPCR was carried out using a SYBR® Green Premix Pro Taq HS RT-qPCR Kit AG11701 (ACCURATE BIOLOGY, China), performed with a Thermal® Cycler Dice Real Time System III (TaKaRa) in final volumes of 20 μL, each containing 1 μL of cDNA, 10 μL SYBR® Green Premix Pro Taq HS RT-qPCR Kit AG11701 (ACCURATE BIOLOGY, China), 0.5 μL each of forwards and reverse primers (10 μM), and 8 μL sterile water. Each sample was analyzed in triplicate along with the internal control gene. The target gene/β-actin mRNA ratio was calculated using the formula $2^{-\Delta Ct}$, and the raw data were simply transformed into the selected gene-to-actin Ct ratio for statistical analysis.

Data transformation and statistical analysis

For RT-qPCR, the expression levels of target genes were routinely normalized as a ratio of β-actin mRNA detected in the same sample. For RT-qPCR and GSI measurements, the data expressed as the mean±SE (standard error) were exported using TaKaRa DiceReal Time software and analyzed by using Student's t test or one-way ANOVA followed by Fisher's least significant difference (LSD) test.

TABLE 1 Sequences of qPCR primers.

Gene ID	Forward primer sequences (5'-3')	Reverse primer sequences (5'-3')
differentially expressed genes(DEGs)		
low-density lipoprotein receptor-related protein 1 (LDLR)	GACCTGGGCAGATACATCC	CTTCGCCTCGACCACAAAC
beta-1,3-glucan-binding protein(BGBP)	CGAGAACGGACAAGAAGTG	CAGCATAGAAGCCATCAGG
beta, beta-carotene 15,15'-dioxygenase(BCMO1)	AGAAGATGACGGTGTAGTGTT	AAAGTATGGACGGACCCTG
vitellogenin receptor (VgR)	TGCTGGCATAGCTTTGATT	CTCGTTAGGACGGTTGGGT
vitellogenin (Vg)(O)	TTGGGATGCCGATAATGCT	CCAGTTTGGCGTGGTAAGG
vitellogenin (Vg)(H)	TCAGGCTTGACGACGATG	CTTGGCTATGTCTGGTGTTG
cytochrome P450 9e2-like, transcript variant X1(9E2)	TTTGCTGCCTTTCAGTTGG	TTCATGCTGGCCCTGTTCT
cytochrome P450 3A13-like(3A13)	CCTCAAGTCGGCTCAAAGTC	CGCGATGTAGAAGCTGGTTAA
cytochrome P450 3A1-like, transcript variant X1(3A1)	TTCCACGAGCCATTGTTAT	TTGAGGCAGAAGGAGACGA
β-actin	GCATCCACGAGACCACTTACA	CTCCTGCTTGCTGATCCACATC

Results

Effect of eyestalk ablation and nutritional reinforcement on ovarian maturation

Unilateral eyestalk ablation (UEA) and nutritional enrichment were applied to artificially induce ovarian maturation in female L. vannamei (Figure 1A). Based on our histological results (Figure 1D), the ovaries were found to develop to stage I at 0–3 days (Ov-I, Hp-I), to stage II at 1–4 days (Ov-II, Hp-II), to stage III at 3–6 days (Ov-III, Hp-III) and to stage IV at 4–6 days (Ov-IV, Hp-IV) and to spawn at 4–6 days after these administrations (Figure 1B). In this case, the mean gonadosomatic index (GSI) of the ovaries increased from 1.15 to 6.03 from day 0 to day 6 (Figure 1C), and the GSIs for stages I, II, III and IV were 0.82, 1.95, 3.29 and 7.11, respectively (Figure 1D). The GSI increasing pattern indicated a large amount of nutrient accumulation in ovaries during the exogenous vitellogenesis period from stage III to stage IV.

Quality control, trimming, de novo assembly and mapping

After filtering out low-quality reads using Illumina HiSeq 6000, fastp and SeqPrep software, we obtained data for shrimp ovaries and hepatopancreas in four stages. For the ovarian samples, 44,267,292, 44,175,442, 44,359,992 and 44,208,868 clean reads were generated for stages I, II, III and IV, respectively, and for the hepatopancreas samples, 44,630,016, 40,197,512, 44,540,914 and 44,043,748 clean reads were generated for stage I and for stages I, II, III and IV, respectively (Table 2). All sequence reads are deposited in the National Center for Biotechnology Information (NCBI) sequence read archive (SUB10677615). The Q20 values of all samples were higher than 95% by FastQC26 analysis, indicating high sequencing quality (Reference Gene Source: Penaeus_vannamei; GenBank GCA_003789085.1).

Clean reads were pooled and assembled into nonredundant transcripts with a reference genome, and a total of 52192 transcripts were generated with an average length of more than 1800 bp (Table 3).

Comparison of raw and clean data (reads) after quality control with the reference genome using HISAT2 revealed unique mappings of 29,617,891 (66.91%), 28,914,804 (65.45%), 29,535,553 (66.58%) and 29,529,228 (66.79%) for the four ovarian stages. The unique mapping of the four stages of the hepatopancreas reached 32,624,482 (73.1%), 28,488,888 (70.87%), 30,954,251 (69.5%) and 33,394,407 (75.82%),

TABLE 2 Quality control and data statistics for clean reads.

Sample	Read reads	Raw bases	Q20(%)	GC%
HP-1	44630854	6694628100	98.65	51.03
HP-2	40202508	6030376200	98.88	51.08
HP-3	44541714	6681257100	98.7	49.45
HP-4	44045422	6606813300	98.62	48.29
OV-1	44268076	6640211400	98.62	49.39
OV-2	44176264	6626439600	98.65	48.41
OV-3	44360814	6654122100	98.66	47.91
OV-4	44209682	6631452300	98.64	47.78

TABLE 3 Length distribution of transcripts.

Length	Number
0~200	2942
201~400	3290
401~600	4756
601~800	4617
801~1000	4067
1001~1200	3761
1201~1400	3276
1401~1600	2884
1601~1800	2594
>1800	20005
total	52192

respectively (Table 4). The NR database annotated with the most functional information on transcripts.

Functional annotation and classification of genes

All genes were annotated using BLASTx with the NCBI nonredundant (Nr), KEGG, SWISS-PROT, GO, COG and PFAM protein databases. Annotation information was retrieved from proteins with the highest sequence similarity. In this study, 36,025 (90.9%) genes were annotated, and among them, 19,214, 9,695, 12,927, 14,095, 14,082 and 14,077 genes were annotated in the Nr, KEGG, SWISS-PROT, GO, COG, and PFAM databases, respectively (Figure 2A). The Venn diagram shows the annotation of expressed genes across databases, with 7,530 genes annotated to multiple libraries simultaneously, in addition to 2,540 genes annotated to the NR database. (Figure 2B).

Based on the Gene Ontology (GO) database, the genes were annotated and assigned to three categories. Within the biological process category, "cellular process" (2,502 genes) and "metabolic process" (1,855 genes) were the dominant groups. Within the cellular component category, "membrane part" (2,705 genes) and "cell part" (2,375 genes) were the most abundant groups. Within the molecular function category, "binding" (3,396 genes) and "catalytic activity" (3,143 genes) were the dominant groups (Figure 2C). Based on the Kyoto Encyclopedia of Genes and Genomes (KEGG) database, a total of 15,902 genes were mapped to six specific pathways, including cellular processes, environmental information processing, genetic information processing, metabolism, human diseases, and organism systems (Figure 2D). These annotated genes were further subdivided into 43 subcategory pathways. Among them, we focused on the most annotated Metabolism section in the First Category; most genes fell under Amino acid metabolism (289 genes), Carbohydrate metabolism (414 genes), lipid metabolism (422 genes), and Glycan biosynthesis and metabolism (289 genes).

Differentially expressed genes and their functional enrichment analysis

The analysis of the relationship between samples from different stages of the hepatopancreas and ovary was demonstrated by a Venn diagram (Figure 3A). In this case, a total of 6730 genes were expressed in both tissues, of which 4079 and 1227 were genes specifically expressed in the hepatopancreas and ovary, respectively. Within the hepatopancreas, 8524 transcripts were commonly expressed at four stages, while at stages I, II, III and IV, the numbers of transcripts coexpressed in the hepatopancreas and ovary were 5541, 6098, 7508 and 6917, respectively (Figure 3A).

To identify DEGs involved in ovarian development, we used the RPKM value to compare the expression differences between different groups (Figure 3B). A large number of DEGs were screened with adjusted $q < 0.05$ and $|\log2Ratio| \geq 1$. A total of 10288 differentially expressed genes (DEGs) were identified between ovarian and hepatopancreatic samples, including 3077 upregulated transcripts and 7211 downregulated transcripts. The ovarian and hepatopancreatic samples were divided into four stages for further comparison. Among them, 3267 and 5138 transcripts were upregulated and downregulated at stage II, and 2737 and 6337

TABLE 4 Sequence Mapping Analysis.

Sample	Total reads	Total mapped	Multiple mapped	Uniquely mapped
Hp_I	44630016	38851014(87.05%)	6226532(13.95%)	32624482(73.1%)
Hp_II	40197512	34882655(86.78%)	6393767(15.91%)	28488888(70.87%)
Hp_III	44540914	39270864(88.17%)	8316613(18.67%)	30954251(69.5%)
Hp_IV	44043748	38545508(87.52%)	5151101(11.7%)	33394407(75.82%)
Ov_I	44267292	41472570(93.69%)	11854679(26.78%)	29617891(66.91%)
Ov_II	44175442	41171411(93.2%)	12256607(27.75%)	28914804(65.45%)
Ov_III	44359992	41393017(93.31%)	11857464(26.73%)	29535553(66.58%)
Ov_IV	44208868	41214096(93.23%)	11684868(26.43%)	29529228(66.79%)

10.3389/fmars.2022.948105

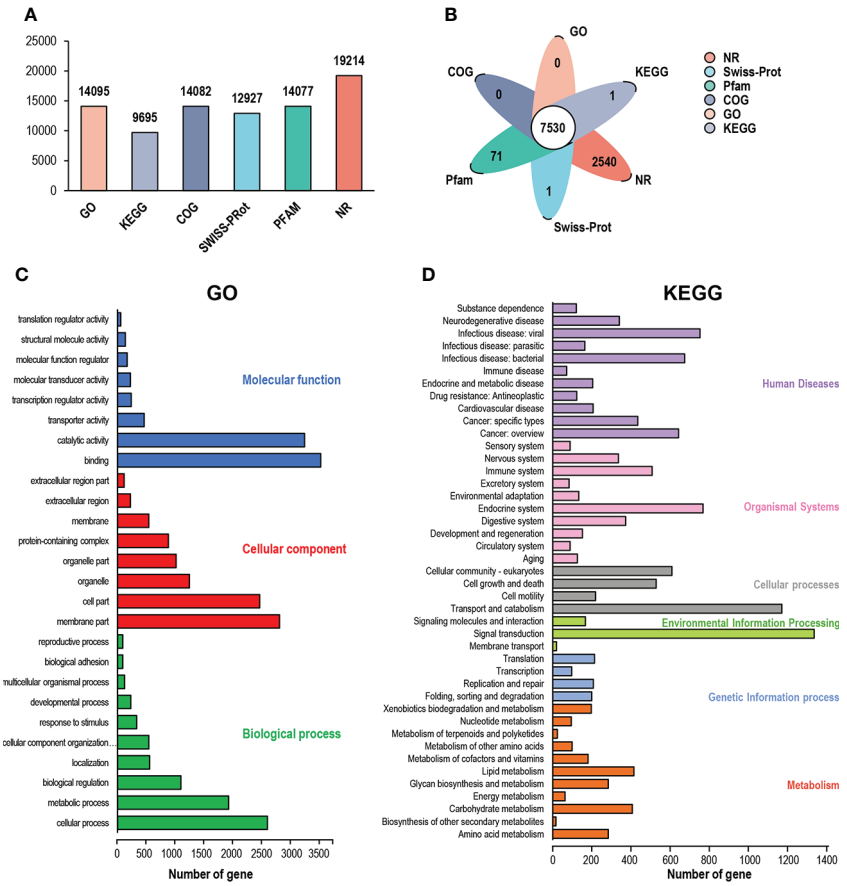

FIGURE 2
(A) All genes and transcripts obtained from the transcriptome assembly of Penaeus vannamei were compared with six major databases (NR, Swiss-Prot, Pfam, EggNOG, GO, and KEGG), and the Venn diagram shows the comparison of the data from the major databases. **(B)**Venn diagram of six databases, the white part is the number of common genes **(C)** GO classification results are summarized into three main GO categories (cellular components, molecular functions, and biological processes). The Y-axis represents the GO ontology. The X-axis indicates the number of genes. **(D)** KEGG classification of all transcripts. Columns represent the number of transcripts in each subcategory.

DEGs were upregulated and downregulated at stage III in the hepatopancreas and ovary, respectively (Figure 3C).

Expression analysis of transcripts of genes related to lipid metabolism

The three most enriched pathways of metabolism were selected from the KEGG enriched pathways amino acid metabolism, carbohydrate metabolism, and lipid metabolism, and the gene sets of the three pathways were established separately. Pathway enrichment analysis was performed using the same principle as GO functional enrichment analysis, and the KEGG pathway function was considered to be significantly enriched when the corrected P value (Padjust) was <0.05. The enrichment results (Figure 4A) showed that most of the metabolism-related transcripts were upregulated in the hepatopancreas, while fewer were upregulated in the ovary. Three pathways related to lipid transport were identified from the lipid metabolism gene set: fatty acid biosynthesis (map00061), fatty acid degradation (map00062), and biosynthesis of unsaturated fatty acids (map01040), and the heatmap showed that the majority of transcripts associated with lipid transport were upregulated in the hepatopancreas and less in the ovary (Figure 4B).

Identification and expression patterns of lipoprotein and their receptor genes

Apolipoproteins are important carriers for lipid transportation, providing the required nutrients during the shrimp ovarian development cycle. In this study, the expression levels of

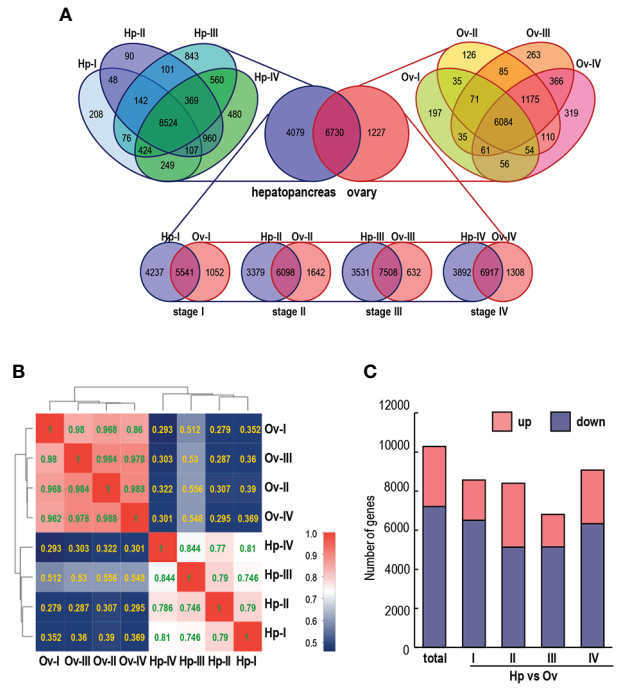

FIGURE 3
(A) Venn diagrams of unique and common genes in different stages of hepatopancreas and ovary development. **(B)** Correlation analysis of the four stages of ovary and hepatopancreas. The value is the correlation coefficient of the two samples; the larger the value is, the greater and more similar the correlation between the two samples. **(C)** Number of up- and down-regulated DEGs in each hepatopancreatic group compared to the ovarian group (first combinatorial bar) and pairwise comparison of four different staged hepatopancreatic and ovarian groups (last four combinatorial bars).

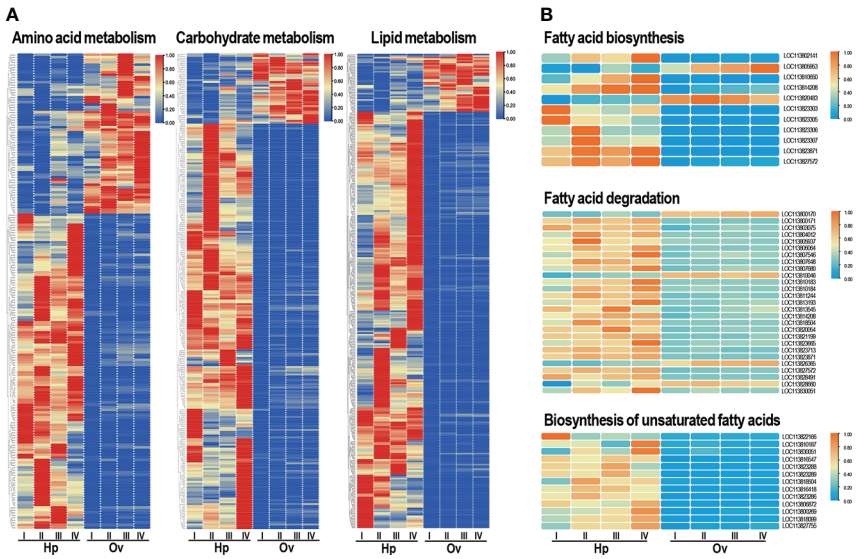

FIGURE 4
(A) KEGG analysis of three metabolic pathway transcripts up- and downregulated at different stages in the ovary and hepatopancreas. **(B)** Fatty acid metabolic pathway transcripts up- and down-regulated at different stages in the ovary and hepatopancreas. Orange and blue represent upwards and downwards shifts, respectively.

apolipoproteins and their receptors were selected for analysis and illustrated by a heatmap (Figure 5A). The apolipoprotein included vitellogenin (Vg, LOC11380422), apolipoprotein D (ApoD, LOC113810220 and LOC113815027), beta-1,3-guucan-binding protein (BGBP, LOC113813397 and LOC113807239), hemolymph protein (BGBP, LOC113813397 and LOC113807239) and hemolymph clottable protein (CP, LOC113819742 and LOC113807427), and the apolipoprotein receptor included vitellogenin receptor (VgR, LOC113811544 and LOC113811783), very low-density lipoprotein receptor (VLDLR, LOC113811553 and LOC113802323) and low-density lipoprotein receptor-related protein 1 (LDLR-RP1, LOC113824560) (Jia et al., 2016; Hoeger and Schenk, 2020; Li et al., 2021). In this case, Vg, ApoD, BGBP, BP, VLDLR and LDLR-RP1 transcripts were predominantly expressed in the hepatopancreas but not in the ovary, while one of the VgR transcripts appeared to have low ovarian expression and high hepatopancreas expression. The RT-qPCR results for BGBP, VgR and LDLR were consistent with the RNA-seq results (Figure 5B). However, the expression of Vg genes appeared in two different expression patterns for the two isoforms, which will be covered later in the section.

Quantification and structural domain analysis of two Vg isoforms

By RT-qPCR, two transcripts of Vg genes showed completely opposite expression sites (Figure 6A), in which LOC113804022 had high expression in the hepatopancreas and was defined as hepatopancreatic vitellogenin (Hp-Vg), and LOC113826723 had high expression in the ovary and was defined as ovarian vitellogenin (Ov-Vg). Compared with Ov-Vg, HP-Vg transcriptional levels are higher than ovarian fragments. The nucleotide sequence similarity between the two Vg transcripts was 71.6%, indicating that the two genes do not encode the same protein. As shown in Figure 6B, prediction of structural domains indicated the presence of DUF1943, Pfam : DUF1081 and VWD domains in both Vg proteins. Ov-Vg contained the LPD_N domain, while it was replaced by the Pfam : Vitellogenin_N domain in Hp-Vg (Figure 6B). In addition, gene organizations showed that both types of Hp-Vg and Ov-Vg genes contain 15 exons separated by 14 introns, and all introns start with GT and end with AG, conforming to the GT/AG rule for intron splicing (Figure 6B).

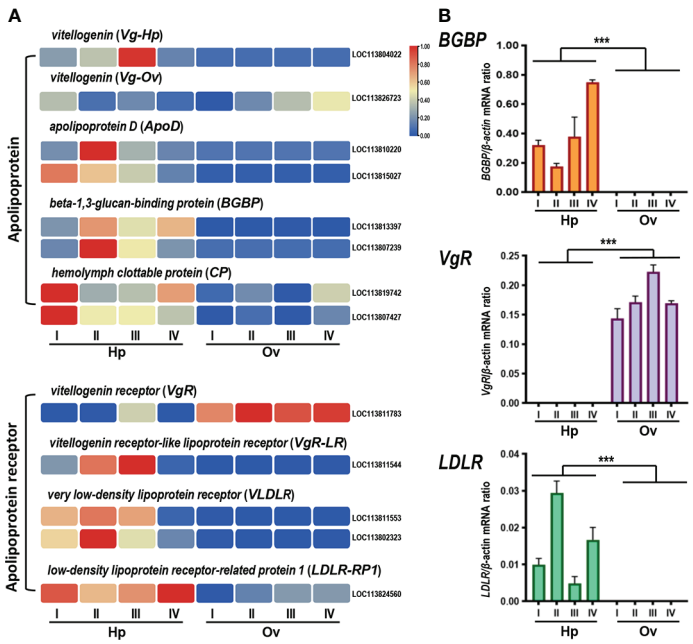

FIGURE 5
(A) Apolipoprotein and apolipoprotein receptor clustering heatmap analysis. **(B)** Quantitative realtime PCR validation of lipoprotein RNA-seq data. Three single genes were selected for validation, including *beta-1,3-glucan binding protein* (*BGBP*), *vitellogenin receptor* (*VgR*), and *low density lipoprotein receptor* (*LDLR*). The x-axis represents the developmental stage. Columns and bars represent the mean and standard error of the relative expression levels from RT-qPCR results (Y-axis on the left). Values with different superscripts indicate statistical significance ($P < 0.05$), calculated by one-way ANOVA. *** means significant difference.

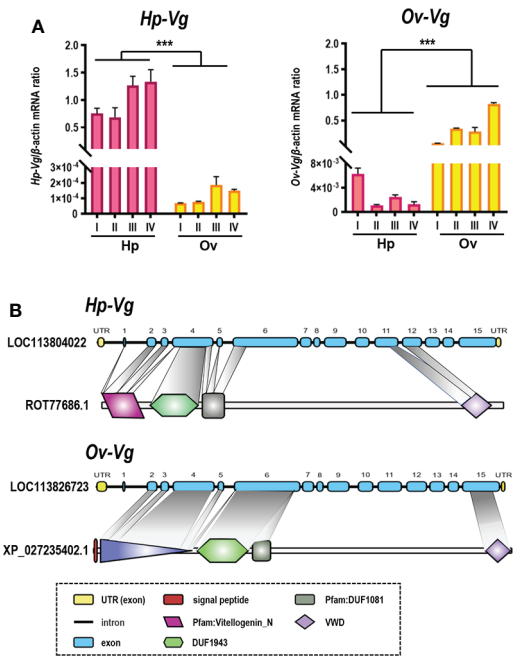

FIGURE 6
(A) RT-qPCR validation of two differentially expressed *vitellogenin*, named *Hp-Vg* as the hepatopancreatic type and *Ov-Vg* as the ovarian type. The X-axis is staging, left is hepatopancreatic, right is ovarian, Y-axis is sample CT to *β-actin* CT ratio. Values with different superscripts indicate statistical significance ($P < 0.05$), calculated by one-way ANOVA. **(B)** Comparison of Hp-Vg and Ov-Vg structural domains (Hp-Vg: ROT77686.1, Ov-Vg: XP_027235402.1) and exon/intron organization of genes (Hp-Vg: LOC11380422, Ov-Vg: LOC113826723). The ORF and UTR of exons are marked with dark blue and empty boxes, respectively, and introns are marked with solid lines. Solid lines. The lengths of the elements are indicated as nucleotides. *** means significant difference.

Expression analysis of transcripts of genes related to carotenoid metabolism

The primary pathway associated with carotenoid metabolism is metabolism of cofactors and vitamins, and the heatmap shows that transcripts of this pathway were more highly expressed in the hepatopancreas than in the ovary (Figure 7A). The results for the secondary pathway retinol metabolism were similar to those for the primary pathway (Figure 7B), with most transcripts highly expressed in the hepatopancreas. Four typical genes on the pathway were screened for heatmap and quantitative analysis (Figures 7C, D), and the enzyme BCOM1 (LOC113809949), associated with carotenoid cleavage, was found to be highly expressed in the hepatopancreas and almost absent from the ovary, while other representative genes cytochrome P450 3A1-like (3A1), transcript variant X1 cytochrome P450 3A13-like (3A13), and cytochrome P450 9e2-like, transcript variant X1 (9e2), which are CYP family member genes related to carotenoid processing, were also highly expressed only in the hepatopancreas, which was consistent with the RT-qPCR results.

Discussion

In this study, it was shown that the ovaries of L. vannamei could develop from stage I to stage IV within 4-6 days post-unilateral eyestalk ablation and 11-13 days of nutritional enrichment feeding the fresh clam worms, squid and oysters, respectively (Figure 1A), which was much shorter than the previous report on these shrimp without nutritional reinforcement (generally need 15-37 days to reach spawning after eyestalk ablation) (Du et al., 2018). This study suggested a synergistic effect between nutritional reinforcement with fresh food and eyestalk ablation on ovarian development of L. vannamei, similar to a previous report on black tiger shrimp Penaeus monodon (Hoeger and Schenk, 2020). Based on that, this study investigated the contributions of the hepatopancreas and ovaries to vitellin accumulation in the oocyte maturation of female shrimp by transcriptomic sequencing.

RNA-Seq is a type of NGS that provides important tools for the discovery of genes and the analysis of gene structure, genetic evolution and population genetics (Hoeger and Schenk, 2020). In recent years, a number of genes

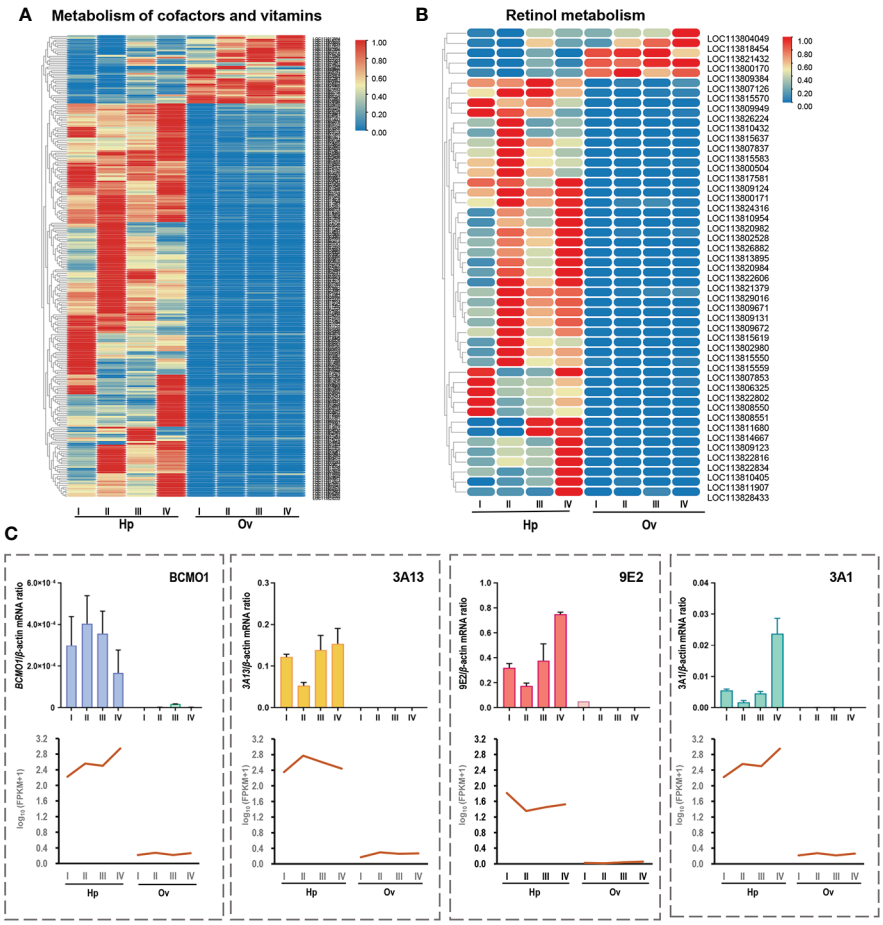

FIGURE 7
(A) Clustering heatmap analysis of vitamin metabolism genes in the primary pathway of carotenoid metabolism. **(B)** Clustering heatmap analysis of retinoid metabolism genes in the secondary pathway of carotenoid metabolism. **(C)** Realtime quantitative PCR validation of carotenoid metabolism-related RNA-seq data. Four representative genes were selected for validation, including beta, beta-carotene 15,15'-dioxygenase (BCMO1), cytochrome P450 3A13-like (3A13), cytochrome P450 3A1-like, transcript variant X1 (3A1) and cytochrome P450 9e2-like, transcript variant X1 (9E2). The X-axis represents developmental stages. Columns and bars represent the mean and standard error of the relative expression levels of RT-qPCR results (Y-axis on the left). Values with different superscripts indicate statistical significance ($P < 0.05$), calculated by one-way ANOVA.

associated with crustacean ovarian development have been identified by genome (Zhang et al., 2019) and transcriptome (Sittikankaew et al., 2020) analyses. In this study, we identified transcripts associated with lipoprotein transportation, such as Vg, ApoD, BGBP, CP, VgR, VLDLR and LDLR-RP1, and with carotenoid metabolism, such as BCMO1, 3A13, 9E2 and 3A1, from the hepatopancreatic and ovarian transcriptomes of L. vannamei.

For analysing DEGs in different stages of the ovary and hepatopancreas in shrimp, the results showed that more DEGs were upregulated than downregulated in the hepatopancreas during the ovarian maturation cycle, particularly for lipid metabolism and transportation (Figures 4A, B), indicating that the hepatopancreas was the major lipid metabolism centre and supplied more lipids to the developing ovaries during ovarian development.

Based on the ultrastructural features of the crustacean hepatopancreas, nutrients are considered mainly absorbed by R-cells (Samuel and Bähler, 2010), the most abundant cell type in the hepatopancreas. R-cells can store large amounts of energy reserves, such as lipids and glycogen. In P. monodon and Palaemon elegans, rough endoplasmic reticulum (rER) vesicles often transport degraded lipid globules in a central direction, and peroxisomes and mitochondria are close to the lipid globule-rER complex for catabolism and further ß-oxidation (Wang et al., 2014).

The hepatopancreas synthesizes hemolymph proteins with different functions, such as hemocyanin, lipoproteins,

antimicrobial peptides and coagulating proteins (Ahearn, 2010). Within the hemolymph proteins, lipoprotein is a kind of biochemical assembly whose primary function is to transport hydrophobic lipid molecules in hydrophilic plasma or other extracellular fluids (Vogt, 1994).

Most of the high-density lipoprotein HDL-BGBPs circulating in the hemolymph are thought to originate in the hepatopancreas, although they seem to be ubiquitously expressed (Holdich, 2002). The expression levels of HDL-BGBP vary based on species and tissues (Abdu et al., 2000). These lipoproteins differ from mammalian HDL because they include phospholipids as a major lipid component instead of triglycerides. The lipoproteins are probably synthesized in the R-cells and exported *via* the basal tubule system (Gloria et al., 2000). The results of this study showed that lipoprotein genes were predominantly expressed in the hepatopancreas rather than in the ovary, except for an Ov-Vg (Figures 5A, 6A), indicating that the hepatopancreas is the major site for lipoprotein synthesis even during ovarian development. Given that only VgR but not other lipoprotein receptors was mainly expressed in the ovary, it is logical to speculate that self-circulation from the hepatopancreas to the hepatopancreas is the normal form of lipoprotein transport in shrimp and that transportation from the hepatopancreas to ovary is a specific form for lipoprotein transport during female reproduction.

In this study, multiple Vg or Vg-like transcripts were identified from the transcriptome of L. vannamei, with different expression patterns during ovarian development. Hepatopancreas-expressed Vg (Hp-Vg) and ovary-expressed Vg (Ov-Vg) are considered to provide the greatest contributions to ovarian vitellin deposition (Figure 5A), and they share only 44.74% identity with each other at the amino acid (a.a.) sequence level. By BLAST screening, Hp-Vg and Ov-Vg transcripts were found to correspond to LOC113804022 and LOC113826723 in the L. vannamei genome and XR_003475567.1 and XM_027379601.1, respectively, as previously reported (Dai et al., 2021). Different Vg genes and multiple Vg isoforms with different expression patterns have been found in L. vannamei (Wang et al., 2020). However, their contribution to vitellin accumulation in oocytes is unclear. Based on the transcriptomes of the hepatopancreas and ovary from the banana shrimp F. merguiensis, black tiger shrimp P. monodon and lobster Panilus homarus, multiple Vg transcripts have also been identified (Vogt, 2019), indicating the presence of multiple Vg genes in crustaceans. Our study showed that one Vg gene (Hp-Vg) was restrictedly expressed in the hepatopancreas, while another Vg gene (Ov-Vg) was specifically expressed in the ovaries during the whole ovarian maturation of L. vannamei (Figure 6A).

Interestingly, the results of the current study showed that the signal peptide was only found in the a.a. sequences of Ov-Vg but not Hp-Vg (Figure 6B). It is speculated that Hp-Vg is transported from the hepatopanscreas to the ovary *via* the vitellogenin apolipoprotein, which does not require a signal peptide (Wang et al., 2020). In contrast, Ov-Vg is secreted and absorbed by ovaries independently *via* a paracrine pathway. Similarly, Vg isoforms with and without signal peptides have been reported in the mud crab S. paramamosain (Yang et al., 2016).

Carotenoids are the major pigments for crustaceans. Previous studies have shown crustaceans have to obtain carotenoids from their diets and can further convert some carotenoids, such as β-carotene and zeaxanthin, into Axn (Babin et al., 2020). During crustacean ovarian maturation, carotenoids first absorb and accumulate in the hepatopancreas in free and esterified forms and

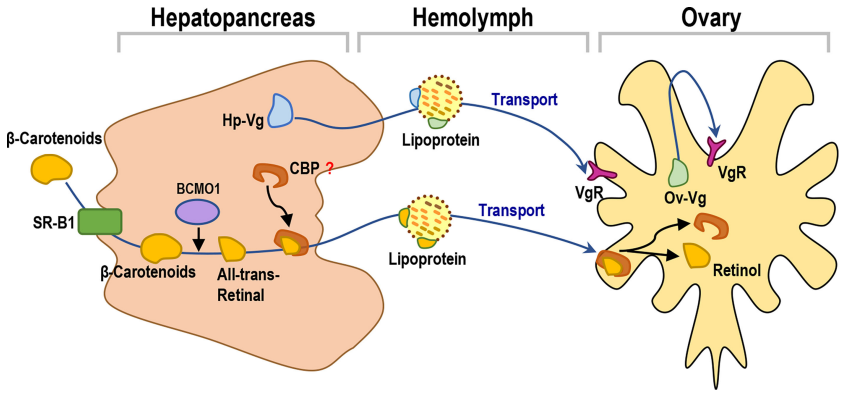

FIGURE 8
A working model for yolk nutrition production, transportation and accumulation pathways from the hepatopancreas to ovary in Pacific white shrimp.

are then transported to the ovary *via* the hemolymph during vitellogenesis (Goodwin, 1986). Carotenoids are highly hydrophobic and therefore require special transport by lipoproteins, such as low-density lipoprotein in mammals and lipophorin in insects, through plasma or hemolymph for deposition in target tissues (Sachindra et al., 2005). However, to date, no lipoprotein for transporting carotenoids has been functionally identified in crustaceans.

Furthermore, retinols and other retinoid derivatives play a critical role in the developmental processes of crustaceans, including ovarian and larval development (Boonyaratpalin et al., 2001), which are generally produced from the central cleavage at the 15,15'-double bond of β-carotene by the carotenoid cleaving enzyme (BCMO) (M et al., 1988). The results of the current study showed that the transcripts related to carotenoid metabolism were associated with the map00830 pathway in ko00515 by KEGG alignment (Supplementary Figure S1). One major carotenoid cleaving enzyme (BCMO1) we identified in the L. vannamei transcriptome (Figure 8) from the current study. The high expression level of BCMO1 mRNA in the hepatopancreas indicates the accumulation of large carotenoids in the hepatopancreas. However, the actual absorption, transportation, deposition and metabolism of dietary carotenoids in crustaceans remain unclear and warrant further investigation.

Data availability statement

The datasets presented in this study can be found in online repositories. The names of the repository/repositories and accession number(s) can be found below: BioProject, accession number: PRJNA438564.

Author contributions

ZL, TC and XW designed and drafted the manuscript. MZ, YR, XC, JL and LZ performed animal collection and prepared samples. ZL, MZ, HY and XZ performed data processing and bioinformatic analysis. ZL, TC and XW conceived the study and experimental design and helped draft the manuscript. HL, CH and TC contributed reagents/materials/analysis tools. TC and XW supervised and conceived the experiments and corrected the manuscript. All authors read and approved the final manuscript.

Funding

This research was funded by the Guangdong Provincial Special Fund for Modern Agriculture Industry Technology Innovation Teams (2019KJ149) and the National Natural Science Foundation of China (31402287).

Acknowledgments

The authors thank Ms. Min Zhang and Ms. Ziyue Zhao for their help in data collection and Dr. Xiao Jiang for her help in manuscript preparation. The authors also thank the Majorbio Cloud Platform (Shanghai, China) for bioinformatics support.

Conflict of interest

Authors JL and HL are/were employed by Jinyang Biotechnology Co. Ltd.

The remaining authors declare that the research was conducted in the absence of any commercial or financial relationships that could be construed as a potential conflict of interest.

Publisher's note

Supplementary material

The Supplementary Material for this article can be found online at: https://www.frontiersin.org/articles/10.3389/fmars.2022.948105/full#supplementary-material

SUPPLEMENTARY FIGURE 1
Retinol metabolism pathway by KEGG analysis showing different genes of action (yellow - known genes, green - new genes, red border - upregulated genes, blue border - downregulated genes). The KEGG pathway map 000830 is adapted from https://www.genome.jp/kegg-bin/show_pathway map00830, and the KEGG database has been previously described.

References

Abdu, U., Yehezkel, G., and Sagi, A. (2000). Oocyte development and polypeptide dynamics during ovarian maturation in the red-claw crayfish cherax quadricarinatus. *Invertebrate Reprod. Dev.* 37, 75–83. doi: 10.1080/07924259.2000.9652402

Ahearn, G. A. (2010). Nutrient transport by the crustacean gastrointestinal tract: recent advances with vesicle techniques. *Biol. Rev.* 62, 45–63. doi: 10.1111/j.1469-185X.1987.tb00625.x

Arcos, F. G., Ibarra, A. M., and Racotta, L. S. (2011). Vitellogenin in hemolymph predicts gonad maturity in adult female *Litopenaeus (Penaeus) vannamei* shrimp. *Aquaculture* 316, 93–98. doi: 10.1016/j.aquaculture.2011.02.045

Avarre, J. C., Lubzens, E., and Babin, P. J. (2007). Apolipocrustacein, formerly vitellogenin, is the major egg yolk precursor protein in decapod crustaceans and is homologous to insect apolipophorin II/I and vertebrate apolipoprotein b. *BMC Evol. Biol.* 7, 3. doi: 10.1186/1471-2148-7-3

Babin, A., Motreuil, S., Teixeira, M., Bauer, A., and Moreau, Y.. (2020). Origin of the natural variation in the storage of dietary carotenoids in freshwater amphipod crustaceans. *PloS One* 15, e0231247. doi: 10.1371/journal.pone.0231247

Bae, S. H., Okutsu, T., Tsutsui, N., Kang, B. J., Chen, H. Y., and Wilder, M. N. (2017). Involvement of second messengers in the signaling pathway of vitellogenesis-inhibiting hormone and their effects on vitellogenin mRNA expression in the whiteleg shrimp, litopenaeus vannamei. *Gen. Comp. Endocrinol.* 246, 301–308. doi: 10.1016/j.ygcen.2017.01.006

Boonyaratpalin, M., Thongrod, S., Supamattaya, K., Britton, G., and Schlipalius, L. E. (2001). Effects of ß-carotene source, dunaliella salina, and astaxanthin on pigmentation, growth, survival and health of penaeus monodon. *Aquacult Res.* 32 (Suppl 1), 182–190. doi: 10.1046/j.1355-557x.2001.00039.x

Britton, G. (1995). Structure and properties of carotenoids in relation to function. *FASEB J. Off. Publ. Fed. Am. Societies Exp. Biol.* 9, 1551. doi: 10.1006/excr.1995.1406

Ceballos-Vázquez, B. P., Palacios, E., Aguilar-Villavicencio, J., and Racotta, I. S. (2010). Gonadal development in male and female domesticated whiteleg shrimp, litopenaeus vannamei, in relation to age and weight. *Aquaculture* 308, 116–123. doi: 10.1016/j.aquaculture.2010.08.020

Chen, T., Lin, T., Li, H., Lu, T., Li, J., Huang, W., et al. (2018). Heat shock protein 40 (HSP40) in pacific white shrimp (Litopenaeus vannamei): Molecular cloning, tissue distribution and ontogeny, response to temperature, Acidity/Alkalinity and salinity stresses, and potential role in ovarian development. *Front. Physiol.* 9. doi: 10.3389/fphys.2018.01784

Chen, T., Zhang, L. P., Wong, N. K., Zhong, M., Ren, C. H., and Hu, C. Q. (2014). Pacific white shrimp (Litopenaeus vannamei) vitellogenesis-inhibiting hormone (VIH) is predominantly expressed in the brain and negatively regulates hepatopancreatic vitellogenin (VTG) gene expression. *Biol. Reprod.* 90, 47. doi: 10.1095/biolreprod.113.115030

Dai, H., Lv, Z., Huang, Z., Ye, N., Li, S., Jiang, J., et al. (2021). Dietary hawthorn-leaves flavonoids improves ovarian function and liver lipid metabolism in aged breeder hens. *Poultry Sci.* 100, 101499. doi: 10.1016/j.psj.2021.101499

Du, J. L., Zhang, X. J., Yuan, J. B., Zhang, X. X., Li, F. H., and Xiang, J. H. (2018). Wnt gene family members and their expression profiling in litopenaeus vannamei - ScienceDirect. *Fish Shellfish Immunol.* 77, 233–243. doi: 10.1016/j.fsi.2018.03.034

Gloria, Y.-P., Teresa, G. G., Vargas-Albore, F., and García-Bañuelos, M. (2000). Synthesis of hemolymph high-density lipoprotein β-glucan binding protein by penaeus vannamei shrimp hepatopancreas. *Mar. Biotechnol* 2, 485–492. doi: 10.1007/s101260000030

Gong, J., Ye, H., Xie, Y., Yang, Y., Huang, H., Li, S., et al. (2015). Ecdysone receptor in the mud crab Scylla paramamosain: a possible role in promoting ovarian development. *J. Endocrinol.* 224, 273–287. doi: 10.1530/JOE-14-0526

Goodwin, W. ,. T. (1986). Metabolism, nutrition, and function of carotenoids. *Annu. Rev. Nutr.* 6, 273. doi: 10.1146/annurev.nu.06.070186.001421

Heras, H., Gonzalez-Baró, M., and Pollero, R. J. (2000). Lipid and fatty acid composition and energy partitioning during embryo development in the shrimp macrobrachium borellii. *Lipids* 35, 645–651. doi: 10.1007/s11745-000-0569-z

Hiramatsu, N., Todo, T., Sullivan, C. V., Schilling, J., Reading, B. J., Matsubara, T., et al. (2015). Ovarian yolk formation in fishes: Molecular mechanisms underlying formation of lipid droplets and vitellogenin-derived yolk proteins. *Gen. Comp. Endocrinol.* 221, 9–15. doi: 10.1016/j.ygcen.2015.01.025

Hoeger, U., and Schenk, S. (2020). Crustacean hemolymph lipoproteins. *Subcell Biochem.* 94, 35–62. doi: 10.1007/978-3-030-41769-7_2

Holdich, D. M. (2002). Biology of freshwater crayfish. *Biol. Freshw. Crayfish.* doi: 10.1038/238113b0

Jia, X., Chen, Y., Zou, Z., Lin, P., Wang, Y., and Zhang, Z. (2013). Characterization and expression profile of vitellogenin gene from Scylla paramamosain. *Gene* 520, 119–130. doi: 10.1016/j.gene.2013.02.035

Jia, W., Ke-Cai, X., Ying-Hong, L., and Ying, X. (2016). *De novo* transcriptome analysis of Chinese citrus fly, bactrocera minax (Diptera: Tephritidae), by high-throughput illumina sequencing. *PloS One* 11, e0157656. doi: 10.1371/journal.pone.0157656

Jinxia, P., Pinyuan, W., Bin, Z., et al. (2015). Gonadal transcriptomic analysis and differentially expressed genes in the testis and ovary of the pacific white shrimp (Litopenaeus vannamei). *BMC Genomics*. doi: 10.1186/s12864-015-2219-4

Kang, B. J., Okutsu, T., Tsutsui, N., Shinji, J., Bae, S. H., and Wilder, M. N. (2014). Dynamics of vitellogenin and vitellogenesis-inhibiting hormone levels in adult and subadult whiteleg shrimp, litopenaeus vannamei: relation to molting and eyestalk ablation. *Biol. Reprod.* 90, 12. doi: 10.1095/biolreprod.113.112243

Lee, C. Y., Lee, B. D., Na, J. C., and An, G. (2010). Carotenoid accumulation and their antioxidant activity in spent laying hens as affected by polarity and feeding period. *Asian Australas. J. Anim. Sci.* 23, 799–805. doi: 10.5713/ajas.2010.90296

Liaaen-Jensen, S. (1997). Stereochemical aspects of carotenoids. *Pure Appl. Chem.* 69, 2027–2038. doi: 10.1351/pac199769102027

Lin, K. H., Lin, K. C., Lu, W. J., Philip-Aloysius, T., Thanasekaran, J., and Joen-Rong, S. (2015). Astaxanthin, a carotenoid, stimulates immune responses by enhancing IFN-γ and IL-2 secretion in primary cultured lymphocytes *in vitro* and *ex vivo*. *Int. J. Mol. Sci.* 17, 44. doi: 10.3390/ijms17010044

Li, Y. T., Tang, B. P., Zhang, S. P., Tang, Y. Y., and Zhang, M. L. (2021). Transcriptome analysis of immune-related genes in sesarmops sinensis hepatopancreas in reaction to peptidoglycan challenge. *Genomics* 946–954. doi: 10.1016/j.ygeno.2021.01.011

Luo, X., Chen, T., Zhong, M., Jiang, X., Zhang, L., Ren, C., et al. (2015). Differential regulation of hepatopancreatic vitellogenin (VTG) gene expression by two putative molt-inhibiting hormones (MIH1/2) in pacific white shrimp (Litopenaeus vannamei). *Peptides* 68, 58–63. doi: 10.1016/j.peptides.2014.11.002

Mak, A. S., Choi, C. L., Tiu, S. H., Hui, J. H., He, J. G., Tobe, S. S., et al. (2005). Vitellogenesis in the red crab charybdis feriatus: Hepatopancreas-specific expression and farnesoic acid stimulation of vitellogenin gene expression. *Mol. Reprod. Dev.* 70, 288–300. doi: 10.1002/mrd.20213

M, V., L, R., and L, O. (1988). And quantitative variations in carotenoid pigments in the ovary and. - *Arch. Int. Physiol. Biochim.* 96 (5), 155–164.

Nagaraju, G. P. (2011). Reproductive regulators in decapod crustaceans: an overview. *J. Exp. Biol.* 214, 3–16. doi: 10.1242/jeb.047183

Ni, J. B., Zeng, Z., Kong, D. Z., Hou, L., Huang, H. Q., and Ke, C. H. (2014). Vitellogenin of fujian oyster, crassostrea angulata: Synthesized in the ovary and controlled by estradiol-17 beta. *Gen. Comp. Endocrinol.* 202, 35–43. doi: 10.1016/j.ygcen.2014.03.034

Quackenbush, L. S. (2001). Yolk synthesis in the marine shrimp, penaeus vannamei. *Integr. Comp. Biol.* 41, 458–464. doi: 10.1093/icb/41.3.458

Raviv, S., Parnes, S., Segall, C., Davis, C., and Sagi, A. (2006). Complete sequence of litopenaeus vannamei (Crustacea: Decapoda) vitellogenin cDNA and its expression in endocrinologically induced sub-adult females. *Gen. Comp. Endocrinol.* 145, 39–50. doi: 10.1016/j.ygcen.2005.06.009

Sachindra, N. M., Bhaskar, N., and Mahendrakar, N. S. (2005). Carotenoids in different body components of Indian shrimps. *J. Sci. Food Agric.* 85, 167–172. doi: 10.1002/jsfa.1977

Samuel, Margueratjürg, and Bähler, J. (2010). RNA-Seq: from technology to biology. *Cell. Mol. Life Sci* 67, 569–579. doi: 10.1007/s00018-009-0180-6

Sittikankaew, K., Pootakham, W., Sonthirod, C., Sangsrakru, D., Yoocha, T., Khudet, J., et al. (2020). Transcriptome analyses reveal the synergistic effects of feeding and eyestalk ablation on ovarian maturation in black tiger shrimp. *Sci. Rep.* 10, 3239. doi: 10.1038/s41598-020-60192-2

Teruhisa, K., Yoko, K., Shimaya, M., Simpson, K. L, and Chichester, C. O. (1973). The biosynthesis of astaxanthin–XIV. the conversion of labelled β-carotene-15,15′-3H2 into astaxanthin in the crab, portunus trituberculatus. *Comp. Biochem. Physiol. Part B Comp. Biochem and Molecular Biology* 46, 269–272. doi: 10.1016/0305-0491(73)90317-9

Thongda, W., Chung, J. S., Tsutsui, N., Zmora, N., and Katenta, A. (2015). Seasonal variations in reproductive activity of the blue crab, callinectes sapidus: Vitellogenin expression and levels of vitellogenin in the hemolymph during ovarian development. *Comp. Biochem. Physiol. Part A Mol. Integr. Physiol.* 179, 35–43. doi: 10.1016/j.cbpa.2014.08.019

Tian, X., Gautron, J., Monget, P., and Pascal, G. (2010). What makes an egg unique? clues from evolutionary scenarios of egg-specific genes. *Biol. Reprod.* 83, 893–900. doi: 10.1095/biolreprod.110.085019

Tiu, S. H. K., Hui, J. H. L., Mak, A. S. C., He, J.-G., and Chan, S.-M. (2006). Equal contribution of hepatopancreas and ovary to the production of vitellogenin

(PmVg1) transcripts in the tiger shrimp, penaeus monodon. *Aquaculture* 254, 666–674. doi: 10.1016/j.aquaculture.2005.11.001

Tseng, D. Y., Chen, Y. N., Liu, K. F., Kou, G. H., Lo, C. F., and Kuo, C. M. (2002). Hepatopancreas and ovary are sites of vitellogenin synthesis as determined from partial cDNA encoding of vitellogenin in the marine shrimp, penaeus vannamei. *Invertebrate Reprod. Dev.* 42, 137–143. doi: 10.1080/07924259.2002.9652770

Tsukimura, B. (2001). Crustacean vitellogenesis: Its role in oocyte development. *Integr. Comp. Biol.* 41, 465–476. doi: 10.1093/icb/41.3.465

Tsutsui, N., Ohira, T., Okutsu, T., Shinji, J., Bae, S. H., Kang, B. J., et al. (2013). Molecular cloning of a cDNA encoding vitellogenesis-inhibiting hormone in the whiteleg shrimp litopenaeus vannamei and preparation of its recombinant peptide using an e. coli expression system. *Fisheries Sci.* 79, 357–365. doi: 10.1007/s12562-013-0603-z

Tufail, M., and Takeda, M. (2008). Molecular characteristics of insect vitellogenins. *J. Insect Physiol.* 54, 1447–1458. doi: 10.1016/j.jinsphys.2008.08.007

Vogt, G. (1994). Life-cycle and functional cytology of the hepatopancreatic cells of astacus astacus (Crustacea, decapoda). *Zoomorphology* 114, 83–101. doi: 10.1007/BF00396642

Vogt, G. (2019). Functional cytology of the hepatopancreas of decapod crustaceans. *J. Morphology* 280, 1405–1444. doi: 10.1002/jmor.21040

Wade, N. M., Gabaudan, J., and Glencross, B. D. (2017). A review of carotenoid utilisation and function in crustacean aquaculture. *Rev. Aquaculture* 9(2), 141–156. doi: 10.1111/raq.12109

Wang, W., Li, B., Zhou, T., Wang, C., and Chan, S. (2020). Investigation of gene sequence divergence, expression dynamics, and endocrine regulation of the vitellogenin gene family in the whiteleg shrimp litopenaeus vannamei. *Front. Endocrinol.* 11. doi: 10.3389/fendo.2020.577745

Wang, W., Wu, X., Liu, Z., Zheng, H., and Cheng, Y. (2014). Insights into hepatopancreatic functions for nutrition metabolism and ovarian development in the crab portunus trituberculatus: gene discovery in the comparative transcriptome of different hepatopancreas stages. *PloS One* 9, e84921. doi: 10.1371/journal.pone.0084921

Wouters, R., Molina, C., Lavens, P., and Calderon, J. (2001). Lipid composition and vitamin content of wild female litopenaeus vannamei in different stages of sexual maturation. *Aquaculture* 198, 307–323. doi: 10.1016/S0044-8486(01)00522-1

Yang, Y., Zheng, B., Bao, C., Huang, H., and Ye, H. (2016). Vitellogenin2: spermatozoon specificity and immunoprotection in mud crabs. *Reproduction* 152, 235. doi: 10.1530/REP-16-0188

Zhang, X. J., Yuan, J. B., Sun, Y. M., Li, S. H., Gao, Y., Yu, Y., et al. (2019). Penaeid shrimp genome provides insights into benthic adaptation and frequent. - *Nat. Commun.* 10 (1), 356. doi: 10.1038/s41467-018-08197-4

Zmora, N., Trant, J., Chan, S. M., and Chung, J. S. (2007). Vitellogenin and its messenger RNA during ovarian development in the female blue crab, callinectes sapidus: gene expression, synthesis, transport, and cleavage. *Biol. Reprod.* 77, 138–146. doi: 10.1095/biolreprod.106.055483

Zmora, N., Trant, J., Zohar, Y., and Chung, J. S. (2009). Molt-inhibiting hormone stimulates vitellogenesis at advanced ovarian developmental stages in the female blue crab, callinectes sapidus 1: an ovarian stage dependent involvement. *Saline Syst.* 5, 7. doi: 10.1186/1746-1448-5-7

frontiers | Frontiers in Marine Science

TYPE Original Research
PUBLISHED 15 August 2022
DOI 10.3389/fmars.2022.976754

OPEN ACCESS

EDITED BY
Haihui Ye,
Jimei University, China

REVIEWED BY
Sirinart Techa,
National Science and Technology Development Agency (NSTDA), Thailand
An Liu,
Jimei University, China

*CORRESPONDENCE
Xi Xie
xiexi@nbu.edu.cn
Dongfa Zhu
zhudongfa@nbu.edu.cn

SPECIALTY SECTION
This article was submitted to Aquatic Physiology, a section of the journal Frontiers in Marine Science

RECEIVED 23 June 2022
ACCEPTED 25 July 2022
PUBLISHED 15 August 2022

CITATION
Tu S, Ge F, Han Y, Wang M, Xie X and Zhu D (2022) Putative role of corazonin in the ovarian development of the swimming crab *Portunus trituberculatus*. *Front. Mar. Sci.* 9:976754. doi: 10.3389/fmars.2022.976754

Putative role of corazonin in the ovarian development of the swimming crab *Portunus trituberculatus*

Shisheng Tu, Fuqiang Ge, Yaoyao Han, Mengen Wang, Xi Xie* and Dongfa Zhu*

School of Marine Science, Ningbo University, Ningbo, China

Corazonin (Crz) is a neuropeptide that widely distributed in insects and crustaceans. The Crz is proposed to have pleiotropic functions in insects, but its physiological roles in crustaceans are poorly understood. In the present study, *Crz* and its putative receptor (*CrzR*) were identified from the swimming crab, *Portunus trituberculatus*, and their interaction was validated using the Dual-Luciferase reporter assay system. Tissue distribution analysis showed the *PtCrz* was mainly derived from center nerve system, while its receptor was highly expressed in Y-organ, the main site for ecdysteroids synthesis. Exposure of YO to synthetic Crz and CrzR dsRNA respectively led to the transcriptional changes of two ecdysteroidogenesis genes, further indicating a putative role of Crz signaling on ecdysteroids synthesis. During the ovarian development, the mRNA levels of *PtCrz* and *PtCrzR* increased significantly in vitellogenic stages, suggesting a potential role of Crz signaling in vitellogenesis. The hypothesis was further strengthened by *in vitro* experiments that the expression of *vitellogenin* (*Vg*), *Vg receptor* (*VgR*), *cyclinB*, and *Cdc2* in ovary explants could be induced by synthetic Crz, whereas reduced by CrzR dsRNA. In addition, since 20-hydroxyecdysone also showed a stimulating effect on *Vg* expression, an indirect regulation of Crz signaling on ovarian development *via* ecdysteroids might also exist.

KEYWORDS

corazonin, corazonin receptor, ovarian development, ecdysteroid, *Portunus trituberculatus*.

Introduction

Corazonin (Crz) is a neuropeptide that widely distributed in insects and crustaceans (Roch et al., 2011; Patel et al., 2014; Veenstra, 2016). Due to its structural relevance to the vertebrate gonadotropin-releasing hormone (GnRH), Crz is known as a member of the GnRH-related peptides. In arthropods, the GnRH-related peptides also include

adipokinetic hormone/corazonin-related peptide (ACP) and red pigment-concentrating hormone (RPCH) (Hauser and Grimmelikhuijzen, 2014; Zandawala et al., 2015). A typical Crz prepropeptide normally consists of a predicted signal peptide, a conserved 11 amino acid corazonin mature peptide, and an additional sequence called corzaonin-precursor-related peptide (CrzRP) (Veenstra, 1994; Baggerman et al., 2002; Verleyen et al., 2006; Predel et al., 2007; Hillyer et al., 2012). In insects, there are 6 isoforms of mature Crzs, differing from each other by only one amino acid (Verleyen et al., 2006; Predel et al., 2007). Among them, the [Arg^7]-corazonin is the most common Crz isoform in insects, and the only isoform found in crustaceans (Dircksen et al., 2011; Bao et al., 2015; Veenstra, 2016).

The first Crz was identified as a cardioacceleratory peptide in the cockroach *Periplaneta Americana* (Veenstra, 1989). Similar function was found in the blood-sucking bug *Rhodnius prolixus* (Patel et al., 2014), but not in other insects (Predel et al., 1999; Hillyer et al., 2012). Crz was also proposed as a regulator of color polymorphism in some locusts (Tawfik et al., 1999; Roller et al., 2003). Recently, emerging evidence suggests that Crz peptides may have broader physiological roles. For example, injection of [Arg^7]-corazonin can reduce the silk spinning rate and prolong the pupal development of the silkworm *Bombyx mori* (Tanaka et al., 2002). The [Arg^7]-corazonin contributes to the early release of ecdysis-triggering hormone (ETH) in the moth *Manduca sexta*, which initiates the ecdysis behavior (Kim et al., 2004). In the fruit flies, Crz is involved in sperm transfer (Hou et al., 2018) and fertility (Gospocic et al., 2017; Ben-Menahem, 2021), the ethanol intoxication behavior (Varga et al., 2016), and regulation of metabolism (Nassel et al., 2013). Compared with insects, the reports about Crz in crustaceans are limited. In the redclaw crayfish *Cherax quadricarinatus*, the synthetic Crz showed abilities in inducing some molting behavioral responses (Minh Nhut et al., 2020), while in the green shore crab *Carcinus maenas*, Crz peptide did not affect heart activity, blood glucose levels, lipid mobilization, or pigment distribution in chromatophores (Alexander et al., 2018).

Most neuropeptides perform their physiological roles by binding to specific G protein-coupled receptors (GPCRs) (Xu et al., 2016). The CrzR is a typical GPCR that was firstly identified is the fruit fly *D. melanogaster* (Cazzamali et al., 2002). To date, the CrzR has been identified in many insects, including the moth *M. sexta* (Kim et al., 2004), the malaria mosquito *Anopheles gambiae* (Belmont et al., 2006), the silkworm *B. mori* (Yang et al., 2013), the house fly *Musca domestica* (Sha et al., 2012), the mosquito *Aedes aegypti* (Oryan et al., 2018), and the blood-sucking bug *R. prolixus* (Hamoudi et al., 2016). The insect CrzRs are hallmarked with a DRY motif at the border of the cytoplasmic end of the third transmembrane domain and a NSXXNPXXY motif in the seventh transmembrane domain (Oldham and Hamm, 2008). Based on these features, *CrzR* has been found in several crustaceans, including the green shore crab *C. maenas* (Alexander et al., 2018), the blackback land crab *Gecarcinus lateralis* (Tran et al., 2019), and the spiny lobster *Sagmariasus verreauxi* (Buckley et al., 2016). In *C. maenas*, the CrzR showed high sensitivity in binding to the Crz with an EC50 value of 0.75 nM (Alexander et al., 2018).

In the present study, *Crz* and its putative receptor (*CrzR*) were identified from the swimming crab, *Portunus trituberculatus*, and their interaction was validated using the Dual-Luciferase reporter assay system. Based on the spatial and temporal expression patterns of *PtCrzR*, the involvement of Crz signaling in ecdysteroids biosynthesis and ovarian development was speculated. The hypothesis was further strengthened by Crz treatment and *PtCrzR* silencing in the *in vitro* assays.

Materials and methods

Ethical care considerations

This study was carried out in accordance with the recommendations of the Institutional Animal Care and Use Committee (IACUC) of the Ningbo University. All experimental procedures were approved by the Committee on the Ethics of Animal Experiments of the Ningbo University.

Animals and tissue sampling

Wild-caught female swimming crabs *Portunus trituberculatus* (body weight of 120-360 g) were purchased from local fish markets in Zhenhai, Ningbo, China. The ovarian development stage of each crab was determined according to previously reported (Wu et al., 2007). The female crabs of exogenous vitellogenic stage were placed on ice for anesthetization before sacrificed. Tissues including brain (Br), eyestalk ganglion (Es), gill (Gi), hepatopancreas (Hp), heart (Ht), Y-organ (YO), muscles (Ms), thoracic ganglion (TG), and ovaries (Ov) were collected for each crab and stored in RNA preservation fluid (CWBIO, Taizhou, Jiangsu Province, China) at -80°C.

RNA extraction, molecular clone and bioinformatics analysis

Total RNA was extracted from tissues using RNA-Solv® Reagent (Omega, USA) following the manufacturer's instructions. The quantity and quality of the RNA were determined using a Nanodrop 2000 spectrophotometer (Thermo Scientific, USA), and the genomic DNA was removed with DNase I (RNase-free DNase I, Takara). The first cDNA was synthesized with the Perfect Real-Time

PrimerScript®RT reagent Kit (Takara), and 5`/3` RACE-cDNA were synthesized with the BD SMARTer™ RACE cDNA amplification kit (Clontech). The full-length sequence was cloned according to the user manual guide for the BD SMARTer™ 5`/3`RACE kit. All PCR products were 1% agarose gel examined, purified (Sangon, Shanghai, China), cloned into PMD19-T vector (Takara), and sequenced by Zhejiang Youkang Biotechnology Co., Ltd (Hangzhou, Zhejiang Province, China). The open reading frame (ORF) was predicted using ORF finder, and the putative signal peptide was predicted using SignalP 5.0 Server program. For *Pt*Crz, the deduced amino acid sequence was further analyzed using the NeuroPred website to predict the prohormone cleavage sites, the mature peptide and the post-translational modifications. For *Pt*CrzR, the transmembrane regions were predicted by GPCRHMM webserver. Multiple sequence alignment was conducted using Clustal X software. The phylogenetic tree was constructed *using* the MEGA7.0.14 software with Neighbor-Joining (NJ) algorithm method. GenBank accession numbers of these species are shown in Supplementary Table 1.

Cell culture and transient transfection

The plasmid for transient expression was constructed by inserting the ORF of *PtCrzR* into the expression vector pEGFP-N1 using restriction enzymes *BamH I* and *EcoR I* (NEB, USA). The construct was sequenced to validate the sequence and orientation. Human embryonic kidney 293T cells (HEK293T) were cultured in high glucose dulbecco's modified eagle medium (DMEM, Corning, USA) supplemented with 10% fetal bovine serum (Bovogen, Australia), 100 U/mL penicillin, and 100 μg/mL streptomycin (Hyclone, USA). Cells were maintained in T25 flasks at 37°C in a humidified incubator containing 5% CO_2. Cells were seeded overnight in a 60 mm culture dish and transiently co-transfected with 3 μg of the *Pt*CrzR/pEGFP-N1 plasmid, 3 μg of the reporter gene pCRE-luc, and 1.2 μg of internal control gene pRL-TK using 15 μL Lipofectamine 3000 (GLPBIO, USA) transfection reagent following the manufacturer's instructions. The empty pEGFP-N1 plasmid was used for mock transfection.

Confocal microscopy

To verify the membrane localization of *Pt*CrzR, the HEK293T cells transiently transfected with *Pt*CrzR/pEGFP-N1 plasmid were used for confocal microscope analysis. The transfected cells were fixed with 4% paraformaldehyde (PFA) for 20 min, and then stained with the cell membrane probe 1,1'-dioctadecyl-3,3,3',3'-tetramethylindocarbocyanine perchlorate (DiI, Beyotime) at 37°C for 10 min. After removing the DiI solution, the cells were washed three times with PBS and further incubated with a nuclear dye 2-(4-Amidinophenyl)-6-indolecarbamidine dihydrochloride (DAPI, Beyotime) at 37°C for 10 min. After removing the DAPI solution, the cells were washed three times with PBS, mounted in an anti-fade mounting medium (Solarbio), and imaged using a Zeiss laser scanning confocal microscope (LSM880, 294 Carl Zeiss, Oberkochen, Germany). The fluorescence detection was used green channel of 505-550 nm, blue channel of 430-490 nm and red channel of 550-585 nm with excitation of 488 nm, 405 nm and 557 nm respectively.

Dual-luciferase reporter assays

The mature *PtCrz* peptide (pQTFQYSRGWTN-NH_2) was synthesized by Sangon Biotech (Shanghai, China), with a purity of 98%. The transfected HEK293T was co-incubated with synthetic Crz peptide in various concentrations (10^{-4}-10^{-11} M). After incubation for 8 h, ligand-induced changes in luciferase activity were detected by the Dual-Luciferase® Reporter Assay System kit (Promega, USA). The dose-response curve was established and fitted in the Logistic equation utilizing GraphPad Prism 7.00.

In vitro assays

20-hydroxyecdysone (20E) was purchased from Tokyo Chemical Industry Development Co., Ltd. (Tokyo, Japan), dissolved in 95% ethanol, and then serially diluted to appropriate working concentrations using crab saline. The female crabs of exogenous vitellogenic stage were used for *in vitro* assays. Hepatopancreas, ovary and YO explants were cultured in 24-well plates as previously described (Xie et al., 2018). After pre-incubation for 1 h, the hepatopancreas and ovary explants were treated with synthetic Crz and 20E respectively, while the YO explants were treated with synthetic Crz. The working concentrations for synthetic Crz were 10^{-5} M, 10^{-6} M, and 10^{-7} M, and 0.05 μM, 0.5 μM and 5 μM for 20E. After incubated for another 8 h, tissues were collected in RNA preservation fluid for qPCR analysis. For Crz treatments, expression levels of *PtVg* and *PtCrzR* in hepatopancreas, *PtVg*, *PtVgR*, *PtCrzR*, *PtcyclinB* and *PtCdc2* in ovary, and *PtSpo, PtSad* and *PtCrzR* in Y-organs were investigated. For 20E treatments, expression levels of *PtVg* and *PtEcR* in hepatopancreas, and *PtVg*, *PtVgR*, *PtEcR*, *PtcyclinB* and *PtCdc2* in ovary were investigated.

RNA interference

cDNA fragments of the *PtCrzR* transmembrane region (565 bp) and the green fluorescent protein (*GFP*, 568 bp) were

cloned into the pMD19-T vector (Takara), respectively. The dsRNA was prepared as previously described (Xie et al., 2016). The female crabs of exogenous vitellogenic stage were used for this experiment. The RNAi experiments were taken on ovary and YO explants, and were divided into 3 groups. The group 1 and 2 were treated with 5 μg of CrzR dsRNA and the group 3 was treated with 5 μg of GFP dsRNA. For group 1 and 3, the tissues were collected after 8 h incubation for qPCR analysis. For group 2, after 8 h incubation, the culture media was replaced by fresh M199 media containing 10^{-6} M of synthetic Crz peptide, and the tissues were collected after incubating for another 8 h.

Gene expression analysis

The relatively mRNA levels in the present study were determined by qPCR, using the primers listed in Supplementary Table 2. The amplification efficiency of primers was 95%-105% (Supplementary Table 3). For tissue distribution analysis, RT-PCR was also carried out to test the accuracy of qPCR. The qPCR system and condition were carried out as previously described (Xie et al., 2016). The β-actin gene was used as an internal control. The specificity of the PCR products was verified using melting curve analysis. For each sample, qPCR reactions were repeated three times. The qPCR data were calculated using the $2^{-\Delta\Delta CT}$ method (Livak and Schmittgen, 2001), and presented as the mean ± standard error (SE). The statistical differences were analyzed by one-way ANOVA followed by Tukey and Duncan test or student`s T-tests (SPSS statistics 25.0). A P value <0.05 was considered to be statistically significant different.

Results

Molecular characterization of *PtCrz* and *PtCrzR*

The deduced amino acid sequence of *PtCrz* consists of a signal peptide, a mature peptide, an RKR cleavage site, and a Crz precursor-related peptide (CrzRP) (Supplementary Figure 1). The predicted Crz mature sequence was pQTFQYSRGWTNamide, which is identical to the insect [Arg^7]-corazonins (Supplementary Figure 2). The putative *Pt*CrzR was predicted to have seven transmembrane helix regions (Supplementary Figure 3), and the phylogenetic analysis showed it was clustered with other known CrzR sequences (Supplementary Figure 4), belonging to the rhodopsin-like GPCR family. The sequence of the *PtCrz* and *PtCrzR* were deposited in GenBank with accession number OL694705 and OL694706.

Functional Characterization of *PtCrzR*

Confocal microscopy showed that *Pt*CrzR/pEGFP-N1 mainly localized to the cell membrane (Figure 1), indicating the *Pt*CrzR is a transmembrane protein. For ligand-receptor binding assays, the HEK293T cells were transiently co-transfected with *Pt*CrzR/pEGFP-N1, pCRE-luc, and pRL-TK. The transfected HEK293T cells showed concentration-dependent cAMP responses when activated with Crz peptide. The median effective concentration (EC50) value for Crz was 22.91 nM (Figure 2). HEK293T cells transfected with empty vector showed no response to different concentrations of Crz peptide.

Spatial and temporal expression of *PtCrz* and *PtCrzR*

The mRNA expression levels of *PtCrz* and *PtCrzR* were detected in a variety of crab tissues. The level of *PtCrz* expression was highest in the eyestalk ganglion, and second in the brain (Figures 3A, C). The *PtCrzR* mRNA was at extremely high level in the Y-organ, while at much lower levels in the eyestalk ganglion, brain, ovary, gill, hepatopancreas, heart, thoracic ganglion and muscle (Figures 3B, D). During the ovarian development, the relative expression level of *PtCrz* in eyestalk ganglion gradually increased, and reached to a peak in the near-mature stage, while *PtCrzR* transcripts in Y-organ was expressed at the highest level in the exogenous vitellogenic stage, and decreased in the near-mature stage (Figure 4).

Effects of *Pt*Crz/*Pt*CrzR on ecdysteroidogenesis related genes

Highly expression of *PtCrzR* in Y-organs suggested the Crz signaling might be involved in ecdysteroids biosynthesis. Therefore, transcriptional changes of two ecdysteroidogenesis related genes, *PtSpo* and *PtSad*, were analyzed in the following *in vitro* assays. The synthetic Crz could induce the expression of *PtCrzR*, as well as *PtSpo* and *PtSad* (Figure 5A). The CrzR dsRNA treatments showed high efficiency in interfering the *PtCrzR* expression, and significant decrease of the *PtSpo* and *PtSad* expression (Figure 5B).

Effects of *Pt*Crz/*Pt*CrzR on genes related to ovarian development

Since the *PtCrzR* transcripts were also slightly expressed in hepatopancreas and ovaries, the direct effects of Crz signaling on ovarian development were also investigated. Changes in the expression of several related genes were examined in the

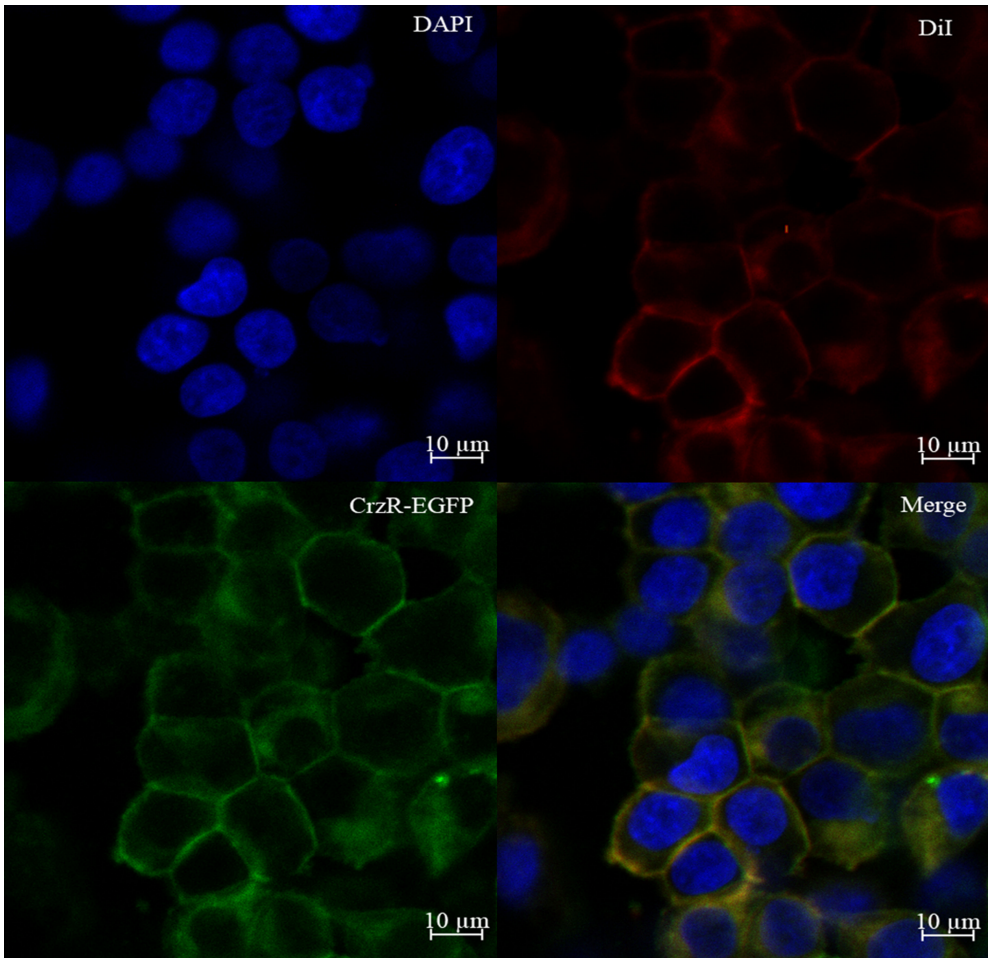

FIGURE 1
Expression of *PtCrzR* in HEK293T cells. Cells expressing *Pt*CrzR/pEGFP-N1 fusion protein were stained with a nuclei probe (DAPI) and a membrane plasma probe (DiI).

hepatopancreas and ovary explants after treated with synthetic Crz and CrzR dsRNA, respectively. Treatment with synthetic Crz could induce the expression of *PtCrzR* in hepatopancreas and ovary, suggesting the Crz signaling is existed in both tissues (Figures 6A, B). However, the synthetic Crz failed to regulate the *PtVg* in hepatopancreas, but showed stimulatory effects on the expression of *PtVg*, *PtVgR*, *PtcyclinB*, and *PtCdc2* in ovaries (Figures 6A, B). Expressions of these genes in ovary explants could be significantly down-regulated by the CrzR dsRNA, but the reduction could be rescued by adding Crz peptide (Figure 7).

Effects of 20E on genes related to ovarian development

The effects of 20E on the expression of genes related to ovarian development was verified in hepatopancreas and ovary explants. Compared with the control group, the mRNA expression levels of *PtEcR* and *PtVg* were significantly up-regulated in both hepatopancreas and ovary explants. For the ovary explants, exposure to 20E induced the expression of *PtcyclinB*, but had no effect on *PtVgR* and *PtCdc2* expression (Figure 8).

Discussion

Neuropeptides are the largest and most diverse group of signaling molecules in multicellular organisms, which act as neurotransmitters, neuromodulators, hormones, or growth factor, regulating various physiological processes and myriad behavioral actions (Schoofs et al., 2017). Insects and crustaceans have long been used to study the mode of action of neuropeptides, but only a few of neuropeptides are well

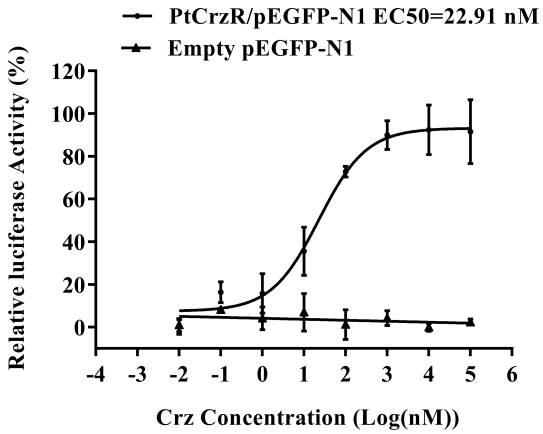

FIGURE 2
Dose-response curves for *PtCrzR* heterogeneously expressed in HEK293T cells. Different concentrations of *PtCrz* peptides were treated and the concentration of cAMP was determined. Each data point was a mean value ± SE from three independent biological replicates.

characterized in some model species. Especially for crustaceans, the large-scale identification of neuropeptides has only emerged in recent years, relatively little is known about most neuropeptides.

The Crz is a typical peptide that were extensively studied in insects, but poorly understood in crustaceans. The mature peptide sequence of *Pt*Crz was predicted as pQTFQYSRGWTNamide, which is identical to the known crustacean Crzs and insect [Arg^7]-corazonins. Since [Arg^7]-corazonins is the main isoform for insect Crzs, and since no other Crzs were identified in crustaceans, this type of Crz could be evolutionarily considered as an ancestor Crz. The tissue expression analysis showed that the *PtCrz* transcripts were mainly expressed in center nerve system, concurred with the CNS dominated expression of Crzs in both insects and crustaceans (Hou et al., 2017; Alexander et al., 2018; Hou et al., 2018). Compared to the conservation in sequence and distribution, the Crz function seems to be divergent between insects and crustaceans. As being a pleiotropic neuropeptide in insects, only its function in the regulation of molting behavior has been revealed in a crustacean (Minh Nhut et al., 2020). In the green shore crab, *C. maenas*, it was shown that the *Cm*Crz lacks functions that proposed for insect Crzs, such as cardio regulation, glucose metabolism, lipid mobilization, and chromatophore pigment migration (Alexander et al., 2018).

Although the physiological roles of the crustacean Crz remains unclear, its receptor has been found in several species by searching for the conserved DRY and NSXXNPXXY motifs (Veenstra, 2015; Buckley et al., 2016; Alexander et al., 2018). Given the importance of a receptor in signal transduction, the behavioral patterns of CrzR may be indicative for the possible functions of Crz peptides. In this study, the putative *PtCrzR* sequence was therefore identified. In addition to the membrane location and evolutionary conservation, the obtained *Pt*CrzR could be activated by the synthetic Crz in a dose-dependent manner, with EC50 of 22.91 nM and which resulted in cAMP accumulation. In further *in vitro* assays, the gene expressions that induced by the synthetic Crz treatment were reduced by *PtCrzR* silencing, again suggesting the obtained *Pt*CrzR is a *bona*

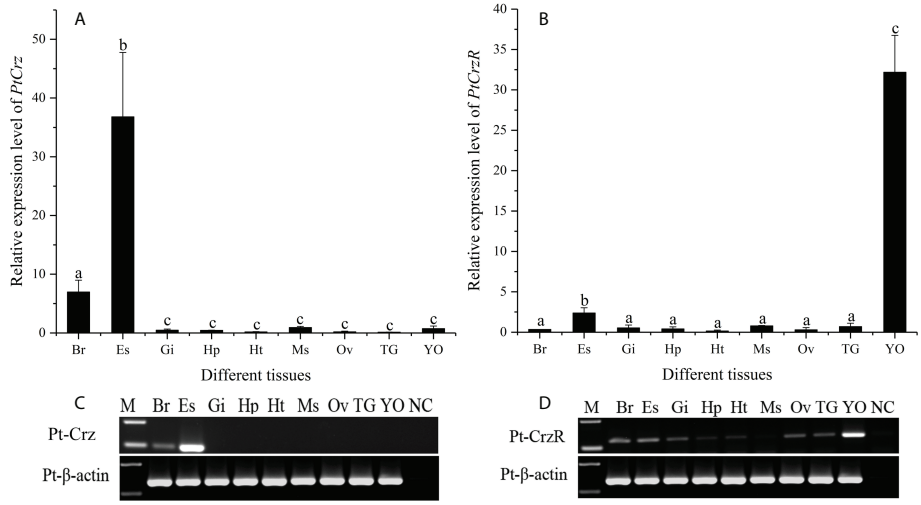

FIGURE 3
Tissue distribution of *PtCrz* **(A, C)** and *PtCrzR* **(B, D)** mRNA in the swimming crab (n=5). Different letters indicate statistically significant differences ($P < 0.05$) within each tissue. Br, brain; Es, eyestalk ganglion; Gi, gill; Hp, hepatopancreas; Ht, heart; Ms, muscle; Ov, ovary; TG, thoracic ganglion; YO, Y-organ.

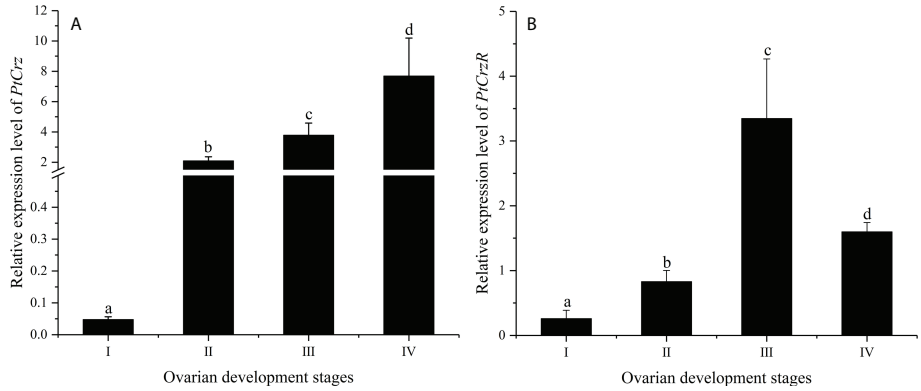

FIGURE 4
The expression of *PtCrz* **(A)** and *PtCrzR* **(B)** in the eyestalk ganglion and the Y-organ during the ovarian development were quantified respectively by qPCR analysis (n=4). Different letters indicate statistically significant differences ($P < 0.05$) within each stage. I: previtellogenic stage; II: endogenous vitellogenic stage; III: exogenous vitellogenic stage; IIV: near-mature stage.

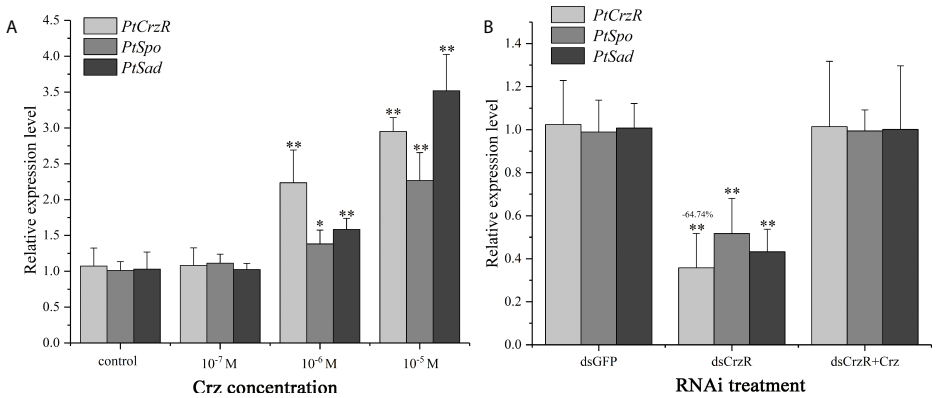

FIGURE 5
In vitro effect of synthetic Crz **(A)** or CrzR dsRNA **(B)** on the expression of *PtCrzR*, *PtSpo*, and *PtSad* in Y-organ explants from *P. trituberculatus*. Data are shown as mean ± SE (n=4). "*" represents significant differences ($P < 0.05$) and "**" represents extremely significant differences ($P < 0.01$) from the control group.

fide receptor for *Pt*Crz. However, it should be noted that this reduction could be rescued by adding Crz in CrzR dsRNA treatment. Since it is common for a neuropeptide to activate two or more related receptors (Schoofs et al., 2017), our results might suggest the existence of other Crz receptors.

The *PtCrzR* was strongly expressed in Y-organ, and the level was significantly higher than other tissues. As the molting gland in crustacean, the Y-organ is mainly responsible for the production of ecdysteroids. Therefore, our results elicited an indication that the Crz might be involved in regulating the ecdysteroidogenesis. Similar distribution was also observed for the *CrzR* of *C. maenas* (Alexander et al., 2018), but in that study, application of Crz peptide to Y-organ had barely effect on ecdysteroids secretion. In this study, interestingly, contrary evidence might be presented, as the gene expressions of *PtSpo* and *PtSad* in Y-organ explants were remarkably induced by Crz treatment, whereas reduced by *PtCrzR* silencing. As members of Halloween gene family, *Spo* and *Sad* encode cytochrome P450 enzymes CYP307A1 and CYP315A1, respectively, which are responsible for the early and late steps of ecdysteroids biosynthesis (Mykles, 2011). However, although the transcription levels of the Halloween genes have been shown to be closely related to ecdysone levels in many studies (Iga et al., 2010; Xie et al., 2016; Yang et al., 2021), future studies to detect the ecdysone levels after Crz treatment are still needed to confirm the stimulatory effects of Crz peptide.

The expressions of *PtCrz* and *PtCrzR* were observed to increase during the vitellogenic stages, whereas the *PtCrzR*

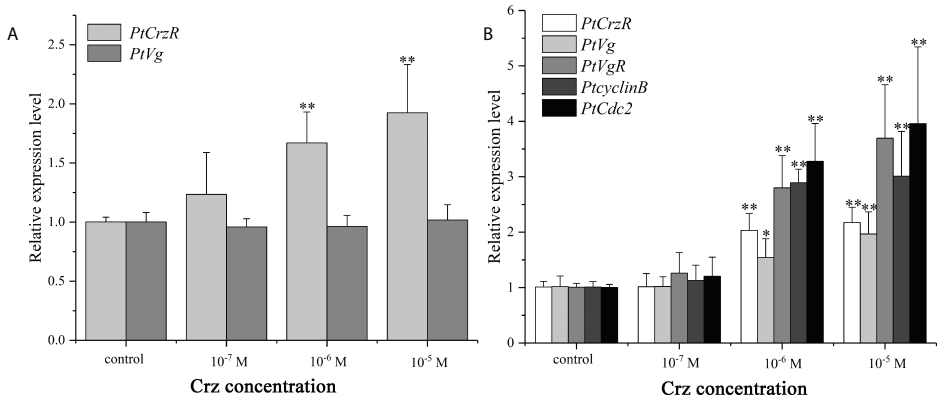

FIGURE 6
In vitro effect of synthetic Crz on the expression of *PtCrzR* and *PtVg* in the hepatopancreas explants **(A)**, and the expression of *PtCrzR*, *PtVg*, *PtVgR*, *PtcyclinB*, and *PtCdc2* in the ovary explants **(B)**. Data are shown as mean ± SE (n=4). "*" represents significant differences (P < 0.05) and "**" represents extremely significant differences (P < 0.01) from the control group.

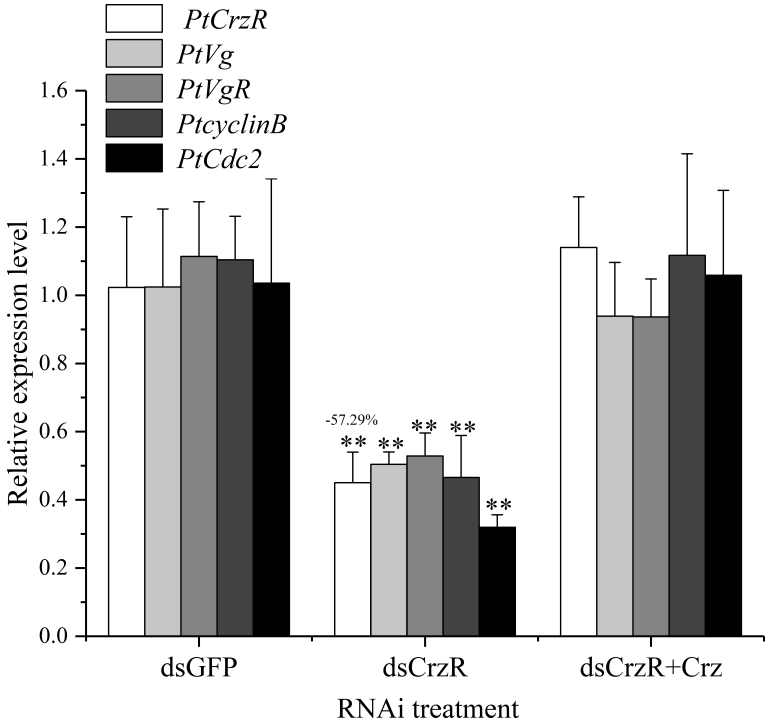

FIGURE 7
Effect of CrzR dsRNA on the expression of *PtCrzR*, *PtVg*, *PtVgR*, *PtcyclinB*, and *PtCdc2* in the ovary explants from *P. trituberculatus*. Data are shown as mean ± SE (n=4). "**" represents extremely significant differences (*P* < 0.01) from the control group.

expression declined in the near-mature stage, which might suggest a potential role of Crz signaling in vitellogenesis. Combined with the possible effects of Crz on ecdysteroidogenesis, this result could be reminiscent of the vitellogenic promoting role for 20-hydroxyecdysone (20E), the main active form of ecdysteroids (Li et al., 2000; Tiu et al., 2010; Gong et al., 2015; Yang and Liu, 2021). In this study, 20E treatment induced the *Vg* expression in both hepatopancreas

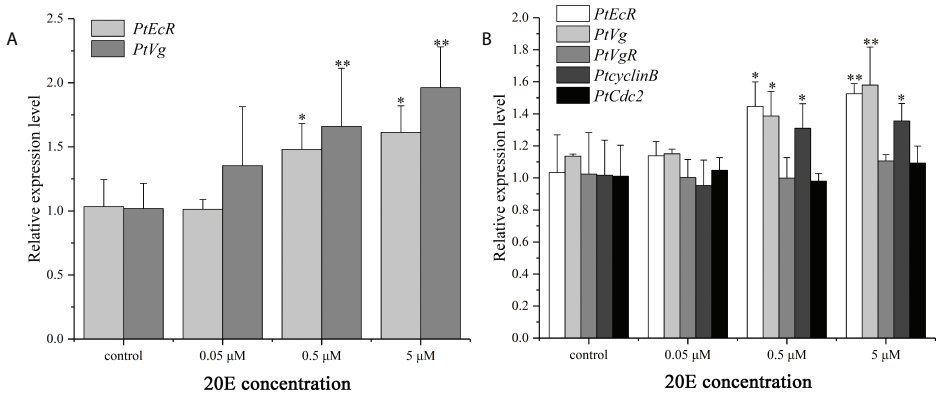

FIGURE 8
In vitro effect of 20E on the expression of *PtEcR* and *PtVg* in the hepatopancreas explants **(A)**, and the expression of *PtEcR*, *PtVg*, *PtVgR*, *PtcyclinB*, and *PtCdc2* in the ovary explants **(B)**. Data are shown as mean ± SE (n=4). "*" represents significant differences ($P < 0.05$) and "**" represents extremely significant differences ($P < 0.01$) from the control group.

and ovary explants, further illustrating its role in the ovarian development of *P. trituberculatus*. However, as mentioned in last paragraph, whether Crz signaling can regulate ovarian development *via* ecdysteroids needs more evidences in hormone levels.

Since the *PtCrzR* transcripts were also slightly expressed in hepatopancreas and ovaries, the direct effects of Crz signaling on ovarian development should not be ignored. The increase in *PtCrzR* expression in hepatopancreas and ovary exposed to Crz indicated the existence of Crz signaling in both tissues. However, only the *Vg* expression in ovaries but not hepatopancreas was induced by Crz exposure, which may suggest other switch pathways for Crz signaling. As a GnRH-like peptide, the effects of Crz on ovarian development were compared with those from RPCH, another member in this group. In the whiteleg shrimp *Litopenaeus vannamei*, *in vivo* injection of RPCH caused significant increase in ovarian *Vg* mRNA levels (Chen et al., 2018). Similar results were also observed in mud crab *Scylla paramamosain*, but the induction of *Vg in vitro* required the presence of nerve tissues (Zeng et al., 2016). It was also found in *S. paramamosain* that *in vivo* treatment of RPCH could also induced the *Vg* expression in hepatopancreas, which was not observed in our *in vitro* studies.

In addition to *Vg*, several other ovarian-related genes were also selected to investigate their transcriptional response to the Crz exposure. Among them, the VgR is a crucial protein in mediating the endocytosis which incorporating the exogenous Vg into developing oocytes (Zmora et al., 2007). As for *cyclinB* and *Cdc2*, which are components of maturation promoting factor (MPF), emerging evidences indicated they are also involved in the oocyte maturation of crustaceans (Fang et al., 2009; Qiu and Liu, 2009; Han et al., 2012). It was observed that the expressions of *VgR*, *cyclinB*, and *Cdc2* were also up-regulated by synthetic Crz. This induction was further confirmed by treating with CrzR dsRNA, which might suggest an integrative role of Crz signaling during ovarian development. Moreover, this result conforms to the properties of CrzR as a GPCR, as in many studies, the intracellular cAMP level plays pivotal roles in regulating the expression of *Vg*, *cyclinB*, and *Cdc2* (Chen et al., 2018; Mani et al., 2019; Feng et al., 2021; Wan et al., 2022).

Although the Crz peptides are structurally related to the vertebrate GnRHs (Hauser and Grimmelikhuijzen, 2014; Zandawala et al., 2015), the present study was the first to explore its putative role in ovarian development. Comparably, another GnRH-related peptide RPCH has been reported to be involved in ovarian development in several species (Zandawala et al., 2015; Zeng et al., 2016; Chen et al., 2018; Ben-Menahem, 2021). Interestingly, although the RPCHR has been identified from several crabs (Alexander et al., 2018; Ma et al., 2018), its paralogous sequence cannot be found in the transcriptome (Tu et al., 2021) and the genome of *P. trituberculatus* (NCBI database: PRJNA555262). In addition, another study in our group has confirmed the ligand activation of *Pt*CrzR by RPCH (data not shown), which suggests that the RPCH might use the *Pt*CrzR as its receptor in *P. trituberculatus*. It would be intriguing to define the overlapping roles of these two peptides, as well as their crosstalk during signal transduction.

Data availability statement

The datasets presented in this study can be found in online repositories. The names of the repository/repositories and accession number(s) can be found in the article/Supplementary Material.

Ethics statement

The animal study was reviewed and approved by Committee on the Ethics of Animal Experiments of the Ningbo University.

Author contributions

ST: conceptualization, sample collection, experiment, data analysis and writing-original draft. FG and YH: sample collection and experiment. MW: experiment. XX and DZ: editing and supervision. All authors contributed to the article and approved the submitted version.

Funding

This study was supported by the National natural Science Foundation of China (Nos. 41776165 and 31802265), Natural Science Foundation of Zhejiang province (LY20C190004), and the K. C. Wong Magna Fund in Ningbo University.

Conflict of interest

The authors declare that the research was conducted in the absence of any commercial or financial relationships that could be construed as a potential conflict of interest.

Publisher's note

All claims expressed in this article are solely those of the authors and do not necessarily represent those of their affiliated organizations, or those of the publisher, the editors and the reviewers. Any product that may be evaluated in this article, or claim that may be made by its manufacturer, is not guaranteed or endorsed by the publisher.

Supplementary material

The Supplementary Material for this article can be found online at: https://www.frontiersin.org/articles/10.3389/fmars.2022.976754/full#supplementary-material

References

Alexander, J. L., Oliphant, A., Wilcockson, D. C., Audsley, N., Down, R. E., Lafont, R., et al. (2018). Functional characterization and signaling systems of corazonin and red pigment concentrating hormone in the green shore crab, *Carcinus maenas*. *Front. Neurosci.* 11. doi: 10.3389/fnins.2017.00752

Baggerman, G., Cerstiaens, A., De Loof, A., and Schoofs, L. (2002). Peptidomics of the larval *Drosophila melanogaster* central nervous system. *J. Biol. Chem.* 277, 40368–40374. doi: 10.1074/jbc.M206257200

Bao, C., Yang, Y., Huang, H., and Ye, H. (2015). Neuropeptides in the cerebral ganglia of the mud crab, *Scylla paramamosain*: Transcriptomic analysis and expression profiles during vitellogenesis. *Sci. Rep.* 5, 17055. doi: 10.1038/srep17055

Belmont, M., Cazzamali, G., Williamson, M., Hauser, F., and Grimmelikhuijzen, C. J. (2006). Identification of four evolutionarily related G protein-coupled receptors from the malaria mosquito *Anopheles gambiae*. *Biochem. Biophys. Res. Commun.* 344, 160–165. doi: 10.1016/j.bbrc.2006.03.117

Ben-Menahem, D. (2021). GnRH-related neurohormones in the fruit fly *Drosophila melanogaster*. *Int. J. Molr. Sci.* 22, 5035. doi: 10.3390/ijms22095035

Buckley, S. J., Fitzgibbon, Q. P., Smith, G. G., and Ventura, T. (2016). *In silico* prediction of the G-protein coupled receptors expressed during the metamorphic molt of *Sagmariasus verreauxi* (Crustacea: Decapoda) by mining transcriptomic data: RNA-seq to repertoire. *Gen. Comp. Endocrinol.* 228, 111–127. doi: 10.1016/j.ygcen.2016.02.001

Cazzamali, G., Saxild, N., and Grimmelikhuijzen, C. (2002). Molecular cloning and functional expression of a drosophila corazonin receptor. *Biochem. Biophys. Res. Commun.* 298, 31–36. doi: 10.1016/s0006-291x(02)02398-7

Chen, H.-Y., Kang, B. J., Sultana, Z., and Wilder, M. N. (2018). Molecular cloning of red pigment-concentrating hormone (RPCH) from eyestalks of the whiteleg shrimp (*Litopenaeus vannamei*): Evaluation of the effects of the hormone on ovarian growth and the influence of serotonin (5-HT) on its expression. *Aquaculture* 495, 232–240. doi: 10.1016/j.aquaculture.2018.04.027

Chen, T., Ren, C., Jiang, X., Zhang, L., Li, H., Huang, W., et al. (2018). Mechanisms for type-II vitellogenesis-inhibiting hormone suppression of vitellogenin transcription in shrimp hepatopancreas: Crosstalk of GC/cGMP pathway with different MAPK-dependent cascades. *PloS One* 13, e0194459. doi: 10.1371/journal.pone.0194459

Dircksen, H., Neupert, S., Predel, R., Verleyen, P., Huybrechts, J., Strauss, J., et al. (2011). Genomics, transcriptomics, and peptidomics of *Daphnia pulex* neuropeptides and protein hormones. *J. Proteome Res.* 10, 4478–4504. doi: 10.1021/pr200284e

Fang, J. J., and Qiu, G. F. (2009). Molecular cloning of cyclin b transcript with an unusually long 3' untranslation region and its expression analysis during oogenesis in the Chinese mitten crab, *Eriocheir sinensis*. *Mol. Biol. Rep.* 36, 1521–1529. doi: 10.1007/s11033-008-9346-9

Feng, Q. M., Liu, M. M., Cheng, Y. X., and Wu, X. G. (2021). Comparative proteomics elucidates the dynamics of ovarian development in the Chinese mitten crab *Eriocheir sinensis*. *Comp. Biochem. Physiol. Part D. Genomics Proteomics* 40, 100878. doi: 10.1016/j.cbd.2021.100878

Gong, J., Ye, H., Xie, Y., Yang, Y., Huang, H., Li, S., et al. (2015). Ecdysone receptor in the mud crab *Scylla paramamosain*: A possible role in promoting ovarian development. *J. Endocrinol.* 224, 273–287. doi: 10.1530/joe-14-0526

Gospocic, J., Shields, E. J., Glastad, K. M., Lin, Y., Penick, C. A., Yan, H., et al. (2017). The neuropeptide corazonin controls social behavior and caste identity in ants. *Cell* 170, 748–759. doi: 10.1016/j.cell.2017.07.014

Hamoudi, Z., Lange, A. B., and Orchard, I. (2016). Identification and characterization of the corazonin receptor and possible physiological roles of the corazonin-signaling pathway in *Rhodnius prolixus*. *Front. Neurosci.* 10. doi: 10.3389/fnins.2016.00357

Han, K., Dai, Y., Zou, Z., Fu, M., Wang, Y., and Zhang, Z. (2012). Molecular characterization and expression profiles of cdc2 and cyclin b during oogenesis and spermatogenesis in green mud crab (*Scylla paramamosain*). *Comp. Biochem. Physiol. B. Biochem. Mol. Biol.* 163, 292–302. doi: 10.1016/j.cbpb.2012.07.001

Hauser, F., and Grimmelikhuijzen, C. J. (2014). Evolution of the AKH/corazonin/ACP/GnRH receptor superfamily and their ligands in the protostomia. *Gen. Comp. Endocrinol.* 209, 35–49. doi: 10.1016/j.ygcen.2014.07.009

Hillyer, J. F., Estevez-Lao, T. Y., Funkhouser, L. J., and Aluoch, V. A. (2012). *Anopheles gambiae* corazonin: Gene structure, expression and effect on mosquito heart physiology. *Insect Mol. Biol.* 21, 343–355. doi: 10.1111/j.1365-2583.2012.01140.x

Hou, Q. L., Chen, E. H., Jiang, H. B., Yu, S. F., Yang, P. J., Liu, X. Q., et al. (2018). Corazonin signaling is required in the male for sperm transfer in the oriental fruit fly *Bactrocera dorsalis*. *Front. Physiol.* 9. doi: 10.3389/fphys.2018.00660

Hou, Q.-L., Jiang, H.-B., Gui, S.-H., Chen, E.-H., Wei, D.-D., Li, H.-M., et al. (2017). A role of corazonin receptor in larval-pupal transition and pupariation in

the oriental fruit fly *Bactrocera dorsalis* (Hendel) (Diptera: Tephritidae). *Front. Physiol.* 8. doi: 10.3389/fphys.2017.00077

Iga, M., and Smagghe, G. (2010). Identification and expression profile of Halloween genes involved in ecdysteroid biosynthesis in *Spodoptera littoralis*. *Peptides* 31, 456–467. doi: 10.1016/j.Peptides.2009.08.002

Kim, Y. J., Spalovska-Valachova, I., Cho, K. H., Zitnanova, I., Park, Y., Adams, M. E., et al. (2004). Corazonin receptor signaling in ecdysis initiation. *Proc. Natl. Acad. Sci. U.S.A.* 101, 6704–6709. doi: 10.1073/pnas.0305291101

Li, C., Kapitskaya, M. Z., Zhu, J., Miura, K., Segraves, W., and Raikhel, A. S. (2000). Conserved molecular mechanism for the stage specificity of the mosquito vitellogenic response to ecdysone. *Dev. Biol.* 224, 96–110. doi: 10.1006/dbio.2000.9792

Livak, K. J., and Schmittgen, T. D. (2001). Analysis of relative gene expression data using real-time quantitative PCR and the 2(-delta delta C(T)) method. *Methods* 25, 402–408. doi: 10.1006/meth.2001.1262

Mani, T., Subramaniya, B. R., Chidambaram Iyer, S., Sivasithamparam, N. D., and Devaraj, H. (2019). Modulation of complex coordinated molecular signaling by 5-HT and a cocktail of inhibitors leads to ovarian maturation of *Penaeus monodon* in captivity. *Mol. Reprod. Dev.* 86, 576–591. doi: 10.1002/mrd.23135

Ma, K. Y., Zhang, S. F., Wang, S. S., and Qiu, G. F. (2018). Molecular cloning and characterization of a gonadotropin-releasing hormone receptor homolog in the Chinese mitten crab, *Eriocheir sinensis*. *Gene* 665, 111–118. doi: 10.1016/j.gene.2018.05.006

Minh Nhut, T., Mykles, D. L., Elizur, A., and Ventura, T. (2020). Ecdysis triggering hormone modulates molt behaviour in the redclaw crayfish *Cherax quadricarinatus*, providing a mechanistic evidence for conserved function in molt regulation across pancrustacea. *Gen. Comp. Endocrinol.* 298, 113556. doi: 10.1016/j.ygcen.2020.113556

Mykles, D. L. (2011). Ecdysteroid metabolism in crustaceans. *J Steroid Biochem Mol. Biol.* 127, 196–203. doi: 10.1016/j.jsbmb.2010.09.001

Nassel, D. R., Kubrak, O. I., Liu, Y., Luo, J., and Lushchak, O. V. (2013). Factors that regulate insulin producing cells and their output in drosophila. *Front. Physiol.* 4. doi: 10.3389/fphys.2013.00252

Oldham, W. M., and Hamm, H. E. (2008). Heterotrimeric G protein activation by G-protein-coupled receptors. *Nat. Rev. Mol. Cell Biol.* 9, 60–71. doi: 10.1038/nrm2299

Oryan, A., Wahedi, A., and Paluzzi, J. V. (2018). Functional characterization and quantitative expression analysis of two GnRH-related peptide receptors in the mosquito, *Aedes aegypti*. *Biochem. Biophys. Res. Commun.* 497, 550–557. doi: 10.1016/j.bbrc.2018.02.088

Patel, H., Orchard, I., Veenstra, J. A., and Lange, A. B. (2014). The distribution and physiological effects of three evolutionarily and sequence-related neuropeptides in *Rhodnius prolixus*: Adipokinetic hormone, corazonin and adipokinetic hormone/corazonin-related peptide. *Gen. Comp. Endocrinol.* 195, 1–8. doi: 10.1016/j.ygcen.2013.10.012

Predel, R., Kellner, R., and Gade, G. (1999). Myotropic neuropeptides from the retrocerebral complex of the stick insect, *Carausius morosus* (Phasmatodea : Lonchodidae). *Eur. J. Entomology.* 96, 275–278. doi: 10.1046/j.1570-7458.1999.00427.x

Predel, R., Neupert, S., Russell, W. K., Scheibner, O., and Nachman, R. J. (2007). Corazonin in insects. *Peptides* 28, 3–10. doi: 10.1016/j.peptides.2006.10.011

Qiu, G. F., and Liu, P. (2009). On the role of Cdc2 kinase during meiotic maturation of oocyte in the Chinese mitten crab, *Eriocheir sinensis*. *Comp. Biochem. Physiol. B. Biochem. Mol. Biol.* 152, 243–248. doi: 10.1016/j.cbpb.2008.12.004

Roch, G. J., Busby, E. R., and Sherwood, N. M. (2011). Evolution of GnRH: diving deeper. *Gen. Comp. Endocrinol.* 171, 1–16. doi: 10.1016/j.ygcen.2010.12.014

Roller, L., Tanaka, Y., and Tanaka, S. (2003). Corazonin and corazonin-like substances in the central nervous system of the pterygote and apterygote insects. *Cell Tissue Res.* 312, 393–406. doi: 10.1007/s00441-003-0722-4

Schoofs, L., De Loof, A., and Van Hiel, M. B. (2017). Neuropeptides as regulators of behavior in insects. *Annu. Rev. Entomol.* 62, 35–52. doi: 10.1146/annurev-ento-031616-035500

Sha, K., Conner, W. C., Choi, D. Y., and Park, J. H. (2012). Characterization, expression, and evolutionary aspects of corazonin neuropeptide and its receptor from the house fly, *Musca domestica* (Diptera: Muscidae). *Gene* 497, 191–199. doi: 10.1016/j.gene.2012.01.052

Tanaka, Y., Hua, Y., Roller, L., and Tanaka, S. (2002). Corazonin reduces the spinning rate in the silkworm, *Bombyx mori*. *J. Insect Physiol.* 48, 707–714. doi: 10.1016/s0022-1910(02)00094-x

Tawfik, A. I., Tanaka, S., De Loof, A., Schoofs, L., Baggerman, G., Waelkens, E., et al. (1999). Identification of the gregarization-associated dark-pigmentotropin in locusts through an albino mutant. *Proc. Natl. Acad. Sci. U.S.A.* 96, 7083–7087. doi: 10.1073/pnas.96.12.7083

Tiu, S. H.-K., Chan, S.-M., and Tobe, S. S. (2010). The effects of farnesoic acid and 20-hydroxyecdysone on vitellogenin gene expression in the lobster, *Homarus americanus*, and possible roles in the reproductive process. *Gen. Comp. Endocrinol.* 166, 337–345. doi: 10.1016/j.ygcen.2009.11.005

Tran, N. M., Mykles, D. L., Elizur, A., and Ventura, T. (2019). Characterization of G-protein coupled receptors from the blackback land crab *Gecarcinus lateralis* y organ transcriptome over the molt cycle. *BMC Genomics* 20, 74. doi: 10.1186/s12864-018-5363-9

Tu, S., Xu, R., Wang, M., Xie, X., Bao, C., and Zhu, D. (2021). Identification and characterization of expression profiles of neuropeptides and their GPCRs in the swimming crab, *Portunus trituberculatus*. *PeerJ* 9, e12179. doi: 10.7717/peerj.12179

Varga, K., Nagy, P., Arsikin Csordas, K., Kovacs, A. L., Hegedus, K., and Juhasz, G. (2016). Loss of Atg16 delays the alcohol-induced sedation response *via* regulation of corazonin neuropeptide production in drosophila. *Sci. Rep.* 6, 34641. doi: 10.1038/srep34641

Veenstra, J. A. (1989). Isolation and structure of corazonin, a cardioactive peptide from the american cockroach. *FEBS Lett.* 250, 231–234. doi: 10.1016/0014-5793(89)80727-6

Veenstra, J. A. (1994). Isolation and structure of the drosophila corazonin gene. *Biochem. Biophys. Res. Commun.* 204, 292–296. doi: 10.1006/bbrc.1994.2458

Veenstra, J. A. (2015). The power of next-generation sequencing as illustrated by the neuropeptidome of the crayfish *Procambarus clarkii*. *Gen. Comp. Endocrinol.* 224, 84–95. doi: 10.1016/j.ygcen.2015.06.013

Veenstra, J. A. (2016). Similarities between decapod and insect neuropeptidomes. *PeerJ* 4, e2043. doi: 10.7717/peerj.2043

Verleyen, P., Baggerman, G., Mertens, I., Vandersmissen, T., Huybrechts, J., Van Lommel, A., et al. (2006). Cloning and characterization of a third isoform of corazonin in the honey bee *Apis mellifera*. *Peptides* 27, 493–499. doi: 10.1016/j.peptides.2005.03.065

Wan, H., Zhong, J., Zhang, Z., Zou, P., and Wang, Y. (2022). Comparative transcriptome reveals the potential modulation mechanisms of spfoxl-2 affecting ovarian development of *Scylla paramamosain*. *Mar. Biotechnol. (NY).* 24, 125–135. doi: 10.1007/s10126-022-10091-6

Wu, X. G., Yao, G. G., Yang, X. Z., Cheng, Y. X., and Wang, C. L. (2007). A study on the ovarian development of *Portunus trituberculatus* in East China Sea during the first reproductive cycle. *Acta Oceanologica. Sin.* 29, 120–127. doi: 10.3321/j.issn:0253-4193.2007.04.014

Xie, X., Liu, M., Jiang, Q., Zheng, H., Zheng, L., and Zhu, D. (2018). Role of kruppel homolog 1 (Kr-h1) in methyl farnesoate-mediated vitellogenesis in the swimming crab *Portunus trituberculatus*. *Gene* 679, 260–265. doi: 10.1016/j.gene.2018.08.046

Xie, X., Liu, Z., Liu, M., Tao, T., Shen, X., and Zhu, D. (2016). Role of Halloween genes in ecdysteroids biosynthesis of the swimming crab (*Portunus trituberculatus*): Implications from RNA interference and eyestalk ablation. *Comp. Biochem. Physiol. A. Mol. Integr. Physiol.* 199, 105–110. doi: 10.1016/j.cbpa.2016.06.001

Xu, G., Gu, G. X., Teng, Z. W., Wu, S. F., Huang, J., Song, Q. S., et al. (2016). Identification and expression profiles of neuropeptides and their G protein-coupled receptors in the rice stem borer *Chilo suppressalis*. *Sci. Rep.* 6, 28976. doi: 10.1038/srep28976

Yang, J., Huang, H., Yang, H., He, X., Jiang, X., Shi, Y., et al. (2013). Specific activation of the G protein-coupled receptor BNGR-A21 by the neuropeptide corazonin from the silkworm, *Bombyx mori*, dually couples to the g(q) and g(s) signaling cascades. *J. Biol. Chem.* 288, 11662–11675. doi: 10.1074/jbc.M112.441675

Yang, X., and Liu, J. (2021). Effect of 20-hydroxyecdysone on vitellogenesis in the ixodid tick *Haemaphysalis longicornis*. *Int. J. Acarol.* 48, 20–26. doi: 10.1080/01647954.2021.2009568

Yang, Z. M., Yu, N., Wang, S. J., Korai, S. K., and Liu, Z. W. (2021). Characterization of ecdysteroid biosynthesis in the pond wolf spider, *Pardosa pseudoannulata*. *Insect Mol. Biol.* 30, 71–80. doi: 10.1111/imb.12678

Zandawala, M., Haddad, A. S., Hamoudi, Z., and Orchard, I. (2015). Identification and characterization of the adipokinetic hormone/corazonin-related peptide signaling system in *Rhodnius prolixus*. *FEBS J.* 282, 3603–3617. doi: 10.1111/febs.13366

Zeng, H., Bao, C., Huang, H., Ye, H., and Li, S. (2016). The mechanism of regulation of ovarian maturation by red pigment concentrating hormone in the mud crab *Scylla paramamosain*. *Anim. Reprod. Sci.* 164, 152–161. doi: 10.1016/j.anireprosci.2015.11.025

Zmora, N., Trant, J., Chan, S. M., and Chung, J. S. (2007). Vitellogenin and its messenger RNA during ovarian development in the female blue crab, *Callinectes sapidus*: Gene expression, synthesis, transport, and cleavage. *Biol. Reprod.* 77, 138–146. doi: 10.1095/biolreprod.106.055483

Advantages of publishing in Frontiers

OPEN ACCESS
Articles are free to read for greatest visibility and readership

FAST PUBLICATION
Around 90 days from submission to decision

HIGH QUALITY PEER-REVIEW
Rigorous, collaborative, and constructive peer-review

TRANSPARENT PEER-REVIEW
Editors and reviewers acknowledged by name on published articles

Frontiers
Avenue du Tribunal-Fédéral 34
1005 Lausanne | Switzerland

Visit us: www.frontiersin.org
Contact us: frontiersin.org/about/contact

REPRODUCIBILITY OF RESEARCH
Support open data and methods to enhance research reproducibility

DIGITAL PUBLISHING
Articles designed for optimal readership across devices

FOLLOW US
@frontiersin

IMPACT METRICS
Advanced article metrics track visibility across digital media

EXTENSIVE PROMOTION
Marketing and promotion of impactful research

LOOP RESEARCH NETWORK
Our network increases your article's readership